THE COMPUTATION OF THE VERTICAL VELOCITY ON THE SYNOPTIC SCALE

Thesis submitted by

ROBERT WILLIAM RIDDAWAY, B. Sc. (Edinburgh)

for the degree of

Doctor of Philosophy

Department of Meteorology,

University of Edinburgh.

May, 1973.

SUMMARY

Several sets of equations which can be used to find the vertical velocity are examined. A distinction is made between assumptions that are based on physical considerations and those based on computational necessity. Since the equations are solved as boundary value problems it is necessary to impose boundary conditions. These are discussed.

Investigations are made into the use of the overrelaxation method for solving partial differential equations with either Dirichlet or Neumann boundary conditions. Emphasis is placed upon the determination of the optimum overrelaxation factor. A simple method of calculating this factor for the ω-equation is tested.

The derivation, meaning and solution of the balance equation is discussed. New methods of solving this equation are introduced and are compared with existing methods. The boundary conditions for the linear balance equation are investigated and this leads to the derivation of a new boundary condition for the balance equation.

The geostrophic ω-equation is examined and the elliptic condition is derived. Appropriate boundary conditions for ω are discussed and the effects of the form of the static stability on ω and Φ_t are investigated. Simple models of the atmosphere are used from which several inferences are drawn. These are tested with case studies. The inconsistency of the usual boundary conditions for ω and Φ_t is also examined.

CONTENTS

PREFACE

The research described in this thesis was conducted in the Meteorology Department under the supervision of Dr. D.H. McIntosh.

LIST OF FIGURES

LIST OF TABLES

LIST OF SYMBOLS

Symbols are defined where they are introduced in the text. However, many symbols are used throughout and these are listed below.

ω	$\frac{dp}{dt}$
ζ	vertical component of vorticity
ζ_g	$\frac{1}{f}\nabla^2\phi$
η	absolute vorticity
T	temperature
ϕ	geopotential
Ψ	streamfunction
χ	velocity potential
ϕ_t	geopotential tendency
Ψ_t	streamfunction tendency
D	divergence
p	pressure
R	gas constant
C_p	specific heat at constant pressure
$\varkappa$	R/C_p
ρ	density
u	$\frac{dx}{dt}$
v	$\frac{dy}{dt}$
w	$\frac{dz}{dt}$
g	apparent acceleration due to gravity
ϑ	potential temperature
m	mapping factor
d	gridlength
f	Coriolis parameter
$\underline{V}$	horizontal velocity

LIST OF SYMBOLS (contd.)

$\underline{V}_1$	rotational part of $\underline{V}$
$\underline{V}_2$	divergent part of $\underline{V}$
$\underline{V}_g$	geostrophic wind in the p direction
$\underline{k}$	unit vector
σ	static stability
$J(u,v)$	$\frac{\partial u}{\partial x}\frac{\partial v}{\partial y} - \frac{\partial u}{\partial y}\frac{\partial v}{\partial x}$
$\nabla^2\omega$	$(\omega_{i+1,j} + \omega_{i-1,j} + \omega_{i,j+1} + \omega_{i,j-1} - 4\omega_{i,j})$
β	overrelaxation factor
β_o	optimum overrelaxation factor
i,j,k	label of gridpoints in the x,y and p directions
n_i,n_j,n_k	number of gridpoints in the x,y and p directions

INTRODUCTION

It is generally accepted that a realistic description of the large-scale vertical velocity can be obtained by solving an ω-equation. This equation is derived by eliminating $\frac{\partial \zeta}{\partial t}$ and $\frac{\partial T}{\partial t}$ between some form of the vorticity equation and thermal equation. To do this it is necessary to use hydrostatic equation (which relates T to Φ) and some form of the divergence equation (which relates ζ to Φ and perhaps Ψ). The resulting ω-equation is such that if Φ is known there is an equation, or set of equations, from which ω may be computed.

A knowledge of the vertical velocity is of both practical and theoretical interest. Thus there have been many investigations involving the solution of an ω-equation.

Several people have investigated the relationship between the large-scale vertical velocity and the "weather" (Smebye (1958), Haltiner et al.(1963), O'Neill (1966)). They all found that the distributions of cloud and precipitation were consistent with that of ω. Danard (1964, 1966) considered a problem that is closely related to this. He investigated the influence of released latent heat (which depends upon ω) on cyclone development and found that latent heat did affect the growth of cyclones.

There are many different forms of the ω-equation that may be used to compute ω. The choice of the equation is often based upon order of magnitude considerations (e.g. Stuart (1964)). Other authors have chosen an equation that is consistent with certain integral properties of the vorticity and energy equations. These were deduced by Wiin-Nielsen (1959) and Lorenz (1960) and used, for example, by O'Neill (1966). However for most diagnostic studies, these integral constraints do not have to be satisfied.

Both Stuart (1964) and Haltiner et al.(1963) have investigated the effect of excluding certain terms in the ω-equation. Stuart made the geostrophic approximation and looked at the effect on the vertical velocity excluding both the differential vertical advection of vorticity, and the differential twisting of the vortex tubes. He found that the combined effect of neglecting these two terms was small. Haltiner et al.investigated the remaining terms of the ω-equation used by Stuart. In particular, they looked at the effect of making different assumptions about the way in which the static stability varied. It was found that the form of the static stability had a marked effect upon ω. They also investigated many other facets of the ω-equation and their report contains a comprehensive discussion of the equation.

Krishnamurti (1968a) and Pedersen et al.(1969) introduced and discussed diagnostic balanced models which can be used to initialise a primitive equation model. In both models the wind was split into two parts which depend upon either a stream function or a velocity potential. The resulting ω-equation is such that a system of three or four equations must be solved simultaneously in order to compute ω. Pedersen compared his solution of ω with that derived from an equation similar to a geostrophic ω-equation. He found that there was a difference of about 30% between these solutions. Also, from Krishnamurti's results (1968b), it can be inferred that when ω is large, the corresponding difference is less than about 60%. However, when ω is small the difference can be about 1000%. These results show that a simple geostrophic ω-equation gives a reasonable description of the vertical velocity field. However the more sophisticated ω-equations can produce results that give valuable insight into the mechanics of weather systems.

It is possible to derive and solve an ω-equation that

includes terrain effects, frictional contributions at the lower boundary, sensible heat transfer from water surfaces and latent heat release. Krishnamurti (1968a) describes a way in which this may be done. His next paper (1968b) evaluates, amongst other things, the importance of these processes. He found that the terrain effect and the transfer of sensible heat are comparatively unimportant, whilst the other processes are important.

Before an ω-equation can be solved it is necessary to make several decisions.

First consider a geostrophic ω-equation. There are several forms of the static stability that may be used. The effect of these on the solution has been investigated but the literature provides no information about how the effects may be predicted for a given static stability function, or a given meteorological situation. Thus it is difficult to decide if it is valid to use an approximate form of the static stability.

Once the precise form of the static stability has been chosen, it is necessary to specify the boundary conditions for ω. The boundary conditions at the top and bottom of the atmosphere can be deduced by physical considerations. This is not so for the lateral boundaries. Usually $\omega = 0$ has been used on these boundaries and has produced reasonable results. However there is little information about the effect of using this boundary condition or the possibility of using a different type of boundary condition.

An ω-equation is usually solved by the successive over-relaxation method. This requires the specification of the over-relaxation factor and it is desirable that the optimum value be used. There are sets of equations that give this value if the equation considered has constant coefficients and Dirichlet boundary conditions. However there is little information about how to choose the optimum

value when the equation has variable coefficients (as in most ω-equations) or when Neumann boundary conditions are used.

Now consider non-geostrophic models. As well as having to decide the same things as for the geostrophic ω-equation it is necessary to choose a method of solving some form of the balance equation. There are many methods to choose from, but scant information on the choice of the best.

It can be shown that the balance equation is related to the gradient wind equation. However the usual boundary condition used for Ψ is derived from the geostrophic wind. Thus there is some doubt about the suitability of the boundary condition that is usually chosen for Ψ.

I initially intended to undertake investigations that were similar to those of Krishnamurti (1968a, 1968b). However before beginning this work I found that it was essential to investigate the problems mentioned above. This thesis is a report on the results of these investigations.

CHAPTER I

The Basic Equations

1.1 Introduction

In this section the equations of hydrodynamics are transformed from spherical coordinates to map coordinates. The equations are then put in terms of an arbitary vertical coordinate, α , and the vorticity and divergence equations are derived. The most suitable choice of α is then discussed.

The ways in which the system of equations can be approximated are investigated. It is shown that the system of equations is only solvable if the $\frac{\partial D}{\partial t}$ term in the divergence is ignored. This is the minimum approximation.

The choice of the finite difference scheme, the boundary conditions and the numerical techniques are discussed. Then, the relationship between the boundary conditions for χ and ψ_t is investigated. Finally, the data used in the case studies is described.

1.2 The Hydrodynamic Equations

The atmosphere is a fluid. Therefore, the behaviour of the atmosphere is described by the hydrodynamic equations. There are six equations which are drived from Newton's second law, the conservation of mass, the first law of thermodynamics and the equation of state of the fluid. If the presence of water vapour is included then there is a seventh equation that represents the conservation of water vapour.

For convenience, it is assumed that the atmospheric motions are adiabatic and frictionless.

The equation of motion of the atmosphere relative to the earth is

$$\frac{d\underline{U}}{dt} + 2\underline{\Omega}\times\underline{U} - \nabla_3(\tfrac{1}{2}\,\Omega^2 R^2) = -\frac{1}{\rho}\nabla_3 p - \nabla_3\phi^*$$

The vector $\underline{U}$ is the three dimensional velocity and $\underline{\Omega}$ and R are respectively the angular velocity vector and the distance from the earth's axis. The parameter Φ^* is the gravitational potential.

The continuity equation is

$$\frac{1}{\rho}\frac{d\rho}{dt} + \nabla_3 \cdot \underline{U} = 0$$

For adiabatic motions, the first law of thermodynamics becomes

$$\frac{d\vartheta}{dt} = 0 \qquad \vartheta = T\left[\frac{1000}{p}\right]^{\varkappa} \qquad \varkappa = \frac{R}{C_p}$$

The equation of state of the atmosphere is taken to be the perfect gas law

$$p = \rho RT$$

If it is assumed that the earth is a sphere with radius a, and that the thickness of the atmosphere is very much less than a, then in spherical coordinates (λ, φ, r) the equations of motion become

$$\frac{du}{dt} - \frac{uv}{a}\tan(\varphi) - fv = \frac{-1}{\rho a \cos(\varphi)}\frac{\partial p}{\partial \lambda} \tag{1.1}$$

$$\frac{dv}{dt} + \frac{u^2}{a}\tan(\varphi) + fu = \frac{-1}{\rho a}\frac{\partial p}{\partial \varphi} \tag{1.2}$$

$$\frac{dw}{dt} = \frac{-1}{\rho}\frac{\partial p}{\partial r} - \frac{\partial \Phi}{\partial r} \tag{1.3}$$

Here $\underline{U} = (u, v, w)$ and $\Phi = \Phi^* - \frac{1}{2}\left[\Omega a \cos(\varphi)\right]^2$. Also $\frac{\partial \Phi}{\partial r}$ is the apparent acceleration due to gravity (g).

For motions on the synoptic scale, it is found that the vertical accelerations are very small compared with those due to gravity and vertical pressure gradients. Thus it is assumed that the atmosphere is in hydrostatic equilibrium. Equation (1.3) then becomes

$$\frac{-1}{\rho}\frac{\partial p}{\partial r} - g = 0 \tag{1.4}$$

Since maps are used in meteorological analysis it is necessary to transform the above equations from spherical coordinates into map coordinates. In the following work a polar stereographic projection was used. With this projection, it can be shown that if the derivatives of the mapping factor $\left(m = \frac{2}{1+\sin(\varphi)}\right)$ are ignored the hydrodynamic equations become

$$\frac{d\underline{V}}{dt} + f\,\underline{k} \times \underline{V} = -\frac{1}{\rho}\nabla p \qquad (1.5)$$

$$-\frac{1}{\rho}\frac{\partial p}{\partial z} + g = 0 \qquad (1.6)$$

$$\frac{1}{\rho}\frac{d\rho}{dt} + \nabla . \underline{V} + \frac{\partial w}{\partial z} = 0 \qquad (1.7)$$

$$\frac{d\vartheta}{dt} = 0 \qquad (1.8)$$

Here the differentical operators $\frac{d}{dt}$ and ∇ are defined by

$$\frac{d}{dt} = \frac{\partial}{\partial t} + m\underline{V} . \nabla + w\frac{\partial}{\partial z}$$

$$\nabla = m\left(i\frac{\partial}{\partial x} + j\frac{\partial}{\partial y}\right)$$

The spherical nature of the atmosphere is taken into account in these equations by allowing f and m to vary with latitude.

Thompson (1961) showed that the above equations imply that the vertical velocity is

$$w = -\int_0^z \nabla . \underline{V}\, dz' + \frac{1}{\gamma}\int_0^z\int_{z'}^{\infty}\left(\frac{\partial \underline{V}}{\partial z''} . \nabla p - \frac{\partial \rho}{\partial z''}\nabla . \underline{V}\right) dz''\, dz'$$

Thus if u, v and p are known the vertical velocity can, in theory, be calculated. However, in practice u and v are not known sufficiently well.

Equations (1.5) to (1.8) are usually called the primitive equations. They can be used to make a numerical weather prediction if suitable initial conditions are chosen. The formulation of these conditions required the computation of the wind field (u, v, w) from the distribution of Φ at time t = o.

Thus the problem of initialising a primitive equation model is essentially the same as deriving the necessary fields for a diagnostic study.

The initialisation can be achieved in two ways. Firstly there are methods which involve the direct use of the primitive equations and secondly there are those methods which use equations derived from the primitive equations. Haltiner (1971) discussed these methods and concluded that the first type of method is best. However, in the following diagnostic studies the second type of method was used because of its greater flexibility.

When the second type of method is used, it is necessary to split the horizontal velocity, $\underline{V}$, into its rotational and divergent parts ($\underline{V}_1$ and $\underline{V}_2$)

$$\underline{V} = \underline{V}_1 + \underline{V}_2$$

If Ψ and X are the streamfunction and velocity potential, then

$$\underline{V}_1 = \underline{k} \times \nabla\Psi \qquad \underline{V}_2 = \nabla X$$

Therefore the vertical component of vorticity (ζ) and the divergence (D) are given by

$$\zeta = \nabla^2\Psi \qquad D = \nabla^2 X$$

The vorticity and divergence equations are derived by "multiplying" equation (1.5) by $\underline{k}.\nabla\times$ and ∇.

Until now the vertical coordinate has been z, but this is not essential. Therefore the equations can be transformed to another coordinate system (x, y, α) and α may be chosen so as to simplify the equations. Since α most vary monotonically with z, it must be a function of ρ, p or ϑ.

The form of equations (1.5) to (1.8), in (x, y, α) coordinates, will be described in the next section.

1.3.1 The Equations In (x, y, α) Coordinates

The transformation of the equations from (x, y, z) to (x, y, α) coordinates was discussed by Hinkelmann (1969). In (x, y, α) coordinates Equations (1.5) to (1.8) become

$$\frac{d\underline{V}}{dt} + f\,\underline{k}\times\underline{V} = -\frac{1}{\rho}\nabla p - \nabla\Phi \tag{1.9}$$

$$\frac{\partial\Phi}{\partial\alpha} = -\frac{1}{\rho}\frac{\partial p}{\partial\alpha} \tag{1.10}$$

$$\frac{\partial}{\partial t}\left(\frac{\partial p}{\partial\alpha}\right) + \nabla.\left(\frac{\partial p}{\partial\alpha}\underline{V}\right) + \frac{\partial}{\partial\alpha}\left(\dot{\alpha}\frac{\partial p}{\partial\alpha}\right) = 0 \tag{1.11}$$

$$\frac{\partial\vartheta}{\partial t} + \underline{V}.\nabla\vartheta + \dot{\alpha}\frac{\partial\vartheta}{\partial p} = 0 \tag{1.12}$$

The vorticity equation can then be derived from Equation (1.9). If the divergence, D, is eliminated between the vorticity and continuity equations, then the vorticity and continuity equations, then the vorticity equation becomes

$$\frac{\partial\zeta}{\partial t} + \underline{V}.\nabla\eta + \dot{\alpha}\frac{\partial\zeta}{\partial\alpha} - \eta\left[\frac{\partial}{\partial t}\left(\frac{\partial p}{\partial\alpha}\right) + \underline{V}.\nabla\frac{\partial p}{\partial\alpha} + \frac{\partial}{\partial\alpha}\left(\dot{\alpha}\frac{\partial p}{\partial\alpha}\right)\right]\Big/\frac{\partial p}{\partial\alpha}$$

$$-\underline{k}.\frac{\partial\underline{V}}{\partial\alpha}\times\nabla\dot{\alpha} - \underline{k}.\nabla p\times\nabla\left(\frac{1}{\rho}\right) = 0 \tag{1.13}$$

In this new coordinate system, the divergence and adiabatic equations are

$$\frac{\partial D}{\partial t} + \underline{V}.\nabla D + \dot{\alpha}\frac{\partial D}{\partial\alpha} + \nabla u.\frac{\partial\underline{V}}{\partial x} + \nabla v.\frac{\partial\underline{V}}{\partial y} + \nabla\dot{\alpha}.\frac{\partial\underline{V}}{\partial\alpha}$$

$$-f\,\underline{k}.\nabla\times\underline{V} + \underline{V}.\underline{k}\times\nabla f + \nabla p.\nabla\left(\frac{1}{\rho}\right) + \frac{1}{\rho}\nabla^2 p + \nabla^2\Phi = 0 \tag{1.14}$$

$$\frac{\partial T}{\partial t} + \underline{V}.\nabla T + \dot{\alpha}\frac{\partial T}{\partial\alpha} = \frac{\varkappa T}{p}\left[\frac{\partial p}{\partial t} + \underline{V}.\nabla p + \frac{\partial p}{\partial\alpha}\dot{\alpha}\right] \tag{1.15}$$

The temperature, T, is derived from the hydrostatic equation and the equation of state, and therefore

$$T = -\frac{p}{R}\frac{\frac{\partial\Phi}{\partial\alpha}}{\frac{\partial p}{\partial\alpha}}$$

Equations (1.13) to (1.15) can be written schematically as

$$\frac{\partial D}{\partial t} = F_1(u, v, \dot{\alpha}, p, \rho, \Phi, \zeta, D)$$

$$\frac{\partial \zeta}{\partial t} = F_2(u, v, \dot{\alpha}, p, \rho, \frac{\partial p}{\partial t}, \zeta)$$

$$\frac{\partial T}{\partial t} = F_3(u, v, \dot{\alpha}, p, \frac{\partial p}{\partial t}, T)$$

Also the diagnostic equations, namely the hydrostatic equation and the gas law, become

$$F_5(p, T, \Phi) = 0$$

$$F_6(p, T, \rho) = 0$$

Finally, the continuity equation is

$$\frac{\partial}{\partial t}\frac{\partial p}{\partial \alpha} = F_4(u, v, \dot{\alpha}, p)$$

If the functions Ψ and X are introduced and if the equations $F_5 = 0$ and $F_6 = 0$ are used, then these equations become

$$\begin{aligned} \nabla^2\frac{\partial X}{\partial t} &= F_1(\Psi, X, \dot{\alpha}, p, \Phi) \\ \nabla^2\frac{\partial \Psi}{\partial t} &= F_2(\Psi, X, \dot{\alpha}, p, \Phi, \frac{\partial p}{\partial t}) \\ \frac{\partial}{\partial p}\frac{\partial \Phi}{\partial t} &= F_3(\Psi, X, \dot{\alpha}, p, \Phi, \frac{\partial p}{\partial t}) \\ \frac{\partial}{\partial t}\frac{\partial p}{\partial \alpha} &= F_4(\Psi, X, \dot{\alpha}, p) \end{aligned} \qquad (1.16)$$

If the distribution of p, Φ or ϑ is known as a function of α, then Equation (1.16) represent four equations in seven unknowns ($\frac{\partial \Psi}{\partial t}$, $\frac{\partial X}{\partial t}$, $\frac{\partial \Phi}{\partial t}$, Ψ, X, α and $\frac{\partial p}{\partial t}$). The large number of unknowns is the result of the need to compute the horizontal velocity components (and hence Ψ and X) from the single variable describing the state of the atmosphere.

It is now necessary to choose α so that the above set of equations are comparatively easy to solve.

1.3.2 The Choice Of α

If $\alpha = p$ then $\frac{\partial p}{\partial t} = 0$ and therefore there are only six unknowns in Equation (1.16). If $\dot{\alpha} = \omega$, these equations become

$$\begin{aligned} \nabla^2 \frac{\partial \chi}{\partial t} &= G_1(\psi, \chi, \omega, \phi) \\ \nabla^2 \frac{\partial \psi}{\partial t} &= G_2(\psi, \chi, \omega) \\ \frac{\partial}{\partial p}\frac{\partial \phi}{\partial t} &= G_3(\psi, \chi, \omega, \phi) \\ 0 &= G_4(\chi, \omega) \end{aligned} \tag{1.17}$$

The choice of $\alpha = p$ has the important effect of turning the continuity equation into a diagnostic equation.

For adiabatic motion, the choice of $\alpha = \vartheta$ has the effect of eliminating one of the unknowns since $\dot{\alpha} = \dot{\vartheta} = 0$. But atmospheric motions are not adiabatic and when this is taken into consideration the advantage of ϑ coordinates disappears.

When $\alpha = z$ and $\dot{\alpha} = w$, the equations become

$$\begin{aligned} \nabla^2 \frac{\partial \chi}{\partial t} &= H_1(\psi, \chi, w, p) \\ \nabla^2 \frac{\partial \psi}{\partial t} &= H_2(\psi, \chi, w, p, \frac{\partial p}{\partial t}) \\ g \frac{\partial}{\partial t}\left(\frac{1}{\frac{\partial p}{\partial z}}\right) &= H_3(\psi, \chi, w, p, \frac{\partial p}{\partial t}) \\ \frac{\partial}{\partial t}\frac{\partial p}{\partial z} &= H_4(\psi, \chi, w, p) \end{aligned} \tag{1.18}$$

A comparison of Equations (1.17) and (1.18) shows that the equations in p coordinates are far simpler than those in z coordinates. The reasons for this are that, for the z coordinates, the continuity equation is predictive and the forcing function of the thermal equation contains a time derivative $\frac{\partial p}{\partial t}$.

A further advantage of the pressure coordinate system is manifested if only the largest terms in the equations are considered.

p coord.		z coord.	
$0 = G_1'(\Psi,\phi)$	(p1)	$0 = H_1'(\Psi,p)$	(z1)
$\nabla^2\frac{\partial\Psi}{\partial t} = G_2'(\Psi,\omega)$	(p2)	$\nabla^2\frac{\partial\Psi}{\partial t} = H_2'(\Psi,w)$	(z2)
$\frac{\partial}{\partial p}\frac{\partial\phi}{\partial t} = G_3'(\Psi,\dot{\omega},\phi)$	(p3)	$g\frac{\partial}{\partial t}\left(\frac{1}{\frac{\partial p}{\partial z}}\right) = H_3'(\Psi,w,p,\frac{\partial p}{\partial t})$	(z3)

For both sets of coordinates, the first equation can be used to eliminate the time derivatives on the left-hand side of the other two equations. The resulting equations are

$0 = G'(\omega,\Psi,\phi)$	(p4)	$0 = H'(w,\Psi,p,\frac{\partial p}{\partial t})$	(z4)

Therefore, for the p system, once Ψ has been found using Equation (p1), Equation (p4) can be solved for ω. Equation (p4) is usually known as the ω-equation. For the z system, a knowledge of Ψ and p is not sufficient to solve Equation (z4) for w.

If the term depending upon $\frac{\partial p}{\partial t}$ is ignored in the forcing function of Equation (z3), then the resulting w-equation is very similar to the ω-equation. Houghton et al. (1971) used this to compute w and found that it gave a reasonable pattern of vertical velocity. However, they made no attempt to estimate the effect of neglecting the $\frac{\partial p}{\partial t}$ term. In general, it is unwise to ignore a large term in an equation.

When $\alpha = \rho$ or $\alpha = p/ps$ (where ps is the surface pressure) is used in Equation (1.16), the equations become very complicated. Therefore it was decided that these forms of α were not suitable for a diagnostic study.

In the following work, the pressure is taken as the vertical coordinate because of the simple form of the equations.

However it is realised that the choice of coordinate system must be determined by the initial data and the ultimate objective of the analysis.

1.4 The Equations In Pressure Coordinates

In pressure coordinates, Equations (1.13), (1.14), (1.15) and (1.11) become

$$\frac{\partial D}{\partial t} + \underline{V}.\nabla D + \omega\frac{\partial D}{\partial p} + D^2 - 2J(u,v) + \frac{\partial \underline{V}}{\partial p}.\nabla\omega - f\zeta + \underline{k}\times\underline{V}.\nabla f + \nabla^2\phi = 0 \quad (1.19)$$

$$\frac{\partial \zeta}{\partial t} + \underline{V}.\nabla\eta + \omega\frac{\partial \zeta}{\partial p} + \underline{k}.\nabla\omega\times\frac{\partial \underline{V}}{\partial p} - \eta\frac{\partial \omega}{\partial p} = 0 \quad (1.20)$$

$$\frac{\partial}{\partial p}\left(\frac{\partial \phi}{\partial t}\right) + \underline{V}.\nabla\frac{\partial \phi}{\partial p} + \sigma\omega = 0 \quad (1.21)$$

$$\nabla^2\chi + \frac{\partial \omega}{\partial p} = 0 \quad (1.22)$$

The static stability , σ , in Equation (1.21) is given by

$$\sigma = \frac{R}{p}\left(\varkappa\frac{T}{p} - \frac{\partial T}{\partial p}\right)$$

Some important integral relations can be derived from the above equations. If these equations are approximated then, in certain circumstances, it is essential that the approximate equations satisfy the same integral relations as the full equations. The integral relations have been discussed at some length by Haltiner (1971) and the important points of his analysis will be described below.

If $K = \frac{1}{2}\,\underline{V}.\,\underline{V}$ and if E is the total potential energy, the energy equation derived from Equations (1.19), (1.20) and (1.22) is

$$\frac{\partial}{\partial t}\int (K + E)\, dM = 0$$

Here M is the mass of the atmosphere. The following sets of equations satisfy an integral relation similar to the one

above

(i) the full vorticity equation (Equation (1.20)) and the divergence equation minus the term $\frac{\partial D}{\partial t}$ (see Equation (1.19)).

(ii) $$\frac{\partial \zeta}{\partial t} + \underline{V}.\nabla\eta + \omega\frac{\partial \zeta}{\partial p} + \underline{k}.\nabla\omega\times\frac{\partial \underline{V}_1}{\partial p} - \eta\frac{\partial \omega}{\partial p} = 0$$
$$f\nabla^2\psi + 2(\psi_{xx}\psi_{yy} - \psi_{xy}^2) + \nabla f.\nabla\psi - \nabla^2\phi = 0$$

These equations, with Equation (1.21) are often called the balanced system

(iii) $$\frac{\partial \zeta}{\partial t} + \underline{V}_1.\nabla\eta + \underline{V}_2.\nabla f - f\frac{\partial \omega}{\partial p} = 0$$
$$f\nabla^2\psi + \nabla f.\nabla\psi - \nabla^2\phi = 0$$

These are often called the linear balanced system

(iv) the quasi-geostrophic system

$$\frac{\partial \zeta}{\partial t} + \underline{V}_1.\nabla\eta - \bar{f}\frac{\partial \omega}{\partial p} = 0$$
$$\bar{f}\nabla^2\psi - \nabla^2\phi = 0$$

With this set of equations the term $\underline{V}_2.\nabla\frac{\partial \phi}{\partial p}$ should be omitted from Equation (1.21) and σ must be treated as a function of pressure only.

From Equation (1.20) it can be shown that the generation of vorticity over a complete isobaric surface is zero. The approximate forms of Equation (1.20) which have this property correspond to those described in (i) to (iv).

The relative importance of each term in an equation can be investigated by using scale analysis. A comprehensive discussion of scale analysis has been given by Haltiner (1971). However, a less rigorous method gives the same results as Haltiner's analysis (see Gambo (1957)). Gambo's method of analysis was used in the following work.

Let L and U be the characteristic horizontal and velocity scales of the synoptic scale motions in the atmosphere. If

f_o is the characteristic Coriolis parameter, then the Rossby number, R, is defined by

$$R = \frac{U}{f_o L}$$

For synoptic scale motions in mid-latitudes $R \approx \frac{1}{10}$.

Following Gambo, it can be assumed that

$$\frac{|\underline{V}_2|}{|\underline{V}_1|} \approx R \qquad \frac{\Phi}{f_o U L} \approx 1$$

Here Φ is the characteristic geopotential scale. The second expression represents the condition for geostrophic equilibrium.

In non-dimensional variables, Equations (1.19) to (1.21) become

$$R^3\left[\omega\frac{\partial D}{\partial p} + D^2 + \underline{V}_2.\nabla D + \frac{\partial \underline{V}_2}{\partial p}.\nabla\omega - 2J(u_2,v_2)\right]$$
$$+R^2\left[\frac{\partial D}{\partial t} + \underline{V}_1.\nabla D + \frac{\partial \underline{V}_1}{\partial p}.\nabla\omega + \underline{k}\times\underline{V}_2.\nabla f - 2J(u_1,v_2) - 2J(u_2,v_1)\right]$$
$$+R\left[\underline{k}\times\underline{V}_1.\nabla f - 2J(u_1,v_1)\right] + \left[-f\zeta + \nabla^2\phi\right] = 0 \qquad (1.23)$$

$$R^2\left[\underline{k}.\nabla\omega\times\frac{\partial \underline{V}_2}{\partial p}\right] + R\left[\omega\frac{\partial \zeta}{\partial p} + \underline{V}_2.\nabla\eta - \zeta\frac{\partial\omega}{\partial p} + \underline{k}.\nabla\omega\times\frac{\partial \underline{V}_1}{\partial p}\right]$$
$$+\left[\frac{\partial\zeta}{\partial t} + \underline{V}_1.\nabla\eta - f\frac{\partial\omega}{\partial p}\right] = 0 \qquad (1.24)$$

$$R\left[\underline{V}_2.\nabla\frac{\partial\phi}{\partial p}\right] + \left[\frac{\partial}{\partial p}\left(\frac{\partial\phi}{\partial t}\right) + \underline{V}_1.\nabla\frac{\partial\phi}{\partial p} + \sigma\omega\right] = 0 \qquad (1.25)$$

If only the largest terms are considered (those of order R^o), the equations become

$$-f\zeta + \nabla^2\phi = 0 \qquad (1.26)$$

$$\frac{\partial\zeta}{\partial t} + \underline{V}_1.\nabla\eta - f\frac{\partial\omega}{\partial p} = 0 \qquad (1.27)$$

$$\frac{\partial}{\partial p}\left(\frac{\partial\phi}{\partial t}\right) + \underline{V}_1.\nabla\eta + \sigma\omega = 0 \qquad (1.28)$$

$$\underline{V}_1 = \underline{k}\times\nabla\Psi \qquad \zeta = \nabla^2\Psi$$

From Equation (1.26) it can be shown that

$$\underline{V}_1 \approx \underline{V}_g = \frac{1}{f}\underline{k}\times\nabla\Phi$$

Here $\underline{V}_g$ is the geostrophic wind. Thus Equation (1.26) to (1.28) define what is essentially a geostrophic system.

If VE, DE and TE represent the vorticity equation, the divergence equation and the thermal equation, then the ω-equation is defined as the equation derived from (see Pedersen et al.(1969)).

$$\nabla^2(TE) - f\frac{\partial(VE)}{\partial p} - \frac{\partial}{\partial t}\frac{\partial(DE)}{\partial p} = 0 \qquad (1.29)$$

When Equations (1.26) to (1.28) are used for DE, VE and TE Equation (1.29) gives

$$\nabla^2(\sigma\omega) + f^2\frac{\partial^2\omega}{\partial p^2} = f\frac{\partial(\underline{V}_1.\nabla\eta)}{\partial p} - \nabla^2(\underline{V}_1.\nabla\frac{\partial\phi}{\partial p}) \qquad (1.30)$$

Equations (1.23) to (1.25) were reduced to Equations (1.26) to (1.28) by using scale analysis. Therefore the ω-equation should be derived in a consistent manner. Thus Equations (1.23) to (1.25) should be used in Equation (1.29) and a scale analysis performed on the resulting equation. If only terms of order R^o are considered, then the resulting equation is Equation (1.30).

If $\underline{V}_g$ is used in place of $\underline{V}_1$, Equation (1.30) becomes the geostrophic ω-equation. The distributions of calculated from Equation (1.30) using $\underline{V}_1$ and $\underline{V}_g$ are almost the same. But, the use of $\underline{V}_g$ has several advantages that will become obvious when the solution of this system of equations is discussed.

Nearly all diagnostic studies have used Equation (1.30) (or a similar equation) with either $\underline{V}_1$ or $\underline{V}_g$. But this may not be suitable if the results are to be used to investigate energy or vorticity budgets. This is because Equations (1.26) to (1.28) do not satisfy the integral constraints described earlier. However, the following work is not

concerned with these budgets and therefore the ω-equation was used in its unaltered form.

The distribution of Φ is known and since there are four unknowns Φ_t^*, Ψ_t, ω and Ψ four sets of boundary conditions must be specified. Equations (1.26) to (1.30) can then be solved. Initially, Ψ is computed from Equation (1.26) and ω is calculated from the ω-equation. Then either Ψ_t or Φ_t or both can be calculated from Equation (.127) with

$$f\nabla^2\Psi_t - \nabla^2\Phi_t = 0$$

If the geostrophic approximation is used, there are only two unknowns ω and Φ_t and thus only two sets of boundary conditions are required. The reduction of the number of unknowns to two greatly simplifies the procedure for solving the system of equations.

When the geostrophic approximation is used, the wind field is derived from Φ and thus it is not necessary to solve Equation (1.26) for Ψ. Once Equation (1.30) has been solved for ω, Φ_t is computed from

$$\nabla^2\Phi_t + f\,\underline{V}_g\cdot\nabla\eta - f^2\frac{\partial\omega}{\partial p} = 0$$

It is suspected that the errors introduced by using $\underline{V}_g$ instead of $\underline{V}_1$ will be less than the errors produced by having to specify a large number of boundary conditions that are neither accurate nor consistent with one another.

Using Equations (1.23) to (1.25) higher-order equations can be derived and these lead to higher-order ω-equations. These higher-order equations are considered in the next section.

*Henceforth any dependent variable that involves a time derivative (e.g. $\frac{\partial\Phi}{\partial t}$) will be written with t as a subscript (e.g. Φ_t).

1.5 Non-Geostrophic Models

Consider the complete set of hydrodynamic equations shown schemmatically by Equation (1.17) and in detail by Equations (1.23) to (1.25).

Equation (1.23) clearly shows that the divergence equation should not be used to calculate $\frac{\partial D}{\partial t}$ (or χ_t), but that it can be used to compute Ψ. Thus the divergence equation should be written as

$$\nabla^2 \Psi = \tilde{G}_1^+(\Psi, \chi, \omega, \Phi, \chi_t) \tag{1.31}$$

Due to the form of the hydrodynamic equations, Φ_t can always be eliminated by using Equation (1.29). The resulting ω-equation has the form

$$\nabla^2(\sigma\omega) + f^2 \frac{\partial^2 \omega}{\partial p^2} = G(\Psi, \chi, \omega, \Phi, \Psi_t, \chi_t, \chi_{tt}) \tag{1.32}$$

Once ω is known, the continuity equation is solved for χ and thus the continuity equation will be written as

$$\nabla^2 \chi = G_4^+(\omega) \tag{1.33}$$

Equations (1.31), (1.32), (1.33) and the vorticity equation form a set of four partial differential equations which can be solved as boundary value problems. Unfortunately there are still six unknowns $\Psi, \chi, \omega, \Psi_t, \chi_t, \chi_{tt}$ and only four equations. The derivation of more equations by differentiating some of the equations with respect to time does nothing to alleviate this problem. Thus, to solve the above set of equations, some approximations or assumptions have to be made.

If $\frac{\partial D}{\partial t}$ is ignored in the divergence equation and if the vorticity equation is used in full, the system of equations becomes that described in (i) of section 1.4. These two equations conserve energy and also produce a zero generation

of vorticity. Hence if these equations could be solved for Ψ, Ψ_t and ω these fields would satisfy the energy relation

$$\int (\underline{k} \times \nabla \Psi_t) \cdot (\underline{k} \times \nabla \Psi) \, dM = - \int \omega \alpha \, dM \qquad (1.34)$$

When $\frac{\partial D}{\partial t}$ is ignored Equation (1.31) will not contain X_t but it will still be contained in Equation (1.32). Thus this approximation is not sufficient to produce a solvable set of equations.

If it is assumed that $\frac{\partial D}{\partial t} = \frac{\partial^2 D}{\partial t^2} = 0$ then neither the divergence equation nor ω-equation will contain X_t and hence it is possible to solve the resulting set of equations. Pedersen et al.(1969) used this set of equations and the iteration proceedure is shown schematically in Fig. 1.1.

Due to the fact that these assumptions alter the ω-equation as well as the divergence equation, the computed fields of Ψ, Ψ_t and ω will not satisfy Equation (1.34).

Pedersen et al. justified their assumptions on the grounds that they led to a divergence equation that would give a balanced wind. But the main advantage in using a balanced wind is that gravity waves may be eliminated. However, Thompson (1961) showed that gravity waves can only be eliminated if $\frac{dD}{dt} = 0$. Thus the wind used by Pedersen will not be free of gravity waves.

An examination of Equation (1.23) shows that Pedersen's assumptions cannot be justified by scale considerations because terms of both equal and smaller magnitude are included.

The above discussion shows that the equations used by Pedersen do not conserve energy or eliminate gravity waves. Also the equations cannot be derived by scale analysis. Thus, it is suspected that his assumptions were based on

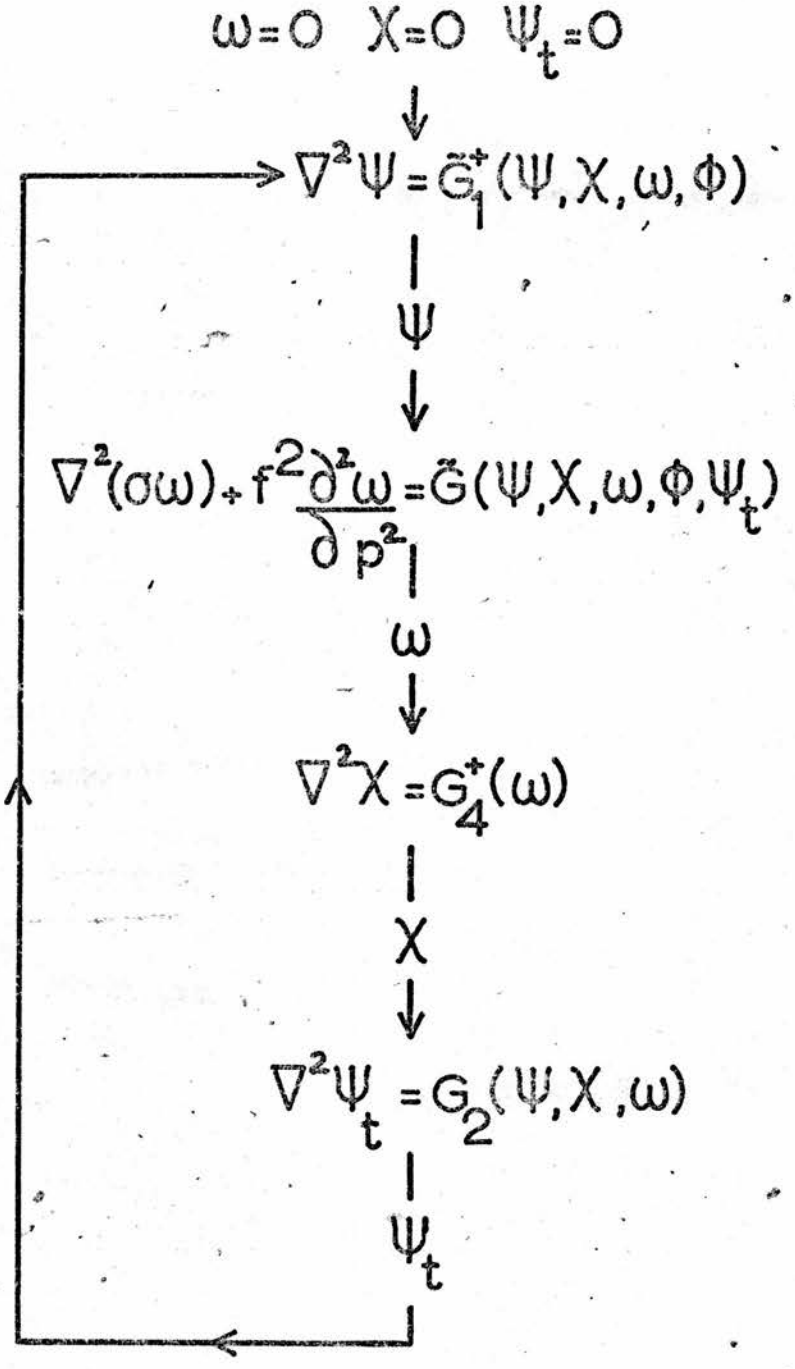

FIGURE 1.1

Pedersen et al. (1969)

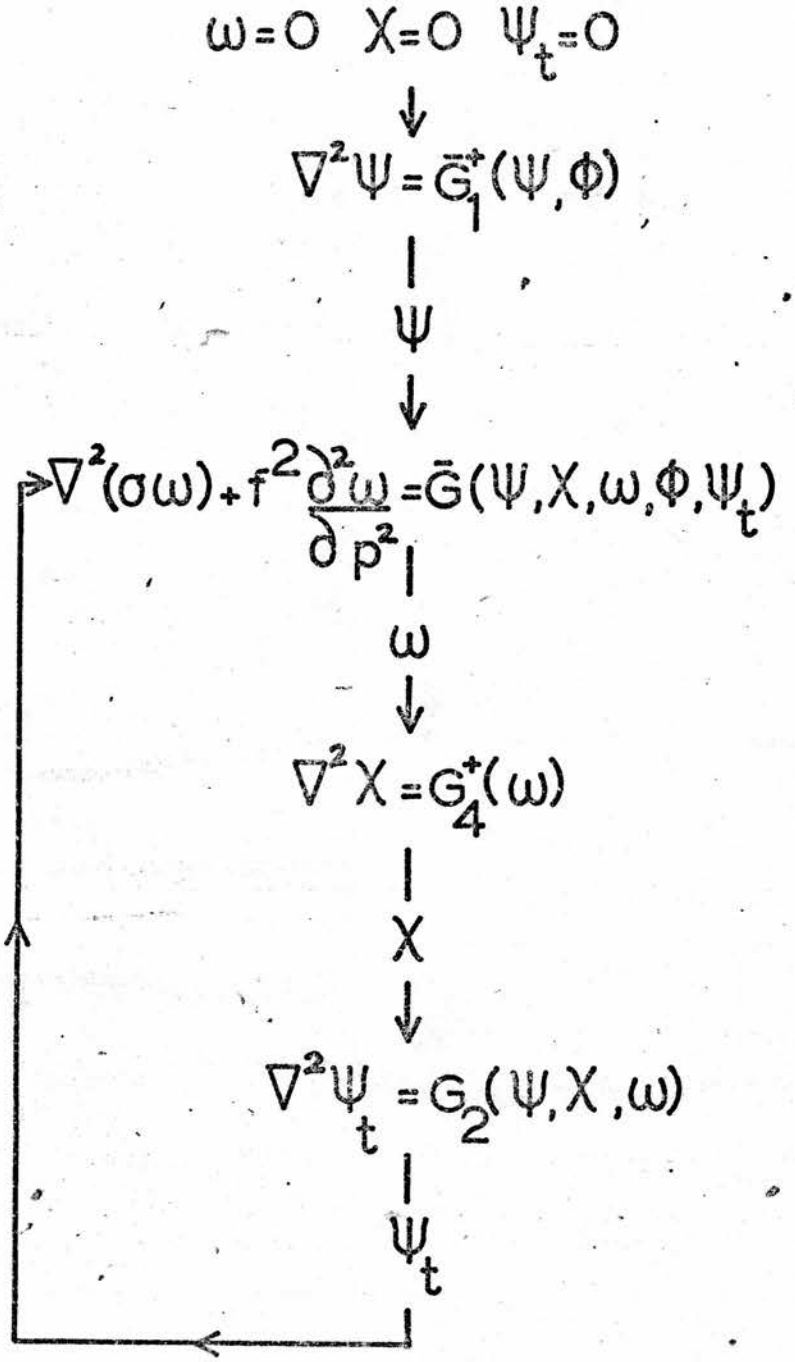

FIGURE 1.2

Krishnamurti (1968)

computational necessity.

Krishnamurti (1968) used the system of equations described in (ii) of section 1.4. These equations conserve energy and produce a zero generation of vorticity. Also, since no approximations are made to the ω-equation, the computed fields of Ψ, Ψ_t and ω should satisfy Equation (1.34). Further, Equations (1.23), (1.24) and (1.25) show that Krishnamurti's equations can be derived from the divergence, vorticity and thermal equations by only including terms of order R^o and R^1.

This system of equations is solvable because χ_t does not appear in either the divergence equation or ω-equation. The iteration scheme used to solve this system of equations is shown in Fig. 1.2.

The above discussion shows that Krishnamurti's choice of equations can be justified and that the system of equations can be solved. Also, a comparison of Figs. 1.1 and 1.2 shows that in Krishnamurti's scheme the divergence equation (in this case the balance equation) has to be solved only once, whereas Pedersen had to solve his form of the divergence equation for every iteration.

Once the system of equations has been chosen there are many other problems that have to be overcome.

1.6 The Solution Of A System of Equations

Before a system of equations can be solved it is necessary to consider the following problems.

(i) the ellipticity of the equations

(ii) the choice of a finite difference scheme

(iii) the type and nature of the boundary conditions

(iv) the choice of a numerical technique for solving the equations.

Each equation, in a system of equations, can only be solved as a boundary value problem if it is elliptic.

An equation is elliptic if, and only if, it can be transformed into an equation of the form

$$\frac{\partial^2 \Psi}{\partial x_1^2} + \frac{\partial^2 \Psi}{\partial x_2^2} + \cdots\cdots + \frac{\partial^2 \Psi}{\partial x_n^2} = 0 \qquad (1.35)$$

For a two dimensional equation

$$F (\Psi_{xx}, \Psi_{yy}, \Psi_{xy}, \Psi_x, \Psi_y, \Psi, x, y) = 0$$

this is possible if

$$4 F_r . F_t - F_s^2 > 0 \qquad (1.36)$$

Here, $r = \Psi_{xx}$, $t = \Psi_{yy}$ and $s = \Psi_{xy}$ and also $F_r = \frac{\partial F}{\partial r}$ etc. (see Arnason (1958)).

Both the vorticity and continuity equations are used in the form of a Poisson equation

$$\nabla^2 X = G$$

For the former equation $X = \Psi$ and for the latter $X = \chi$ Equation (1.36) clearly shows that these equations are always elliptic with respect to Ψ and χ respectively.

The divergence equation is usually used in the form

$$f \nabla^2 \Psi + 2(\Psi_{xx} \Psi_{yy} - \Psi_{xy}^2) + \nabla f . \nabla \Psi = G'$$

This is a non-linear equation and thus the elliptic condition derived from Equation (1.36) is a function of Ψ. Hence it is not possible to make a general statement on when this equation is elliptic. This problem will be pursued further in section 3.31.

All ω-equations are similar to Equation (1.32). It is not easy to transform this into the form of Equation (1.35), but some insight into the elliptic criterion can be gained by considering a related problem. If $\sigma = \sigma(\rho)$, then it is easy to show that the ω-equation is elliptic if

$\sigma(p) > 0$. It is suspected that the elliptic criterion for the complete equation is approximately $\sigma > 0$.

If an equation is solved numerically, then the elliptic criterion is very closely linked to the condition under which the numerical scheme will converge. Thus the elliptic criterion is only significant when it is discussed in terms of the finite difference scheme and the iteration scheme. This aspect of the elliptic criterion will be discussed later.

Although the meteorological fields may be arranged so that each equation in the system yields a convergent solution, there is no guarantee that the complete system will produce convergent solutions. However, the experience of others is that the solutions do converge.

When a diagnostic study is undertaken, it is necessary to specify boundary conditions for some or all of Ψ, ω, X, Φ_t and Ψ_t .

The boundary condition for Ψ is usually derived by assuming that the wind perpendicular to the boundary is geostrophic. The appropriate boundary conditions for will be discussed in sections 3.6.1 and 3.6.3.

When the ω-equation is solved it is usual to set $\omega = 0$ on all the boundaries. This is a realistic assumption on the upper and lower boundaries but not on the lateral boundaries. An alternative condition on the lateral boundary is $\frac{\partial \omega}{\partial n} = 0$. The relative merits of the boundary conditions will be discussed at length in Chapter IV.

It is usually assumed that X , Ψ_t and Φ_t are zero on the lateral boundaries. Therefore, these boundary conditions are independent of the meteorological situation.

It can be shown that some of these boundary conditions

are not consistent with one another. For instance, the use of $\phi_t = 0$ and $\omega = 0$ implies that on the boundary

$$J(\Psi, \frac{\partial \phi}{\partial p}) + \nabla X . \nabla \frac{\partial \phi}{\partial p} = 0$$

There is no reason why this should be so. This inconsistency is also illustrated by the fact that if Equations (1.31) to (1.33) are used to find ϕ_t, X and ω with $\phi_t = X = \omega = 0$ on the boundary, then the solutions will not satisfy the thermal equation

$$\frac{\partial \phi}{\partial p^t} + J(\Psi, \frac{\partial \phi}{\partial p}) + \nabla X . \nabla \frac{\partial \phi}{\partial p} + \sigma \omega = 0$$

It can be shown that the use of $\omega = 0$ and $X = 0$ on the boundary is not inconsistent. This is also true for $\phi = 0$ and $\Psi_t = 0$. It is shown above that the boundary conditions $\omega = 0$ and $\phi_t = 0$ are inconsistent. Therefore the boundary conditions $X = 0$ and $\Psi_t = 0$ are also inconsistent.

In the next section a method will be described by which, in theory, consistent boundary conditions for X and Ψ_t may be derived.

Some form of overrelaxation was used to solve all partial differential equations. Chapter II consists of a discussion of the methods that are used to solve linear equations and a particular non-linear equation is considered in Chapter III.

1.7 Consistent Boundary Conditions For X And Ψ_t

If a Gambo (1957) type analysis is carried out on Equation (1.9) (in p coordinates), then the equation becomes in non-dimensional form

$$R^3 \left[\underline{V}_2 . \nabla \underline{V}_2 + \omega \frac{\partial \underline{V}_2}{\partial p} \right] + R^2 \left[\frac{\partial \underline{V}_2}{\partial t} + \underline{V}_1 . \nabla \underline{V}_2 + \underline{V}_2 . \nabla \underline{V}_1 + \omega \frac{\partial \underline{V}_1}{\partial p} \right]$$

$$+ R \left[\frac{\partial \underline{V}_1}{\partial t} + \underline{V}_1 . \nabla \underline{V}_1 + f \underline{k} \times \underline{V}_2 \right] + \left[f \underline{k} \times \underline{V}_1 + \nabla \Phi \right] = 0$$

If only terms of order R^0 and R^1 are considered and if Ψ and X are introduced, then,

$$\frac{\partial \Psi}{\partial x_t} + f\frac{\partial X}{\partial x} = \frac{\partial \Psi}{\partial y}\frac{\partial^2 \Psi}{\partial x^2} - \frac{\partial \Psi}{\partial x}\frac{\partial^2 \Psi}{\partial x \partial y} + f\frac{\partial \Psi}{\partial y} - \frac{\partial \phi}{\partial y} \qquad (1.38)$$

$$\frac{\partial \Psi}{\partial y_t} + f\frac{\partial X}{\partial y} = \frac{\partial \Psi}{\partial y}\frac{\partial^2 \Psi}{\partial x \partial y} - \frac{\partial \Psi}{\partial x}\frac{\partial^2 \Psi}{\partial y^2} - f\frac{\partial \Psi}{\partial x} + \frac{\partial \phi}{\partial x}$$

These equations show that the gradients of X and Ψ_t along the boundary cannot both be zero. Thus using $X=\Psi_t=0$ on the boundary produces an inconsistency.

If X, Ψ and Φ are known around the boundary then the gradient of Ψ_t along the boundary may be found. If s is the coordinate around the boundary then

$$\frac{\partial \Psi}{\partial s_t} = F(\Psi, \Phi, X)$$

Therefore, if Δ represents the difference between two grid-points on the boundary, this equation becomes

$$\Delta \Psi_t = \frac{F\,d}{m} = F^*$$

Clearly the sum around the boundary of F^*, $\sum F^*$ say, should be zero. This not so when real data is used and therefore the above equation must be replaced by

$$\Delta \Psi_t = F^* - \frac{\delta\, d}{m} \qquad \delta = \frac{\sum F^*}{\sum \frac{d}{m}}$$

This process ensures that $\sum \Delta \Psi_t = 0$.

If X is not known on the boundary, then Equation (1.38) may be written as

$$\Delta \Psi_t + f\,\Delta X = G(\Psi, \Phi)$$

It can be shown that if $\sum \Delta \Psi_t = 0$ and $\sum \Delta X = 0$ the solution of this equation for $\Delta \Psi_t$ and ΔX are unique. Unfortunately the author was unable to find these unique solutions.

1.8.1 The Grids And The Finite Differences

The computations were carried out on the same grid as that used for the 10- level model (Benwell et al.(1971)). This consisted of a square grid, of gridlength d = 108.844545 km, on a polar stereographic map. The mapping factor, m, was given by $m = 2/(1 + \sin\varphi)$ where φ is the latitude.

Three different regions were used and these will be referred to as areas 11, 51 and 91. They are illustrated in Fig. 1.3. The dimensions of the areas are 23d by 31d, 15d by 23d and 15d by 11d. In all figures showing the distribution of a field on an isobaric surface, one gridlength corresponds to 0.7 cm.

Unless stated otherwise, the finite differences were derived from Stirling's Interpolation Formula

$$y(x_o + qd) = y_o + \binom{q}{1}\mu\delta y_o + \frac{q}{2}\binom{q}{1}\delta^2 y_o + \ldots\ldots \qquad y_o = y(x_o)$$

The operators μ and δ are defined by

$$\delta f(x) = f(x + \tfrac{d}{2}) - f(x - \tfrac{d}{2})$$

$$\mu f(x) = \left[f(x + \tfrac{d}{2}) + f(x - \tfrac{d}{2})\right]/2$$

The finite differences calculated in this way are often called centred finite differences. Those used had a truncation error of order d^2.

Suppose that primed operators refer to the earth, whilst unprimed operators refer to the map. By the definition of m

$$\frac{\partial' f}{\partial x} = m\frac{\partial f}{\partial x}$$

It can then be shown that

$$\nabla'^2 f = m^2\nabla^2 f + m\nabla m.\nabla f$$

However the gradient of m is very small and thus the following expression was used

$$\nabla'^2 f = m^2\nabla^2 f$$

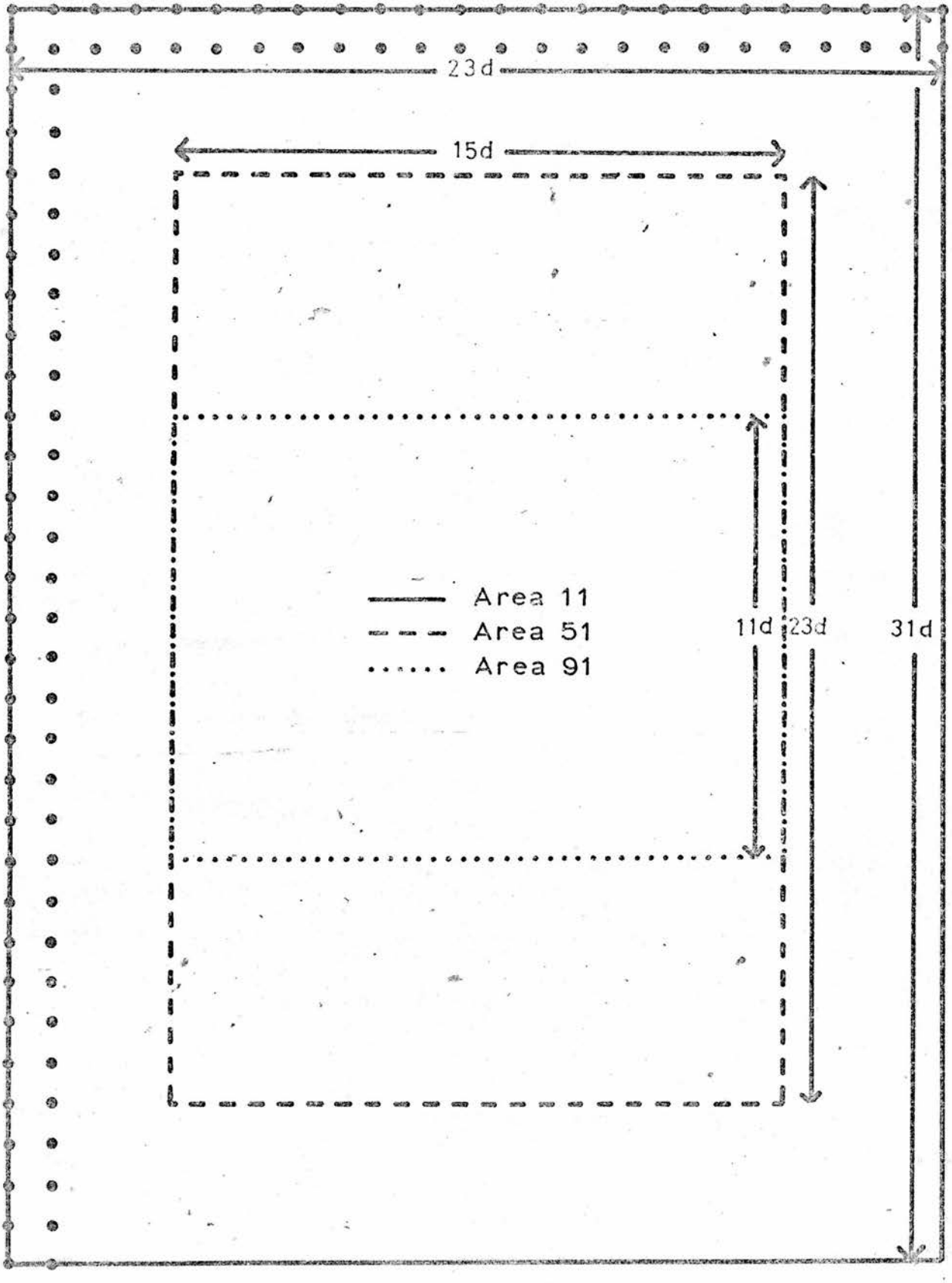

FIGURE 1.3

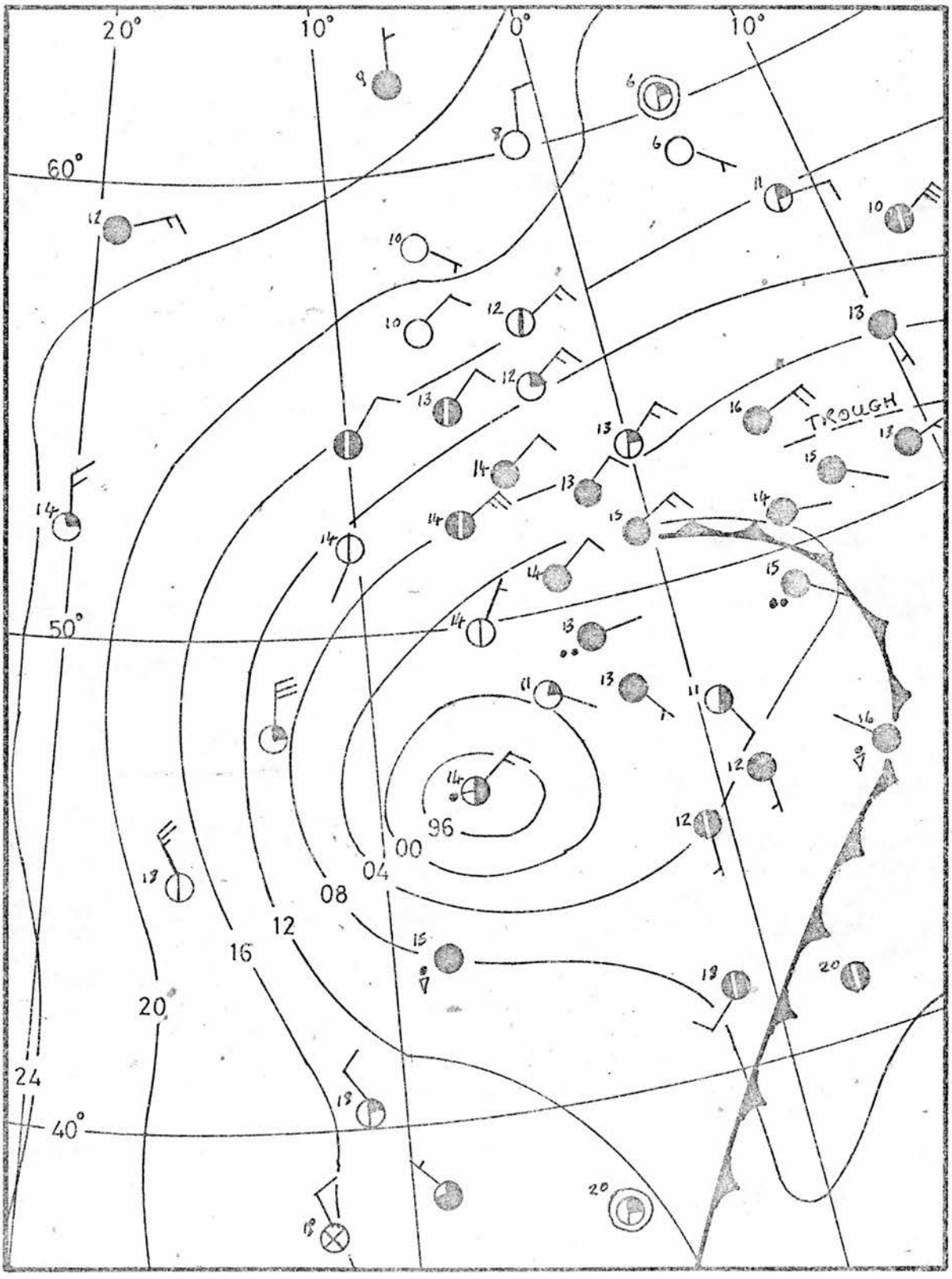

0000 GMT 15.9.68

FIGURE 1.4

It is the unprimed quantities that are put in terms of finite differences.

The next section contains a description of both the meteorological situation and the basic data used in this thesis.

1.8.2 The Data

This thesis is mainly concerned with the equations for Ψ , ω and Φ_t and the methods of their solution, rather than with the significance of the solutions. Therefore the actual meteorological situation considered is of little importance. However for completeness the surface chart for area 11 is exhibited in Fig. 1.4.

All computations were carried out with data for 0000GMT 15.9.68. This was chosen because analysed data, which had been used to test the 10 level model (Benwell et al.(1971)), was available. The actual data consisted of height fields which had been vertically smoothed, convectively adjusted and then horizontally smoothed. The fields for nine isobaric surfaces between 1000mb and 200mb, separated by 100mb, were used. The heights were used only to the nearest meter because the line printer output, from which they were copied, gave the heights to the nearest meter.

C H A P T E R II

The Overrelaxation Method And The Determination Of The Optimum Overrelaxation Factor

2.1 Introduction

This chapter is concerned with the successive overrelaxation method (hereafter called SOR), and the symmetric successive overrelaxation method (SSOR) of solving elliptic partial differential equations. The Helmholtz, Poisson and omega equations are considered, and both Dirichlet and Neumann boundary conditions are used.

Special emphasis is placed on the determination of the optimum overrelaxation factor.

A list of the experiments carried out is shown in Table 2.1.

2.2.1 Methods of Solving Linear Elliptic Equations

Consider the linear, elliptic partial differential equation given by

$$\Gamma x = f \qquad (2.1)$$

Γ is a continuous partial differential operator, x is the dependent variable and f is the forcing function which is independent of x. An analytic solution of this equation cannot usually be found, and thus a numerical technique must be used. For all numerical methods the partial derivatives are replaced by finite differences, so that Equation (2.1) becomes a matrix equation

$$A X = B \qquad (2.2)$$

Here, X and B are matrices of x and f, and A is a matrix depending upon the form of Γ and the boundary conditions.

The two types of method that may be used to solve

The code used in Table 2.1 is as follows

Equ.	- Type of equation	H	- Helmholtz equ.
		P	- Poisson equ.
		W	- ω.- equ.
B.C.	- Type of boundary condition	1	- Dirichlet
		2	- Neumann .
Method	- Method of solution	SOR	-
		SSOR	-
Data	- Type of data	R	- Real
		A	- Artificial
Fig.	- Figures showing $n(E)/\beta$ or $n(E)/\alpha$ curves		

Case	Equ.	B.C.	Method	Data	Fig.	Comments
1a	H	1	SOR	R	2.1) 2.2)	
1b	H	1	SOR	R	2.2	similar to 1a but with a different initial guess.
2a	H	1	SOR	R	2.3	similar to 1a but with a larger area
2b	H	1	SOR	R	2.3	similar to 2a but with a variable b
3	H	1	SSOR	R	2.1) 2.8)	same data as for case 1a
4a	H	1	SOR	A	2.9	S $\propto$ (i-6.5) x (j-4.5)
4b	H	1	SSOR	A	2.9	
5a	H	2	SOR	R	2.10	scheme A
5b	H	2	SOR	R	2.10) 2.11)	scheme B
6	H	2	SSOR	R	2.11) 2.15)	same data as for case 5b
7a	H	2	SOR	A	2.16	same data as for cases 4a and 4b
7b	H	2	SSOR	A	2.16	
8a	P	1	SOR	A	2.17	S $\propto$ (i-6.5)
8b	P	1	SSOR	A	2.17	
9a	P	1	SOR	A	-	S $\propto$ (i-6.5) x (j-4.5)
9b	P	1	SSOR	A	2.18	
10a	P	2	SOR	A	2.20	same data as for cases 8a and 8b
10b	P	2	SSOR	A	2.20	
11a	P	2	SOR	A	2.22	S $\propto$ (j-4.5)
11b	P	2	SSOR	A	2.22	
12a	W	1	SOR	R	2.23	σ constant
12b	W	1	SSOR	R	2.23	
13a	W	1	SOR	R	2.24a	$(q) = 1/4q^2$ $q = 1,1,5$
13b	W	1	SOR	R	-	$(q) = 1/q^2$ $q = 1,1,9$
13c	W	1	SOR	R	-	$(q) = 1/q^2$ $q = 1,1,5$
13d	W	1	SOR	R	2.25	4 levels with $\sigma(2) = 4 \times 10^{-2}$ and $\sigma(3) = 40 \times 10^{-2}$
14	W	1	SOR	R	-	different types of ω-equation
15	W	1	SOR	R	2.25	similar to 13d but with flagging
16a	W	1	SOR	R	2.24b) 2.27)	similar to 13a but using α-scheme
16b	W	1	SOR	R	2.26) 2.27)	different $\sigma(q)$ used to investigate α_c and α_o
16c	W	1	SOR	R	2.27	

TABLE 2.1

Equation (2.2) are known as direct and iterative methods.

In the direct methods the inverse of A (A^{-1}) is calculated and then the solution is given by $X = A^{-1} B$. Since A is usually both large and sparse these methods are not practical.

The iterative methods are ideal for large sparse matrices. They require an initial guess of X ($X^{(0)}$) and an algorithm by which the value of X after n iterations ($X^{(n)}$) can be computed from $X^{(n-1)}$. The iteration process is convergent if $X^{(n)} \longrightarrow X$.

There are two classes of iterative methods; point iterative methods and block iterative methods. In point iterative methods $X^{(n)}$ is altered at each gridpoint separately, whilst in block iterative methods groups of $X^{(n)}$ are changed simultaneously.

The three most commonly used point iterative methods are the Jacobi, the Gauss-Seidel and the SOR methods. The SSOR method is basically the same as the SOR method. The relationship between these four methods is described in many textbooks (e.g. Ames (1965)). The Jacobi method is the least efficient of these methods and will not be considered further.

Suppose Equation (2.2) is arranged so that the diagonal elements of A are unity. If L and U are the lower and upper diagonal matrices of A, and I is the unit matrix, then the SOR method is defined by

$$X^{(n+1)} = M X^{(n)} + C$$

$$M = - (\beta L + I)^{-1} [\, \beta U + (\beta - 1) I \,] \qquad (2.3)$$

$$C = (\beta^{-1} I + L)^{-1} B$$

The parameter β is the overrelaxation factor and n is the

A Poisson equation with Dirichlet boundary conditions on a square mesh size h

Method	Number of steps	Work per iteration
Jacobi	2/h	~1
Gauss-Seidel	1/h	~1
SOR	1/2h	1
SSOR	$\sim 1/\sqrt{h}$	~2.5

TABLE 2.2 - Ames (1965)

Number of steps - number of steps needed to reduce the error to a specified factor of its original value

Work per iteration - work per iteration normalised about the SOR method

iteration index. The iteration process continues until $||x^{(n+1)} - x^{(n)}|| < E$.

E will be called the tolerance.

The Gauss-Seidel method uses Equation (2.3) with $\beta = 1$.

For a two-dimensional region with gridpoints labelled i and j, the SSOR method uses Equation (2.3) at all (i + j) odd points, and then at (i + j) even points (i.e. the only difference between the SOR and SSOR methods is the order in which the gridpoints are relaxed).

Ames (1965) compared different iterative methods of solving a Poisson equation with Dirichlet boundary conditions. A selection of his results is shown in Table 2.2. This shows that the SOR method, using the optimum value of β, is far better than the Gauss-Seidel and Jacobi methods. This is true for all elliptic equations. His results also show that the SSOR method is more efficient than the SOR method. However it is not clear if this is true for all elliptic equations.

There are two kinds of block iterative methods known as single line methods and alternating direction implicit methods (ADI). For the Poisson equation with Dirichlet boundary conditions, Ames (1965) has shown that these methods are superior to point iterative methods. However, it is difficult to use block iterative methods to solve an equation as complicated as the ω-equation. Therefore the present investigation is limited to point iterative methods, but it is hoped that the block iterative methods will be investigated in the future.

The next four sections will be concerned with the method by which the optimum overrelaxation factor (β_o) may be found or estimated. Two methods will be described. The first method is based on the Young-Frankel theory of SOR, and is applicable to all elliptic equations (under certain conditions). The second method is based on a detailed analysis of the iteration algorithm.

2.2.2 The Young-Frankel Theory And Carré's Method

If A is a symmetric positive definite matrix with Young's Property 'A', then the iteration scheme defined by Equation (2.3) will converge for $0<\beta<2$. Under these conditions the rate of convergence of the iterative scheme is dependant upon the spectral radius of matrix M (the spectral radius, λ_m, is defined as the absolute value of the largest eigenvalue of a matrix). The convergence is defined as $-\ln(\lambda_m)$*, and β_o is defined as the value of β that minimizes λ_m and thus maximises the convergence.

The average number of iterations (N) that are necessary to reduce $\| X - X^{(n)} \|$ by one tenth is given by *

$$N = \frac{-1}{\log(\lambda_m)} \qquad (2.4)$$

Engeli (1959) pointed out that the values of N for the Gauss-Seidel and SOR methods (using β_o) are related by

$$N(SOR) = \frac{3}{4}\sqrt{N(G\text{-}S)}$$

This indicates that the SOR method is far more efficient than the Gauss-Seidel method.

Young (1954) showed that if μ_m is the spectral radius of (A-I) then β_o is given by

*ln and log will refer to logarithms to the base e and base ten respectively.

$$\beta_o = \frac{2}{1 + \sqrt{1 - \mu_m^2}} \qquad (2.5)$$

In terms of the spectral radius of M this becomes

$$\beta_o = \frac{2}{1 + \sqrt{1 - \frac{(\lambda_m + \beta - 1)^2}{\beta^2 \lambda_m}}} \qquad (2.6)$$

This holds for all values of β such that $1 < \beta < \beta_o$

It can be shown from Equation (2.6) that when $\beta = \beta_o$, the spectral radius (λ_{mo}) is

$$\lambda_{mo} = \beta_o - 1 \qquad (2.7)$$

Therefore the maximum value of N is given by

$$N_o = \frac{-1}{\log(\beta_o - 1)} \qquad (2.8)$$

If λ_m can be found for a given β, then Equation (2.6) can be used to find β_o. Carré (1961) found λ_m by using the fact that the displacement vector ($\delta^{(n)} = X^{(n)} - X^{(n-1)}$) has the property that

$$\lim_{n \to \infty} \frac{\| \delta^{(n)} \|}{\| \delta^{(n-1)} \|} = \lambda_m \qquad (2.9)$$

For convenience the use of this equation with Equation (2.6) will be referred to as Carré's method, although the method described by Carré was more sophisticated.

Carré's method is only effective if $1 < \beta < \beta_o$ and therefore an estimate of β_o is required. A good estimate is advantageous because the rate at which λ_m is approached depends upon ($\beta_o - \beta$).

Miyakoda (1960) derived sets of formulae by which can be calculated for several simple equations with Dirichlet boundary conditions. Unlike Carré's method, this method does not involve the solution of the actual equation for which β_o is required. Thus it is useful to use Miyakoda's method to derive β_o for simple equations.

Also it may be used to estimate β_o for more complicated equations so that Carré's method can be used.

Experimental evidence that will be described later shows that Miyakoda's method can be extended to give accurate values of β_o for complicated equations.

2.2.3 Miyakoda's Method

Let Γ' be the finite difference form of the differential operator Γ in Equation (2.1). Also let x_p and f_p be the values of x and f at point P. At point P, Equation (2.10) becomes

$$\Gamma' x_p = f_p \qquad (2.10)$$

If $x_p^{(n)}$ is the value of x_p after n iterations, then the residual at P is

$$R_p^{(n)} = \Gamma' x_p^{(n)} - f_p$$

The SOR iteration scheme is defined by

$$x_p^{(n+1)} = x_p^{(n)} - \frac{\beta R_p^{(n)}}{M_p} \qquad (2.11)$$

Here M_p is the coefficient of x_p in Equation (2.10). The division of $R_p^{(n)}$ by M_p is equivalent to making the diagonal elements of A unity (see section 2.2).

The iteration scheme defined by Equation (2.11) will be referred to as the β-scheme.

Several authors (e.g. Stuart et al.(1967), Asselin (1967)) have used the iteration scheme defined by

$$x_p^{(n+1)} = x_p^{(n)} + \alpha \tilde{R}_p^{(n)} \qquad (2.12)$$

Here $\tilde{R}_p^{(n)}$ is closely related to $R_p^{(n)}$. The parameter α is treated as a constant and will be referred to as the "α overrelaxation factor". The iteration scheme defined by Equation (2.12), will be called the α-scheme.

If the equation to be solved has constant coefficients

then the α-scheme and β-scheme are equivalent. This is not so if the coefficients are variable. The latter situation will be dealt with in section 2.54.

Unless stated otherwise, the β-scheme was used to solve all partial differential equations.

In both the α-scheme and β-scheme the latest values of x are used to compute $R_p^{(n)}$. Therefore only one field of x has to be stored. When only the values of x from the previous iteration are used to compute $R_p^{(n)}$ the iteration scheme is called simultaneous overrelaxation. This requires the storing of two fields of x and is less efficient than SOR. Therefore it will not be considered further.

The error, $\varepsilon_p^{(n)}$, is defined by

$$\varepsilon_p = x_p - x_p^{(n)}$$

In terms of the error, the iteration process is equivalent to

$$\varepsilon_p^{(n+1)} = \varepsilon_p^{(n)} - \frac{\beta}{M_p} \Gamma' \varepsilon_p^{(n)} \qquad (2.13)$$

Miyakoda's method consists of assuming a distribution of $\varepsilon_p^{(n)}$ which is then used in conjunction with Equation (2.13) to find the value of β that maximises the convergence.

Let i and j be the labels of the gridpoints in a two-dimensional region and let n_i and n_j be the number of grid-points in the i and j directions. Miyakoda assumed that $\varepsilon_{ij}^{(n)}$ had the form

$$\varepsilon_{ij}^{(n)} = K^n A^{i+j} f(i, n_i) f(j, n_j) \qquad (2.14)$$

Here K is the convergence rate and A is the amplitude. The function f (i, n_i) is chosen so that the boundary conditions are satisfied. For Dirichlet boundary conditions the error is zero on the boundary, and therefore f (i, n_i)

was chosen to be

$$f(i, n_i) = \sin\left(\frac{\pi}{n_i - 1} i\right) \qquad (2.15)$$

Miyakoda (1960) derived a set of formulae to give β_o for the Helmholtz equation

$$\nabla^2 \psi - b\psi = c \qquad b = \text{constant}$$

The formulae are

$$\begin{aligned} \tau &= \left[\cos\left(\frac{\pi}{n_i - 1}\right) + \cos\left(\frac{\pi}{n_j - 1}\right) \right] / 2 \\ c &= \left(\frac{4 + b}{2\tau}\right)^2 / 2 - 1 \\ \beta_o &= 1 + c - \sqrt{c^2 - 1} \end{aligned} \qquad (2.16)$$

From these equations it can be shown that

$$\beta_o = \frac{2}{1 + \sqrt{1 - \tau^2}}$$

A comparison of this with Equation (2.5) shows that τ is the spectral radius of (A-I). It can also be shown that K is the spectral radius of M. These facts indicate the relationship between Miyakoda's method and the Young-Frankel theory.

Equation (2.16) can be rearranged to give

$$\begin{aligned} \tau &= \frac{2}{4 + b} \left[\cos\left(\frac{\pi}{n_i - 1}\right) + \cos\left(\frac{\pi}{n_j - 1}\right) \right] \\ c &= \frac{2}{\tau^2} - 1 \\ \beta_o &= 1 + c - \sqrt{c^2 - 1} \end{aligned} \qquad (2.17)$$

The reason for this rearrangement will become apparent later.

When an equation is solved by using an iterative technique it is necessary to specify the tolerance E. But the quantity that is known initially is the acceptable error (AE). Therefore the relationship between AE and E must be derived.

Suppose that the iteration process proceeds until

$$\left\| \frac{\beta R^{(n)}}{4+b} \right\| < E$$

Using the definition of the residual it can be shown that

$$E \approx \beta(1 - A\tau)AE \qquad (2.18)$$

If $v = \beta - 1$ and if β is close to β_o, then this equation gives

$$E \approx (1 - v^2)AE \qquad (2.19)$$

This shows that E is always less than AE. For example, if $\beta_o = 1.5$ then $E \approx .75x$ AE. Also it shows that as $\beta_o \rightarrow 1$, $E \rightarrow AE$.

When b = 0, the Helmholtz equation becomes a Poisson equation. Thus by putting b = 0 the above results can be used to determine β_o and E for a Poisson equation.

Miyakoda also considered an equation that is similar to

$$A\nabla^2\omega + B\frac{D^2\omega}{Dp^2} + F = 0 \qquad (2.20)$$

Here A and B are constants. If Dirichlet boundary conditions are used, then β_o is given by

$$\tau = \frac{2}{4A+2B}\left[A\cos\left(\frac{\pi}{n_i-1}\right) + A\cos\left(\frac{\pi}{n_j-1}\right) + B\cos\left(\frac{\pi}{n_K-1}\right)\right]$$

$$c = \frac{2}{\tau^2} - 1 \qquad (2.21)$$

$$\beta_o = 1 + c - \sqrt{c^2 - 1}$$

The similarity between Equations (2.17) and (2.21) will be discussed in the next section.

The relationship between E and AE for Equation (2.20) is the same as that for the Helmholtz equation (see Equations (2.18 and (2.19).

Miyakoda tried to use his method to find β_o for equations with Neumann boundary conditions. However he had little success. The reason for this will be discussed

later.

So far, only equations with constant coefficients have been considered. This is because Miyakoda's method can only be used with this type of equation. Later it will be shown how his method can be extended to include variable coefficients.

Although Equation (2.14) gives the correct value of β_o, this equation is not strictly correct. If the optimum value of β is used, then it can be shown that

$$K^n A^{i+j} = (\beta_o - 1)^{n+(i+j)/2}$$

Therefore both $\varepsilon_{ij}^{(n)}$ and $x_{ij}^{(n)}$ are known and thus the exact solution of the equation can be found. This result is obviously incorrect and the reason is that Equation (2.14) is not correct. Equation (2.14) should be replaced by

$$\varepsilon_{ij}^{(n)} = \gamma K^n A^{i+j} f(i, n_i) f(j, n_j) \qquad (2.22)$$

Here γ is a constant and is a type of scaling factor.

Miyakoda's method is very similar to the method used by O'Brien (1968). He calculated the eigenvalues of M by using matrix methods, where Miyakoda used algebraic methods. The advantage of O'Brien's method is that it can cope easily with variable coefficients. But this method requires a great deal of computation and thus it is preferable to use Miyakoda's method.

In the next section a set of formulae will be given from which β_o can be calculated for a general equation (of a certain type).

2.2.4 A Generalisation of Miyakoda's Equations

Consider a linear partial differential equation with constant coefficients. Let the dependent variable be x and let there be n independent variables Γ_i (i = 1, 1, n).

Suppose that there are Q terms involving x, with coefficients C_q (q = 1,1,Q) and that f (r_i) is the forcing function. The equation may then be written as

$$\sum_{q=1}^{Q} C_q \Gamma_q x = f(r_i) \qquad (2.23)$$

Here Γ_q are the differential operators and in this analysis they can only be $\frac{\partial^2}{\partial r_i^2}$ or 1.

Let M_q be the coefficient of x at point P once $\Gamma_q x$ has been discretised using centred finite differences. If ϑ_q is a function depending upon the form of Γ_q, then τ is given by

$$\tau = \sum_{q=1}^{Q} C_q M_q \vartheta_q \Big/ \sum_{q=1}^{Q} C_q M_q \qquad (2.24)$$

The values of ϑ_q and M_q are given below.

$\Gamma_q x$	M_q	ϑ_q
x	1	0
$\frac{\partial^2 x}{\partial r_i^2}$	-2	$\cos\left(\frac{\pi}{n_i - 1}\right)$

Here n_i is the number of gridpoints in the direction of r_i.

The value of β_o can now be calculated by using the appropriate value of τ and the following equations

$$c = \frac{2}{\tau^2} - 1$$

$$\beta_o = 1 + c - \sqrt{c^2 - 1}$$

The above equations with Equation (2.24) will be referred to jointly as Equation (2.24).

It can easily be shown that Equations (2.17) and (2.21) can be derived from Equation (2.24).

2.2.5 The Determination Of β_o For the SSOR Method

The SSOR method was described by Sheldon (1962). The only difference between this method and the SOR method is the order in which the points are relaxed

(see section 2.2.1). Therefore, when the Young-Frankel theory applies to the SOR method it will also apply to the SSOR method. This means that Carré's method can be used to calculate β_o for the SSOR method.

Sheldon considered the use of the SSOR method for solving a Poisson equation with Dirichlet boundary conditions. He showed that the mimumum spectral radius was the same as that for the SOR method. This implies that the value of β_o is the same for both methods. If this is so then the maximum convergence rates for these methods must be the same after a sufficient number of iterations. Therefore the relative efficiency of these methods depends upon what happens during the first few iterations.

Jenssen and Straede (1969) compared the efficiency of the SOR and SSOR methods of solving different finite difference forms of a Poisson equation. They found that with $\beta = \beta_o$, the SSOR method was faster than the SOR method.

The above results imply that, for a Poisson equation with $\beta = \beta_o$, the SSOR method requires fewer iterations than the SOR method to reach its maximum convergence rate.

If these deductions are correct then the relative efficiency of the SOR and SSOR methods will depend upon the value of E chosen. This must be taken into consideration in interpreting the results of Jenssen andStraede.

In terms of the error, $\varepsilon_{ij}^{(n)}$, the SSOR iteration scheme for the Poisson equation is

$$\varepsilon_{ij}^{(q+1)} = \varepsilon_{ij}^{(q-1)} + \frac{\beta}{4}\left(\varepsilon_{i+1,j}^{(q)} + \varepsilon_{i-1,j}^{(q)} + \varepsilon_{i,j+1}^{(q)} + \varepsilon_{i,j-1}^{(q)} - 4\,\varepsilon_{ij}^{(q-1)} \right) \qquad (2.25)$$

This is used at all (i + j) even and then (i + j) odd. An examination of Equation (2.25) indicates that $\varepsilon_{ij}^{(q)}$ will

have the form

$$\varepsilon_{ij}^{(q)} = \gamma K^{q} f(i, n_i) g(j, n_j) \qquad (2.26)$$

Consider the case where Dirichlet boundary conditions are used. It can be shown that the value of β_o is the same for the SOR and SSOR methods if $g(j, n_j) = f(j, n_j)$ and if f is given by Equation (2.15). The validity of these assumptions will be considered later.

Later the value of β_o for the SSOR method will be found experimentally and by using Carré's method. Also comparisons will be made between the SOR and SSOR methods for different types of equation and different kinds of boundary condition.

2.3 The Overrelaxation Method For Solving A Helmholtz Equation And The Determination of β_o

If $\omega \propto \sin(lp)$ and if the derivatives of σ are ignored, then the geostrophic ω-equation may be written as

$$\nabla^2\omega - b\omega + S' = 0 \qquad b = \left(\frac{fld}{m}\right)^2 \Big/ \sigma \qquad (2.27)$$

In the atmosphere both f^2 and σ are functions of x and y.

The merits of using the SOR and SSOR methods for solving this equation were investigated. Both types of boundary conditions were considered and b was treated as both a constant and a variable.

The variation of the rate of convergence with β was investigated by finding the number of iterations (n(E)) required before the condition $\|\omega^{(n+1)} - \omega^{(n)}\| < E$ * was satisfied with a given β. The β for which n(E) was a minimum will be referred to as $\beta_o(E)$. Also, the values of β_o found from Miyakoda's method and Carré's method will be

*The norm was the modulus of the numerically largest element. Also, for the Helmholtz equation, E has units of mb s^{-1}.

called $\beta_o(M)$ and $\beta_o(C)$.

The error distribution was computed for both types of boundary condition. This was then used to either verify Miyakoda's method or to extend it. Also, the shape of the constant E curves was deduced from the error distribution and the relationship between E and the acceptable error was investigated.

For Dirchlet boundary conditions, the equations derived by Miyakoda (see Equation (2.17)) were used to investigate the effect of the number of gridpoints on N_o and β_o.

The investigations outlined above were divided into four sections. The first two deal with the SOR and SSOR methods of solving a Helmholtz equation with Dirichlet boundary conditions. The other two sections are concerned with the use of these two methods when Neumann boundary conditions are employed.

2.3.1 The SOR Method Of Solving A Helmholtz Equation With Dirichlet Boundary Conditions

Equation (2.27) was solved with S' derived from data for the 600 mb level for areas 91 and 51. Other distributions of S' were also used and these will be described later.

Unless otherwise stated, both the initial guess and the boundary conditions were $\omega = 0$.

The constant value of b ($\bar{b}$) was derived from the average values of f^2, σ and $\left[\frac{m}{d}\right]^2$. The averages were $1.226 \times 10^{-8}\ s^{-2}$, $1.97 \times 10^{-2}\ m^2\ mb^{-2} s^{-2}$ and $1.098 \times 10^{-10}\ m^{-2}$; thus $b = 8.87 \times 10^{-2}$.

The Helmholtz equation, with b, was solved with real

Case	n_i	n_j	β	N_o	$\beta_o(C)$	$\beta_o(M)$	$\beta_o(E)$	Fig.
1a	14	10	1.46	3.1	1.476	1.476	1.48	2.1
2a	14	22	1.49	3.9	1.558	1.558	1.54	2.2
2b	14	22	1.52	3.8	1.546	-	1.53	2.2

TABLE 2.3

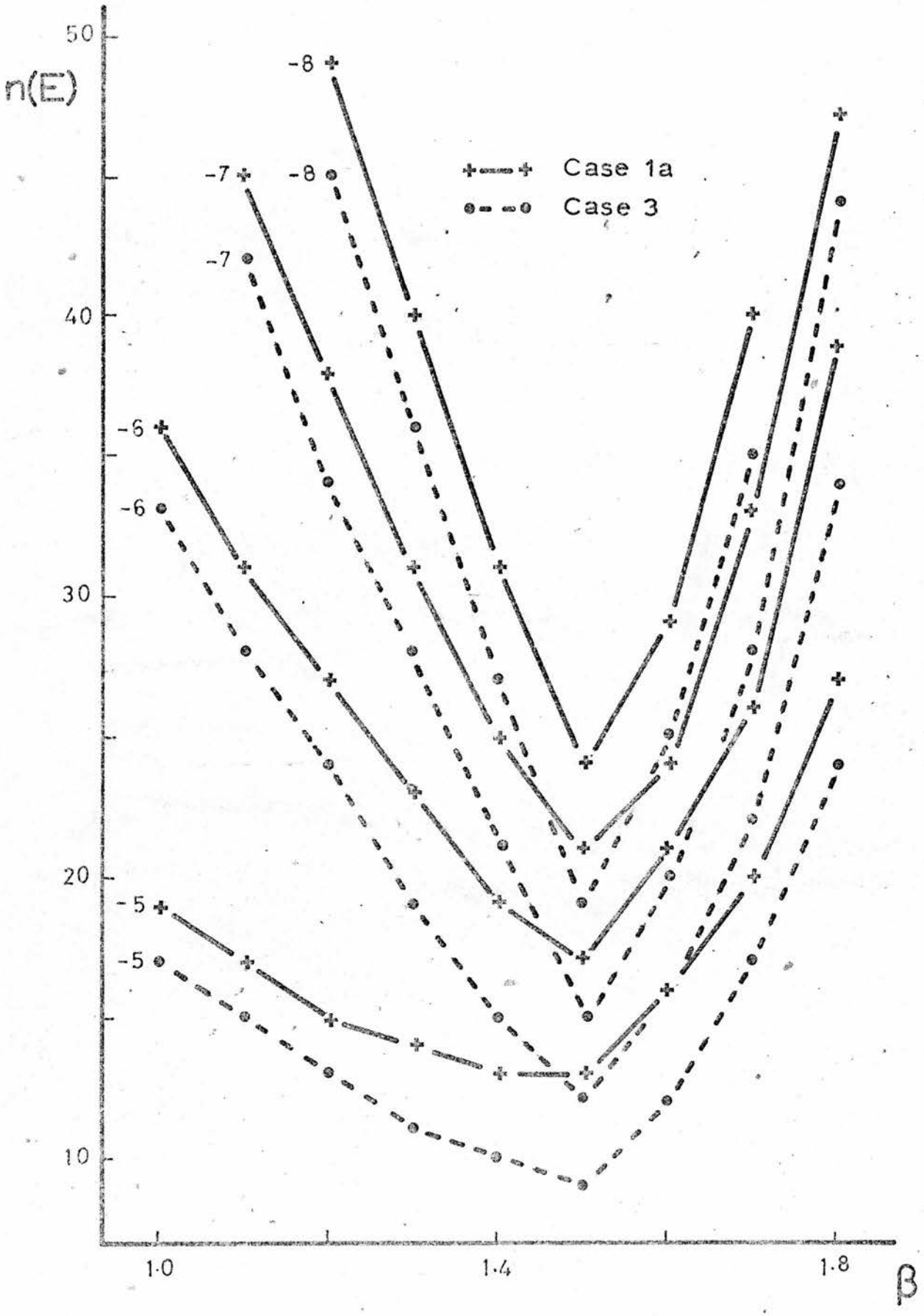

FIGURE 2·1

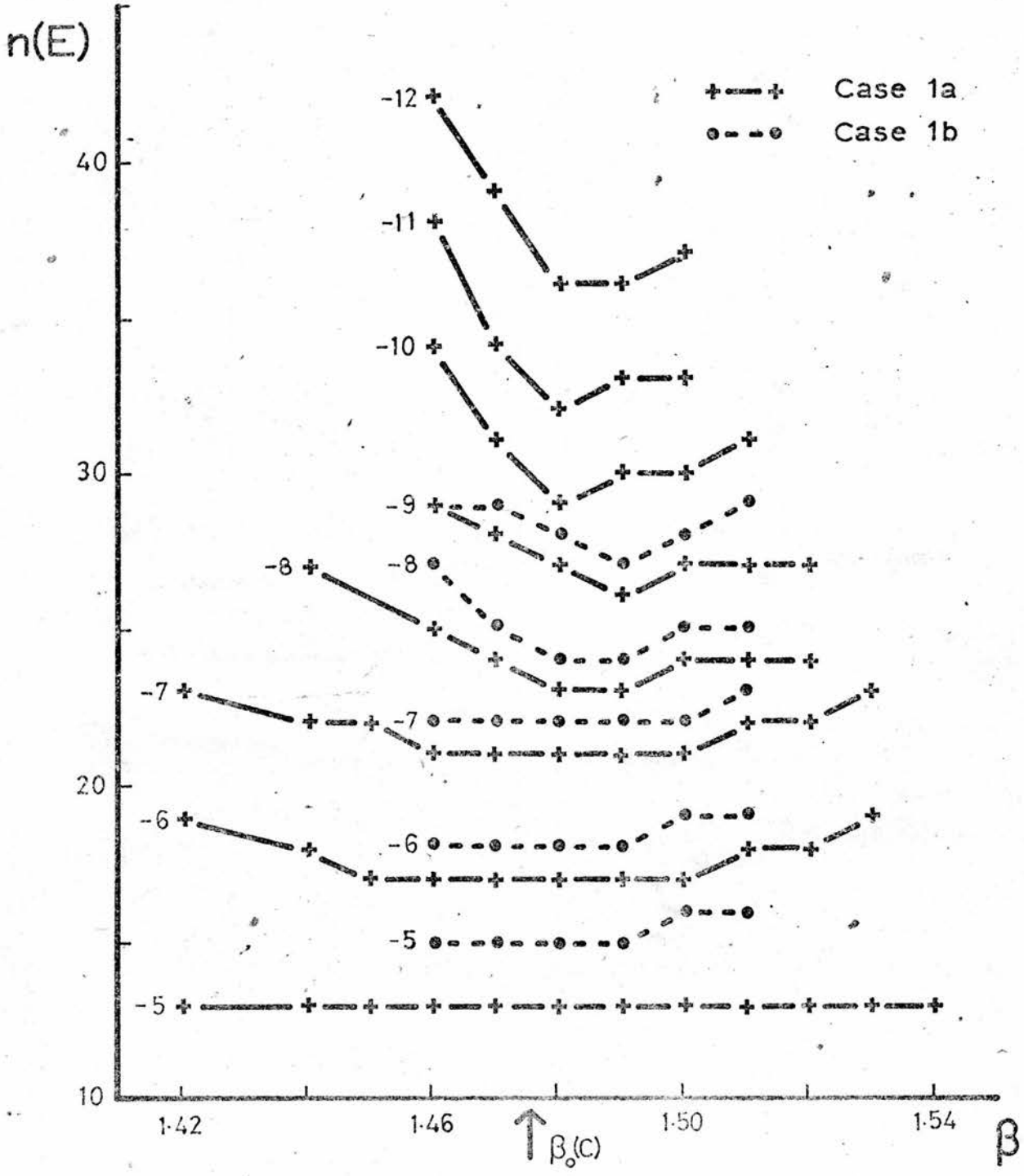
n(E)
40
30
20
10
Case 1a
Case 1b
-12
-11
-10
-9
-8
-8
-7
-7
-6
-6
-5
-5
1·42
1·46
1·50
1·54
β
β₀(C)

FIGURE 2.2

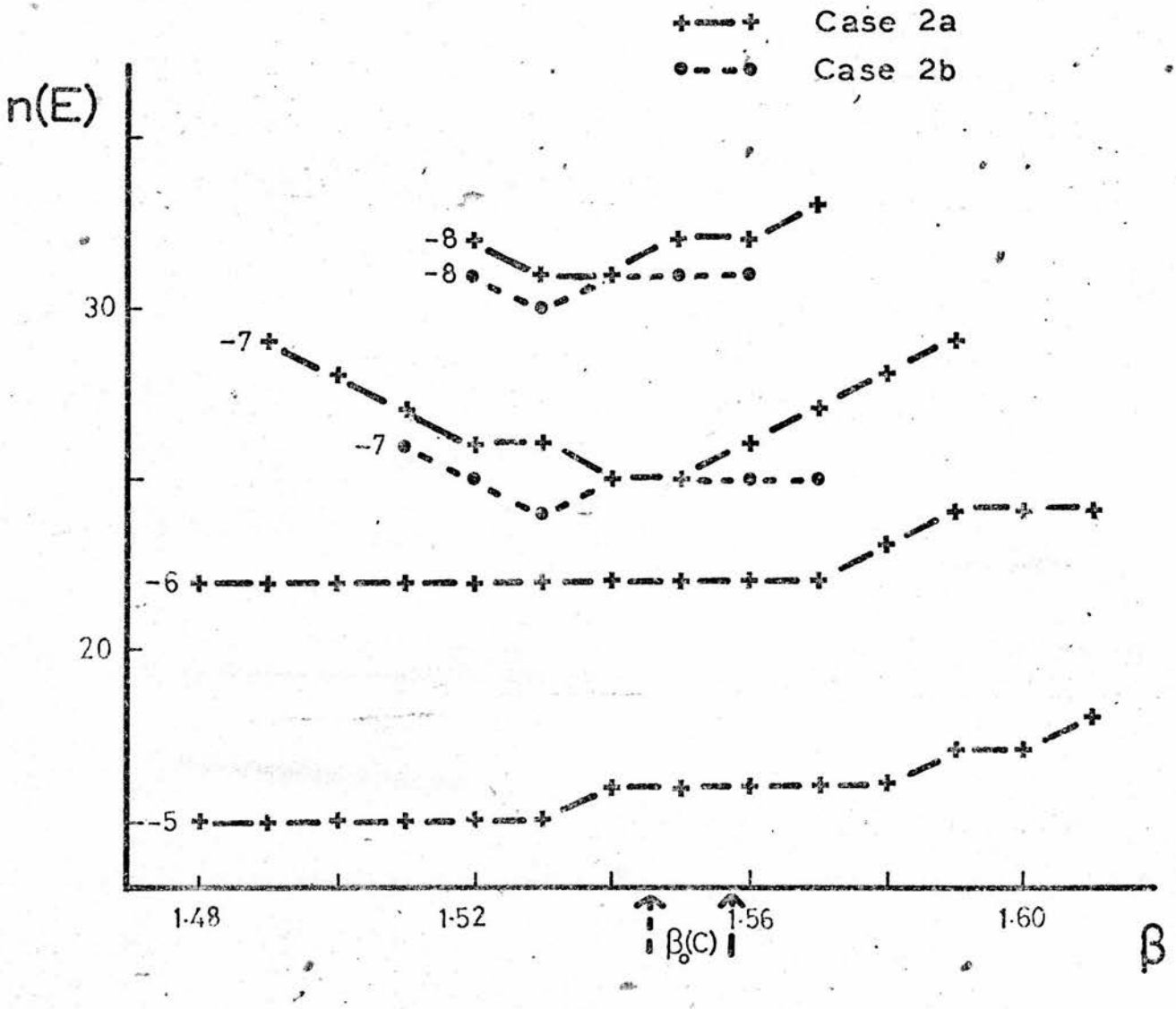

FIGURE 2·3

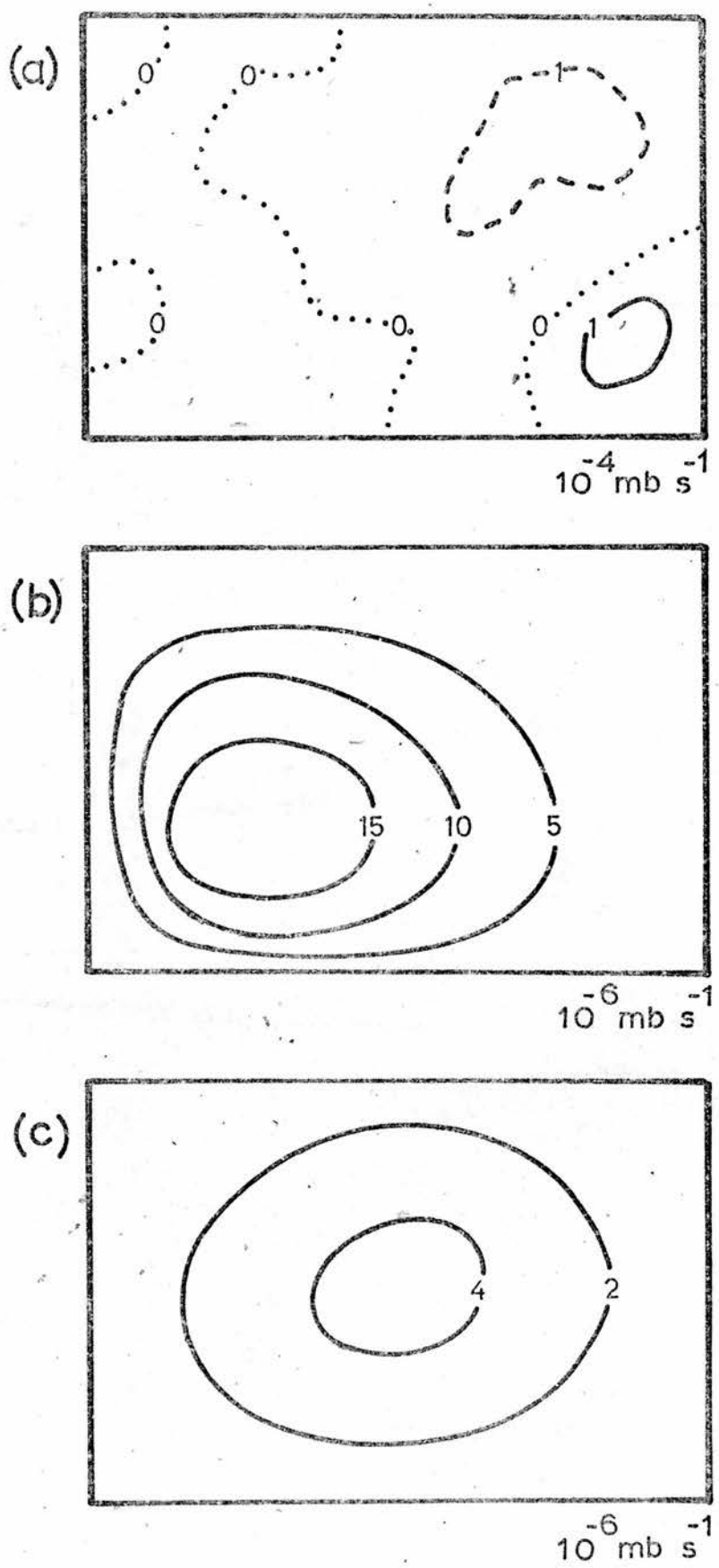

FIGURE 2·4

(a) Solution of Equ.(2·27) with $(\omega)_b = 0$

(b) $\varepsilon_{ij}^{(16)}$, $\beta = 1{\cdot}4$, case 1a (SOR)

(c) $\varepsilon_{ij}^{(16)}$, $(i+j)$ odd, $\beta = 1{\cdot}4$, case 3 (SSOR)

data in areas 91 and 51 (cases 1a and 2a).

The distribution of n(E) with β for case 1a is shown in Fig. 2.1.* This shows that the SOR method with β_o was superior to the Gauss-Seidel method ($\beta = 1$). For example, with $E = 10^{-6}$, the former method required about $\frac{1}{2}$ the iterations of the latter. Clearly it is worthwhile calculating β_o when the SOR method is used.

For cases 1a and 2a, the constant E curves in the vicinity of β_o are shown in Figs. 2.2 and 2.3. Also $\beta_o(M)$, $\beta_o(C)$ and $\beta_o(E)$ are shown in Table 2.3. This table shows that $\beta_o(M)$ and $\beta_o(C)$ are identical and that they are very close to $\beta_o(E)$.

Miyakoda's method predicted the correct β_o and this implies that the error was given by Equation (2.14). This was confirmed by calculating $\varepsilon_{ij}^{(16)}$ for case 1a. This is shown in Fig. 2.4b. The fact that the distribution of $\varepsilon_{ij}^{(n)}$ was independent of the solution of the equation (shown in Fig. 2.4a) implies that β_o depends only upon the iteration scheme and not upon the initial guess, the value of ω on the boundary or the distribution of S.

In both cases 1a and 2a the optimum value of β became better defined as E decreased. This was because the error vector becomes dominated by one eigenvector as the number of iterations increases. Also it is expected that $\beta_o(E) \longrightarrow \beta_o(M)$ as E decreases. These results show that when E was large n(E) was not sensitive to β, but when E was small n(E) varied rapidly with β. Therefore, more care needs to be taken over calculating β_o when E is small than when E is large.

The results for case 1a also show that it is better to

*The curves are labelled with log E. This applies to other figures.

overestimate β_o rather than underestimate it. Engeli (1959) has shown that this is to be expected for all equations with Dirichlet boundary conditions.

Let ω_a be the solution of ω for case 1a. The effect of the initial guess was investigated by using $-\omega_a$ as the initial guess and the results of this computation (case 1b) are shown in Fig. 2.2 . A comparison of cases 1a and 1b shows that the initial guess had little influence on the distribution of n(E) with β . Also, $\beta_o(C)$ was the same in both cases and therefore a bad initial guess may increase the total number of iterations required for a given E, but will not affect the rate of convergence.

The effect of the distribution of S' on $\beta_o(C)$ was investigated. The distributions of S' were made up of combinations of sines and cosines and in all cases $\beta_o(C)$ was the same . Thus the rate of convergence was not affected by the distribution of S'. Also different forms of the Dirichlet boundary condition had no effect upon $\beta_o(C)$.

Case 2a was repeated using a variable b (b(x,y) say) and this will be called case 2b. Since b(x,y) depends upon the distribution of both f and σ, b(x,y) did not vary rapidly. The average value of b(x,y) was the constant value of b used in case 2a (that is $\bar{b}$).

The results for case 2b are shown in Fig. 2.3. This shows that $\beta_o(C)$ and $\beta_o(E)$ were almost the same as those in case 2a (see Table 2.3). Therefore these results imply that the value of β_o for an equation with variable coefficients can be estimated by finding β_o for the equation with the average values of the coefficients.

In the above case, the coefficient b(x,y) varied

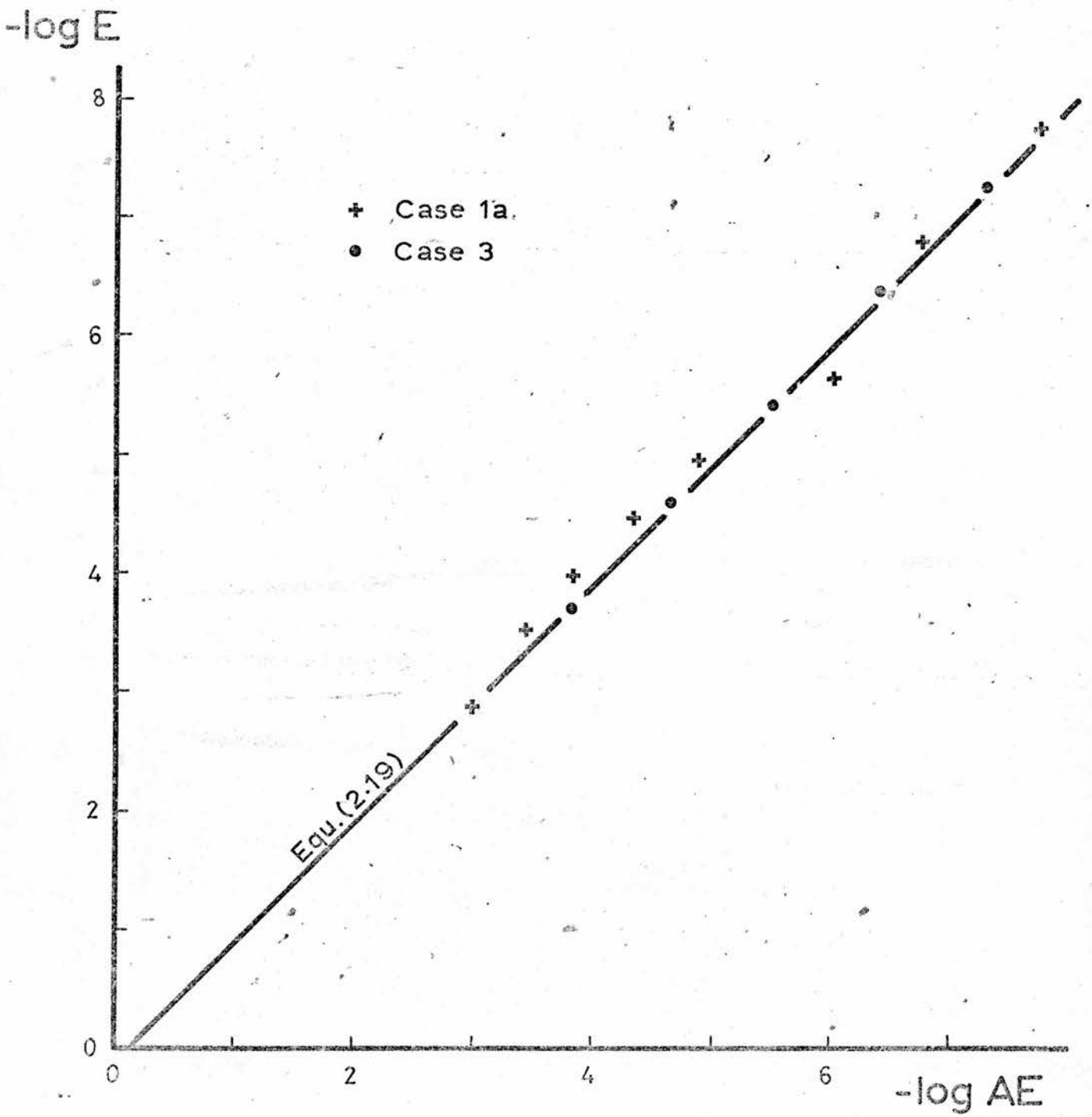

FIGURE 2.5

slowly. However, it will be shown later that the same conclusion holds for rapidly varying coefficients.

The validity of Equation (2.19) was tested for case 1a. The optimum value β_o was used and AE and E were computed for a series of n. It was assumed that AE and E are given by $\left\| \varepsilon_{ij}^{(n)} \right\|$ and $\left\| \omega^{(n+1)} - \omega^{(n)} \right\|$ respectively. Fig. 2.5 shows a graph of log E against log AE. The theoretical results derived from Equation (2.19) are also shown. Bearing in mind that Equation (2.19) gives only the approximate relationship between AE and E, it is concluded that this equation is essentially correct. If this is so, then $E \approx AE$ when v is small (n_i and n_j small). However if v is large (n_i and n_j large), then Equation (2.19) should be used to deduce E.

Miyakoda (1960) showed that $K = A^2$ in Equation (2.14). He also showed that with a given $\beta = 1 + v$, the amplitude is given by

$$A = a \pm \sqrt{a^2 - v}$$

$$a = \frac{(1+v)\tau}{2}$$

An approximate condition for the termination of the iteration process is $\left\| \varepsilon_{ij}^{(n)} \right\| < E$. Therefore, if i_m and j_m are the coordinates of the gridpoints at which $\left| \varepsilon_{ij}^{(n)} \right|$ is a maximum, the iteration process stops when

$$E = \gamma A^{i_m + j_m + 2n} f(i_m, n_i) f(j_m, n_j)$$

Here the function f is given by Equation (2.15). For a given E and v, this equation can be used to compute n since

$$2n = \frac{\log\left[\frac{E}{\gamma F}\right]}{\log\left[R\left(a + \sqrt{a^2 - v}\right)\right]} - (i_m + j_m) \qquad (2.28)$$

$$F = f(i_m, n_i) f(j_m, n_j)$$

This was used to compute the distribution of n(E) with β

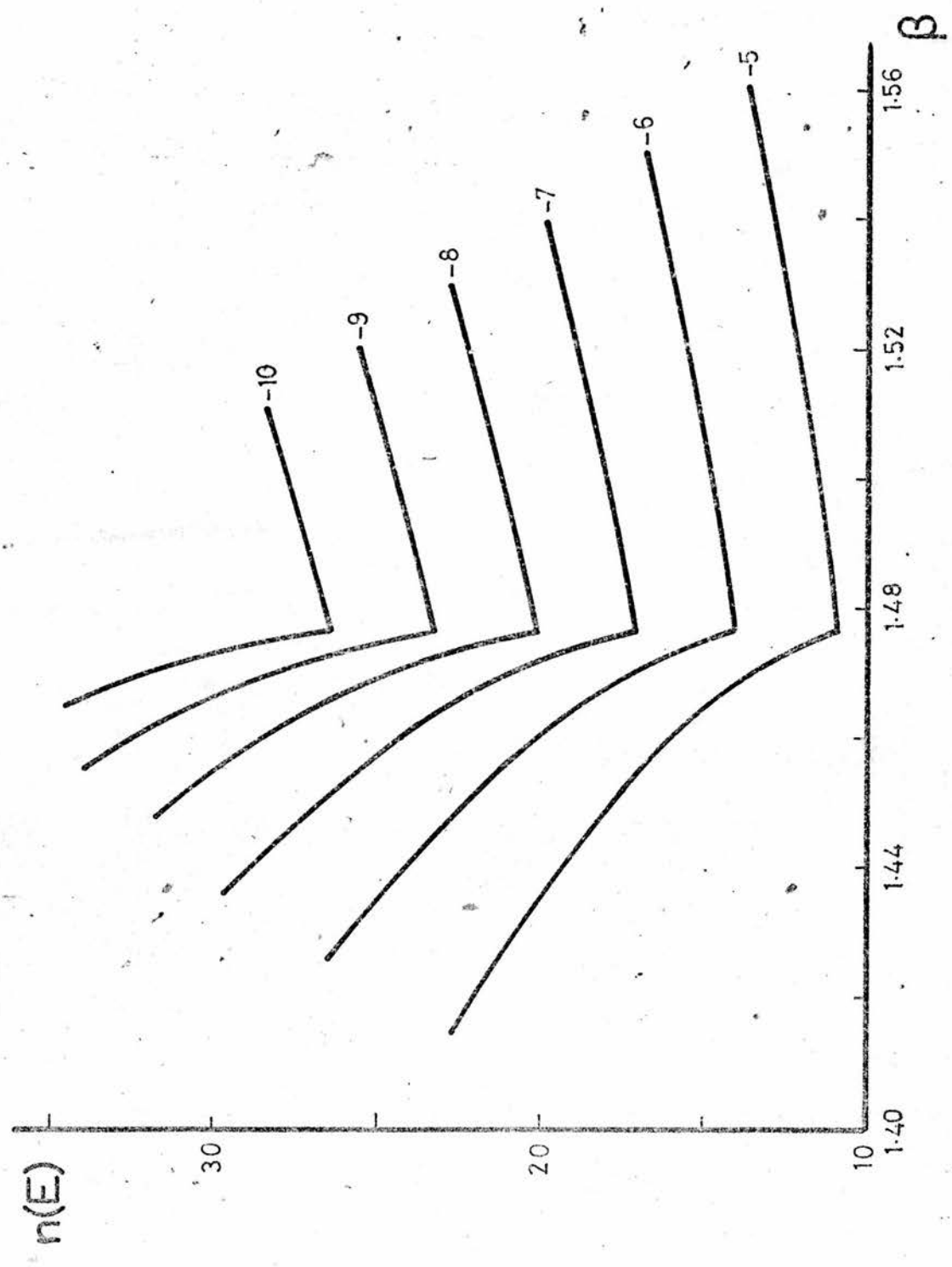

FIGURE 2.6 Equ.(2.28) with γ=1 for case 1a

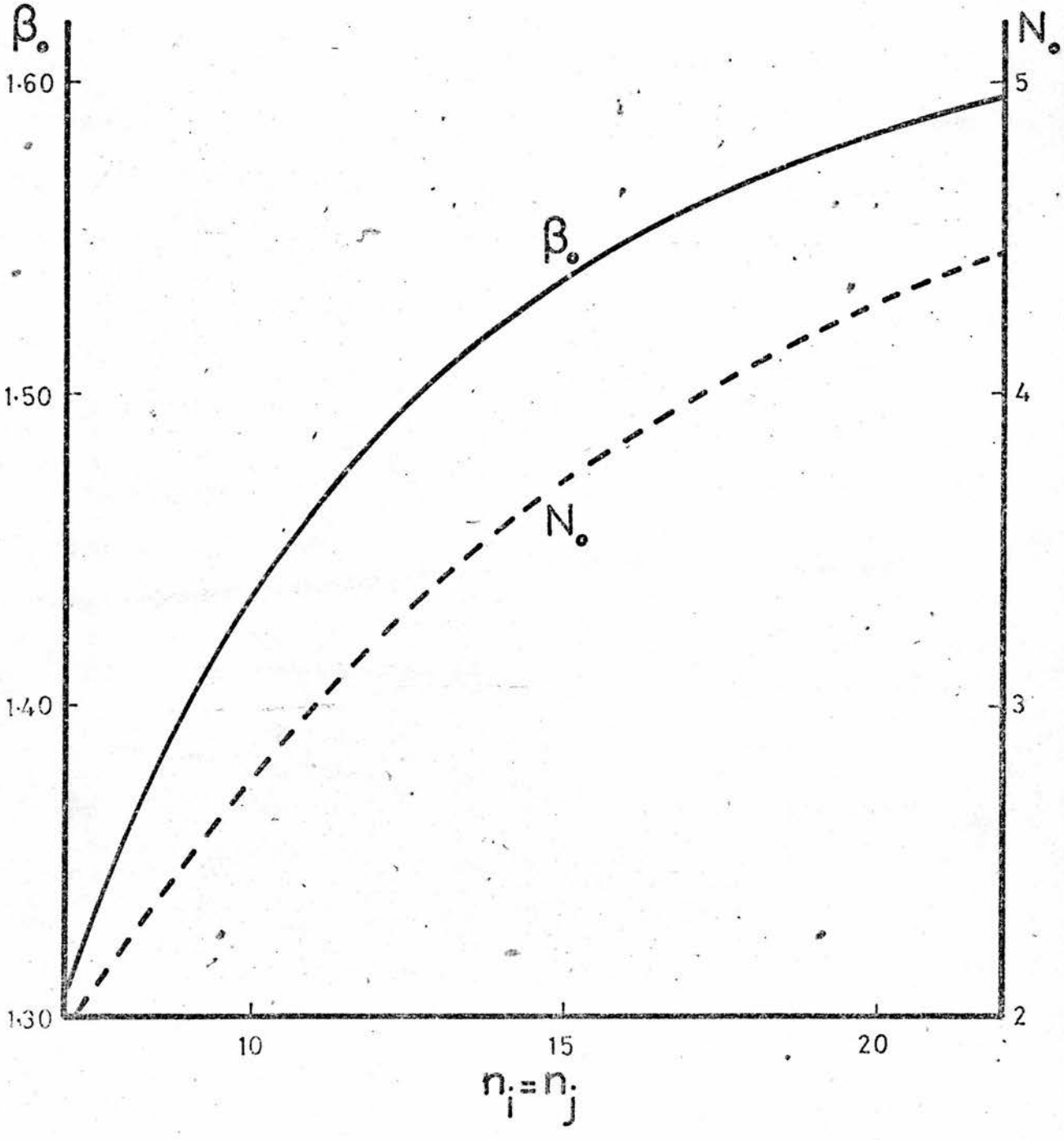

FIGURE 2·7

for case 1a. The results are illustrated in Fig. 2.6. A comparison of this figure with Fig. 2.2 shows that Equation (2.28) gives the correct distribution of n(E) with β.

Fig. 2.6 clearly shows that it is better to overestimate β_o rather than underestimate it. Also, since the magnitude of $\frac{dn(E)}{dv}$ increases with E for $\beta < \beta_o$, the extra number of iterations required when β_o is underestimated increases as E decreases.

The variation of $G(E) = \frac{dn(E)}{dv}$ with E was investigated further by differentiating Equation (2.28) with respect to v. It can be shown that when $\beta < \beta_o$, $G(E) \propto \log \frac{E}{\gamma}$. Since γ is such that $\frac{E}{\gamma} < 1$, this fraction may be written as 10^{-k}. Therefore $G(E) \propto -k$. Hence, for $\beta < \beta_o$, the magnitude of the gradient of the n(E) against β curves increases as E decreases.

Finally the effect of the number of gridpoints on β_o (and hence the convergence rate) was considered. It can be shown that if Equation (2.27) is solved on a grid with $n_i \times n_i$ gridpoints, then

$$\beta_o \propto 2 - \frac{\delta^2}{n_i^2}$$

This shows that as n_i increases $\beta_o \longrightarrow 2$. It also shows that β_o, and hence N_o, will vary rapidly when n_i is small.

Equations (2.16) were solved for β_o with different values of $n_i = n_j$. Using Equation (2.8), the variation of N_o with n_i was also found. The results are shown in Fig. 2.7. This shows that N_o increases with the number of gridpoints. Thus if the number of gridpoints is increased from 10 x 10 to 20 x 20 (a four-fold increase) there will be approximately a six-fold increase in a computer time.

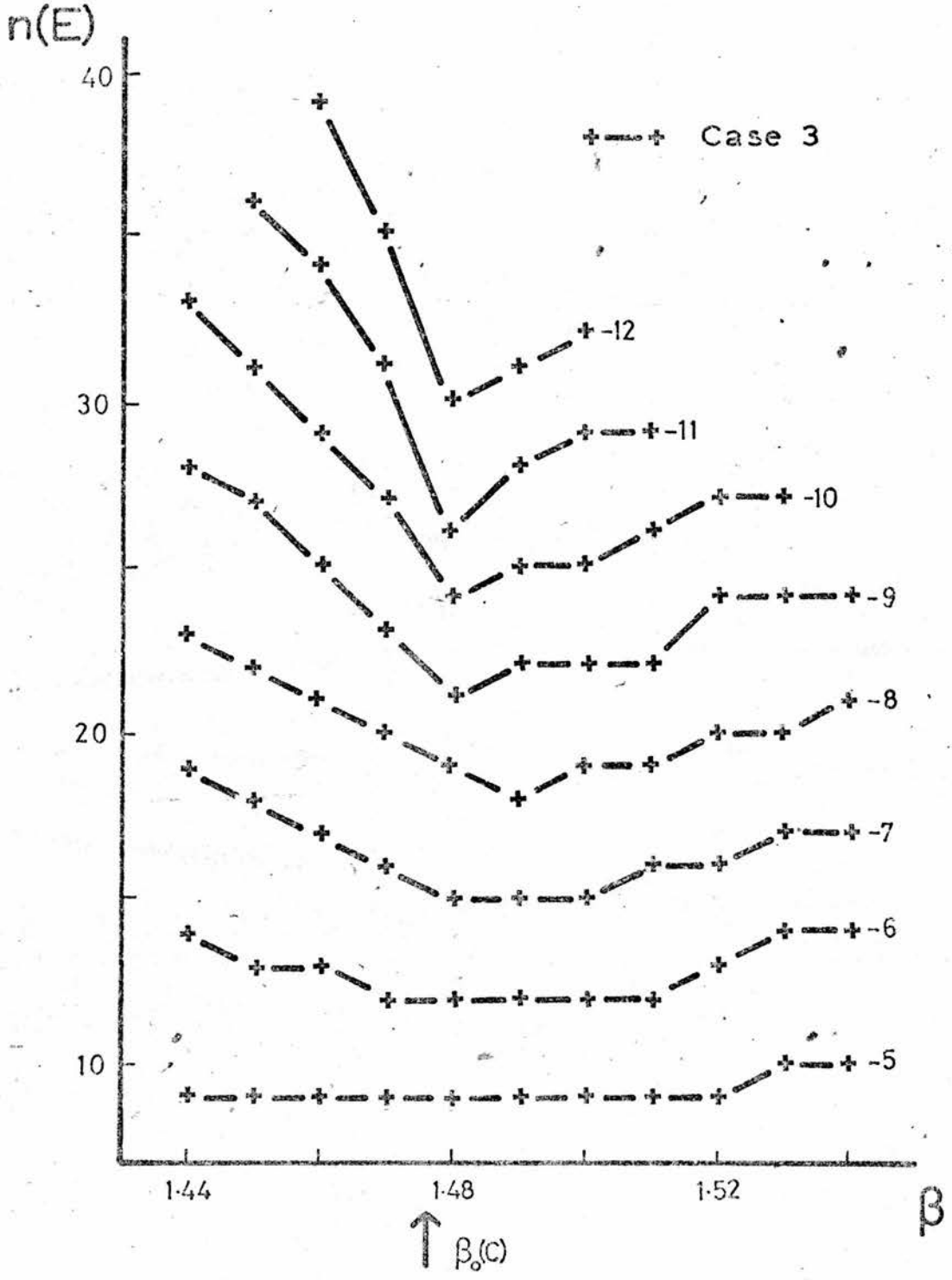

FIGURE 2·8

These results show that when the number of gridpoints is increased, there is an increase in the computer time due to an increase in the number of calculations per iteration and a decrease in the convergence rate.

2.3.2 The SSOR Method For Solving A Helmholtz Equation With Dirichlet Boundary Conditions

A comparison was made between the SSOR and SOR methods by repeating case 1a using the SSOR method (case 3).

Carré's method was used to calculate β_o for the SSOR method. It was found to be the same as for the SOR method.

The distribution of n(E) with β, for both cases 1a and 3, is shown in Fig. 2.1. This shows that the SSOR method was more efficient than the SOR method for $1.0 <= \beta <= 1.8$ ($\beta > 1.8$ was not used due to the slow rate of convergence). This figure also shows that the shapes of the constant E curves are essentially the same for both methods.

A more detailed study of the distribution of n(E) with β, in the vicinity of β_o, was undertaken and the results are shown in Fig. 2.8. The equivalent results for the SOR method are shown in Fig. 2.2. A comparison of these two figures shows the SSOR method was always more efficient than the SOR method in the vicinity of β_o. For example, with $\beta = 1.48$ and $E = 10^{-12}$, the SOR method required 36 iterations whereas the SSOR method required only 30. The superiority of the SSOR method was due to its more rapid convergence during the initial stages of the iteration process. For instance, with $\beta = 1.48$, the SOR method required 17 iterations to reach $E = 10^{-6}$ and a

further 19 to reach $E = 10^{-12}$. The corresponding numbers for the SSOR method are 12 and 18. Thus, below $E = 10^{-6}$, the rate of convergence of both methods was almost the same. This confirms the deductions made in section 2.2.5.

The distribution of the error for case 3 was investigated. It was found that it was composed of two slightly different fields corresponding to (i + j) odd and (i + j) even. Fig. 2.4c shows $\varepsilon_{ij}^{(16)}$ for the (i + j) odd points. This distribution suggests that, in Equation (2.26), $g(j,n_j) = f(j,n_j)$ and that f is given by Equation (2.15). Therefore it is not surprising that β_o was the same for the SOR and SSOR methods.

The efficiency of the SSOR method is reflected by the fact that $\| \varepsilon_{ij}^{(16)} \|$ for the SOR method was larger than that for the SSOR method (see Figs. 2.4b and 2.4c).

The relationship between E and AE for case 3 was investigated in the same way as for case 1a. The results are shown in Fig. 2.5. This shows that Equation (2.19) was applicable to the SSOR method.

For the SOR method it was found that β_o was independent of S'. However this was not so for the SSOR method.

Suppose that the gridpoints are labelled so that $0 <= i <= 13$ and $0 <= j <= 9$, and that $\vartheta = \pi/13$ and $\varphi = \pi/9$. When S' had the form $S' = \sin(r\vartheta i)\sin(s\varphi j)$, r and s integers, it was found that $\varepsilon_{ij}^{(n)} \propto S'$. Also β_o (C) could be predicted by using Equation (2.17) with τ given by

$$\tau = \frac{2}{4+b}\left[\cos(r\vartheta) + \cos(s\varphi)\right]$$

Therefore, it appears that β_o depends upon the wavelength composition of S'. For example, if r = s = 1 then

S x 10^{15}	$\beta_o(C)$
1	1.476
c(1ϑi)	1.379
c(2ϑi)	1.476
c(3ϑi)	1.379
c(1ϑi) c(1φj)	1.476
c(2ϑi) c(2φj)	1.476
c(1ϑi) c(2φj)	1.379
c(3ϑi) c(2φj)	1.379
c(4ϑi) c(2φj)	1.379
c(4ϑi) c(3φj)	1.476
(i-6.5)	1.379
(i-6.5)(j-4.5)	1.476

TABLE 2.4

$$c(2\vartheta i)\ c(2\varphi j) = \cos\left(2\,\frac{\pi}{13}\,i\right)\cos\left(2\,\frac{\pi}{9}\,j\right)$$

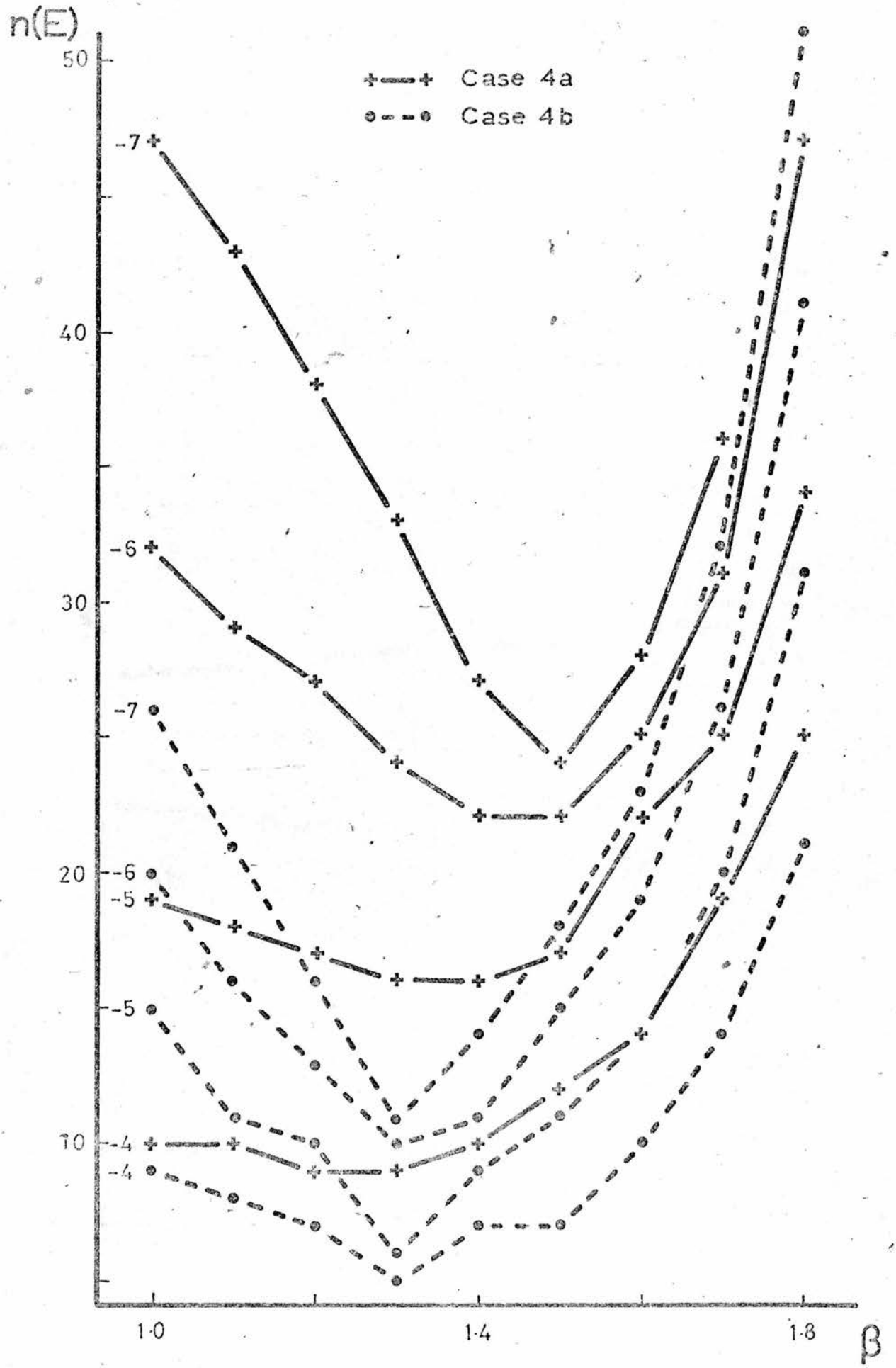

FIGURE 2·9

$\beta_o = 1.476$, whereas if $r = s = 2$ then $\beta_o = 1.259$.

The distributions of S' used above were special because the solution of Equation (2.27) was proportional to S'. Therefore distributions of S' were then used where this was not so. The results are shown in Table 2.4. These results imply that β_o is linked to the symmetry of either S' or ω. Therefore, some of the computations were repeated with $\omega = f(x, y)$ on the boundary; the symmetry of S' then remained while that of ω was destroyed. In these cases β_o always had a value of 1.476. Thus β_o is linked to the symmetry of ω. Where there is no symmetry, the value of β_o is given by Equation (2.17) and $\varepsilon_{ij}^{(q)}$ is

$$\varepsilon_{ij}^{(q)} = \gamma K^q \sin\left(\frac{\pi}{n_i - 1} i\right) \sin\left(\frac{\pi}{n_j - 1} j\right)$$

If real data is used there will be no symmetry and therefore β_o will be the same for the SSOR and SOR methods. But, if artificial data is used, it is possible that the value of β_o will be different for the two methods.

The effect of the use of artificial data on the constant E curves was also considered. The chosen distribution of S' was

$$S = 10^{-15} \times (i - 65)\ (j - 4.5) \qquad S' = \frac{S}{\sigma}\left[\frac{d}{m}\right]^2$$

For this, $\beta_o(C) = 1.476$. The distribution of $n(E)$ with β for both the SOR and SSOR methods is shown in Fig. 2.9 (cases 4a and 4b). A comparison of this figure with Fig. 2.1 shows that the artificial data produced an exaggerated view of the superiority of the SSOR method.

The investigations using artificial data show that great care must be taken in interpreting the results when this type of data is used.

2.3.3 The SOR Method For Solving A Helmholtz Equation With Neumann Boundary Conditions

Equation (2.27) was solved with Neumann boundary conditions using the same data as in case 1a. Whenever this type of boundary condition was used, it took the form of $\frac{\partial \omega}{\partial n} = 0$ and the initial guess was $\omega = 0$. The solution of Equation (2.27) under these conditions is shown in Fig. 2.12a.

The computations were made with the gridpoints ordered in the two ways illustrated below.

A

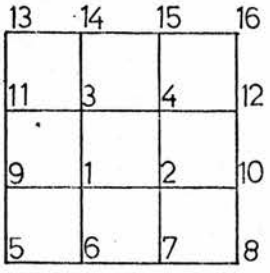

B

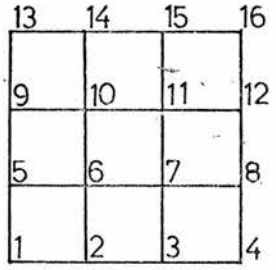

The variation of n(E) with β for both schemes A and B (cases 5a and 5b) is shown in Fig. 2.10. This shows that the constant E curves are almost identical for both schemes. Also the distributions of the error are similar (see Figs. 2.12b and 2.13a) and the slight differences are easily explained when the ordering of the gridpoints is examined.

The above results show that there is little to choose between schemes A and B. But, it was thought desirable to have a scheme for which an analytical expression for the error could be found. Thus scheme B was used in all subsequent computations. The distribution of the error will be discussed later.

Fig. 2.11 shows the distribution of n(E) with β for a large range of β (this is also case 5b). This indicates that the SOR method was much more efficient than the Gauss-

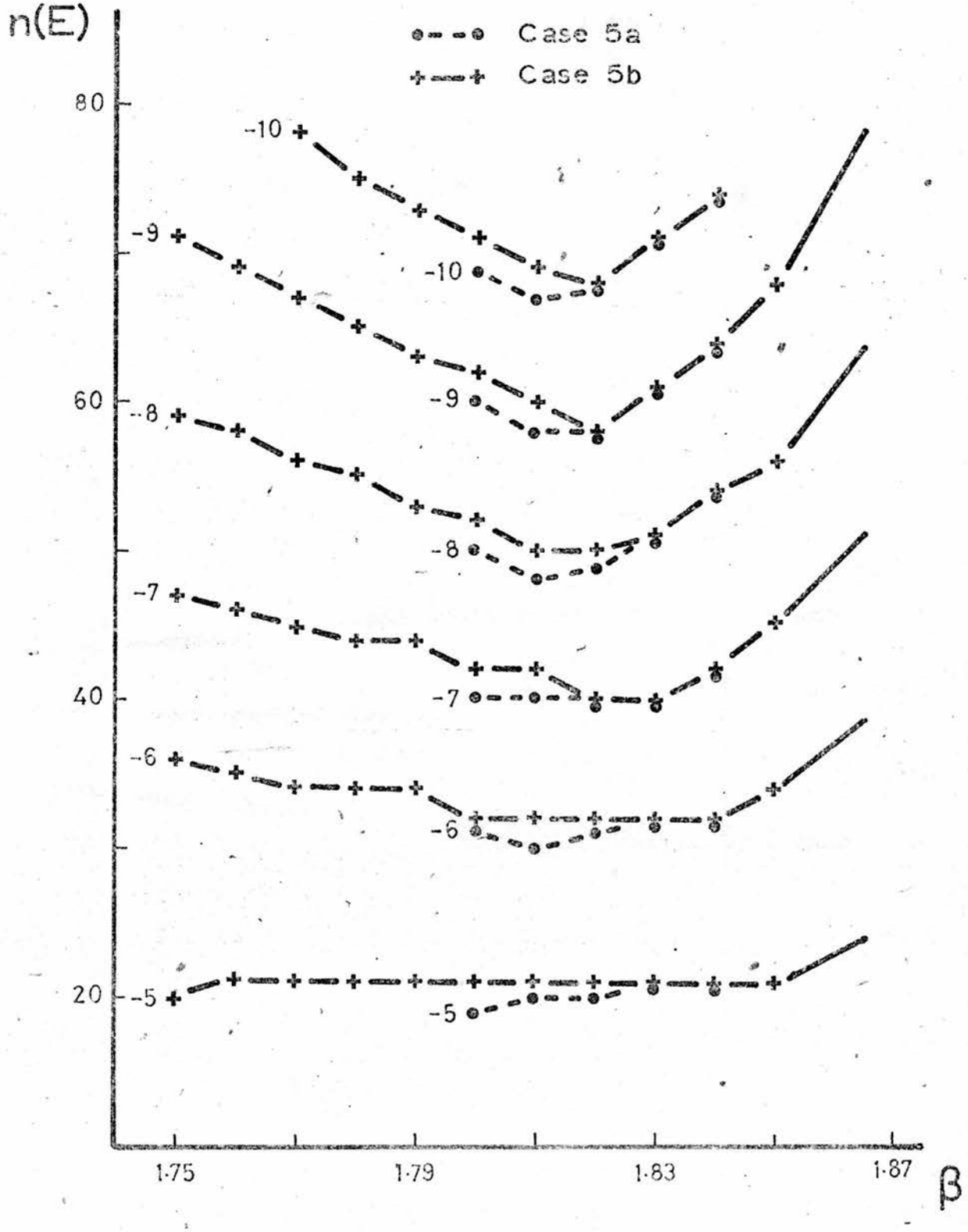

FIGURE 2·10

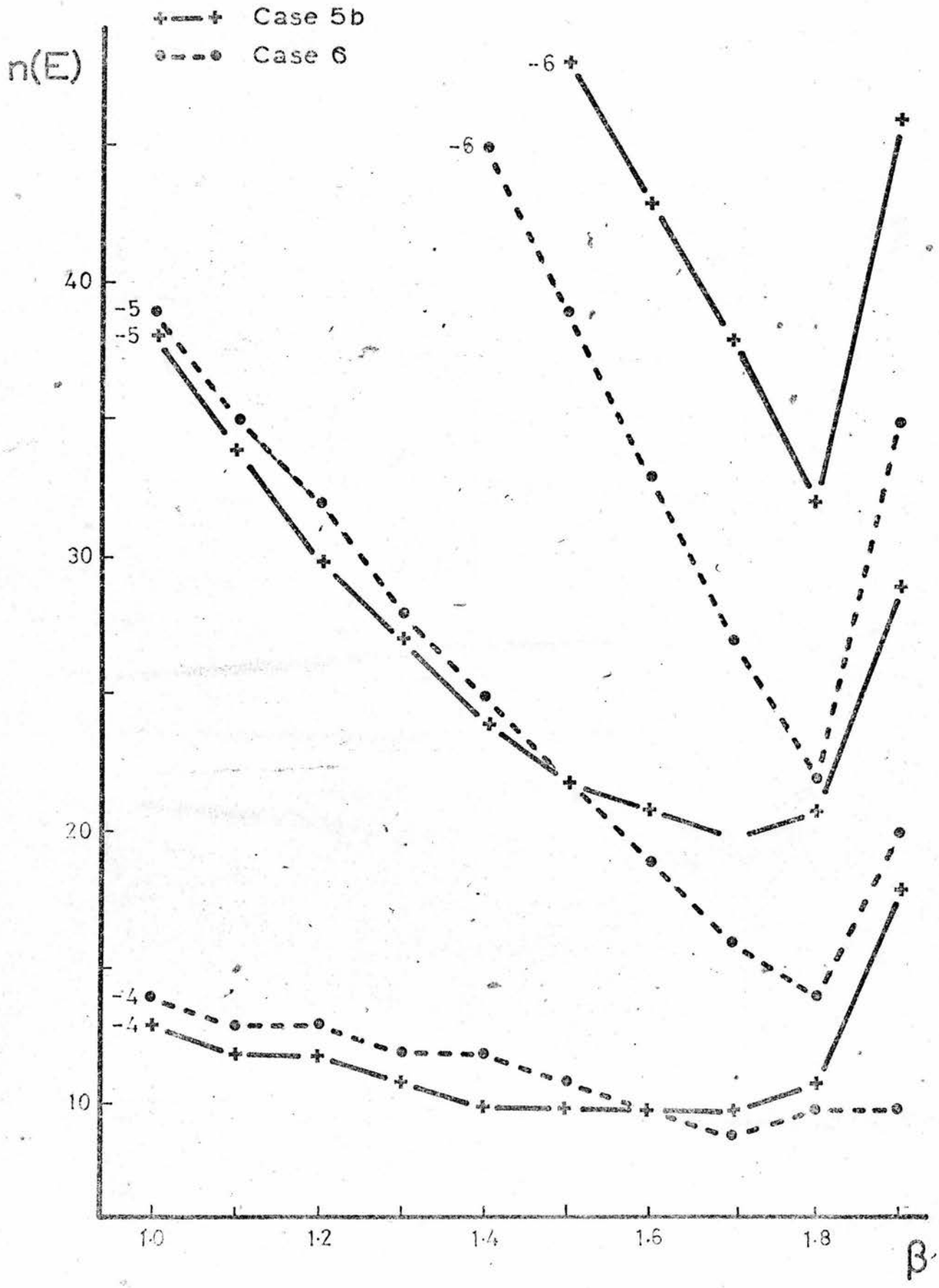

FIGURE 2·11

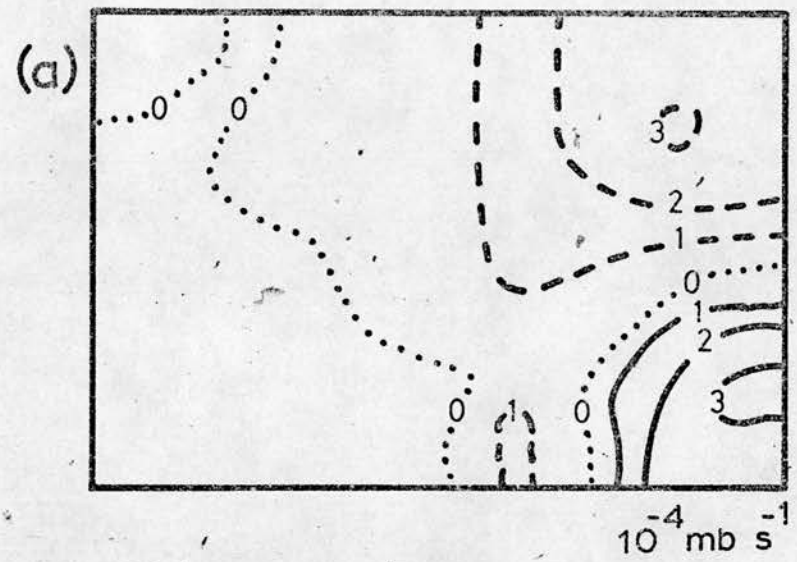

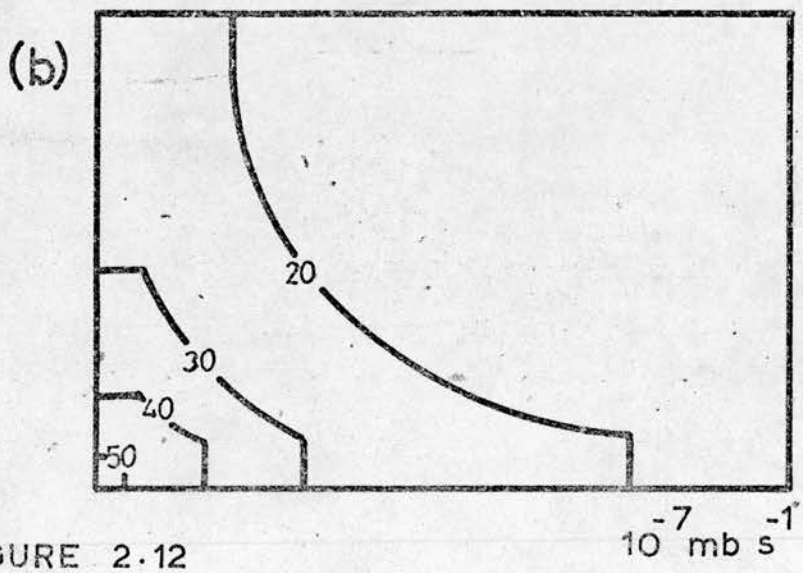

FIGURE 2·12

(a) Solution of Equ.(2·27) with $\left(\frac{\partial \omega}{\partial n}\right)_b = 0$

(b) $\varepsilon_{ij}^{(37)}$, $\beta = 1{\cdot}7$, case 5a (SOR, scheme A)

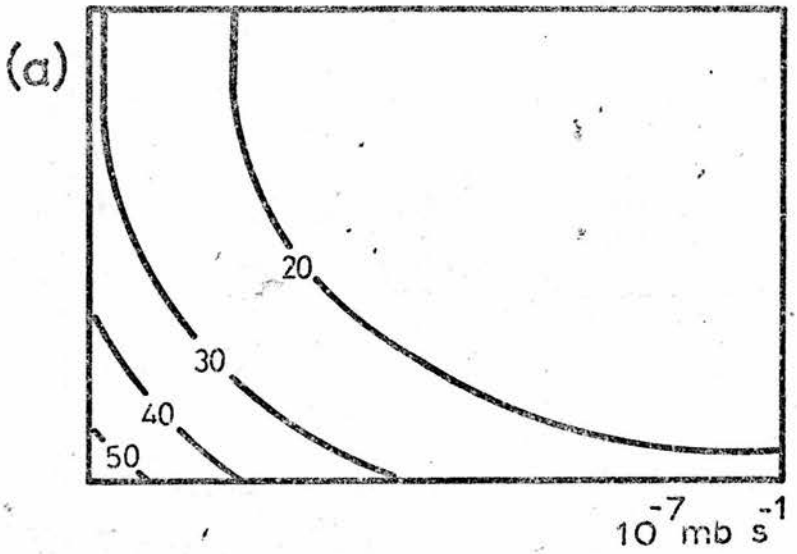

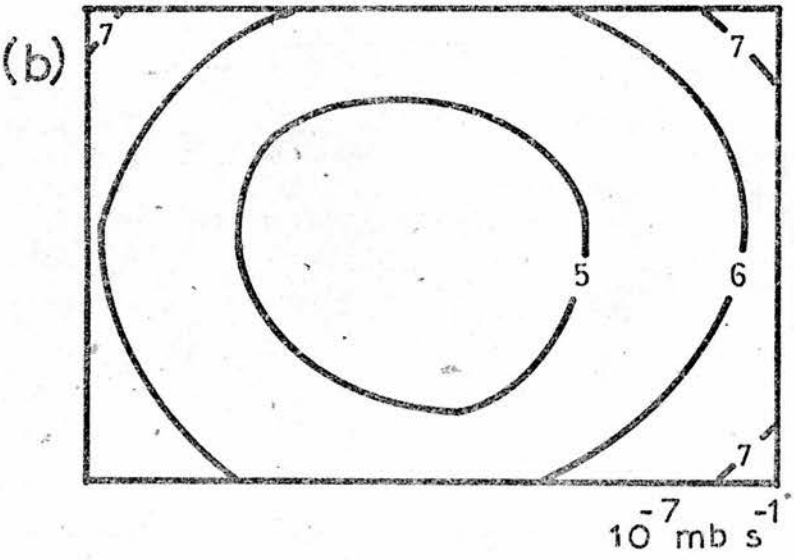

FIGURE 2·13

(a) $\varepsilon_{ij}^{(37)}$, $\beta = 1{\cdot}7$, case 5b (SOR, scheme B)

(b) $\varepsilon_{ij}^{(37)}$, $(i+j)$ odd, $\beta = 1{\cdot}7$, case 6 (SSOR, scheme B)

Seidel method. It also shows that it is advantageous to know β_o accurately (if there is one). For instance, when $E = 10^{-6}$ the use of $\beta = 1.4$ instead of $\beta = 1.8$ increases the number of iterations by about 60%.

Both Figs. 2.10 and 2.11 show that the optimum value of β became better defined as E decreased. For example, Fig. 2.10 shows that if $\beta = 1.77$ is used in place of $\beta = 1.82$ the number of iterations for $E = 10^{-10}$ is increased by ten. For $E = 10^{-6}$ the increase is only two. Thus care must be taken in choosing β if E is small.

When β_o (C) was calculated it was found that it oscillated, and that it tended to approach the value of β that was being used. Therefore it is not clear how much, if any, of the Young-Frankel theory applies to equations with Neumann boundary conditions. However if $\beta_o(E) = 1.82$ is used in Equation (2.8) it is found that $N_o \approx 11.5$. This corresponds well with the experimental value of N_o (see Fig. 2.10).

The only difference between cases 1a and 5b is the type of boundary condition used. When Dirichlet boundary conditions were used N_o was about 3. The corresponding value for the Neumann boundary conditions was about 11. Thus in this particular situation, the use of Neumann boundary conditions involved nearly four times the number of iterations than when Dirichlet boundary conditions were used. Therefore Dirichlet boundary conditions should be used whenever possible.

It has already been shown that it would be useful to be able to calculate β_o. An ideal method would be one that is similar to that proposed by Miyakoda (1960). He

suggested that $\varepsilon_{ij}^{(n)}$ is given by Equation (2.14) with $f(i, n_i) = \cos\left[\frac{\pi}{n_i - 2} + \delta\right]$. This was then used to derive a set of formulae for β_o. He showed that Equation (2.17) could be used with τ given by

$$\tau = \frac{2}{4+b}\left[\cos\left(\frac{\pi}{n_i - 2}\right) + \cos\left(\frac{\pi}{n_j - 2}\right)\right]$$

Using $b = 8.87 \times 10^{-2}$, $n_i = 14$ and $n_j = 10$, these equations give $\beta_o = 1.46$. This is clearly incorrect and the reason is that Miyakoda did not use the correct $f(i, n_i)$.

The distribution of $\varepsilon_{ij}^{(n)}$ was calculated and the results are shown in Fig. 2.13a. This indicates that $f(i, n_i)$ has the form

$$f(i, n_i) = \cosh(\vartheta i) \qquad (2.29)$$

Unfortunately ϑ is not known. However it is expected that ϑ depends upon the number of gridpoints and therefore it might have the form

$$\vartheta = \frac{\vartheta'}{n_i - 1} \qquad (2.30)$$

The value of ϑ' must be found by experiment.

It can be shown that if f is given by Equation (2.29) with the above ϑ, then τ becomes

$$\tau = \frac{2}{4+b}\left[\cosh\left(\frac{\vartheta'}{n_i - 1}\right) + \cosh\left(\frac{\vartheta'}{n_j - 1}\right)\right] \qquad (2.31)$$

By experiment $\beta_o(E) = 1.82$ and therefore the equations can be used in reverse to give ϑ'. It was found that $\vartheta' = 1.94$ and therefore an approximate expression for f is

$$f(i, n_i) = \cosh\left(\frac{2}{n_i - 1} i\right)$$

It was then necessary to test if ϑ' was equal to 2.0 for all values of n_i. An indirect method was used because a large number of iterations would be needed to find $\beta_o(E)$

for given values of n_i and n_j.

For convergence $\tau < 1$. Thus if $\vartheta' = 2.0$ and $n_i = n_j$ the condition for convergence is

$$\cosh\left(\frac{2}{n_i - 1}\right) < \frac{4 + b}{4} \qquad (2.32)$$

Therefore there will only be convergence if $n_i > 11$. When $n_i < 11$ was used it was possible to get a convergent solution. Thus either $\vartheta' = 2.0$ or f is not given by Equation (2.29). The distribution of $\varepsilon_{ij}^{(n)}$ was computed for each n_i and this showed that f was a coshine function. Therefore $\vartheta' \neq 2.0$ and, what is more, ϑ' must be a function of n_i. These results show that there is no justification in supposing that ϑ is related to n_i by Equation (2.30).

The distribution of $\varepsilon_{ij}^{(n)}$ was computed for different distributions of S'. In each case f was given by Equation (2.29).

The above results imply that for the Helmholtz equation, the distribution of $\varepsilon_{ij}^{(n)}$ is always given by Equation (2.14) with Equation (2.29).

Some insight into why it is difficult to deal with Neumann boundary conditions may be gained by considering the distribution of $\varepsilon_{ij}^{(n)}$ in the form

$$\varepsilon_{ij}^{(n)} = A^{i+j+2n} \cosh(\vartheta_1 i) \cosh(\vartheta_2 j)$$

Here ϑ_1 and ϑ_2 are not necessarily the same. Fig. 2.13a shows that at $i = n_i - 1$ and $j = n_j - 1$, $\frac{\partial \varepsilon_{ij}^{(n)}}{\partial i} = \frac{\partial \varepsilon_{ij}^{(n)}}{\partial j} = 0$

From the first of these it is found that at $i = n_i - 1$

$$\ln\left(\frac{1}{A}\right) = \vartheta_1 \sinh\left[(n_i - 1)\vartheta_1\right] \Big/ \cosh\left[(n_i - 1)\vartheta_1\right]$$

Thus ϑ_1 is determined by A and hence ϑ_1 depends upon β. The same is true for ϑ_2. Therefore both ϑ_1 and ϑ_2 depend upon β, n_i and n_j. Thus it appears impossible to derive a set of equations (similar to Equation

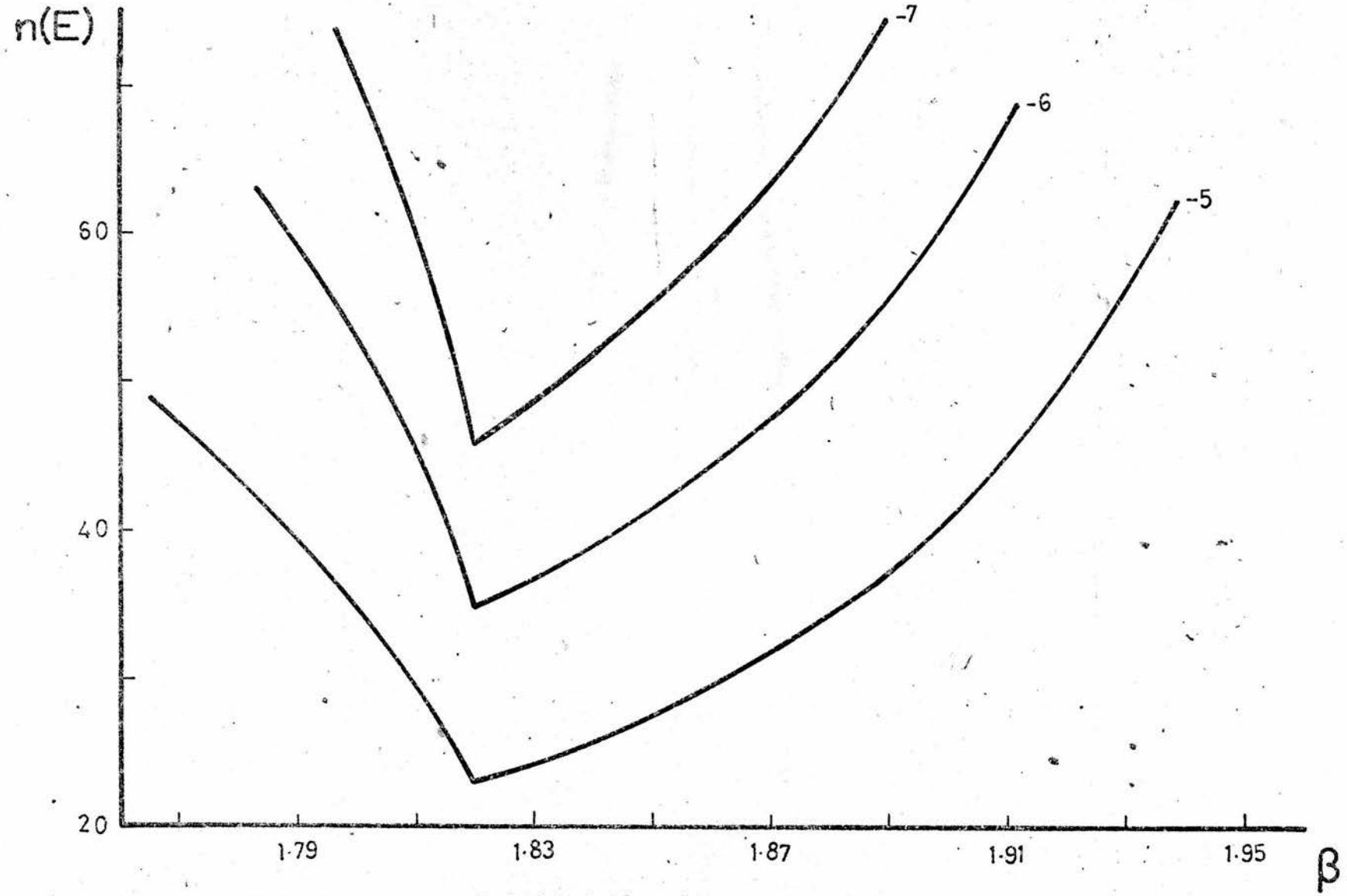

FIGURE 2.14 Equ.(2.28) with $\gamma = 1$ for case 5b

(2.17)) that will give β_o for Neumann boundary conditions.

Equation (2.28) was used to derive a set of curves similar to those in Fig. 2.6. These curves are shown in Fig. 2.14. Figs. 2.6 and 2.14 show that it is undesirable to underestimate β_o for both types of boundary conditions. For Neumann boundary conditions it is also unwise to overestimate β_o by very much.

2.3.4 The SSOR Method For Solving A Helmholtz Equation With Neumann Boundary Conditions

Case 6 is a repetition of case 5b but the SSOR method was used in place of the SOR method. Fig. 2.11 shows the distribution of n(E) with β for both cases. This indicates that $\beta_o(E)$ was approximately the same for both methods.

It also shows that for the smallest E considered ($E = 10^{-6}$) the SSOR method required the smallest number of iterations. This was not so for $E = 10^{-5}$, but it is significant that in the region of $\beta_o(E)$, the SSOR method was always superior.

A detailed study of the constant E curves in the vicinity of $\beta_o(E)$ was also undertaken for case 6. The results are exhibited in Fig. 2.15. The corresponding results for the SOR method are shown in Fig. 2.10. A comparison of these figures reveals that, in the vicinity of $\beta_o(E)$ with $E < 10^{-5}$, the SSOR method required about 10 iterations less than the SOR method. Also it was found that for $E < 10^{-5}$, the experimental value of N_o is almost the same for both methods. Thus the superiority of the SSOR method is due to the rapid convergence in its initial stages. This is also true when Dirichlet boundary conditions are used (see section 2.3.2).

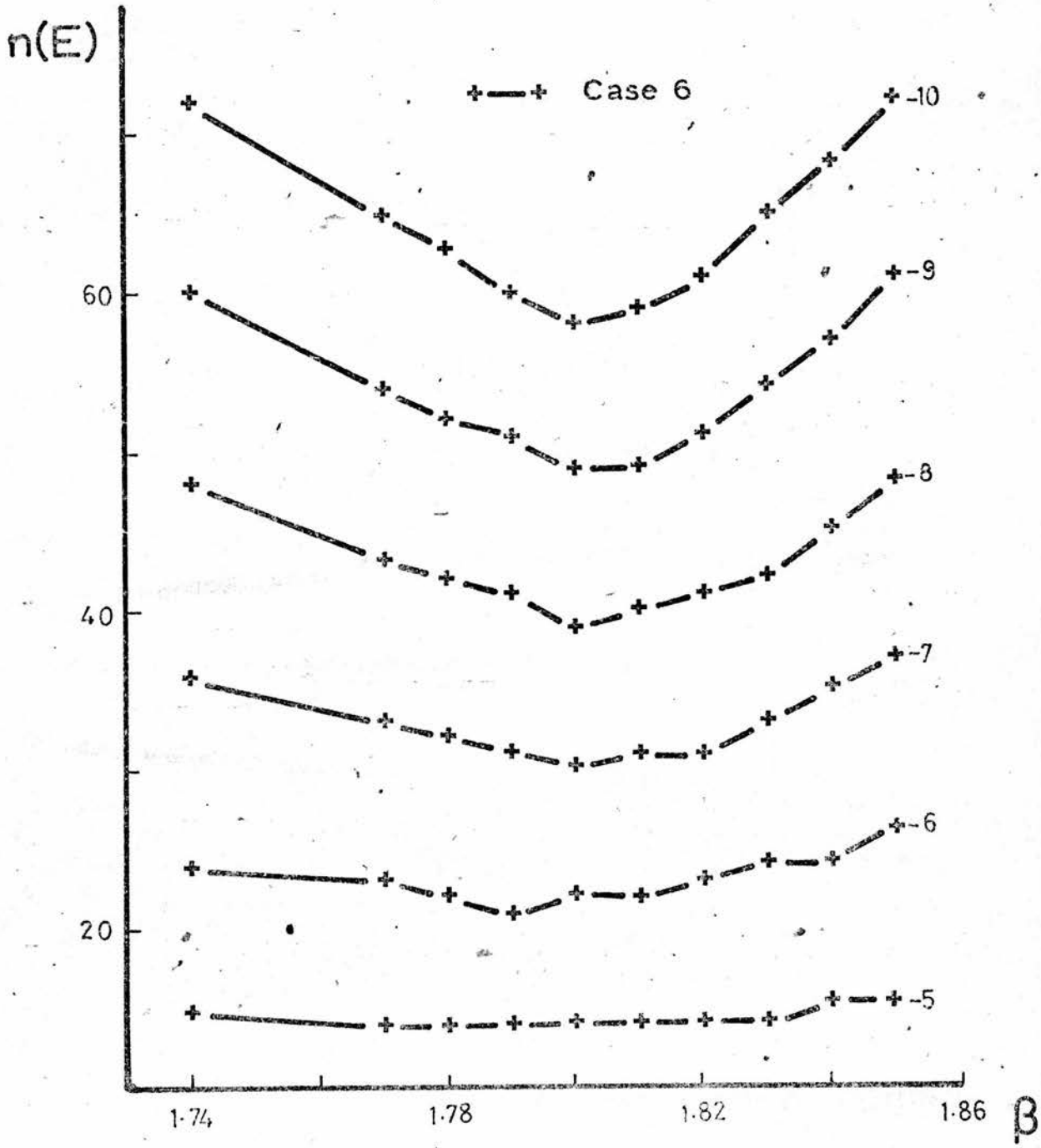

FIGURE 2·15

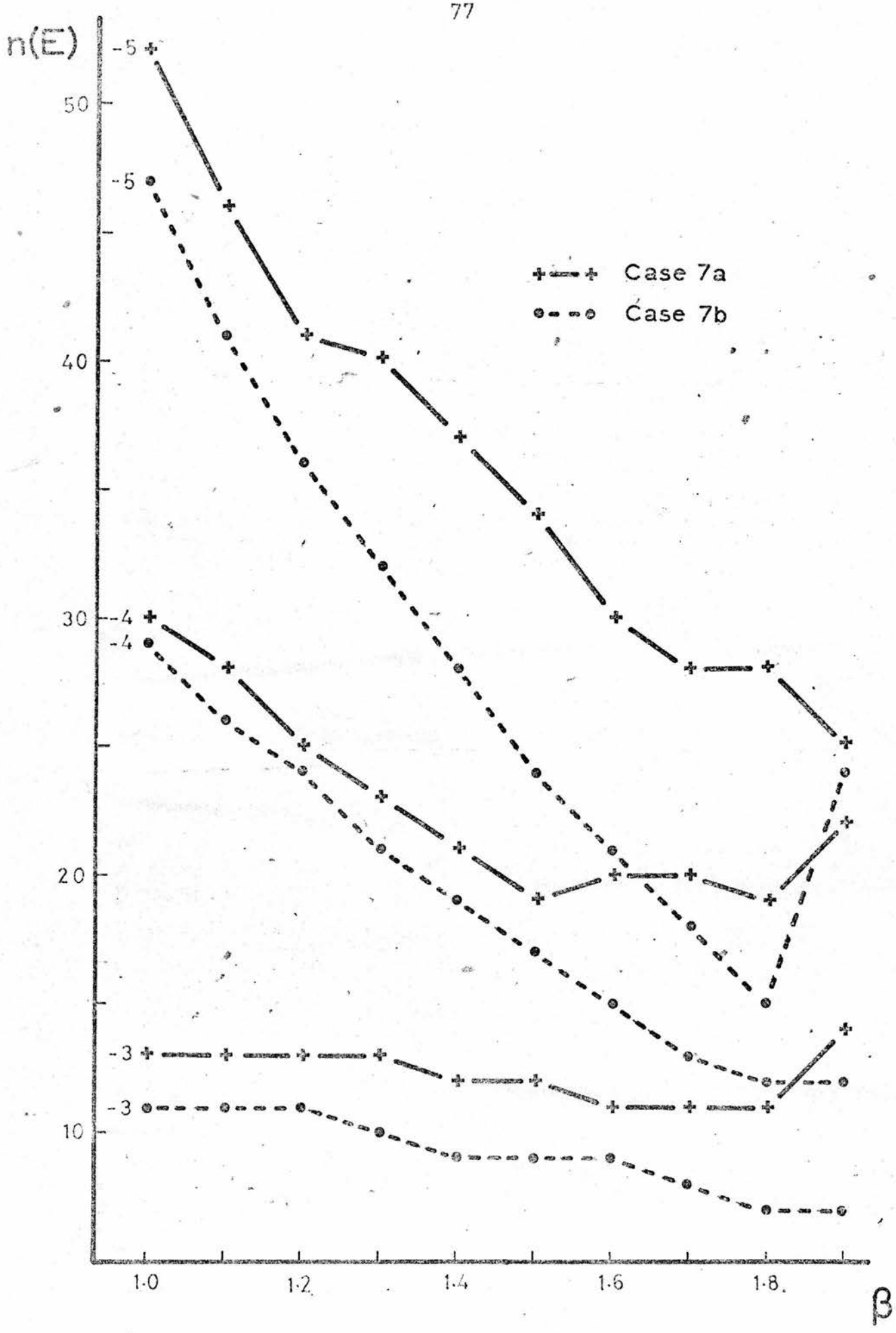

FIGURE 2·16

The values of $\beta_o(E)$ for cases 5b and 6 were 1.82 and 1.80 respectively. It is not clear if the difference between these is significant. But, even if β_o is not exactly the same for both methods, it appears that the optimum values of β are in the same region.

When $\varepsilon_{ij}^{(n)}$ was computed for case 6 it was found that it consisted of two fields. Fig. 2.13b shows $\varepsilon_{ij}^{(37)}$ for (i + j) odd. A superficial examination of this suggests that

$$\varepsilon_{ij}^{(n)} \propto 1 + \cos\left(\frac{2\pi i}{n_i - 1}\right)\cos\left(\frac{2\pi j}{n_j - 1}\right)$$

Since it was not possible to use $\varepsilon_{ij}^{(n)}$ to find β_o for case 5b (see section 2.3.3) a further analysis of the exact form of $\varepsilon_{ij}^{(n)}$ seemed unnecessary.

The effect of using artificial data was also investigated. This was difficult because Carré's method could not be used to calculate β_o. However a qualitative assessment was carried out by computing $\varepsilon_{ij}^{(n)}$ for different forms of S. Once again it was found that the symmetry of the solution sometimes affected $\varepsilon_{ij}^{(n)}$ and thus presumably affected β_o. When there was no symmetry, $\varepsilon_{ij}^{(n)}$ was always composed of two fields of the kind illustrated in Fig. 2.13b.

Finally the distribution of n(E) with β for the data used in cases 4a and 4b was computed. The computations will be referred to as cases 7a and 7b depending upon whether the SOR or the SSOR method was used.

The distribution of $\varepsilon_{ij}^{(n)}$ for cases 7a and 7b were similar to that derived for real data (see cases 5b and 6).

The constant E curves for cases 7a and 7b are exhibited in Fig. 2.16. These have a similar shape to those found

in Fig. 2.11. In particular, Figs. 2.11 and 2.16 show that for both methods, using either type of data, $\beta_o(E)$ was in the vicinity of 1.8. Although the resolution of β was not very good, the results for cases 7a and 7b reinforce the idea that β_o is almost the same for both the SOR and the SSOR methods.

2.4 The Overrelaxation Method For Solving A Poisson Equation And The Determination of β_o

If X and Ψ_t (or Φ_t) are to be calculated from the continuity equation and vorticity equation then it is necessary to solve Poisson type equations. Also it is often necessary to solve this type of equation when solving the balance equation.

In the following sections the determination of β_o for the SOR and the SSOR methods will be considered. Also both types of boundary conditions will be used.

When a Poisson equation is solved with Neumann boundary conditions a consistency condition must be satisfied. Suppose the Poisson equation is written as

$$\nabla^2 X = S \qquad (2.33)$$

It can be shown that if $\frac{\partial X}{\partial n} = f(x, y)$ on the boundary (C), then the integral of Equation (2.33) over the area (A) gives

$$\oint_C f(x, y)\, ds = \iint_A S\, dA$$

In particular, if $f(x, y) = 0$ then the integral of S over the area considered must be zero. This is the consistency condition. If this constraint is not satisfied then the overrelaxation method will not give a convergent solution. Thus to ensure consistency, artificial data was used for $\hat{S}$.

For convenience, the same distribution of S was used when the Dirichlet boundary conditions were used.

The continuity equation was used as an example of a Poisson equation. Thus S in Equation (2.33) corresponds to the divergence which has an order of magnitude of 10^{-7} s^{-1}. In the following four section E has units of $m^{2} s^{-1}$.

2.4.1 The SOR Method For Solving A Poisson Equation with Dirichlet Boundary Conditions

If b = 0 then Equation (2.27) becomes a Poisson equation. Therefore by using b = 0, Equation (2.17) can be used to find β_o (M) for a Poisson equation with Dirichlet boundary conditions.

Equation (2.33) was solved with $n_i = 14$ and $n_j = 10$ and with

$$S = 10^{-7} \times (i - 6.5) \qquad (2.34)$$

This will be referred to as case 8a. It was found that β_o (M) = β_o (C) = 1.544 and that β_o (E) = 1.55 (see Fig. 2.17). This figure also shows that the shapes of the constant E curves are the same as for case 1a.

2.4.2 The SSOR Method Of Solving A Poisson Equation With Dirichlet Boundary Conditions

It was found that the symmetry of the solution of the equation affected the error, and hence β_o, in the same way as for the Helmholtz equation. This is illustrated by the results from the repetition of case 8a with the SSOR method (case 8b). It was found that $\beta_o(C) = 1.420$, and that the value of $\beta_o(M)$ derived from $\varepsilon_{ij}^{(n)}$ was the same as $\beta_o(C)$.

The distribution of n(E) with β for cases 8a and 8b

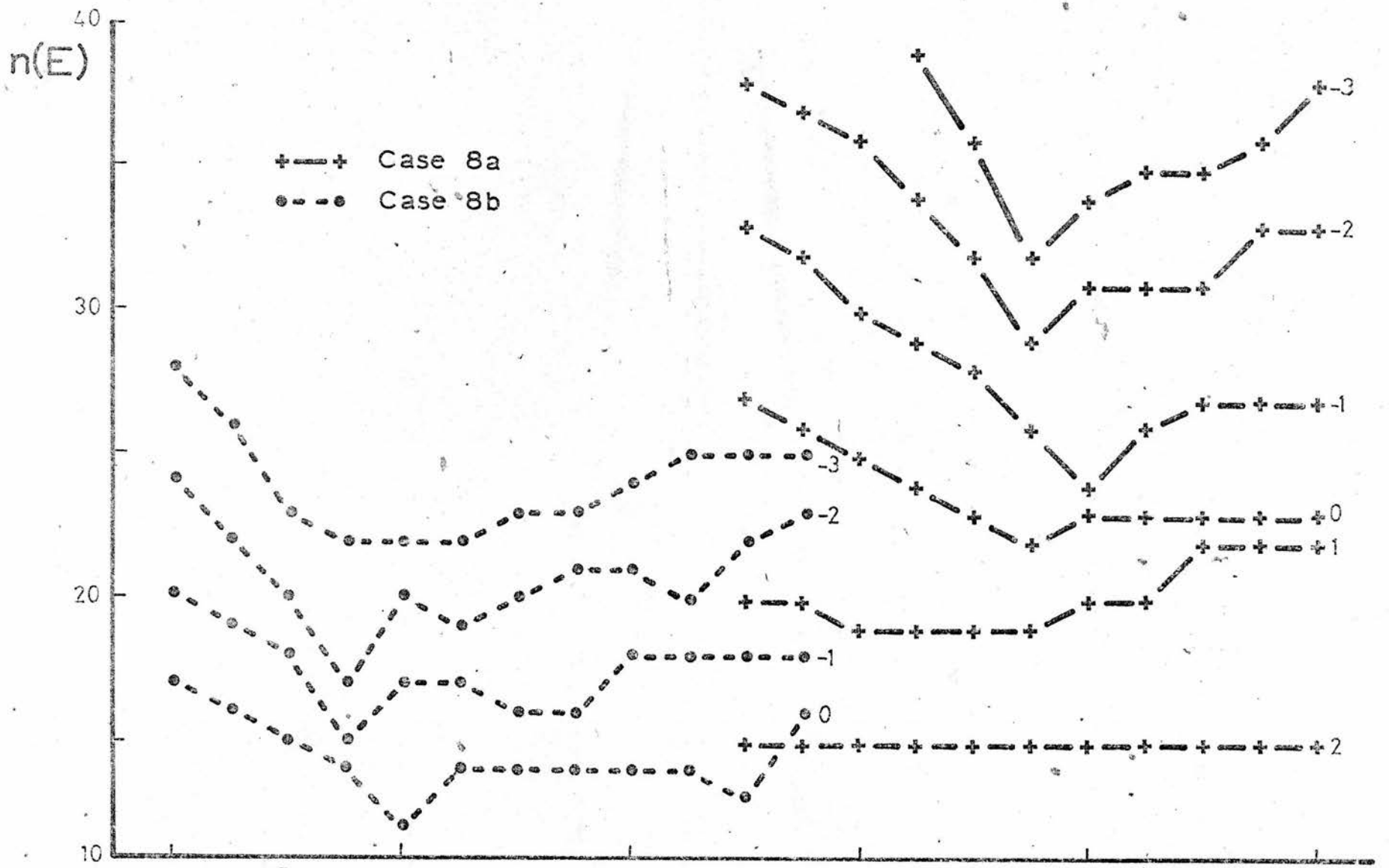
n(E)
40
30
20
10
Case 8a
Case 8b
-3
-2
-1
0
1
2
1·40
1·48
1·56
β
$\beta_o(C)$
$\beta_o(C)$

FIGURE 2·17

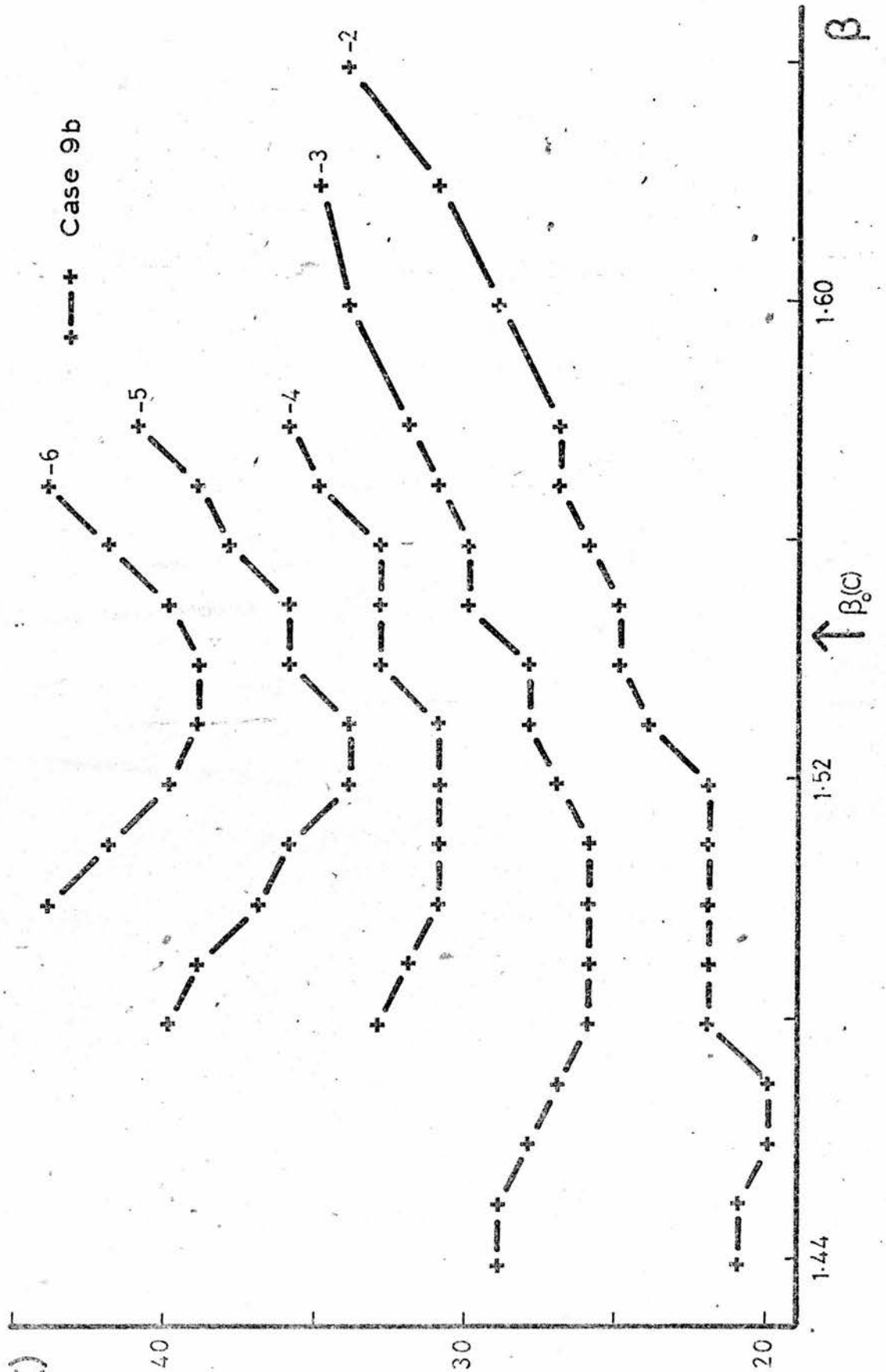

FIGURE 2.18

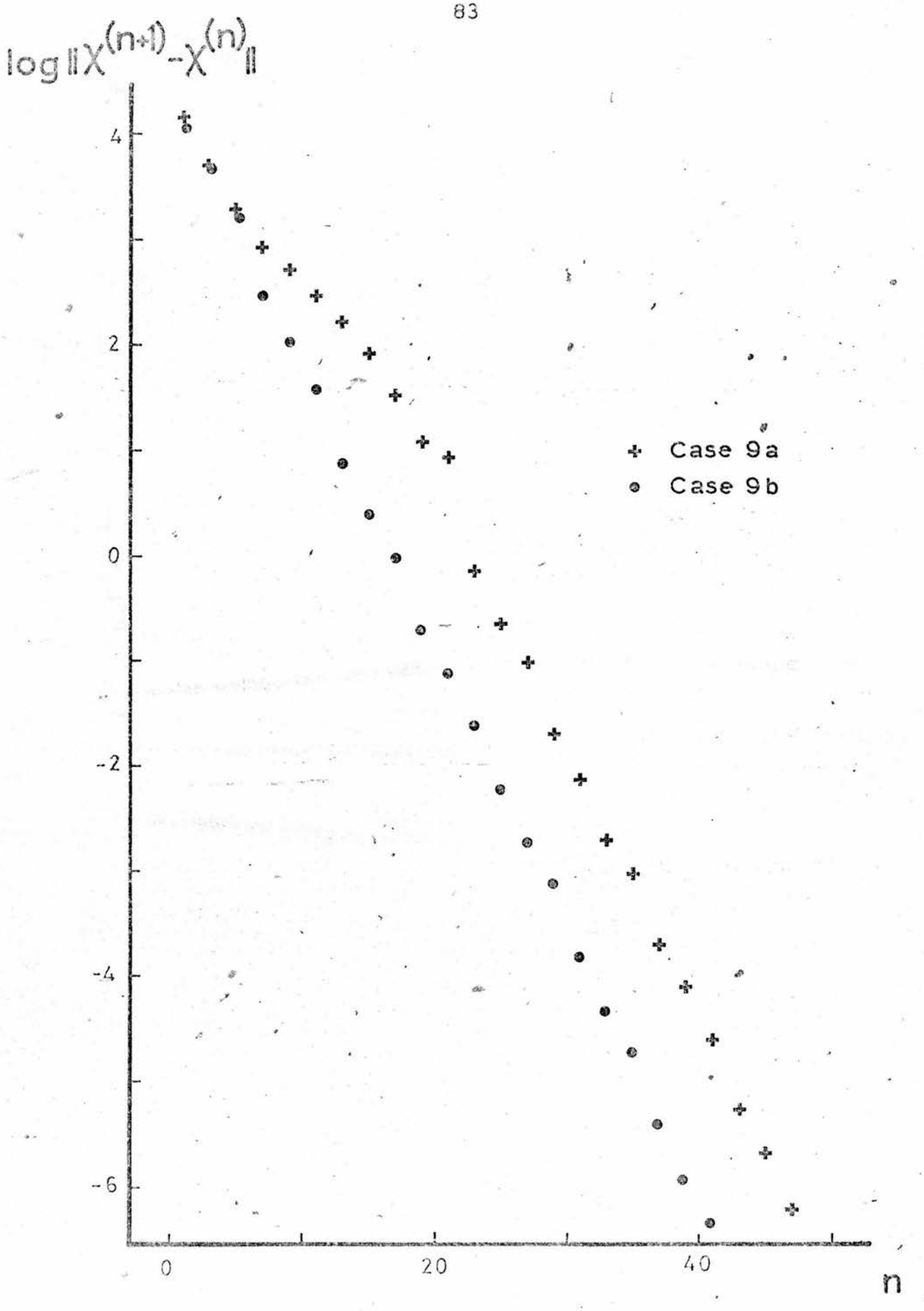

FIGURE 2·19

is shown in Fig. 2.17. This shows that the SSOR method was the most efficient. However this is to be expected because case 8b had a smaller value of β_o than did case 8a.

The SSOR method was used to solve the Poisson equation with

$$S = 10^{-7} \times (i - 6.5) \times (j - 45) \qquad (2.35)$$

This will be referred to as case 9b. It was found that $\beta_o(C) = 1.544$ which was the same as for the SOR method. The distribution of n (E) with β is shown in Fig. 2.18. This shows that when E is large the value $\beta_o(E)$ is much less than $\beta_o(C)$. However this may be of no special significance because this type of behaviour (although on a lesser scale) can be seen in Fig. 2.3.

Since, with this particular S, β_o was the same for both methods, it was expected that their rates of convergence would be the same, when $\beta = \beta_o$ was used. This was checked by plotting log E against n for both methods (with $E = \|\chi^{(n+1)} - \chi^{(n)}\|$). The results are shown in Fig. 2.19, and this illustrates the fact that the SSOR method is more efficient than the SOR method.

Fig. 2.19 also shows that after a sufficient number of iterations, the rate of convergence for both methods is the same. However, the SSOR method achieved this maximum rate of convergence almost immediately, whilst the SOR method achieved it after about 12 iterations. Thus, the SSOR method is superior to the SOR method due to its rapid rate of convergence during the initial stages of the iteration proceedure.

Since $\beta = \beta_o$ was used in the above computations, the

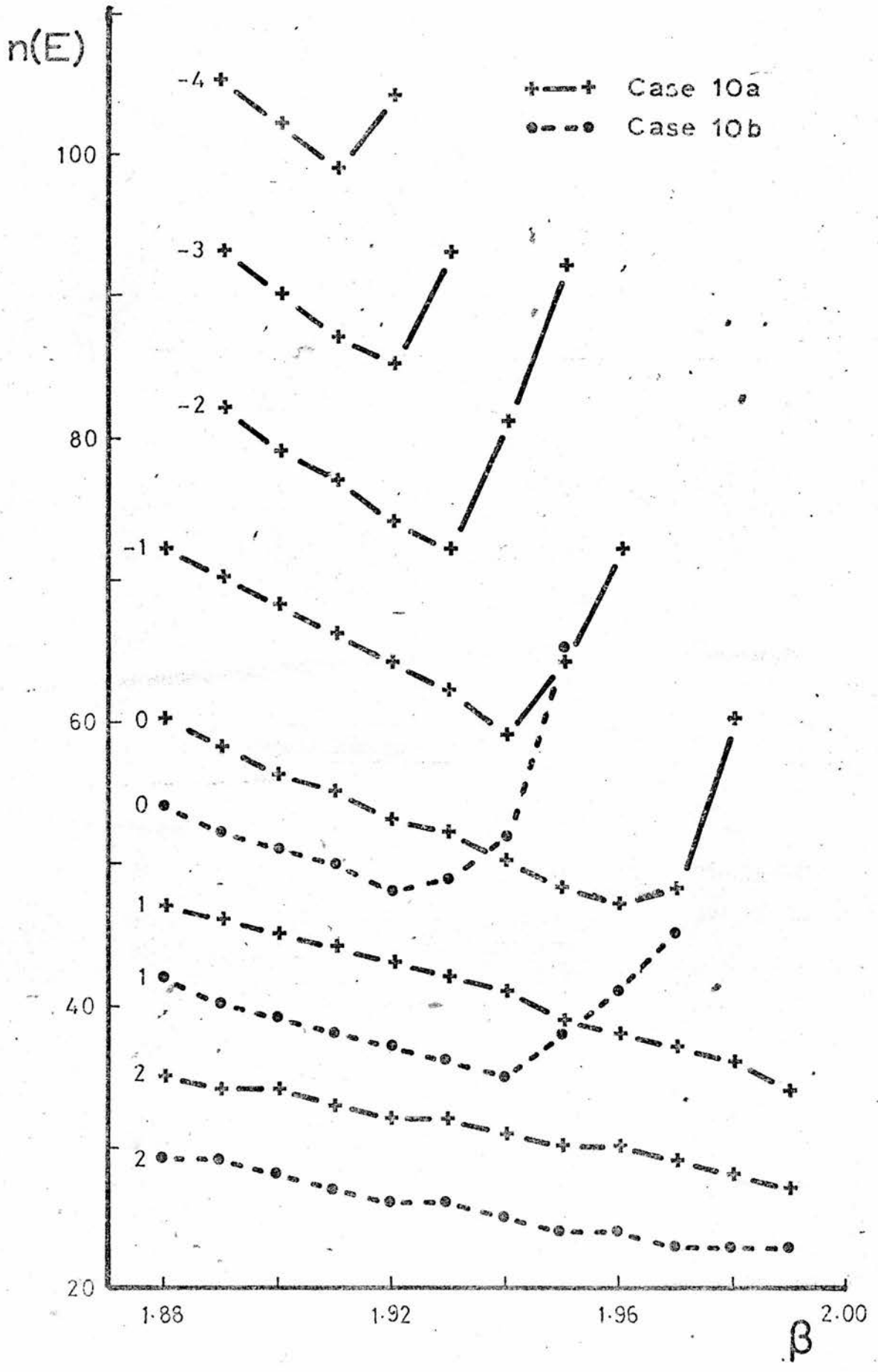
n(E)
Case 10a
Case 10b
-4
-3
-2
-1
0
0
1
1
2
2
100
80
60
40
20
1·88
1·92
1·96
2·00
β

FIGURE 2·20

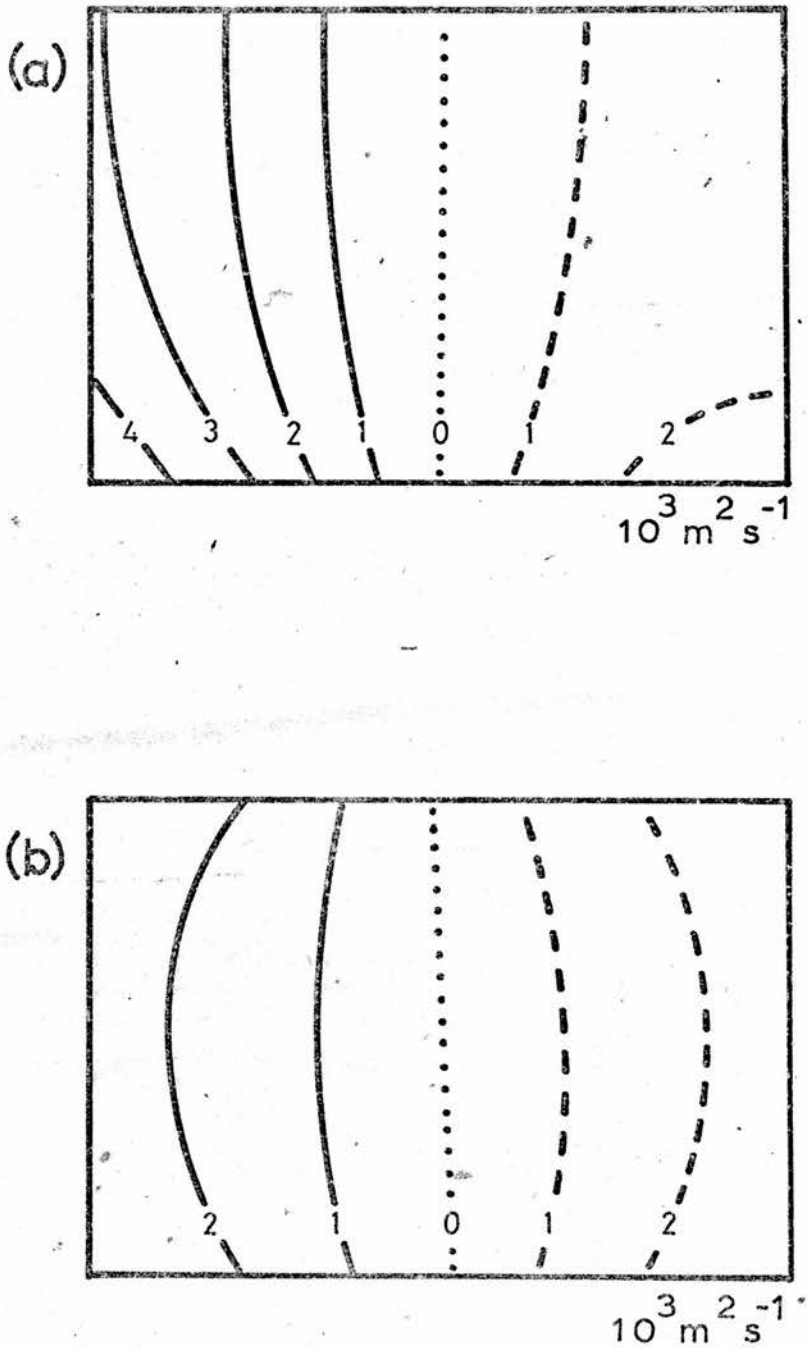

FIGURE 2·21

(a) $\varepsilon_{ij}^{(31)}$, $\beta = 1{\cdot}7$, case 10a (SOR)

(b) $\varepsilon_{ij}^{(31)}$, $(i+j)$ odd, $\beta = 1{\cdot}7$, case 10b (SSOR)

value of N_o can be calculated, and it was found to be 3.8. The experimental value of N_o can be found by calculating the number of iterations required to reduce $\log \| \chi^{(n+1)} - \chi^{(n)} \|$ by one. It also had a value of 3.8.

Finally, when $\beta_o(C)$ was calculated for complicated (i.e. non-symmetric) distributions of S it was found that β_o was the same as for the SOR method.

2.4.3. The SOR Method For Solving A Poisson Equation With Neumann Boundary Conditions

Case 8a was repeated using Neumann boundary conditions (case 10a). The results are shown in Fig. 2.20.

Fig. 2.20 indicates that there may not be an optimum value of β that is independent of E. If this is so, a possible explanation may be that the consistency condition was not satisfied. The reason for this supposition is that the normal derivative of $\varepsilon_{ij}^{(n)}$ on some of the boundaries is not zero (see Fig. 2.21a). This implies that $\frac{\partial \omega}{\partial n} \neq 0$ everywhere and thus having the average of S equal to zero is not sufficient to fulfill the consistency condition.

The results of cases 10a and 8a (Figs. 2.20 and 2.17) show that far more iterations were required to solve the equation with Neumann boundary conditions than with Dirichlet boundary conditions. Thus the latter boundary condition should be used where possible.

A further examination of $\varepsilon_{ij}^{(n)}$ (see Fig. 2.21a) shows that

$$\varepsilon_{ij}^{(n)} \propto \cos\left(\frac{\pi}{n_i - 1} i\right) \cosh(\vartheta j) \qquad (2.36)$$

This has a different form to that for the Helmholtz equation. The reason is that if $\varepsilon_{ij}^{(n)}$ was similar to that for the

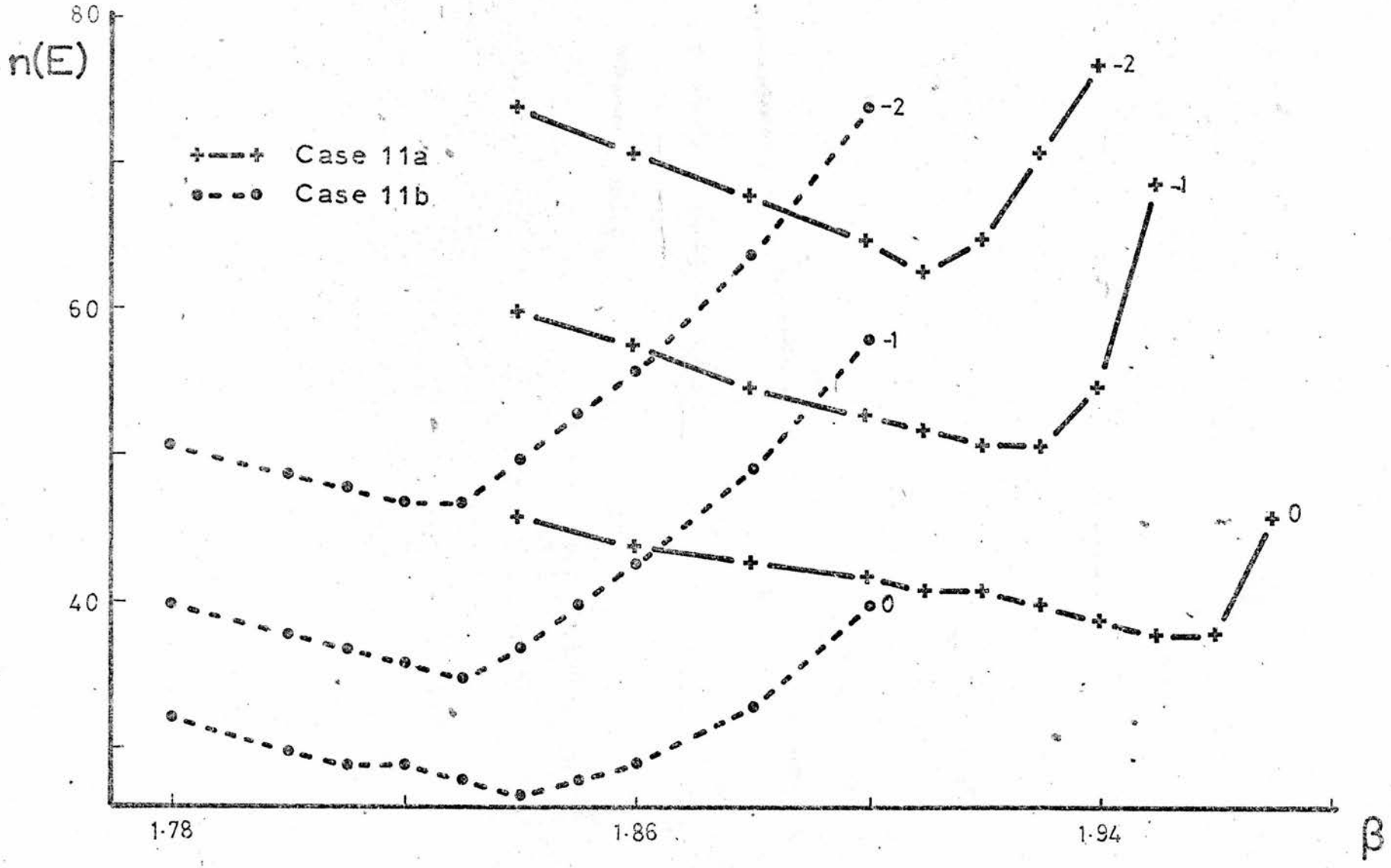

FIGURE 2·22

Helmholtz equation then $\tau > 1$ for all ϑ . Therefore there would not be convergence.

It was unfortunate that in case 10a the distribution of S in the i direction was similar to cos ($\frac{\pi}{n_i - 1}$ i). Therefore the validity of Equation (2.36) was tested by computing the error for distributions of S where this was not so. Equation (2.36) was true in all cases.

The constant E curves were also derived for

$$S = 10^{-7} \times (j - 4.5) \qquad (2.37)$$

This will be referred to as case 11a and the results are shown in Fig. 2.2 2. As in case 10a there did not appear to be a unique value of β_o. Also, a comparison of Figs. 2.20 and 2.22 shows that the constant E curves have the same shape for both cases. Thus the results for cases 10a and 11a are very similar. This implies that these results are characteristic of the results to be expected when more complicated distributions of S are used.

2.4.4 The SSOR Method Of Solving A Poisson Equation With Neumann Boundary Conditions

Cases 10a and 11a were repeated using the SSOR method (cases 10b and 11b). The results are illustrated in Figs. 2.20 and 2.22. These show that the constant E curves are similar in shape for both the SSOR and SOR methods. They also show that $\beta_o(E)$ varies with E for both methods.

Fig. 2.20 shows that, for cases 10a and 10b, the SSOR method was no more efficient than the SOR method. Also, the constant E curves for case 10b were displaced towards low β , and the displacement decreased as E decreased.

The distribution of $\varepsilon_{ij}^{(31)}$ was computed for case 10b

(see Fig. 2.21b). It was found that to a good approximation

$$\varepsilon_{ij}^{(n)} \propto 1 + \cos\left(\frac{\pi}{n_i-1} i\right)\cos\left(\frac{2\pi}{n_j-1} j\right)$$

Once again it was not possible to use this to find $\beta_o(M)$.

When S was given by Equation (2.37) the SSOR method was appreciably more efficient than the SOR method. However the constant E curves for the SSOR method were still displaced towards low β.

It was found that the distribution of the error for both cases 10b and 11b was the same. However this was not always so because the distribution depended upon the symmetry of the solution.

The error distributions for cases 11a and 11b were not related to the solution of the equation. Therefore, it is likely that the results for these cases are characteristic of those to be expected when real data is used. Thus it is suspected that, in general, the SSOR method is a more efficient method of solving a Poisson equation with Neumann boundary conditions than is the SOR method. Also, it appears that for neither iterative method is there a single β_o for all E. However, for a given E, the value of $\beta_o(E)$ for the SSOR method is less than that for the SOR method.

2.5 The Overrelaxation Method Of Solving An ω-Equation And The Determination Of β_o

A comparison was made between the efficiency of using the SOR and SSOR methods for solving Equation (2.21). The coefficients were treated as constants and Dirichlet boundary conditions were used.

When a real situation is considered the coefficients of the ω-equation would not be constants. This is especially true for coefficient A (see Equation (2.20)) because it depends upon σ which varies rapidly with pressure. Therefore it is necessary to have a method of finding β_o when there are variable coefficients. Carré's method is still valid, and therefore this was used to find an empirical extension of Miyakoda's method.

Occasionally flagging has been used in an attempt to reduce the computation time (Stuart (1967)). The effect of this technique on the constant E curves was considered.

Either an α-scheme or β-scheme can be used to solve an ω-equation. The relative merits of these schemes were investigated. Also the optimum and cut-off values of the α-overrelaxation factor were examined.

In the following discussion E has units of $mb\,s^{-1}$ and the static stability has units of $m^2\ mb^{-2}\ s^{-2}$.

2.5.1 A Comparison Of The SOR And SSOR Methods Of Solving An ω-Equation With Constant Coefficients

When certain assumptions are made, the ω-equation takes the form of Equation (2.20), with

$$A = \left[\frac{m}{d}\right]^2 \sigma \quad \text{and} \quad B = \left[\frac{f}{\Delta p}\right]^2$$

In the following computations (cases 12a and 12b), σ was taken to be a constant with a value of 4×10^{-2} .. The values of $\left[\frac{m}{d}\right]^2$ and f^2 were the same as those used in case 1a. There were five levels (q = 1, 1, 5) separated by 200 mb (Δp).

The SSOR method used previously for two-dimensional cases, was extended to cover three dimensions. Therefore

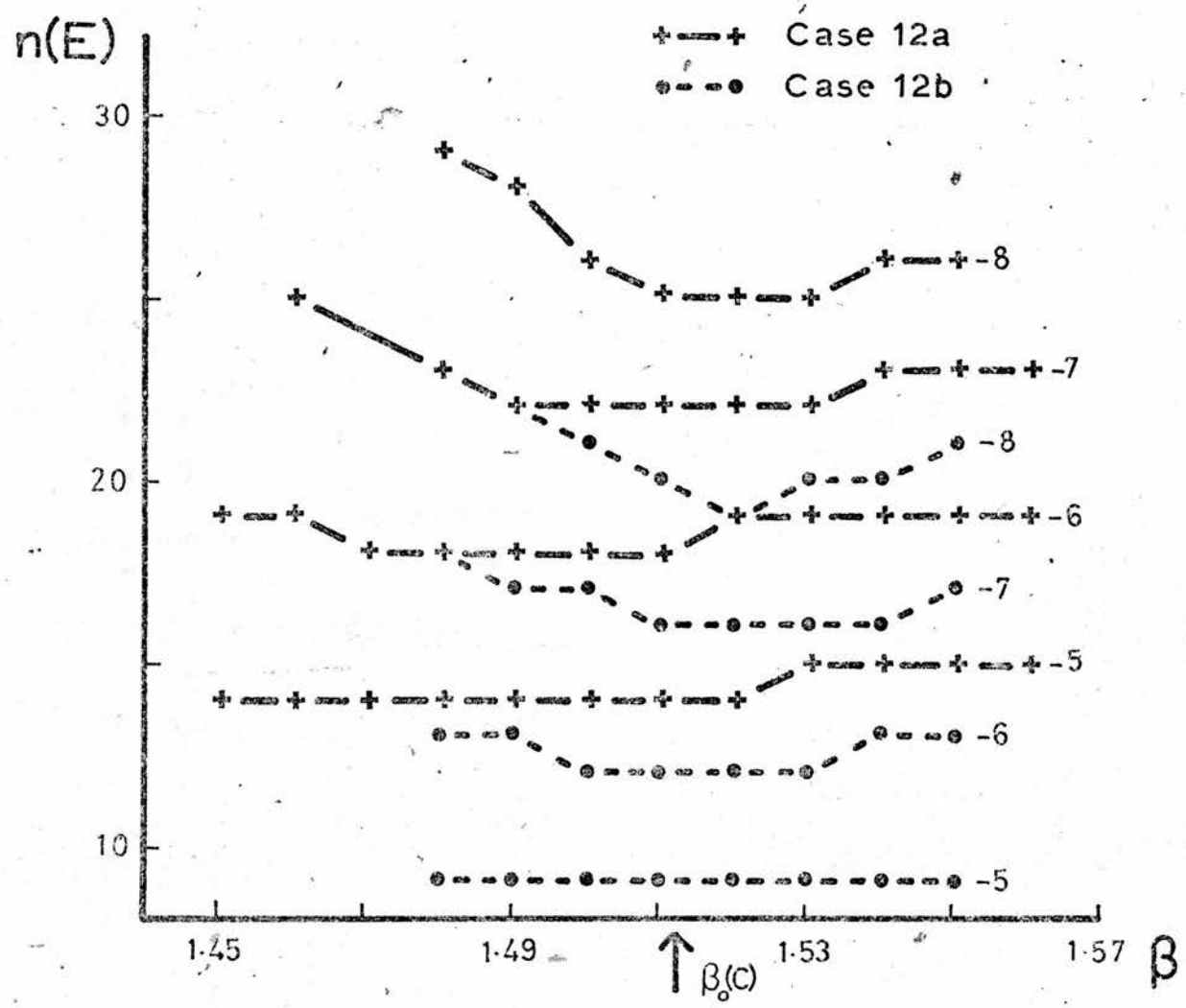

FIGURE 2·23

the order in which the gridpoints were relaxed depended upon whether (i + j + q) was odd or even. In this, and subsequent computations, Dirichlet boundary conditions were used.

For both methods $\beta_o(C)$ was 1.513 and this was the same as the value of $\beta_o(M)$ calculated from Equation (2.21). Thus it was possible to use Miyakoda's method to find β_o for both iterative methods.

The variation of n(E) with β for cases 12a and 12b is shown in Fig. 2.23. This shows that the constant E curves have a similar shape to those calculated for the two-dimensional cases (e.g. see Fig. 2.2). Fig. 2.23 also shows that for a given E and β the SSOR method required fewer iterations than the SOR method. Once again this was due to the rapid convergence of the SSOR method during the first few iterations.

The error was computed for both methods and it was found that the distributions were similar to those for the Helmholtz equation using the corresponding iterative method (see Figs. 2.4b and 2.4c).

These results show that the SSOR method can be easily and usefully extended to three dimensions.

The next section is concerned with the calculation of β_o when σ is variable.

2.5.2 The Computation of β_o For An ω-Equation With Variable Coefficients

In the atmosphere the static stability varies approximately with the inverse of the square of the pressure and thus in the first computation (case 13a), $\sigma(q) = \frac{1}{4q^2}$ was used. Apart from this, the data was the same as in case

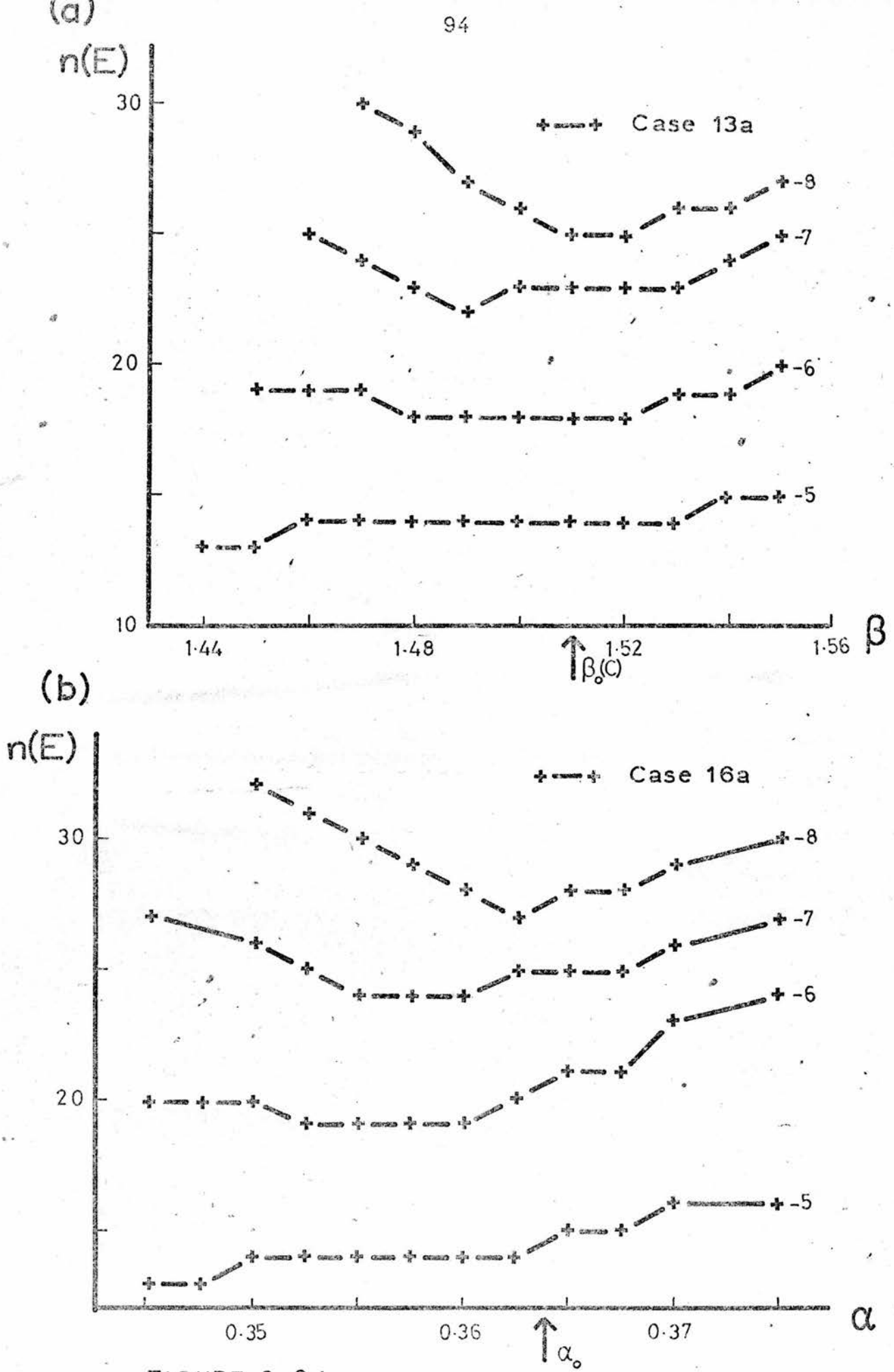
(a)
n(E)
30
20
10
Case 13a
-8
-7
-6
-5
1·44
1·48
1·52
1·56
β
β₀(C)
(b)
n(E)
30
20
Case 16a
-8
-7
-6
-5
0·35
0·36
0·37
α
α₀

FIGURE 2·24

Case	n_i n_j n_k	$\bar{\sigma} \times 10^2$	β	λ_m	$\beta_o(C)$	$\beta_o(\bar{M})$
13a	14 10 5	3.53	1.48	0.642	1.511	1.510
13b	14 10 9	4.14	1.50	0.651	1.528	1.530
13c	14 10 5	4.81	1.48	0.665	1.519	1.518
13d	14 10 4	22.00	1.48	0.700	1.535	1.533

TABLE 2.5

Equation	$\beta_o(C)$
$\bar{\sigma}\nabla^2\omega + \bar{f}^2\frac{\partial^2\omega}{\partial p^2} + S = 0$	1.499
$\sigma\nabla^2\omega + \bar{f}^2\frac{\partial^2\omega}{\partial p^2} + S = 0$	1.499
$\sigma\nabla^2\omega + f^2\frac{\partial^2\omega}{\partial p^2} + S = 0$	1.499
$\nabla^2(\sigma\omega) + f^2\frac{\partial^2\omega}{\partial p^2} + S = 0$	1.509

TABLE 2.6 The bar denotes the isobaric average.

12a. The ω-equation was solved by using the SOR method. This was used in all subsequent computations.

It was found that $\beta_o(C) = 1.511$ for case 13a. This is shown along with the variation of n (E) with β, in Fig. 2.24a. The figure indicates that $\beta_o(C)$ is correct. It also shows that the constant E curves are similar in shape to those found for other equations.

The value of $\beta_o(C)$ was also calculated for different values of n_k and Δp and different distributions of σ.

In case 13b the same data was used as in case 13a but with $n_k = 9$, $\Delta p = 100$ mb and $\sigma(q) = {}^{1}/_{q^2}$ $(q = 1, 1, 9)$. The next case (case 13c) was similar to case 13a, but $\sigma(q) = {}^{1}/_{q}$ was used. Lastly, the $n_k = 4$ and $\Delta p = 200$ mb was used and the values of σ at the two interior levels were 4×10^{-2} and 40×10^{-2}. The values of $\beta_o(C)$ for these cases are shown in Table 2.5.

Although β_o can be calculated by using Carré's method, it would be useful if a method similar to that of Miyakoda could be devised.

The results for cases 2a and 2b showed that, for the Helmholtz equation, the average value of a coefficient could be used with Miyakoda's method to give a good estimate of β_o. Therefore the average values of σ ($\bar{\sigma}$ say) were used in Equation (2.21) to give $\beta_o(\bar{M})$ (see Table 2.5). A comparison of $\beta_o(C)$ and $\beta_o(\bar{M})$ clearly shows that $\beta_o(\bar{M})$ gives the correct value of β_o.

If both coefficients in Equation (2.20) are variable, it is not clear whether the average values that should be used in Equation (2.21) are $\left[\frac{\overline{A}}{\overline{B}}\right]$, $\left[\frac{\overline{B}}{\overline{A}}\right]$ or $\bar{A}$ and $\bar{B}$. It

is suspected that the values of β_o for cases 2a and 2b were slightly different because the wrong averages were used. However the difference was only .012 and therefore the problem was not pursued further.

Many variations of the ω-equation have been used to calculate ω. Some of these are shown in Table 2.6. Using the same data as in case 13a, but with the real distribution of static stability, $\beta_o(C)$ was calculated for each of the equations. This group of computations will be referred to as case 14.

The distributions of σ, f^2 and $\left[\frac{m}{d}\right]^2$ were such that $\bar{\sigma} = 2.53 \times 10^{-2}\ m^2\ mb^{-2}\ s^{-2}$, $\bar{f}^2 = 1.23 \times 10^{-8}\ s^{-2}$ and $\left[\frac{\bar{m}}{d}\right]^2 = 1.09 \times 10^{-10}\ m^{-2}$. Substituting the average values in Equation (2.21) gave $\beta_o(\bar{M}) = 1.498$. This confirms the previous conclusion. The agreement between $\beta_o(C)$ for the first three equations was due to the fact that $\sigma(p)$ and $\bar{f}^2$ were the averages of σ and f^2 over the isobaric surfaces. Since the horizontal variations of σ were small it was not surprising that $\beta_o(C)$ for the last equation was similar to that for the other equations.

The above results show that Miyakoda's method can be extended to give a very good estimate of β_o for the full ω-equation.

2.5.3 The Effect Of Flagging

If flagging is used in solving Equation (2.10) then a point P is only relaxed so long as $\left| x_p^{(n+1)} - x_p^{(n)} \right| > E$. When flagging is not used, relaxation continues whilst $\left\| x_p^{(n+1)} - x_p^{(n)} \right\| > E$.

The effect of the use of the flagging technique was investigated by introducing it into a repeat of case 13d

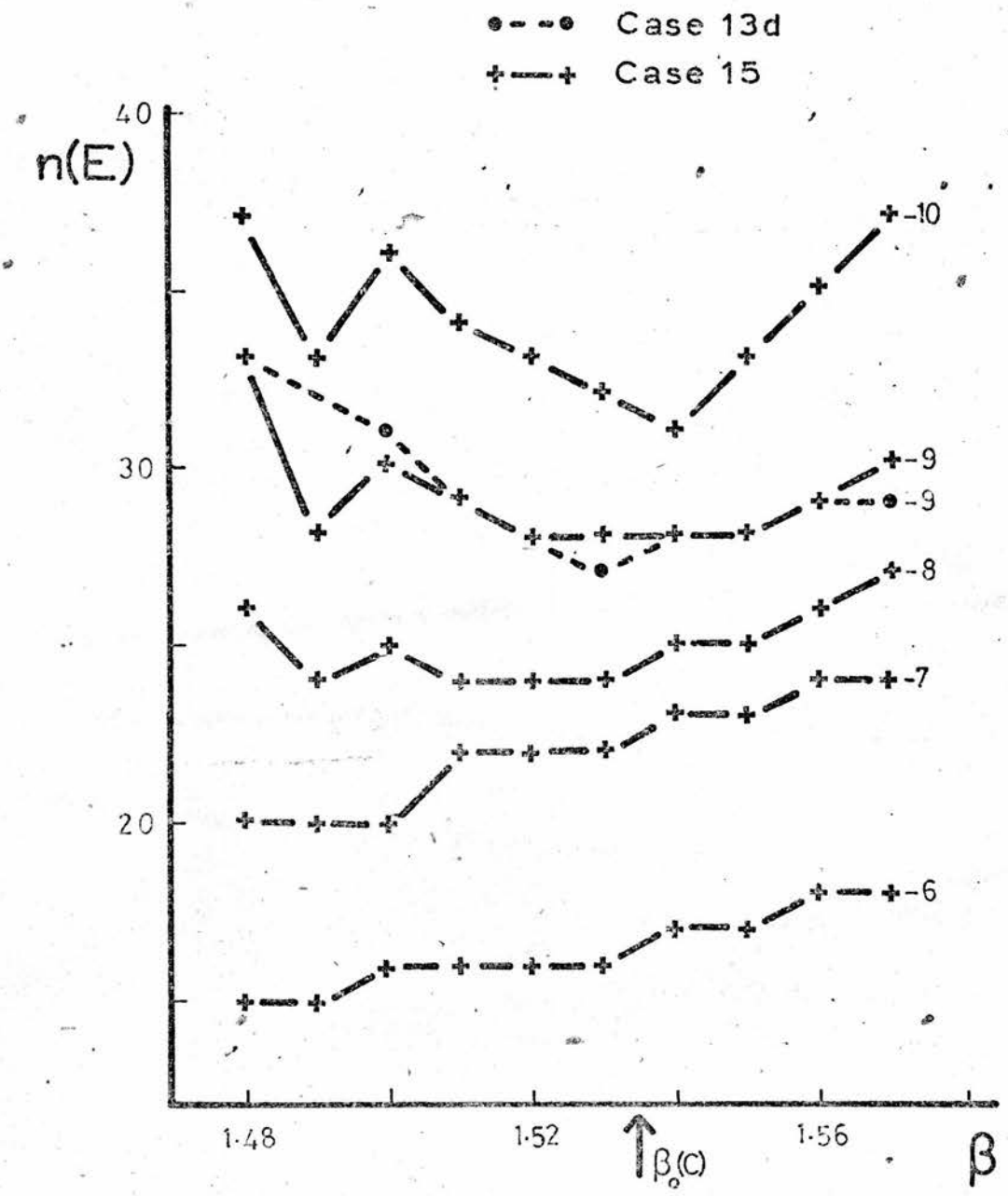

FIGURE 2·25

(case 15). The results are shown in Fig. 2.25. This figure also shows the results for case 13d with $E = 10^{-9}$. These results show that the flagging technique did not reduce the total number of iterations required for a given E. However, there was a slight saving in computer time when flagging was used because fewer points had to be relaxed.

Fig. 2.25 shows that, when E was small, there was a double minimum in the $n(E)$ versus β curves. The main minimum corresponds to the value of β_o that would be found if flagging was not used, namely $\beta_o(M) = 1.535$. The other minimum is due to the flagging and the large difference in stability at the two levels.

The level at which the stability was large had small values of ω since $\omega \propto \frac{1}{\sigma}$ (approximately). Therefore the flagging at this level was completed before that at the other level. Hence, only the level with stability 4×10^{-2} was relaxed during the last few iterations. This means that the secondary minimum corresponds to $\sigma = 4 \times 10^{-2}$ and this gives $\beta_o(M) = 1.49$. This agrees well with the observed value of β at the secondary minimum.

2.5.4 An Introduction To The α Overrelaxation Factor

In the α-scheme is used to solve an equation, then it is advantageous to know the optimum value of α (α_o say). It would also be of interest to know the largest value of α (α_c say) that will give a convergent solution.

First consider a general equation of the form of Equation (2.23). If the coefficients are constant and if C_{qm} is the maximum value of C_q, then α_o is given by

$$\alpha_o = \frac{-\beta_o}{M_{qm} + \sum_{q \neq qm} \left[\frac{C}{C}_q M_q \right]} \qquad (2.38)$$

The value of α_c is given by this equation with $\beta_o = 2$.

It can easily be shown that, when α_o and β_o are used with their respective iteration schemes to solve an equation with constant coefficients, both methods require the same number of iterations.

With respect to Equation (2.20) it can be shown that α_o and α_c are given by

$$\alpha_o = \frac{\beta_o}{4 + \frac{2\lambda^2}{\sigma}} \qquad \lambda^2 = \left[\frac{f\,d}{m\,\Delta p} \right]^2 \qquad (2.39)$$

$$\alpha_c = \frac{2}{4 + \frac{2\lambda^2}{\sigma}} \qquad (2.40)$$

When the ω-equation has constant coefficients, the above equations can be used to calculate α_o and α_c. However, if the coefficients are not constant (e.g. if $\sigma = \sigma(p)$) then these equations cannot be used directly.

Stuart et al.(1967) made an empirical study of α_o and α_c for the ω-equation. They took all the coefficients to be constant except the static stability which they took to be a function of pressure only. The variation of n(E) with α was investigated and from these results the experimental values of α_o and α_c were found ($\alpha_o(E)$ and $\alpha_c(E)$ say). They did this for several different grid sizes. The variation of stability with pressure that was used is shown in Table 2.7 and a summary of the results is in Table 2.8.

Stuart et.al also compared $\alpha_o(E)$ with the value calculated by using $\sigma = 2 \times 10^{-2}$ in Equations (2.21 and (2.39). They found good agreement between these values, but they

	Units				
Pressure	mb	800	600	400	200
Stability	$10^{-2}\ m^{2}\ mb^{-2}\ s^{-2}$	1.178	2.015	4.252	44.664

TABLE 2.7

	$n_i=n_j$	$\alpha_o(E)$	$\sigma_1 \times 10^5$	$\sigma_2 \times 10^2$	α_o^1 α_o^2	$\alpha_c(E)$	$\sigma_c \times 10^2$
A	35	0.400	0.94	1.91	0.411 0.399	0.450	1.11
B	23	0.250	0.86	0.59	0.364 0.347	0.300	4.10
C	17	0.300	2.02	1.90	0.320 0.299	0.350	1.12
D	11	0.225	2.82	2.00	0.244 0.218	0.275	1.34

TABLE 2.8

did not say why this particular value of σ was used. Also no attempt was made to explain the values of $\alpha_c(E)$. Thus the work of Stuart et al. does not suggest a method of calculating either α_o or α_c for a given distribution of σ.

Whilst only a mathematical analysis of the iteration scheme will produce a way of calculating α_o and α_c exactly, it was decided to use the results of Stuart et al. to find a way of estimating their values.

To start with, Equations (2.21) and (2.38) were used to find an equation for σ such that $\alpha_o = \alpha_o(E)$. This was found to be a quadratic equation and the solutions (σ_1 and σ_2 say) are shown in Table 2.8. The solutions σ_1 can be ignored because they are far too small. Also since it is expected that σ_2 depends only upon $\sigma(p)$, the results for case B are suspect. Yamagishi (1968) has also drawn attention to the inconsistency of this result. If case B is ignored, the value of σ_2 is between 1.90×10^{-2} and 2.00×10^{-2}.

It is not immediately obvious how this value of stability can be derived from $\sigma(p)$ (see Table 2.7). However flagging was used and the results in section 2.53 show that this can affect the distribution of n(E). Therefore it is suspected that the combination of flagging and the large stability at 200 mb rendered the effect of this level on $\alpha_o(E)$ negligible. Thus it is necessary to find how σ_2 is related to the stability at the other three levels.

The average value of the stability over the three lower levels is 2.48×10^{-2}. But, if the stability of the

200 mb level is taken to be effectively zero (because of the flagging), then the average value of σ over the four levels is 1.86×10^{-2}. The values of α_o calculated by using these stabilities in Equations (2.21) and (2.39) are shown in Table 2.8 (α_o^1 and α_o^2 say). Both α_o^1 and α_o^2 are close to $\alpha_o(E)$. However, it is not known exactly which value of the static stability should be used because of the complication of flagging. But, it does seem likely that α_o can be estimated by using the average static stability in both Equations (2.21) and (2.39).

Table 2.8 also shows the value of σ (σ_c say) that made $\alpha_c = \alpha_c(E)$ in Equation (2.40). This shows that, apart from case B, the values of σ_c are very close to the smallest value of the stability.

If $\bar{\sigma}$ and σ_{min} are the average and minimum values of σ, then the above results suggest that α_o and α_c may be estimated from

$$\alpha_o = \frac{\beta_o}{4 + \frac{2\lambda^2}{\bar{\sigma}}} \qquad \lambda^2 = \left[\frac{f\,d}{m\,\Delta p}\right]^2 \tag{2.41}$$

$$\alpha_c = \frac{2}{4 + \frac{2\lambda^2}{\sigma_{min}}} \tag{2.42}$$

In the next section these propositions will be tested for cases that are not complicated by flagging.

2.5.5 The Determination of α_o And α_c

The values of α_o and α_c were found experimentally for two sets of data (cases 16a and 16b). The same data was used in case 16a as in case 13a. Also case 16b was the same as case 16a except that the static stability was halved at each level. For case 16a the values of $\bar{\sigma}$ and σ_{min} were 3.53×10^{-2} and 1.56×10^{-2}. The corresponding

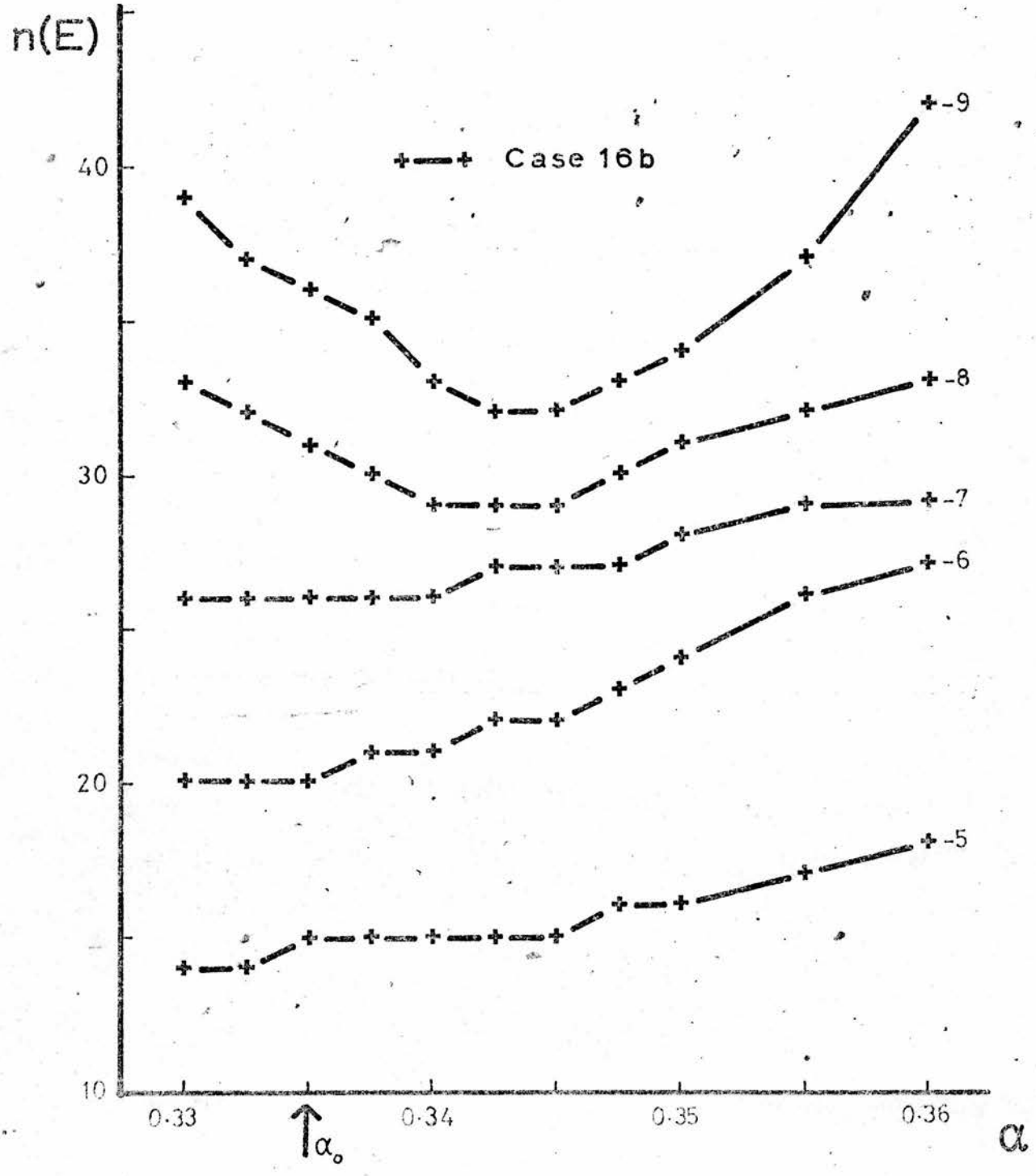

FIGURE 2·26

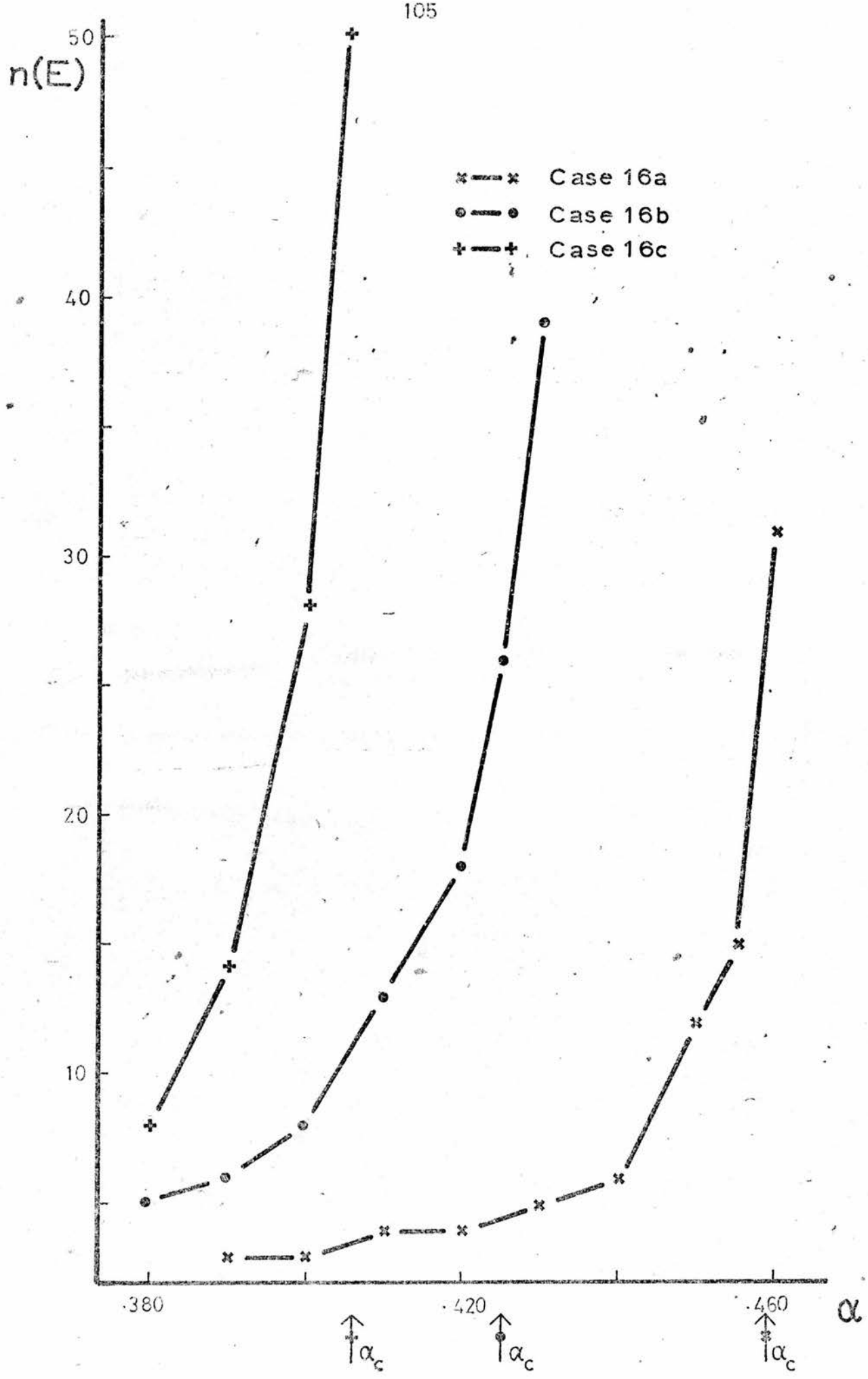
n(E)
50
40
30
20
10
Case 16a
Case 16b
Case 16c
·380
·420
·460
α
α_c
α_c
α_c

FIGURE 2·27

values for case 16b were half of these.

The results for case 16a are shown in Fig. 2.24b. The value of α_o calculated from Equation (2.41) is also shown in this figure. These results show that α_o is a good estimate of $\alpha_o(E)$.

A comparison of Figs. 2.24a and 2.24b shows that, for $E = 10^{-7}$ and $E = 10^{-8}$, the iteration scheme required fewer iterations than the α-scheme. However, for $E = 10^{-6}$ this was reversed. From these results it is not possible to decide which scheme is the most efficient, but it is suspected that the β-scheme will usually require fewer iterations. However, the total computer time required for the α-scheme may be less because it needs fewer computations per iteration.

The value of α_c was computed by finding the value of α for which the iteration scheme would not converge. In these computations $E = 10^{-3}$ was used. The results, with α_c calculated from Equation (2.42), are exhibited in Fig. 2.27. (The last point on the 'curve' shows that when .005 was added to this value of α, there was no convergence). The results show that Equation (2.42) gives a good estimate of $\alpha_c(E)$.

The above experiments were repeated for case 16b and the results are shown in Figs. 2.26 and 2.27. As in case 16a, Equations (2.41) and (2.42) give good estimates of $\alpha_c(E)$.

Finally, case 16a was repeated with a stability of 0.6×10^{-2} at the 800 mb level (case 16c). In this case only α_c was investigated. The results are shown in Fig. 2.27 and they confirm that Equation (2.42) gives a good

estimate of $\alpha_c(E)$.

The above results show that Equations (2.41) and (2.42) estimated $\alpha_o(E)$ and $\alpha_c(E)$ to within 3%. Therefore these equations can be used with some confidence.

2.6 Discussion

The first point of importance is that for all the equations, boundary conditions and iterative schemes considered, it was advantageous to use $\beta>1$. Therefore, the following discussion will be primarily concerned with the value of β that should be used. The discussion will be roughly divided into four parts. These will deal with Dirichlet boundary conditions, Neumann boundary conditions, flagging and the α-scheme.

When Dirichlet boundary conditions were used it was found that the sets of constant E curves had three characteristics in common which are listed below

1. As E decreased, the value of $\beta_o(E)$ became better defined.
2. When E was large, the average value of β for which n(E) was a minimum tended to be less than β_o.
3. The magnitude of the gradient of the constant E curves was greater for $\beta<\beta_o$ than $\beta>\beta_o$.

These facts indicate that if E is relatively small, it is worthwhile estimating β_o accurately. Also, if E is small it is better to slightly underestimate, rather than overestimate β_o. But when E is large the opposite is true. However, in general, it is probably safer to underestimate β_o rather than overestimate it.

The above conclusions apply to both the α and β schemes.

In all the cases considered Carre's method gave the correct value of β_o. But to use this method the equation has to be solved with $1 < \beta < \beta_o$ and thus great attention was paid to Miyakoda's method.

When equations (with constant coefficients and only second derivatives of x and x itself) were solved using the SOR method, it was found that Equation (2.24) predicted β_o correctly. If there were variable coefficients their average values could be used Equation (2.24) to give a good estimate of β_o.

When the SOR method was used it was found that neither the distribution of S nor the initial guess affected β_o. However a bad initial guess did increase the number of iterations required for a given E.

The SSOR method always required few iterations than the SOR method although (provided there was no symmetry) both methods had the same β_o. This was due to the SSOR methods' rapid convergence during the first few iterations.

If there is no symmetry in the solution of an equation, then the prece ding discussion of the SOR method also applies to the SSOR method. Thus, for both methods, an increase in the number of gridpoints will increase N_o. This increase will be large when small numbers of gridpoints are involved.

Equation (2.19) was only tested for the Helmholtz equation. The results confirmed that Equation (2.19) could be used to estimate the value of E that should be used to provide a given AE. It is suspected that Equation (2.19) can be used for all equations.

The results for the Neumann boundary conditions were

less conclusive than those for the other type of boundary condition.

For both the Helmholtz and Poisson equations the value of $\beta_o(E)$ was larger than that for the corresponding equation with Dirichlet boundary conditions. This was reflected in the optimum rate of convergence. Thus the Neumann boundary condition should be used only where absolutely necessary. This applies to both iterative methods.

The results for the Helmholtz equation showed that, in the absence of symmetry, $\beta_o(C)$ was the same for both the SOR and SSOR methods. Also it was found that the SSOR method required fewer iterations than the SOR method.

Since Carré's method could not be used to find β_o, an attempt was made to extend Miyakoda's method. Although analytical expression for the error was found for the SOR method, the set of equations derived from it contained an unknown. Thus it was not possible to find β_o. The distribution of the error was also found for the SSOR method and was used with a similar lack of success.

When the Poisson equation was solved it appeared that there was no value of β_o that was independent of E. When the SOR method was used it was found that, for large E, the value of $\beta_o(E)$ was almost 2. As E decreased, $\beta_o(E)$ also decreased.

The values of $\beta_o(E)$ for the two iterative methods were different. Also, for the most realistic case considered, the SSOR method was superior to the SOR method.

For both iterative methods, approximate analytical expressions for the error was found. However, these

expressions could not be used to predict $\beta_o(E)$.

Due to the disappointing results from the Helmholtz and Poisson equations, the value of $\beta_o(E)$ for the ω-equation with Neumann boundary conditions was not determined.

The above discussion gives rise to two general conclusions.

1. The solution of an equation with Neumann boundary conditions takes far longer than when Dirichlet boundary conditions are used.
2. The SSOR method is more efficient than the SOR method for both types of boundary conditions.

When flagging was used it was found that both $\beta_o(E)$ and $N_o(E)$ were hardly affected. However there was a slight saving in computer time because fewer points had to be relaxed. Thus flagging is a useful technique.

Finally, the use of the α-scheme to solve an ω-equation with variable coefficients was considered. The results indicates that this scheme was less efficient than the β-scheme. But, the α-scheme required fewer computations per iteration and thus it may reduce the computer time by a small amount.

It was found that α_o and α_c could be accurately estimated by Equations (2.41) and (2.42). However it is probably advisable to use the β-scheme becuase this has a theoretical foundation.

The investigations into flagging and the α-scheme indicate that these techniques may produce a marginal saving in computer time.

It is hoped that the observation and deductions in this

chapter will provide the starting point for a more theoretical investigation into the overrelaxation method.

CHAPTER III

The Balance Equation

3.1 Introduction

In this chapter the derivation, meaning and solution of the balance equation are discussed.

A new method of ellipticising the balance equation is introduced, followed by a discussion of the discretisation of the balance equation.

The different methods of solving the balance equation are discussed and two variations of existing methods are introduced. The efficiencies of these methods are compared and the effect of the formulation on the efficiency is investigated.

The last part of the chapter is concerned with the boundary conditions that should be used when solving the balance equation.

3.2 The Origin And Meaning Of The Balance Equation

The divergence equation may be written as

$$\frac{dD}{dt} + D^2 = 2J(u,v) + \frac{\partial \underline{V}}{\partial p}.\nabla\omega - f\zeta + \underline{k}\times\underline{V}.\nabla f + \nabla^2\Phi = 0 \qquad (3.1)$$

Many reasons have been given for simplifying this equation, some of which will be discussed below.

1. Thompson (1961) showed that a fluid in hydrostatic equilibrium was unable to support gravity waves if

$$\frac{dD}{dt} = 0 \qquad (3.2)$$

This assumption turns Equation (3.1) into a diagnostic equation which represents a balance between the wind field ($\underline{V}, \omega$) and the pressure field (represented by Φ). If Ψ and X are introduced this equation becomes

$$\left[D^2 + 2J(u_1,v_2) + 2J(u_2,v_1) + 2J(u_2,v_2) + \underline{k}\times\nabla X.\nabla f + \frac{\partial \underline{V}}{\partial p}.\nabla\omega\right]$$

$$-\left[f\nabla^2\psi + 2(\psi_{xx}\psi_{yy} - \psi_{xy}^2) + \nabla f.\nabla\psi - \nabla^2\phi\right] = 0 \qquad (3.3)$$

For synoptic scale motions the terms in the first bracket are at least an order of magnitude less than those in the second bracket (see Equ. 1.23). Thus if only the large terms are included, Equ. (3.3) becomes

$$f\nabla^2\psi + 2(\psi_{xx}\psi_{yy} - \psi_{xy}^2) + \nabla f.\nabla\psi - \nabla^2\phi = 0 \qquad (3.4)$$

Since f and ϕ are known this is a two dimensional non-linear equation in ψ. It is known as the balance equation.

If the balance equation is elliptic and if boundary conditions are specified for ψ, then it can be solved for ψ for each isobaric surface.

If χ and ω are also known, then Equ. (3.3) can be solved for ψ. This is achieved by treating the terms in the first bracket as part of the forcing function and then solving the equation as if it is the balance equation. The methods that are used to solve the balance equation will be described later.

The use of Equ. (3.4) does not ensure that $\frac{dD}{dt} = 0$ because of the additional assumptions that are made. Thus there may be gravity waves even if the balance equation is used.

2. From the continuity equation it can be shown that

$$\frac{dD}{dt} = -\frac{\partial}{\partial p}\left[\frac{d\omega}{dt}\right] + \frac{\partial \underline{V}}{\partial p}.\nabla\omega + D^2$$

Using this, Equ. (3.1) becomes

$$-\frac{\partial}{\partial p}\left[\frac{d\omega}{dt}\right] + 2(D^2 + \frac{\partial \underline{V}}{\partial p}.\nabla\omega) + 2J(u,v) - f\zeta + \underline{k}\times\underline{V}.\nabla f + \nabla^2\phi = 0 \qquad (3.5)$$

If it is assumed that there are no vertical accelerations (in p co-ordinates), then this reduces to a diagnostic equation. If χ and ω are known, then the diagnostic equation can be solved for Ψ. But, this solution will not be the same as that for Equ. (3.3).

If only large terms are included, then Equ. (3.5) also reduces to the balance equation.

3. Lorenz (1960) considered the forms of the divergence and vorticity equations that are consistent with some form of energy conservation law. It was found that the balance equation was just one variant of the divergence equation for which this was possible.

4. If only the large terms in the balance equation are considered (terms of order R^0 and R^1) then it becomes the balance equation (Equ. 1.23). Also, if only $\frac{\partial D}{\partial t}$ or $\frac{dD}{dt}$ is neglected, then terms of equal or smaller magnitude are still included.

The above discussion shows that basically the balance equation is always derived from the divergence equation by some form of dimensional argument. Therefore, unless a diagnostic study is concerned with vorticity or energy budgets, the use of the balance equation can only be justified by scale considerations.

Some insight into the meaning of the balance equation can be gained by integrating Equ. (3.4). Kuo (1956) has shown that if Ψ_b is the solution of Equ. (3.4) and if $\underline{V}_b = \underline{k} \times \nabla \Psi_b$ then the integral is (if an arbitary function is ignored).

$$\underline{V}_b \cdot \nabla \underline{V}_b + f \underline{k} \times \underline{V}_b = -\nabla \Phi$$

Rearranging, this gives

$$\underline{V}_b - \underline{V}_g = \frac{\underline{k} \times (\underline{V}_b \cdot \nabla \underline{V}_b)}{f} \qquad (3.6)$$

Haltiner (1957) showed that, if the local and vertical contributions to the ageostrophic wind are neglected, then

$$\underline{V} - \underline{V}_g \approx \frac{\underline{k} \times (\underline{V}_g \cdot \nabla \underline{V}_g)}{f} \qquad (3.7)$$

Further, he showed that the right hand side of this equation is large when the isobars are curved or if they are confluent or diffluent. Thus it can be inferred from Equs. (3.6) and (3.7) that the balance equation takes these configurations into account.

For circular isobars, Kuo (1956) showed that the balance equation reduces to the gradient wind equation. Dixon (1972) has also indicated the relationship between the balanced and gradient wind.

There are several other equations that can be used to derive non-divergent balanced winds. Some of these are discussed below.

If the non-linear term in Equ. (3.4) is neglected, the result is the linear balance equation

$$f\nabla^2\psi + \nabla f . \nabla\psi = \nabla^2\phi \qquad (3.8)$$

The solution of this equation will be denoted by ψ_1 and the wind derived from this is $\underline{V}_1 = \underline{k} \times \nabla\psi_1$. The integration of Equ. (3.8) gives

$$\underline{V}_1 - \underline{V}_g = \frac{\underline{k} \times (\nabla \times \underline{M})}{f}$$

The righthand side of this is small and thus $\underline{V}_1$ is similar to $\underline{V}_g$. The advantage of using the linear balance equation is that it is easy to solve.

Wind laws that are a compromise between validity and computational ease are described by

$$f\nabla^2\psi + \nabla f.\nabla\psi + \frac{2}{f^2} J\left(\frac{\partial\phi}{\partial x},\frac{\partial\phi}{\partial y}\right) = \nabla^2\phi$$

$$f\nabla^2\psi + \nabla f.\nabla\psi + 2J\left(\frac{\partial\psi}{\partial x},\frac{\partial\psi}{\partial y}\right) = \nabla^2\phi \qquad (3.9)$$

These equations are usually called quasi-linear balance equations.

Ellsaesser (1968) discussed many wind laws including the balance equation and linear balance equation. He concluded that Equ. (3.8) was the best after taking into account the ellipticisation, reversibility, and computational time. He also considered the effect of the wind laws on barotropic predictions.

Some wind laws were also investigated by Krishnamurti (1968b). He found that both Equs. (3.4) and (3.9) produced winds that were very close to the observed winds. Also, further analysis of his results shows that the behaviour of $\underline{V}_l$ and $\underline{V}_b$ is consistent with them being similar to the geostrophic and gradient winds respectively. For instance, the cross-isobaric flow of $\underline{V}_b$ is consistent with Equ. (3.7).

Krishnamurti concluded that "a large part of the upper tropospheric cross-isobaric flow frequently observed in baroclinic disturbances may be explained from the non-divergent part of the total wind". It should be added that this explanation is only valid if Ψ is computed from an equation that takes the non-linear term into consideration.

Benwell et al.(1971) found that, in certain synoptic situations, the use of Equ. (3.4) gives a much better

prediction than Equ. (3.8).

If the only consideration is the validity of the wind law, then the above results indicate that nothing less simple than the quasi-balance equation should be used to derive the non-divergent wind.

In the following sections only the balance equation will be considered in detail because quasi-balance equations are easy to solve and because more complicated equations are solved in the same way as is a balance equation.

3.3.1 The Elliptic Condition For The Balance Equation

If Equation (3.4) is to be solved as a boundary value problem, it must be elliptic. 'Arnason (1958) showed that the elliptic condition is

$$(f + 2\Psi_{xx})(f + 2\Psi_{yy}) - 4\Psi_{xy}^2 > 0 \qquad (3.10)$$

This condition implies that there are two types of solution for a given boundary condition. In the northern hemisphere the significant solution is such that $f + 2\Psi_{xx} > 0$ and $f + 2\Psi_{yy} > 0$. These conditions imply that $\nabla^2\Psi + f > 0$. Therefore if $\Psi^{(n)}$ is the solution after n iterations, it is required that

$$\nabla^2\Psi^{(n)} + f > 0 \qquad (3.11)$$

It can easily be shown from Equs. (3.4) and (3.10) that the elliptic condition is

$$\nabla^2\phi + \frac{f^2}{2} - \nabla f.\nabla\Psi = E(\Psi) > 0 \qquad (3.12)$$

Therefore at all stages of the iteration procedure the following condition must be satisfied

$$E(\Psi^{(n)}) > 0 \qquad (3.13)$$

Any iteration scheme used to solve the balance

equation must, in order to ensure convergence, include the conditions described by Equs. (3.11) and (3.13).

When the balance equation is written in terms of $E(\Psi)$, it becomes

$$f\nabla^2\Psi + 2(\Psi_{xx}\Psi_{yy} - \Psi_{xy}^2) + \frac{f^2}{2} - E(\Psi) = 0 \qquad (3.14)$$

The methods for solving the balance equation in this form will be discussed later.

There is another useful form of the balance equation which will be derived below.

The deformation field is defined by two parameters $A = -2\Psi_{xy}$ and $B = \Psi_{xx} - \Psi_{yy}$. In terms of these parameters, the non-linear term (NLT) in the balance equation becomes

$$NLT = \frac{\zeta^2 - A^2 - B^2}{2} \qquad (3.15)$$

Using this, Equ. (3.4) becomes a quadratic equation in ζ. In terms of $E(\Psi)$, the solution for ζ is

$$\zeta = -f \pm \sqrt{2E(\Psi) + A^2 + B^2}$$

This clearly shows the existence of two types of solution. In the northern hemisphere the positive sign is chosen so that $\eta > 0$. Thus the balance equation becomes

$$\zeta = -f + \sqrt{2E(\Psi) + A^2 + B^2}$$

$$\nabla^2\Psi = \zeta \qquad (3.16)$$

One of the advantages of using this set of equations is that the condition shown in Equ. (3.11) is implicit in them. The elliptic criterion ensures that there is not a negative quantity under the square root.

Equ. (3.16) also shows that there is another condition on $E(\Psi)$, namely

$$E(\Psi) > -\frac{(A^2 + B^2)}{2} \qquad (3.17)$$

However, if the elliptic criterion holds, then this condition is also satisfied.

The meteorological significance of the two conditions imposed on $E(\Psi)$ has never been fully explained.

Now consider the complete divergence equation. This is elliptic with respect to Ψ if

$$E(\Psi,X,\omega) = \nabla^2\phi + \frac{f^2}{2} - \nabla f.\nabla\Psi + \frac{D^2}{2} + \left[\frac{dD}{dt} + J(X,f) + \nabla\omega.\frac{\partial V}{\partial p}\right] > 0 \qquad (3.18)$$

In terms of E, the divergence equation becomes

$$f\nabla^2\Psi + 2(\Psi_{xx}\Psi_{yy} - \Psi_{xy}^2) + \frac{f^2}{2} - \frac{D^2}{2} - E(\Psi,X,\omega) + 2J(u_1,v_2) + 2J(u_2,v_1) + 2J(u_2,v_2) = 0 \qquad (3.19)$$

This is analagous to Equ. (3.14). An equation that is analagous to Equ. (3.16) can be derived in terms of $A' = u_x - v_y$ and $B' = v_x + u_y$. It can be shown that

$$2J(u,v) = \frac{A'^2 + B'^2 - \zeta^2 - D^2}{2}$$

Thus the divergence equation may be written as

$$\zeta = -f + \sqrt{2E(\Psi,X,\omega) + A'^2 + B'^2} \qquad (3.20)$$

This equation has exactly the same form as Equ. (3.16) and thus the conditions on E have the same form in both cases.

Equs. (3.19) and (3.20) can be solved in the same way as Equs. (3.14) and (3.16).

Miyakoda (1956) noted that if the bracketed terms in Equ. (3.18) are neglected in the divergence equation then the elliptic criterion becomes

$$E = \nabla^2\phi + \frac{f^2}{2} - \nabla f.\nabla\Psi + \frac{D^2}{2} > 0$$

If the elliptic criterion is thought of as a condition on $\nabla^2\phi$, then this condition is less restrictive than that shown in Equ. (3.12). Therefore, in this particular case, the inclusion of extra terms results in a less

restrictive condition on $\nabla^2\Phi$.

When the balance equation is used with real data, it is found that there are regions where the elliptic criterion is not satisfied (hyperbolic regions). The above results suggest that if all, or most, of the terms could be included in the divergence equation, then the hyperbolic regions would disappear.

The next section will be concerned with the ways in which the hyperbolic regions are eliminated when the balance equation is used.

3.3.2 Methods Of Ellipticising The Geopotential Field

Consider the ellipticisation of Φ for the balance equation. When the elliptic criterion (see Equ. (3.12)) is not satisfied, Φ must be changed until it is..

Initially Ψ is not known and thus the elliptic criterion is replaced by

$$E(\Phi) = \nabla^2\Phi - \frac{\nabla f.\nabla\Phi}{f} + \frac{f^2}{2} - \varepsilon > 0 \qquad (3.21)$$

$$\varepsilon = \max\left(\nabla f.\nabla\Psi - \frac{\nabla f.\nabla\Phi}{f}\right)$$

Benwell et al.(1971) suggested that $E = 2 \times 10^{-6}$ f.

If Φ is altered so that $E(\Phi) > 0$, then it is unlikely that the correct elliptic criterion will be violated during the iteration proce dure. However, if a region does become hyperbolic then $E(\Psi^{(n)})$ is set to zero.

If $E(\Phi) < 0$ then $\nabla^2\Phi$ is large and negative (since $\nabla f.\nabla\Psi$ is always small). Kirk (1970) noted that

$$(\nabla^2\Phi)_o \propto (\Phi_m - \Phi_o)$$

Here Φ_m is the average value of Φ in the region of Φ_o. These facts can be used to estimate the change in Φ that is necessary to reduce a negative $E(\Phi)$ to zero.

For simplicity, let the elliptic criterion be

$$E = \nabla^2\phi + \frac{f^2}{2} > 0$$

Suppose that initially the value of E (E_i say) is less than zero and that Φ_o and Φ_m are arranged as shown below

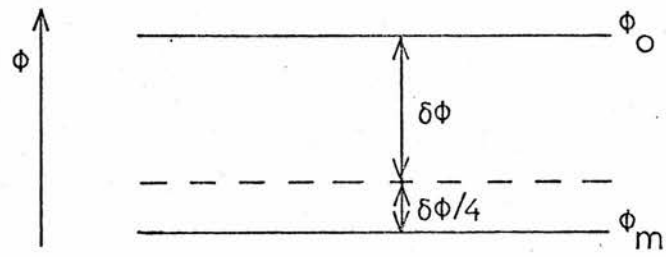

The magnitude of E_i can be decreased by decreasing Φ_o by $\delta\Phi$ and increasing Φ_m by $\frac{\delta\Phi}{4}$. If the final value of E (E_f say) is zero; then

$$E_f = \nabla^2\phi + \frac{5\,\delta\Phi}{4\,d^2} + \frac{f^2}{2} = 0$$

In terms of E_i, this becomes

$$E_i = -\frac{5\,\delta\Phi}{4\,d^2}$$

Using $E_i = -\frac{3}{2} f^2$, $d^2 = 10^{10}$ and $f^2 = 10^{-8}$, this equation gives $\delta\Phi/g = 12m$.

These computations show that the maximum change in height due to ellipticisation will be about 10m. It can also be shown that the above proce dure would change the geostrophic wind by about 10 ms^{-1}.

The above method of changing E is only introduced to obtain an estimate of $\delta\Phi$. The remainder of this section will deal with practical methods by which E may be changed.

The elliptic criterion can be imposed in hyperbolic regions by altering E (Φ) directly or by altering Φ which will then change E (Φ).

Shuman (1957) and Benwell et al.(1971) have suggested methods by which E (Φ) can be altered directly. Shuman's

method starts by scanning $E(\Phi)$ until a negative value is found ($\bar{E}$ at point 0). The value of E at point 0 is then put equal to zero, and $\bar{E}/4$ is added to the value of E at the surrounding four points. This process is repeated until $E(\Phi) > 0$ everywhere. Once $E(\Phi)$ is known, Equ. (3.21) is solved for the new distribution of Φ.

The proceedure adopted by Shuman has the effect of changing $\nabla^2 E$ in the following way

$$(\nabla^2 E)'_o = (\nabla^2 E)_o + 5E_o$$

Here the prime denotes the new value and E_o is a negative quantity. If $\nabla f . \nabla \Phi$ is neglected, then E is given by

$$E = \frac{\nabla^2 \Phi}{d^2} + \frac{f^2}{2}$$

Substituting this into the previous equation gives

$$(\nabla^4 \Phi)'_o = (\nabla^4 \Phi)_o + 5E_o d^2 \qquad (3.22)$$

Let Φ_i and Φ_f be the initial and final geopotentials and let $\tilde{\Phi} = \Phi_f - \Phi_i$. If $\tilde{\Phi}$ varies sinusoidally, then Equ. (3.22) implies that $\tilde{\Phi} \propto E_o$. Thus this process results in a local decrease in the height field.

Fig. 3.1a shows the change in height, in meters, when Shuman's method was applied to the 1000 mb surface in area 51. The hatched regions indicate the areas in which $E(\Phi)$ was originally negative. As expected there was a decrease in Φ in these areas.

One method of altering E by changing Φ, is based on the fact that the geostrophic vorticity is large and negative when $E(\Phi) < 0$. Thus $E(\Phi)$ can be made positive by reducing the magnitude of ζ_g in hyperbolic regions.

Dixon (1970) discussed the smoothing function

$$\Phi'_o = \Phi_o + \frac{(1 - \varkappa)}{4} (\nabla^2 \Phi)_o \qquad (3.23)$$

FIGURE 3.1

(a) The change in height, in meters, when Shumans' method was used to ellipticise Φ for the 1000 mb surface of area 51.

(b) The corresponding results for the author's method.

FIGURE 3.2

The finite difference schemes used to discretise the balance equation.

FIGURE 3.3

(a) ($\Psi 1 - \Psi 2$) - the difference in the streamfunctions when NLT1 and NLT2 are used in the balance equation. The units are 10^{-4} m s^{2-1}.

(b) (u1 - u2) - the corresponding results for the x components of velocity. The units are 10^{-2} m s^{-1}.

(c) (v1 - v2) - the corresponding results for the y component of velocity. The units are 10^{-2} m s^{-1}.

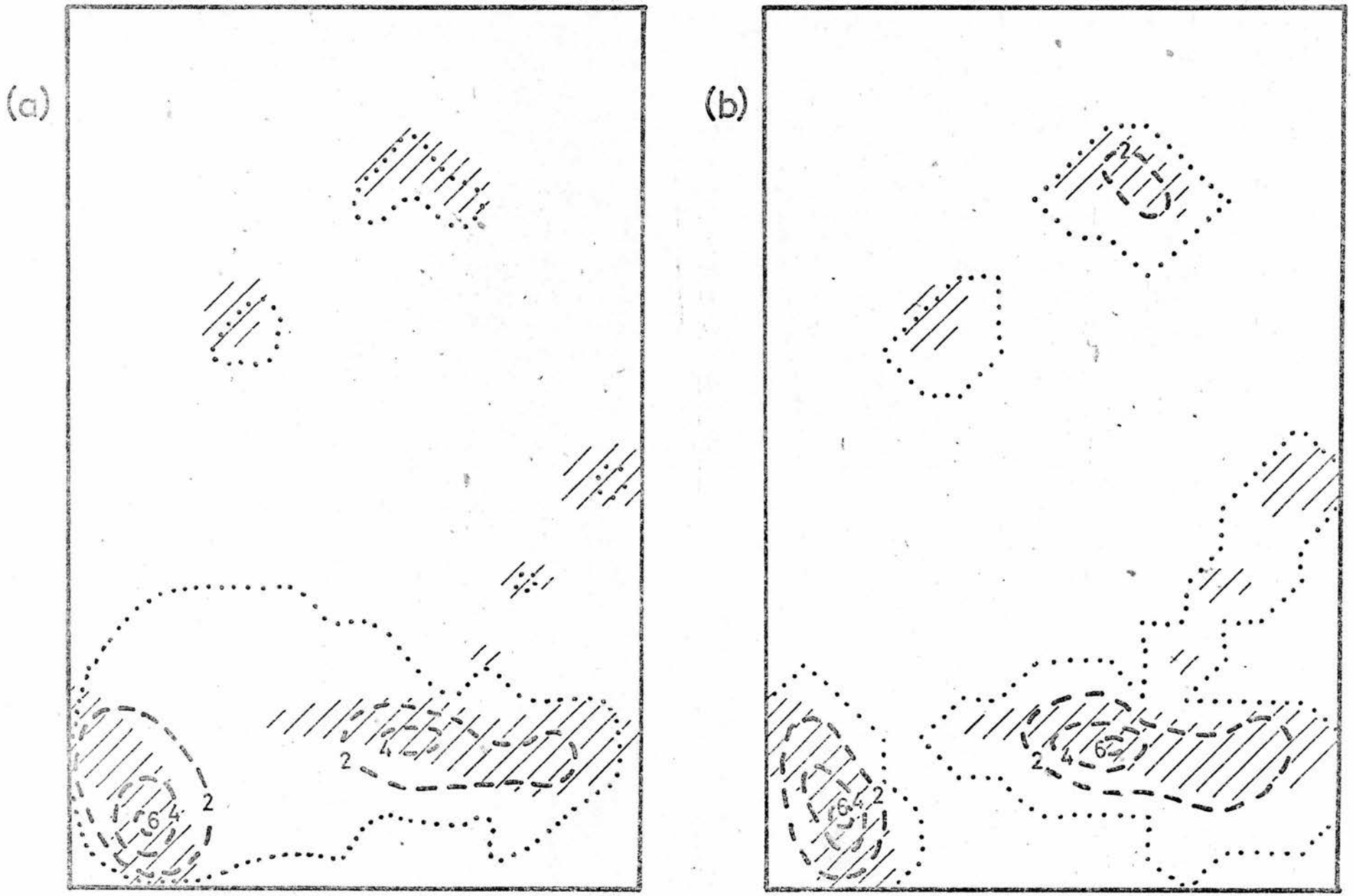

// $E(\Phi) < 0$ FIGURE 3.1 // $E(\Phi) < 0$

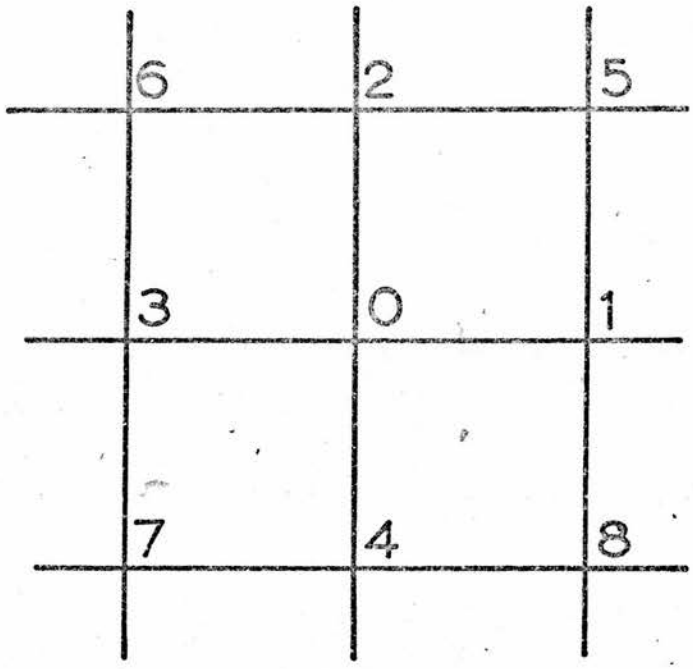

$$^{+}\psi_{xx} = [\psi_1 - 2\psi_0 + \psi_3]/d^2 \qquad ^{+}\psi_{yy} = [\psi_2 - 2\psi_0 + \psi_4]/d^2$$

$$^{+}\nabla^2\psi = {}^{+}\psi_{xx} + {}^{+}\psi_{yy}$$

$$^{+}\psi_{xy} = [\psi_5 - \psi_6 - \psi_8 + \psi_7]/4d^2$$

$$^{+}\nabla f.\nabla\psi = [(f_1 - f_3)(\psi_1 - \psi_3) + (f_2 - f_4)(\psi_2 - \psi_4)]/4d^2$$

$$^{*}\psi_{xx} = [\psi_5 - 2\psi_0 + \psi_7]/2d^2 \qquad ^{*}\psi_{yy} = [\psi_8 - 2\psi_0 + \psi_6]/2d^2$$

$$^{*}\nabla^2\psi = {}^{*}\psi_{xx} + {}^{*}\psi_{yy}$$

$$^{*}\psi_{xy} = [\psi_2 + \psi_4 - \psi_3 - \psi_1]/2d^2$$

FIGURE 3.2

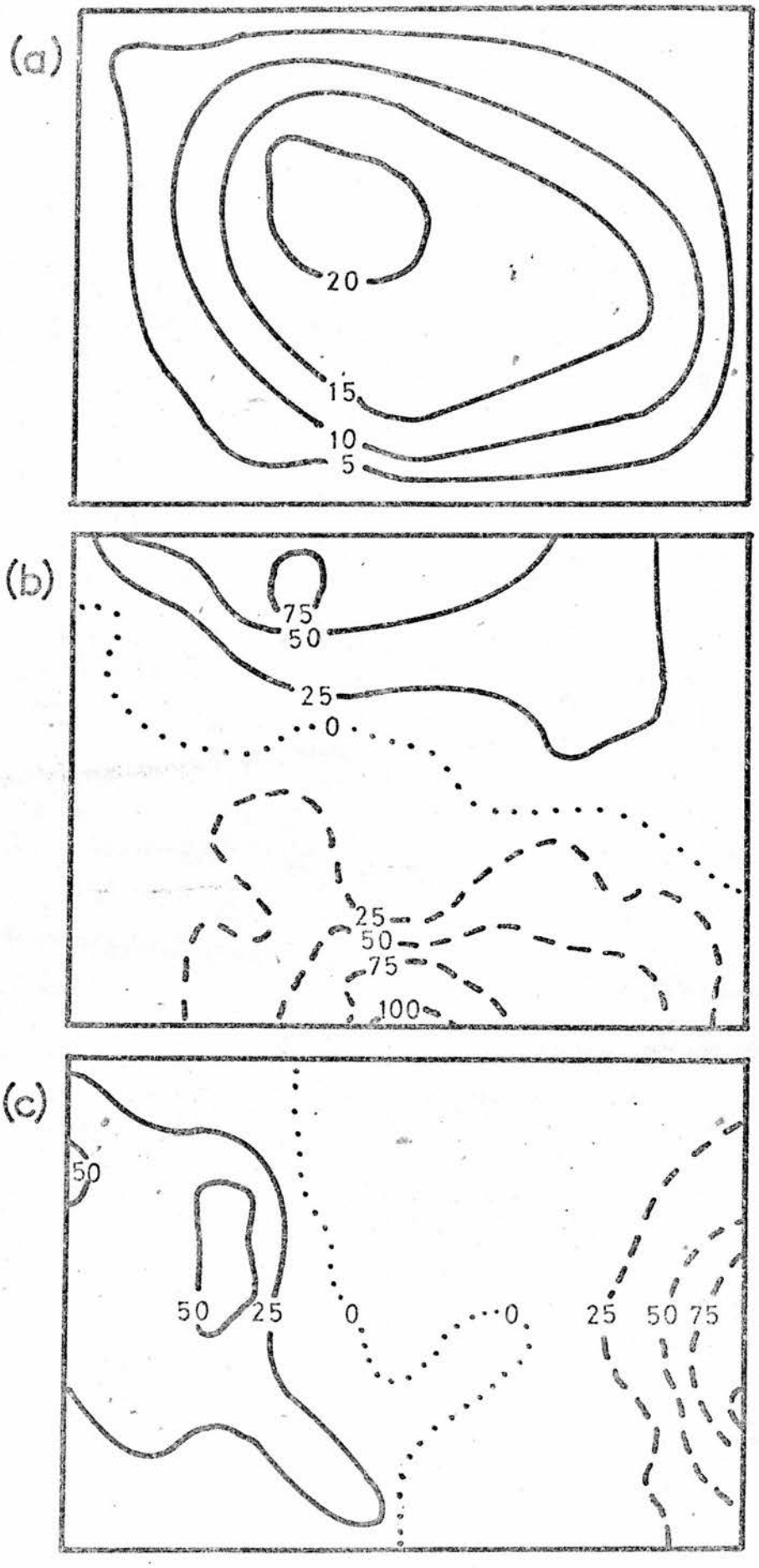

FIGURE 3.3

The effect of this smoothing on ζ_g is described by

$$(\zeta_g)'_o = (\zeta_g)_o + \frac{(1-\varkappa)}{4fd^2}(\nabla^4\phi)_o \qquad (3.24)$$

Since $(\nabla^4\phi)_o \propto (\nabla^2\phi)_m - (\nabla^2\phi)_o$, it can be shown that $(\nabla^4\phi)_o$ will tend to be positive in regions where $E(\phi)<0$. Thus if Equ. (3.23) is used with $\varkappa < 1$ in regions where $E(\phi)<0$, Equ. (3.24) shows that there will be a decrease in the magnitude of the geostrophic vorticity. Also it can be shown that ϕ will decrease when $E(\phi)<0$.

Equ. (3.23) was applied at all points where $E(\phi)<0$ until the elliptic criterion was satisfied. The corresponding results to those found for Shuman's method are shown in Fig. 3.1b. (The straight lines indicate the regions beyond which there was no change in ϕ). It was found that as $\varkappa$ approached unity there was an increase in the number of cycles required and a decrease in the change of ϕ .

Figs. 3.1a and 3.1b show that in both methods the geopotential was changed only in the vicinity of hyperbolic regions. Also these figures show that the resulting change in ϕ was similar for both methods. However it was found that the time taken for the first method was about three times that for the second, (but this may be due to inefficient programming). Another advantage of the second method is that it is not necessary to solve a partial differential equation in order to recover ϕ .

Benwell et al.(1971) used the new ϕ to alter the geopotential at the other levels so as to maintain the temperature structure. But if this is not done, there is

no reason why the new distribution of Φ should be calculated because the balance equation can be written in terms of E (see Equs. (3.14) and (3.16)).

The geostrophic wind was calculated from the initial and final distributions of Φ . It was found that, for both methods, the maximum change was about 3 ms^{-1} .

In the following computations the second method of ellipticisation was used.

3.4 The Finite Difference Scheme

Since the balance equation may only be solved by using numerical techniques, Equ. (3.4) (or those derived from it) must be discretised.

First consider the non-linear term (NLT). There are two common finite difference schemes for this term and they correspond to Miyakoda's methods A and C (Miyakoda 1962). These will be referred to as NLT1 and NLT2. Using the notation shown in Fig. 3.2, these expressions are

$$NLT1 = 2({}^{+}\psi_{xx}\,{}^{+}\psi_{yy} - {}^{+}\psi_{xy}^{2}) \qquad (3.25)$$

$$NLT2 = 2({}^{\times}\psi_{xx}\,{}^{\times}\psi_{yy} - {}^{\times}\psi_{xy}^{2}) \qquad (3.26)$$

NLT1 is derived by using centred finite differences for ψ_{xx}, ψ_{yy} and ψ_{xy}. The resulting truncation error in NLT1 is of the order of d^4. Bolin (1956) argued that there is a systematic error in NLT1 because $\psi_{xx}.\psi_{yy}$ and ψ_{xy}^2 are calculated over different distances.

If the x and y co-ordinates of the grid are rotated through 45 , then the non-linear term is given by NLT2. This also has a truncation error of order d^4 . Also in this case the two parts of NLT are computed over the same distance.

Miyakoda (1962) solved the balance equation using NLT1 and NLT2 and obtained solutions $\Psi 1$ and $\Psi 2$. He found that $\Psi 1 > \Psi 2$ everywhere. The computations were repeated for the 1000 mb surface in area 91. The results in Fig. 3.3 confirm Miyakoda's findings and show that the maximum difference between the wind components derived from $\Psi 1$ and $\Psi 2$ is about 1 ms^{-1} .

Miyakoda speculated that the systematic difference between $\Psi 1$ and $\Psi 2$ was due to NLT2 satisfying a certain integral relationship, whereas NLT1 did not. This assertion was never substantiated.

Some insight into the reason for the systematic difference can be gained by assuming that Ψ is biharmonic

$$\Psi = A \sin(\alpha x)\sin(\beta y)$$

If this is used in Equ. (3.35) and (3.36), it can be shown that

$$\text{NLT1-NLT2} = A^2 \alpha^2 \beta^2 \left(\frac{\alpha^2 + \beta^2}{2}\right) d^2 \sin^2(\alpha x)\sin^2(\beta y)$$

Thus NLT1 > NLT2 everywhere. Now suppose that $\Psi 1$ and $\Psi 2$ are given by

$$\nabla^2 \Psi 1 + \text{NLT1} = \nabla^2 \phi$$

$$\nabla^2 \Psi 2 + \text{NLT2} = \nabla^2 \phi$$

Also let NLT1 = NLT2 + $g^2(x,y)$ so that the subtraction of the above equations

$$\nabla^2(\Psi 1 - \Psi 2) = -g^2(x,y)$$

If ($\Psi 1$ - $\Psi 2$) varies sinusoidally then the left-hand side becomes $-\lambda^2$ ($\Psi 1$ - $\Psi 2$) and thus

$$(\Psi 1 - \Psi 2) = \frac{g^2(x,y)}{\lambda^2}$$

This crude analysis shows that $\Psi 1 > \Psi 2$ everywhere.

It can also be shown that when Ψ is biharmonic, the truncation error in NLT2 is always less than that in NLT1.

Thus it is likely that $\Psi 2$ is a better approximation to the exact solution than is $\Psi 1$.

A method of testing the superiority of either NLT1 or NLT2 might be as follows.

(a) Find the solution of the balance equation and fine grid (m x m gridpoints) using NLT2. Let the solution be $\Psi 2^m$.

(b) Find the solutions of the balance equation using NLT1 or NLT2 on a coarser grid (n x n). Let the solutions be $\Psi 1^n$ and $\Psi 2^n$.

(c) The solution in part (b) that is closest to should indicate the best finite difference form of NLT.

For this method to work, the magnitude of ($\Psi 2^n - \Psi 2^m$) must be much greater than ($\Psi 2^n - \Psi 1^n$). In terms of NLT, it is required that ($NLT2^n - NLT2^m$) must be much larger than ($NLT2^n - NLT1^n$). But both of these expressions vary with x and y and thus, in terms of their root mean square (RMS) values, m and n should be such that

γ RMS ($NLT2^n - NLT1^n$) = RMS ($NLT2^n - NLT2^m$)

Here $\gamma \approx 10$.

If Ψ is biharmonic, it can be shown that the above equation gives

$$\left[\frac{n}{m}\right]^2 = 1 - \frac{3\gamma}{4}\sqrt{\frac{P}{P+Q-2R}}$$

If F and G are defined by $\sin^2(\alpha x)\sin^2(\beta y)$ and $\cos^2(\alpha x)\cos^2(\beta y)$, then P, Q and R are the integrals of F^2, G^2 and FG over the area considered. If P/ (P+Q-2R) is about $\frac{1}{2}$, then $\left[\frac{n}{m}\right]^2$ must satisfy

$$\left[\frac{n}{m}\right]^2 \approx 1 - \frac{\gamma}{2}$$

If $\gamma \approx 10$, this relationship cannot be satisfied and thus

the method described above is of little use.

The affect of the formulation of the non-linear term on the rate of convergence of different iterative schemes will be discussed later.

If the $\nabla^2\psi$ term in the balance equation is replaced by ${}^{\times}\nabla^2\psi$ and if NLT2 is used, then the solution separates into two fields. Thus in all the following computations ${}^{+}\nabla^2\psi$ was used.

Miyakoda suggested a finite difference form of $\nabla f.\nabla\psi$. However, this was not used in these computations because the finite difference depended upon ψ_o which was thought to be undesirable (see section 3.5). Thus $\nabla f.\nabla\psi$ was replaced by ${}^{+}\nabla f.\nabla\psi$ (see Fig. 3.2).

Suppose that the finite difference form of the balance equation is

$$ {}^{+}\nabla^2\psi + {}^{+}\nabla f.\nabla\psi + NLTi = \nabla^2\phi \qquad i = 1,2 \tag{3.27}$$

To derive an equation from this that is analagous to Equ. (3.16), it is necessary that

$$ (A^2 + B^2)_i = ({}^{+}\nabla^2\psi)^2 - 2NLTi \qquad i = 1,2$$

Using the appropriate value of NLTi, this gives

$$ (A^2 + B^2)_1 = (\psi_5 - \psi_6 - \psi_8 + \psi_7)^2/4 + (\psi_1 + \psi_3 - \psi_2 - \psi_4)^2 \tag{3.28}$$

$$ (A^2 + B^2)_2 = 2(\psi_1 + \psi_3 - \psi_2 - \psi_4)^2 + 4(\psi_1 - 2\psi_0 + \psi_3)(\psi_2 - 2\psi_0 + \psi_4) $$

$$ -(\psi_5 - 2\psi_0 + \psi_7)(\psi_6 - 2\psi_0 + \psi_8) \tag{3.29}$$

When A and B are put in terms of (+) finite differences, Equ. (3.28) follows directly. But Equ. (3.29) cannot be derived by using (x) finite differences for A and B. When this is done the result is Equ. (3.28). This inconsistency disappears if $(A^2 + B^2)_2$ is calculated from $({}^{\times}\nabla^2\psi)^2 - 2 \times NLT2$. But this form of $(A^2 + B^2)_2$ cannot

be used because it is necessary for $\nabla^2\Psi$ to be replaced by ${}^{\times}\nabla^2\Psi$ and this is undesirable.

A comparison of Equs. (3.28) and (3.29) shows that the calculation of $(A^2 + B^2)_1$ requires fewer arithmetic operations than does $(A^2 + B^2)_2$. Also the former is independent of Ψ_o whereas the latter depends strongly on Ψ_o. The significance of this will be dealt with later.

3.5 Methods Of Solving The Balance Equation

Two slightly different successive overrelaxation techniques have been used to solve the balance equation.

The first technique is an extension of the SOR method and is known as non-linear overrelaxation (NLOR). This will be referred to as a method of the first type. The main characteristic of this type of method is that the latest values of Ψ are used in all computations.

The second technique consists of linearising either Equ. (3.14) or (3.16). When the former equation is used this will be called a method of the second type. A method of the third type will refer to the use of the latter equation. Both these methods usually, but not always, require the use of two fields of Ψ (or something related to Ψ).

The method described by Endlich (1970) will not be discussed here. However it is hoped that in the future a comparison between his method and those described above will be undertaken.

The ADI method was not considered because of the problem of finding the optimum variation of the iteration of the iteration parameter. Also, there are difficulties

involved in linearising the equation due to the presence of the Ψ_{xy} term.

The NLOR method has been described by Ames (1965). He showed that if $g\ (x_o,\ y_o,\ \Psi_o,\ \Psi_1,\ \Psi_2,\ \ldots\ldots) = 0$ is the finite difference form of the non-linear equation at point 0, then the iteration process is defined by

$$\Psi_o^{(n+1)} = \Psi_o^{(n)} - \frac{\beta g^{(n)}}{\left(\frac{\partial g}{\partial \Psi_o}\right)^{(n)}} \qquad (3.30)$$

Here the latest values of Ψ are used to compute $g^{(n)}$. Ames also pointed out that the optimum value of β depends upon $\Psi^{(n)}$ and therefore it will change during the iteration process. The evaluation of the optimum value of β will be considered later.

If $g = 0$ is a linear equation, then Equ. (3.30) defines the SOR method. This illustrates the relationship between SOR and NLOR.

If $g = 0$ is the balance equation then the presence of Ψ_{xy} in it means that a certain matrix will not have property A (see Ames (1965)). Thus convergence will not necessarily, but will usually, take place.

If $g_1 = 0$ and $g_2 = 0$ are the finite difference form of the balance equation when NLT1 and NLT2 are used, then

$$\frac{\partial g_1}{\partial \Psi_o} = -\frac{4}{d^2}(f \overset{+}{+} \nabla^2\Psi) \qquad \frac{\partial g_2}{\partial \Psi_o} = -\frac{4}{d^2}(f \overset{\times}{+} \nabla^2\Psi)$$

Thus these expressions depend upon the finite difference form of the absolute vorticity. Since the absolute vorticity may be very small, the NLOR method might involve divisions by very small numbers. A method that overcomes this problem will be described later.

The use of the NLOR method to solve the balance

equation will be called NLOR1 and NLOR2. The subscript indicates the form of the non-linear term that was used.

When the NLOR method is used with $\beta = 1$ it becomes identical with the method used by Bolin (1955, 1956).

Asselin (1967) used an iteration scheme that was similar to that used for the NLOR method. This scheme was

$$\psi_o^{(n+1)} = \psi_o^{(n)} + \frac{\alpha g^{(n)}}{\left(\frac{f}{d^2}\right)} \tag{3.31}$$

This has the advantage that the coefficient of $g^{(n)}$ is independent of $\psi^{(n)}$. But, there is the disadvantage that this iteration scheme has never been investigated theoretically. Thus, for instance, the limits of α for which there will be a convergent solution are not known. The use of the above iteration scheme with g_1 or g_2 will be called NLAS1 and NLAS2.

Both the NLOR method and Asselin's method are methods of the first type.

A method of the second type was used by 'Arnason (1958). He solved the linearised equation

$$h^{(n)} = f\nabla^2\psi^{(n)} + \nabla f.\nabla\psi^{(n)} + 2(\psi_{xx}^{(n)}\psi_{yy}^{(n-1)} + \psi_{xx}^{(n-1)}\psi_{yy}^{(n)} - \psi_{xy}^{(n)}\psi_{xy}^{(n-1)}) - \nabla^2\Phi \tag{3.32}$$

If $h_1^{(n)}$ and $h_2^{(n)}$ are the finite difference forms of Equ. (3.32) consistent with the use of NLT1 and NLT2, then the iteration schemes become

$$\psi_o^{(n+1)} = \psi_o^{(n)} + \frac{\beta h_1^{(n)}}{\frac{4}{d^2}\left(f + \frac{\nabla^2\psi^{(n-1)}}{2}\right)}$$

$$\psi_o^{(n+1)} = \psi_o^{(n)} + \frac{\beta h_2^{(n)}}{\frac{4}{d^2}\left(f + \frac{\nabla^2\psi^{(n-1)}}{2}\right)}$$

The use of these schemes will be referred to as NLAR1 and

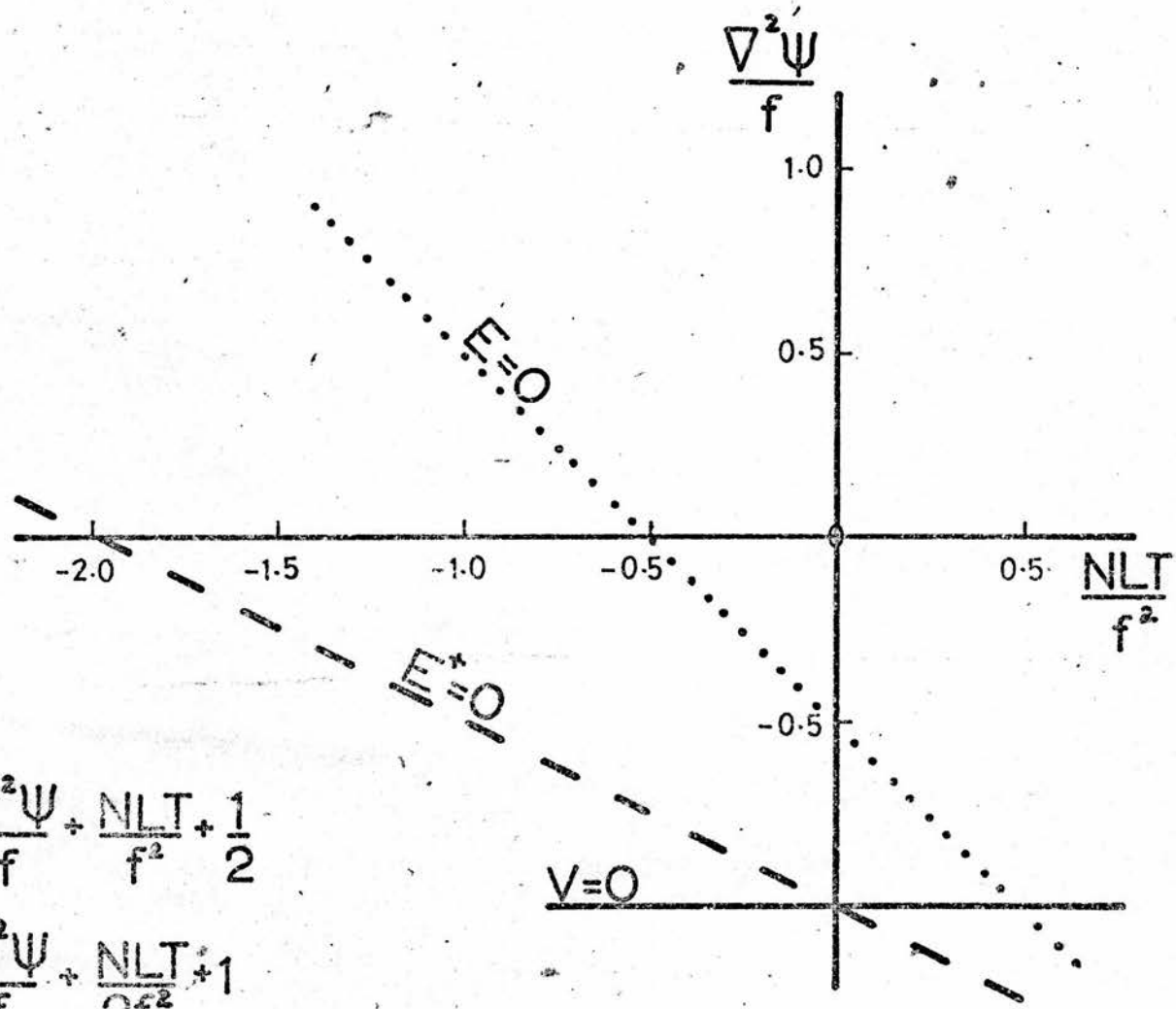

$$E = \frac{\nabla^2\Psi}{f} + \frac{NLT}{f^2} + \frac{1}{2}$$

$$E^{+} = \frac{\nabla^2\Psi}{f} + \frac{NLT}{2f^2} + 1$$

$$V = \frac{\nabla^2\Psi}{f} + 1$$

FIGURE 3·4

NLAR2.

The method used by 'Arnason has two disadvantages when compared with the methods of the first type. Firstly, several extra computations have to be performed and secondly both $\psi^{(n)}$ and $\psi^{(n-1)}$ have to be stored. However the advantages of this method are that for a given n the equation to be solved in linear and that the denominator in the iteration scheme is never small.

The balance equation is elliptic if

$$\frac{\nabla^2\psi^{(n)}}{f} + \frac{NLT^{(n)}}{f^2} + \frac{1}{2} > 0 \qquad (3.33)$$

Equ. (3.32) is elliptic with respect to $\psi^{(n)}$ if

$$\frac{\nabla^2\psi^{(n-1)}}{f} + \frac{NLT^{(n-1)}}{2f^2} + 1 > 0 \qquad (3.34)$$

Fig. 3.4 shows that if Equ. (3.33) holds and if $(\frac{\nabla^2\psi}{f} + 1)>0$ then Equ. (3.34) is satisfied. Thus if the finite difference forms of Equs. (3.11) and (3.13) are satisfied, then Equ. (3.32) is elliptic.

A method that incorporates some of the advantages of both the NLOR and 'Arnason's methods is described by

$$\psi_o^{(n+1)} = \psi_o^{(n)} + \frac{\beta g_1^{(n)}}{\frac{4}{d^2}\left(f + \frac{\nabla^2\psi^{(n)}}{2}\right)} \qquad (3.35)$$

Also a similar iteration scheme can be used to solve $g_2 = 0$. The use of this method will be referred to as NLOR1^x or NLOR2^x depending upon the form of the non-linear term. The NLOR^x method is a method of the first type.

Another method of the second type was discussed by 'Arnason (1958). He considered the equation

$$f\nabla^2\psi^{(n)} + \nabla f.\nabla\psi^{(n)} + NLT^{(n-1)} - \nabla^2\phi = 0$$

With this form of linearisation a Poisson type equation is solved at each iteration. This can be achieved very efficiently. However 'Arnason showed that this method would not produce a convergent solution. The reason is that the non-linear term is strongly dependent upon Ψ_o. This problem may be overcome by solving the balance equation in the form of Equ. (3.16). The methods used to solve the equation in this form will be called methods of the third type.

The general form of the iteration scheme for methods of the third type is

$$\zeta^{(n+1)} = \zeta^{(n)}(1-\alpha) + \alpha F(\Psi) \qquad (3.36)$$

$$\Psi^{(n+1)} = \Psi^{(n)} + \frac{\beta}{\left(\frac{4}{d^2}\right)}(\nabla^2\Psi^{(n)} - \zeta^{(n)}) \qquad (3.37)$$

Here $F(\Psi)$ is the righthand side of Equ. (3.16).

Many variations of the above iteration scheme have been used. Firstly different values of α and β have been used and secondly different numbers of scans per iteration.

A single scan method is defined as a method in which Equs. (3.36) and (3.37) are used at one gridpoint before moving to the next. A double scan method is defined as one in which Equ. (3.36) is used at all gridpoints before Equ. (3.37). Thus in this case each iteration consists of two scans of the grid.

A summary of the methods of the third type that have been used is given in Table 3.1. This shows the ranges of α and β that were used. The number of scans is also indicated. Finally the number of fields that is

Method	Code	α	β	Scans	Fields
Miyakoda A (1956)	NLMA	1	1	1	1
Shuman Slow (1957)	NLSS	1	>1	1	1
Suggested Method	NLAU	<1	>1	1	1
Miyakoda B (1956) / Shuman Fast (1957)	NLMB	1	>1	2	2
White * (1969)	NLWH	<1	>1	2	2

TABLE 3.1

*White used the ADI method to solve the Poisson equation during the second scan of each iteration. In terms of the SOR method, this is equivalent to using $\beta > 1$.

needed is shown.

The relative efficiency of all the methods described was investigated and will be described later.

When methods of the first and second type are used it is desirable to know the optimum value of β. The next section is concerned with estimating this value for a linearised version of the balance equation.

3.6 The Estimation Of The Optimum Overrelaxation Factor

An analysis, similar to that used by Asselin (1967) was performed on the following linear version of the balance equation.

$$f\nabla^2\Psi + A\Psi_{xx} - B\Psi_{xy} + C\Psi_{yy} - \nabla^2\phi = 0 \qquad (3.38)$$

In the analysis the first term was replaced by $f^{+}\nabla^2\Psi$ and two sets of finite differences were used for the "non-linear terms".

The use of ${}^{+}\Psi_{xx}$, ${}^{+}\Psi_{yy}$ and ${}^{+}\Psi_{xy}$ in the "non-linear terms" is analagous to using NLT1. Any quantities derived when these were used will be denoted by a subscript 1. Similarly the use of ${}^{\times}\Psi_{xx}$, ${}^{\times}\Psi_{yy}$ and ${}^{\times}\Psi_{xy}$ is analagous to using NLT2 and a subscript 2 will be used to denote quantities relating to this equation.

If Equ. (3.38) is solved using the SOR method, then the iteration formula for $\varepsilon_{ij}^{(n)} = \Psi_{ij}^{(n)} - \Psi_{ij}$ can be derived.

Suppose $\varepsilon_{ij}^{(n)}$ has the form

$$\varepsilon_{ij}^{(n)} = q^n \exp(\vartheta i + \varphi j) \qquad (3.39)$$

When Dirichlet boundary conditions to solve Equ. (3.38) in an area with $n_i \times n_j$ gridpoints, ϑ and φ will be given by

$$\vartheta = \frac{\pi}{n_i - 1} \qquad \varphi = \frac{\pi}{n_j - 1} \qquad (3.40)$$

If Equs. (3.39) and (3.40) are used in the iteration formula for $\varepsilon_{ij}^{(n)}$, then a complex expression for q can be derived. The magnitude of q, $|q|$ say, is

$$|q| = \sqrt{\frac{(1 - \beta + \beta v)^2 + (\beta w)^2}{(1 - \beta v)^2 + (\beta w)^2}} \qquad (3.41)$$

From this equation it can be shown that $|q|$ is a minimum with respect to β when

$$\beta = \frac{2}{1 + \sqrt{1 - \gamma^2}} \qquad \gamma^2 = 4(v - w^2 - v^2) \qquad (3.42)$$

Let this value of β be denoted by $\beta_o(A)$. The expressions for w and v depend upon the finite differences that are used in Equ. (3.38). These expressions will be given later.

There will be convergence if $|q| < 1$. Equ. (3.41) shows that this is so for all β such that $0 < \beta < 2$. Thus Equ. (3.41) gives the correct range of β for which there is convergence. Also, a comparison of Equs. (3.42) and (2.5) shows that this method produces an expression for β_o that has the correct form.

The method by which $|q|$ was derived is similar to Miyakoda's method. The difference between these methods is associated with the amount of detail that is known about $\varepsilon_{ij}^{(n)}$. Miyakoda used an expression for $\varepsilon_{ij}^{(n)}$ that fitted the results exactly, whereas the above method uses the largest fourier component of $\varepsilon_{ij}^{(n)}$. The latter method is used for Equ. (3.38) because $\varepsilon_{ij}^{(n)}$ is not known.

Let c1, c2, c3, c4, s1, s2, s3 and s4 be defined as follows

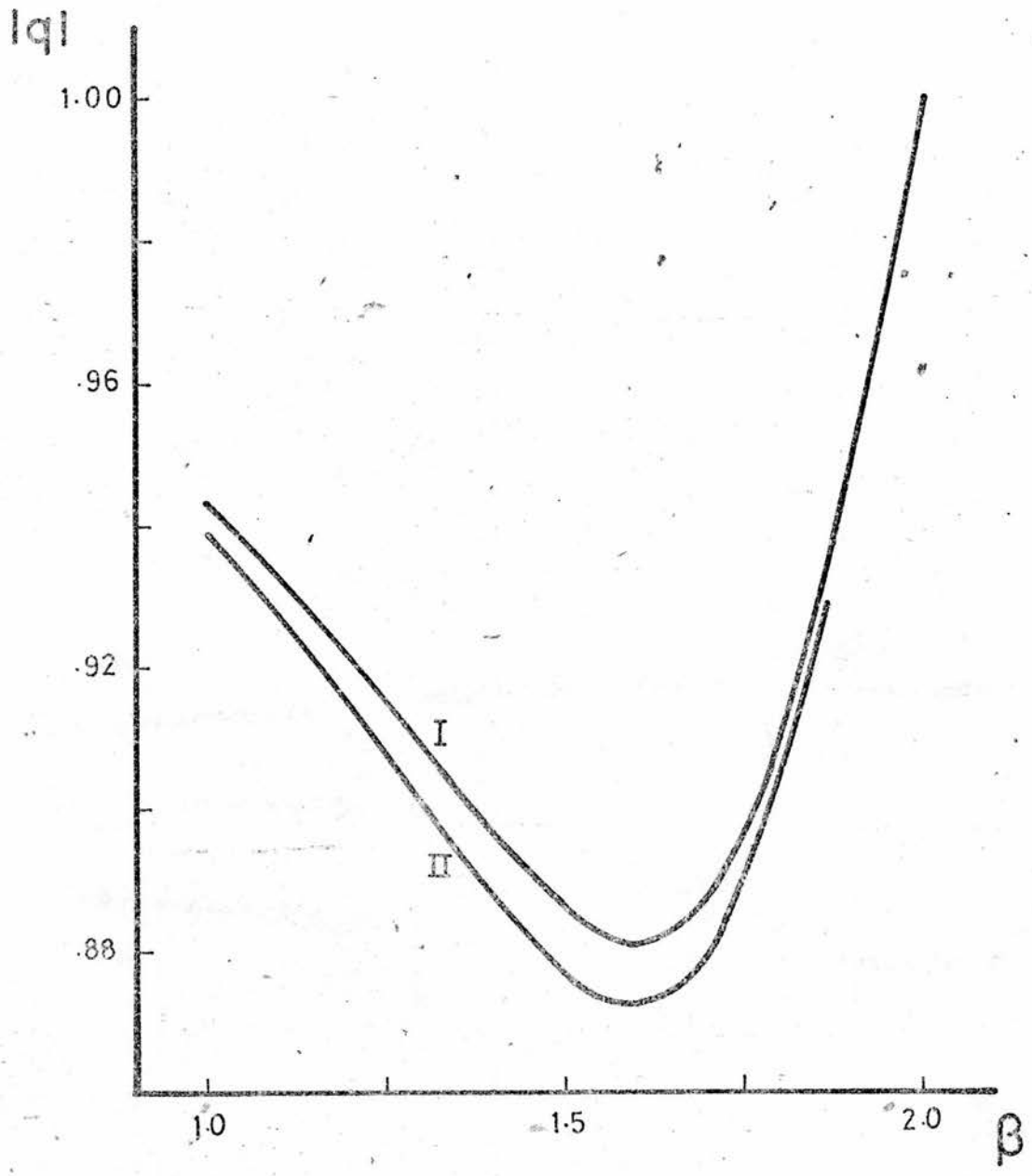

FIGURE 3·5

$c1 = \cos(\vartheta)$ $c2 = \cos(\varphi)$ $c3 = \cos(\varphi+\vartheta)$

$c4 = \cos(\varphi-\vartheta)$

$s1 = \sin(\vartheta)$ $s2 = \sin(\varphi)$ $s3 = \sin(\varphi+\vartheta)$

$s4 = \sin(\varphi-\vartheta)$

It can be shown that v_1 and v_2 are given by

$$v_1 = c1 + c2 + A \times c1 + C \times c2 - \frac{B \times (c3 - c4)}{4} / (4 + 2A + 2C)$$

$$v_2 = c1 + c2 + \frac{A \times c3}{2} + \frac{C \times c4}{2} - \frac{B \times (c2 - c1)}{2} / (4 + A + C)$$

The expressions for w_1 and w_2 are derived from these equations by replacing c1 and s1 etc.

Equs. (3.41) and (3.42) were tested with A = B =C = 0 (a Poisson equation). The variation of $|q|$ with β for this case is shown by curve I in Fig. 3.5. This shows that $|q|$ has a minimum in the region of $\beta = 1.6$. In fact, Equ. (3.42) gives $\beta_o(A) = 1.61$. The corresponding value from Miyakoda's method is $\beta_o(M) = 1.62$. Also it was found that as the number of gridpoints increased $\beta_o(A)$ rapidly approached $\beta_o(M)$. For instance, if there were 10 x 10 gridpoints, $\beta_o(A)$ overestimated $\beta_o(M)$ by only 3%. These results show that $\beta_o(A)$ is a very good approximation to $\beta_o(M)$. The reason for this is that Equ. (3.42) approaches Equ. (2.5) as n_i and n_j increase.

Fig. 3.5 shows that at $\beta_o(A)$, the value of $|q|$ ($q_o(A)$ say) was .88. However if $q_o(M) = \beta_o(M) - 1$ then the theoretical value of the minimum of $|q|$ is $q_o(M) = .62$. Thus $q_o(A)$ was not a good approximation to $q_o(M)$. However, as the number of gridpoints increased, $q_o(A)$ slowly approached $q_o(M)$. This is illustrated by the fact that even for 80 x 80 gridpoints $q_o(A)$ under-

estimated $q_o(M)$ by 6%. Therefore, this method is not a suitable way of estimating the rate of convergence.

The above results indicate that, for a Poisson equation, Equs. (3.41) and (3.42) can be used to estimate β_o, but not q_o. However, $\beta_o(A) - 1$ is a good estimate of q_o. Equ. (3.41) was used to compare the two finite difference schemes used in Equ. (3.38). A, B and C were taken to be the average value of Ψ_{yy}, Ψ_{xx} and $2\ \Psi_{xy}$. The variation of $|q_1|$ and $|q_2|$ with β is shown by curves I and II of Fig. 3.5. (The results for scheme I were the same as those for the Poisson equation). This shows that the optimum values of β were the same for both finite difference schemes. Also, the optimum values were the same as that for the Poisson equation. This is because A, B and C were small.

Fig. 3.5 also shows that $q_o(A)_1 > q_o(A)_2$. This implies that scheme 2 requires fewer iterations than scheme 1. But, this result may not be significant due to the inadequacy of this method in predicting q_o.

The results described in this section indicate that, if A, B and C are small, then the optimum overrelaxation factor for Equ. (3.38) is almost the same as that for a Poisson equation. It is suspected that this will also be true when either NLOR or NLOR^X is used.

3.7 A Comparison Of Different Methods Of Solving The Balance Equation

In the next four sections a comparison is made between the efficiencies of different methods of solving the balance equation.

In all the computations α and β had values of

$\frac{n}{10}$, where n was an integer such that $0 < n < 20$.

The iterative process will be described as divergent if the norm of the residual increases in two successive iterations. Thus if there is divergence when $\beta = 1.5$, it is implied that there is convergence when $\beta = 1.4$ and that it is not known what happens when $1.4 < \beta < 1.5$.

When the norm of the residual decreased monotonically, either + or × was used to indicate points on a graph. However, when this did not happen the symbol • was plotted. D (+) and D (×) indicate the values of the relaxation factor for which there was divergence.

The parts of the computer programmes that were concerned with the iteration process are shown in Appendix I. The programmes for the three basic types of methods are included.

The time taken to solve the balance equation, for a given E, depends upon the number of iterations required (rate of convergence) and the number of computations per iteration. Since a comparison was made between different methods for a given area, a measure of the efficiency is product of the number of iterations and the operational count (the number of multiplications and divisions at each gridpoint per iteration). This will be referred to as the total count (this will depend upon the value of E).

In all computations the geopotential of the 1000 mb surface for area 91 was used ($n_i = 16$, $n_j = 12$). The geopotential was ellipticised by using the second method described in section 3.3.2. Also, except when stated otherwise, the initial guess was Φ/f.

			$E = 10^3$		$E = 10^0$		
Method	β	O.C.	N.I.	T.C.	N.I.	T.C.	Fig.
NLOR1	1.0	16	68	1088	-	-	3.6a
NLOR1[x]	1.0	15	50	750	-	-	3.6a
NLOR1[x]	1.3	16	27	432	-	-	3.6a
NLOR2	1.0	16	71	1136	-	-	3.6b
NLOR2	1.6	17	35	595	-	-	3.6b
NLOR2[x]	1.0	15	53	795	-	-	3.6b
NLOR2[x]	1.6	16	17	272	31	496	3.6b
NLSH2	1.0	15	56	840	-	-	3.7a
NLSH2	1.6	16	19	304	32	512	3.7a
	α						
NLAS1	0.100	14	107	1498	-	-	3.7b
NLAS2	0.225	14	33	462	-	-	3.7b
NLAR1	1.2	26	40	1040	-	-	3.8a
NLAR1[*]	1.6	27	25	675	54	1458	3.8a
NLAR2	1.6	26	22	572	47	1222	3.8b

TABLE 3.2

O.C. - Operational Count

N.I. - Number of Iterations

T.C. - Total Count

3.7.1 A Comparison Of Methods Of The First Type

A comparison of methods of the first type was made. These were the NLOR, NLOR^{X} and NLAS methods. Also, the ordering of the gridpoints as suggested by Sheldon (see section 2.2.1) was used in conjunction with the NLOR method (hereafter called the NLSH method).

The results of using NLOR1 are shown in Fig. 3.6a.* It shows that this method produced convergence for only $\beta = 1.0$. The number of iterations, operational count and total count are shown in Table 3.2.

Fig. 3.6a also shows the results for NLOR1^{X}. With $\beta = 1.0$ and $E = 10^{3}$, the number of iterations was 50 and the total count 750. The corresponding values for NLOR1 were 68 and 1088. Thus, with $\beta = 1.0$, NLOR1^{X} was more efficient than NLOR1.

Unlike NLOR1, NLOR1^{X} gave a convergent solution with $\beta > 1.0$. It was also found that as β increased the convergence rate increased until β had a value of 1.5. At this point there was divergence. Table 3.2 shows that, with $E = 10^{3}$, the number of iterations with $\beta = 1.4$ was almost half the number required when $\beta = 1.0$ was used. Therefore it is worthwhile finding the optimum value of β for NLOR1^{X}. These results also show that NLOR1^{X} was more efficient than NLOR1 for all values of β.

The method (Carré's method) described in section 2.2.2 for calculating β_o for a linear equation, was used with NLOR1^{X}. It gave $\beta_o(C) = 1.56$. The significance of this, if any, is not obvious because with $\beta = 1.56$ there was not a convergent solution.

The disadvantage of using NLOR1^{X} is that it has never

*The curves are labelled with log E. This applies to other figures.

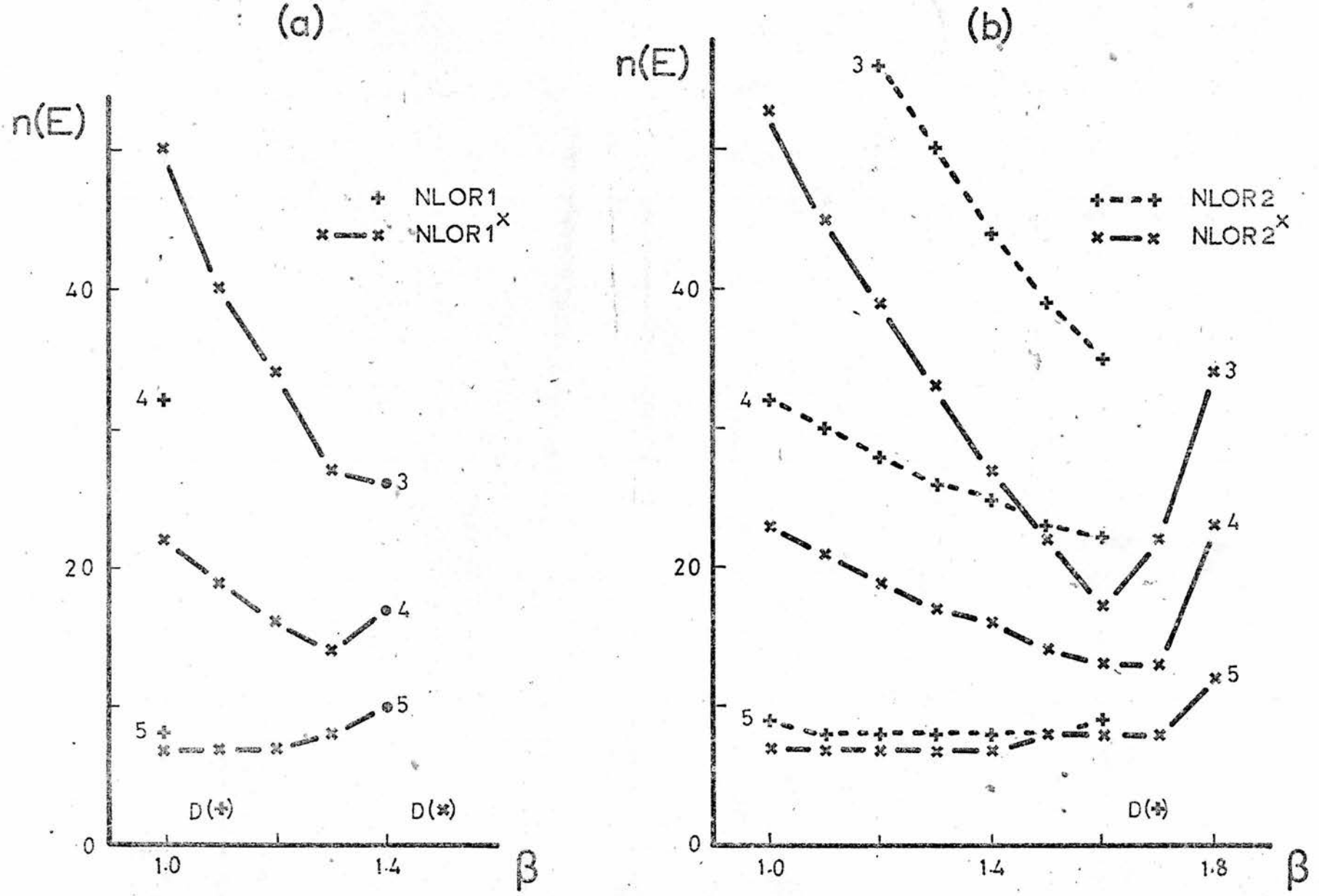
(a)
n(E)
NLOR1
NLOR1×
40
20
0
4
3
4
5
5
D(+)
D(×)
1·0
1·4
β
(b)
n(E)
NLOR2
NLOR2×
40
20
0
3
4
3
4
5
5
D(+)
1·0
1·4
1·8
β

FIGURE 3.6

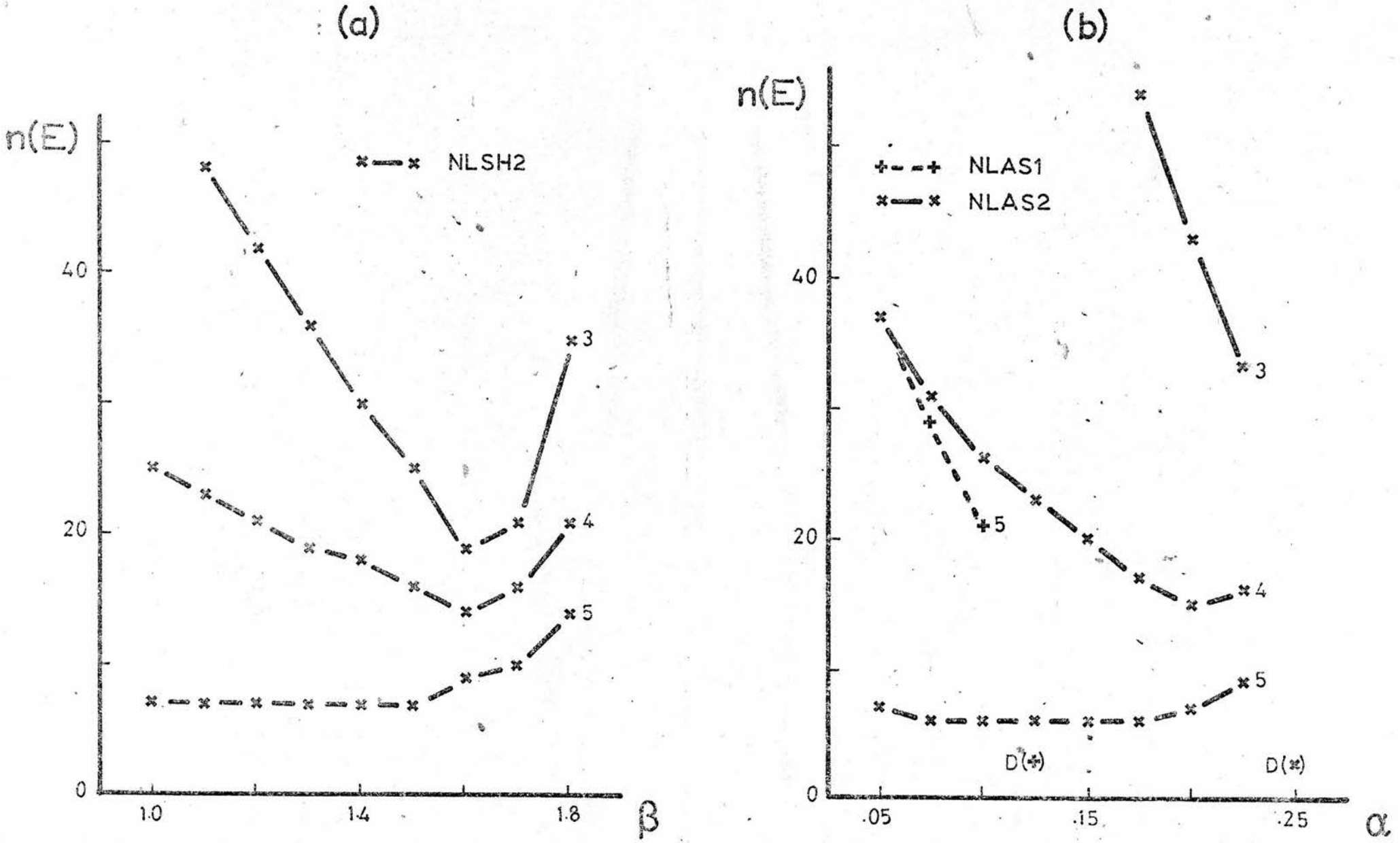
(a)
n(E)
NLSH2
40
20
0
3
4
5
1.0
1.4
1.8
β
(b)
n(E)
NLAS1
NLAS2
40
20
0
3
4
5
D(+)
D(*)
.05
.15
.25
α

FIGURE 3.7

been treated theoretically. Therefore the range of for which there is convergence, and the optimum value of β, must be determined experimentally.

Fig. 3.6b shows the results for NLOR2 and NLOR2^{X}. With $\beta = 1.0$, NLOR2^{X} was more efficient than NLOR2. This figure also shows that the convergence rates increased when $\beta > 1.0$ was used. In both cases $\beta_o(E)$ was 1.6. With this value of β and $E = 10^3$, Fig. 3.6b and Table 3.2 shows that NLOR2^{X} was far more efficient than NLOR2. This was also true when $1.0 < \beta < \beta_o(E)$.

The optimum value of β for NLOR2^{X} became better defined as E decreased. Thus the value of β must be chosen carefully when a small value of E is used.

The value of β_o for a Poisson equation with $n_i = 16$ and $n_j = 12$ is 1.62. This is a very good estimate of $\beta_o(E)$ and supports the suggestion made at the end of section 3.6. Also, Carré's method was applied to NLOR2^{X} and it was found that $\beta_o(C) = 1.58$. Therefore it is possible that Carré's method can be applied to NLOR2^{X}. However, there is no theoretical support for this assertion.

The effect of the initial guess was tested for NLOR2^{X}. An "improved" initial guess was used (the solution of the linear balance equation) and it was found that it had no appreciable effect on the convergence rate.

The ordering of the gridpoints suggested by Sheldon was used in conjunction with NLOR2 (hereafter referred to as NLSH2). The results are shown in Fig. 3.7a. A comparison of this with Fig. 3.6b shows that NLSH2 was slightly less efficient than NLOR2^{X}. The explanation of this may be that when (i + j) even points were relaxed

the non-linear term involved Ψ at other (i + j) even points.

Finally, Asselin's method was investigated. The results of NLAS1 and NLAS2 are shown in Fig. 3.7b. In each of these cases the optimum value of α was the same at the maximum value. However this value of α was different for NLAS1 and NLAS2. Table 3.2 shows that when the optimum value of α was used, NLAS2 was far more efficient than NLAS1.

Asselin's method has never been treated theoretically. Therefore, there is no theory to provide an estimate of the optimum and maximum values of α (α_o and α_c say). However Asselin gained some insight into this problem by analysing a linear version of the balance equation (Equ. 3.38). Using his type of analysis it can be shown that α and β are related by

$$\alpha = \frac{\beta}{4\left(1 + \frac{\nabla^2\Psi}{2f}\right)}$$

The results from sections 2.5.4 and 2.5.5, show that α_o and α_c can be estimated by using

$$\alpha_o = \frac{\beta_o}{AV(x)} \qquad \alpha_c = \frac{2}{MAX(x)} \qquad x = 4\left(1 + \frac{\nabla^2\Psi}{2f}\right)$$

Here AV (x) and MAX (x) refer to the average and maximum values of x.

In the particular case considered, β_o is approximately 1.6 and thus approximate values of α_o and α_c are 0.35 and 0.24. Since $\alpha_o > \alpha_c$ it is expected that the optimum value of α will be its maximum value (i.e. 0.24). These predictions agree well with the experimental

results for NLAS2 (see Fig. 3.7b).

The advantage of using Asselin's method is that it has a smaller operational count than the other method. But, Table 3.2 shows that when the optimum values of the overrelaxation factors were used, NLOR2$^{\times}$ had a smaller total count than NLAS2. Also NLAS1 was the least efficient of all the methods that used NLT1.

Consider the effect of the formulation of the non-linear term on the convergence characteristics of the methods discussed. When NLT1 was used it was found that there was always convergence with $\beta = 1.0$. Also, when it was possible to get convergence with a larger β, there was an increase in the rate of convergence. But it is difficult to estimate the optimum and maximum values of the overrelaxation factors.

When NLT2 was used, it was found that the convergence increased as β increased from 1.0. Also there tended to be a distinct optimum value of β ($\beta_o(E)$) which had a similar value to that for the corresponding Poisson equation. This value could be used to give an estimate of α_o for Asselin's method.

The above results indicate that the methods of the first type were most efficient when NLT2 was used. This result was predicted in section 3.6. However, due to the inadequacy of the analysis described in section 3.6, this may only be a coincidence.

The results in Table 3.2 show that the NLOR2$^{\times}$ method was the most efficient. However the supremacy of this method is only provisional because it has not been extensively tested.

3.7.2 A Comparison Of Methods Of The Second Type

A comparison of methods of the second type was made. The results are summarised in Table 3.2.

Fig. 3.8a shows the results for NLAR1. As β increased from 1.0, the number of iterations required for a given E decreased until $\beta = 1.3$ was reached. With $\beta >= 1.3$ it was found that the solution oscillated. For example the variation of $\log \| \psi^{(n+1)} - \psi^{(n)} \|$ with n is shown in Fig. 3.9.

Miyakoda (1962) noted that the solution of Equ. (3.16) sometimes oscillated. He remedied this by using $(\psi^{(n)} + \psi^{(n-1)})/2$ in the computation of $(A^2 + B^2)^{(n)}$. A similar procedure was used with NLAR1. (hereafter called NLAR1*). The non-linear term took the form

$$4\,NLT = \nabla^2\psi^{(n)}\left(\nabla^2\psi^{(n-1)} + \nabla^2\psi^{(n-2)} \right) - A^{(n)}\left(A^{(n-1)} + A^{(n-2)} \right) - B^{(n)}\left(B^{(n-1)} + B^{(n-2)} \right)$$

The results of NLAR1* are shown in Figs. 3.8a and 3.9.

The use of the above procedure stopped the oscillations and increased the optimum value of β to 1.6. Table 3.2 shows that NLAR1* was more efficient than NLAR1. Another advantage of using NLAR1* is that the value of β_o can be estimated. However the disadvantage of this method is that three fields of ψ have to be stored whereas NLAR1 only requires the storing of two fields.

The results of NLAR2 are shown in Fig. 3.8b. It shows that once again the optimum value of β was 1.6. With this value of β, NLAR2 was the most efficient of all the methods of the second type (see Table 3.2). Therefore it is best to use NLT2 with the NLAS method.

A comparison between the methods of the first and second type (see Table 3.2) shows that NLAR2 had over

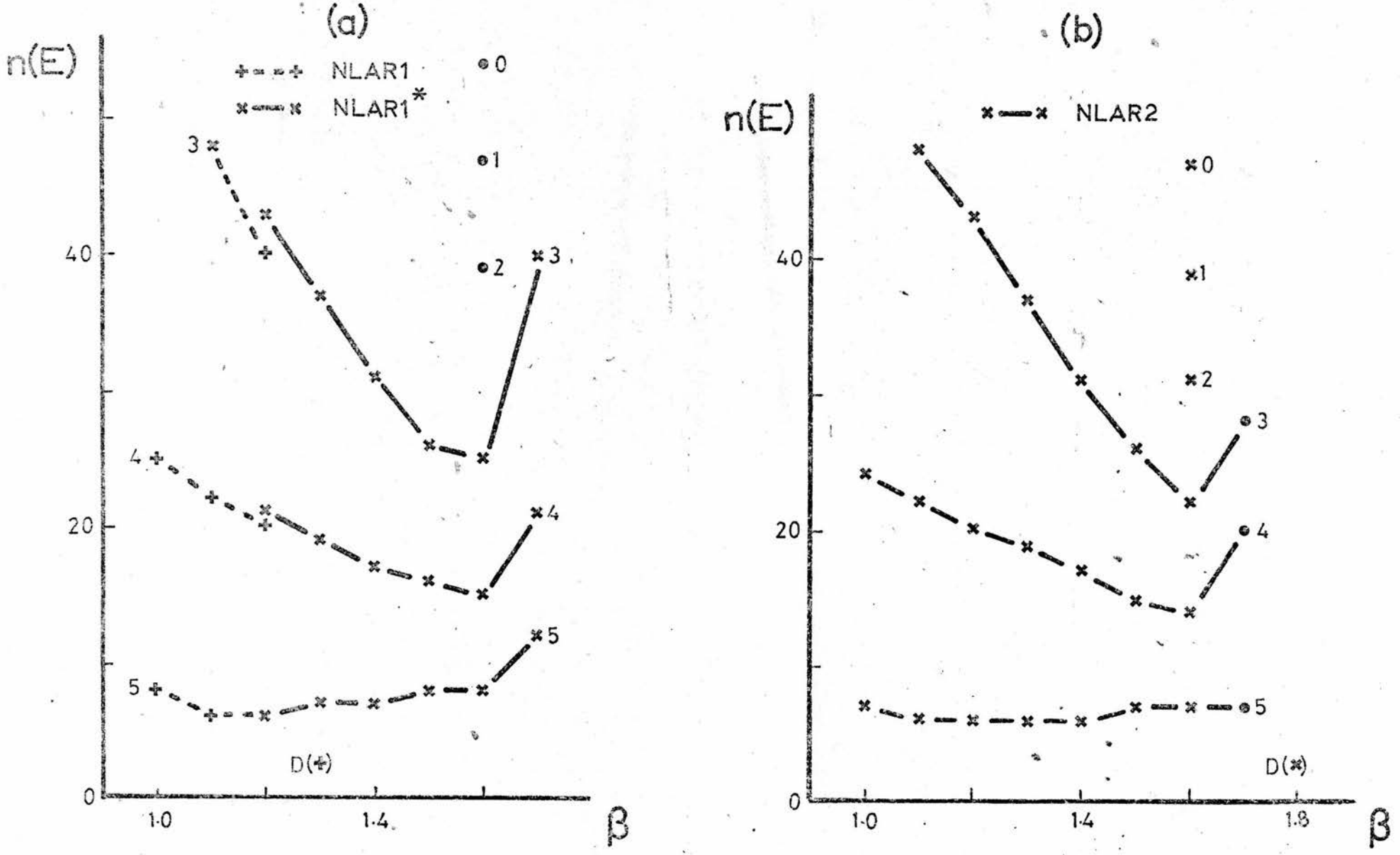
(a)
n(E)
NLAR1
NLAR1*
0
1
2
3
4
5
40
20
0
1·0
1·4
D(+)
β
(b)
n(E)
NLAR2
0
1
2
3
4
5
40
20
0
1·0
1·4
1·8
D(*)
β

FIGURE 3·8

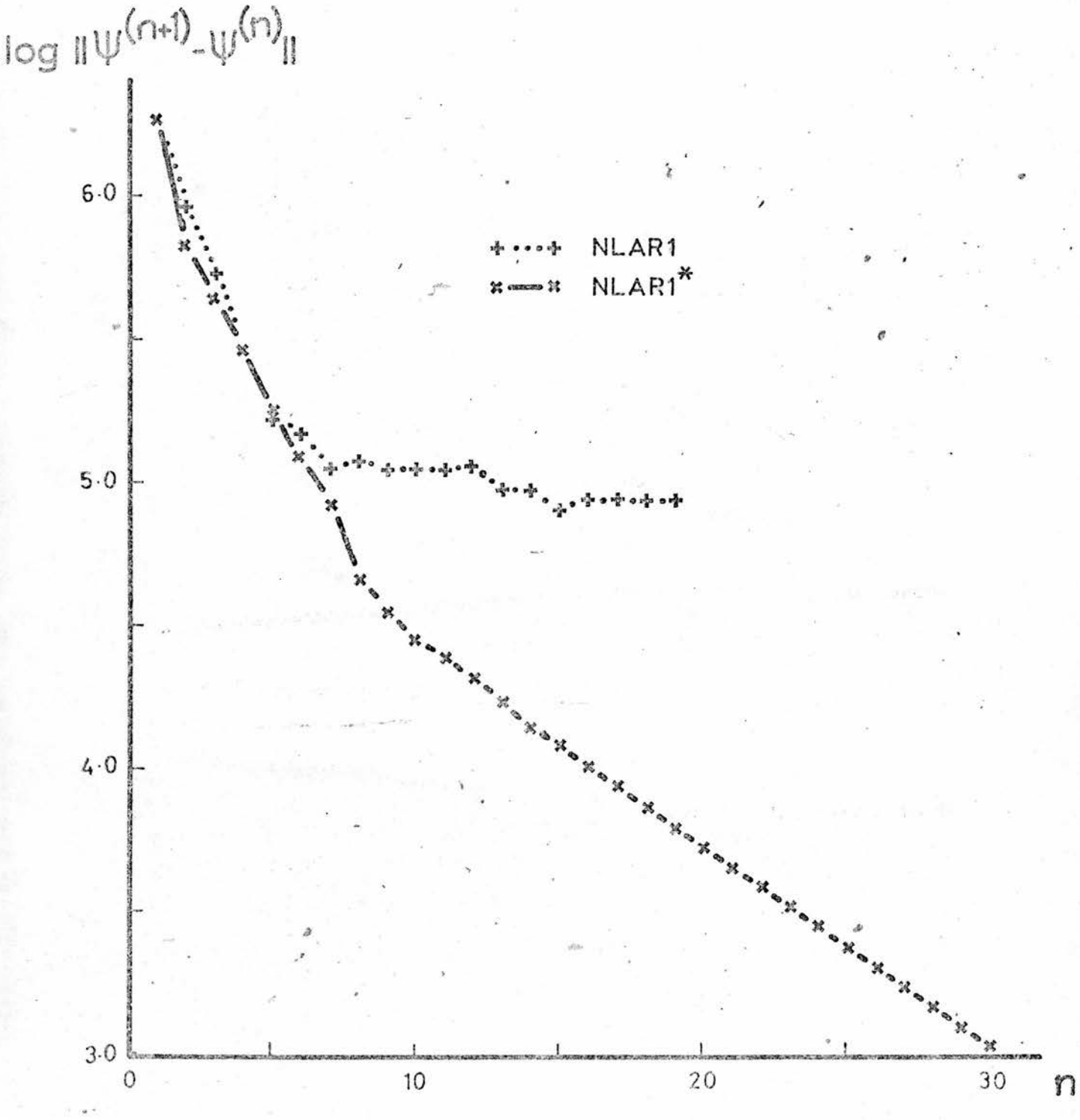

FIGURE 3.9

twice the total count of NLOR2$^{\times}$. However, there was little difference between NLAS2, NLOR2 and NLAR2.

The main disadvantages of methods of the second type are that they have large operational counts and that they require the storage of at least two fields of Ψ .

3.7.3 A Comparison Of Methods Of The Third Type

A comparison of methods of the third type was made. A summary of the results is exhibited in Table 3.3.

When a method of the third type is used it is necessary to specify two parameters α and β . NLWH1 was first investigated by using $\beta = 1.6$ (the optimum value for the Poisson equation) and varying α . The results are shown in Fig. 3.10a. This shows that the convergence rate was not strongly dependent upon α and that it decreased rapidly when $\alpha > 1.0$. In fact there was divergence when $\alpha = 1.2$. In the following computations the optimum α was assumed to be 0.8.

With $\alpha = 1.0$, NLWH1 is equivalent to NLMB1. Fig. 3.10a shows that there was little difference between NLWH1 and NLMB1. But, like β , the optimum value of α became better defined as E decreased. Also it is suspected that α decreases as the number of gridpoints increases. Thus, it is likely that the difference between NLWH1 and NLMB1 is significant if there is a large area or a small value of E.

When a solution oscillated, Miyakoda (1962) used $(\Psi^{(n)} + \Psi^{(n-1)}) /2$ to compute $(A^2 + B^2)$. This technique (hereafter called Miyakoda's technique) was used with NLWH1 when there were no oscillations (NLWH1*). The results are shown in Fig. 3.10b. A comparison of

				$E = 10^3$		$E = 10^0$		
Method	α	β	O.C.	N.I.	T.C.	N.I.	T.C.	Fig.
NLWH1	0.8	1.6	12	21	252	41	492	3.10a
NLWH1*	0.8	1.6	13	22	286	43	559	3.10b
NLMB1	1.0	1.6	11	22	242	-	-	3.10a
NLAU1	0.8	1.6	12	18	216	30	360	3.11a
NLAU1*	0.8	1.6	13	18	234	31	403	3.11b
NLAU1**	0.8	1.6	12	18	216	30	360	-
NLSS1	1.0	1.6	11	18	191	-	-	3.11a
NLMA1	1.0	1.0	10	62	620	-	-	-
NLWH2	0.5	1.6	18	25	450	53	954	3.12a
NLWH2*	0.8	1.6	19	22	418	43	817	3.12b
NLWH2*	1.0	1.6	18	27	484	-	-	3.12b
NLWH2**	0.5	1.6	18	25	450	48	864	-
NLAU2	0.8	1.6	18	34	612	-	-	3.13a
NLAU2*	0.8	1.6	19	34	646	75	1425	3.13b
NLAU2*	1.0	1.6	18	34	612	-	-	3.13b
NLAU2**	0.8	1.6	18	34	612	75	1350	-

TABLE 3.3

O.C. - Operational Count

N.I. - Number of Iterations

T.C. - Total Count

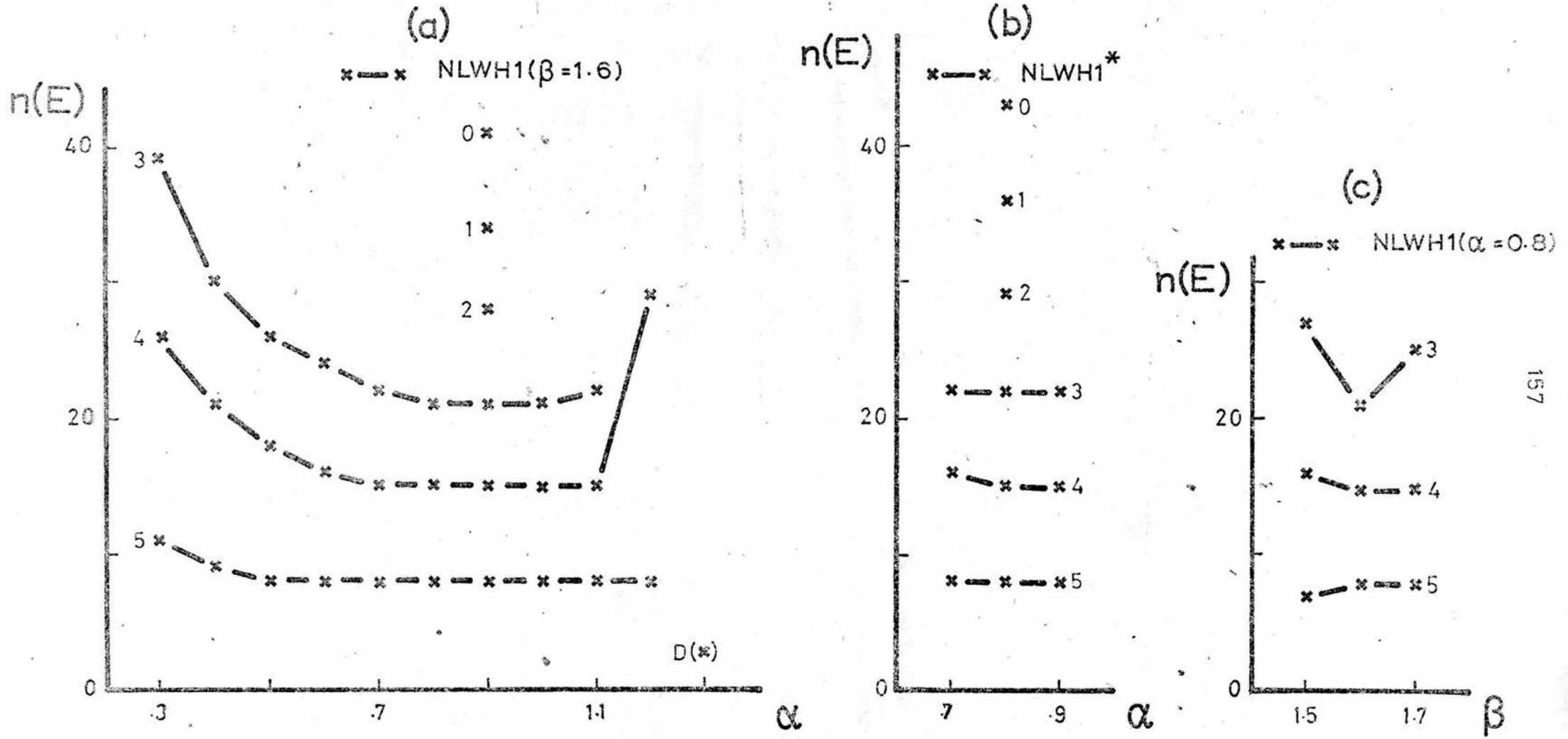
(a)
NLWH1(β=1.6)
n(E)
40
20
0
3
4
5
0
1
2
D(*)
.3
.7
1.1
α
(b)
n(E)
NLWH1*
40
20
0
0
1
2
3
4
5
.7
.9
α
(c)
NLWH1(α=0.8)
n(E)
20
0
3
4
5
1.5
1.7
β

FIGURE 3.10

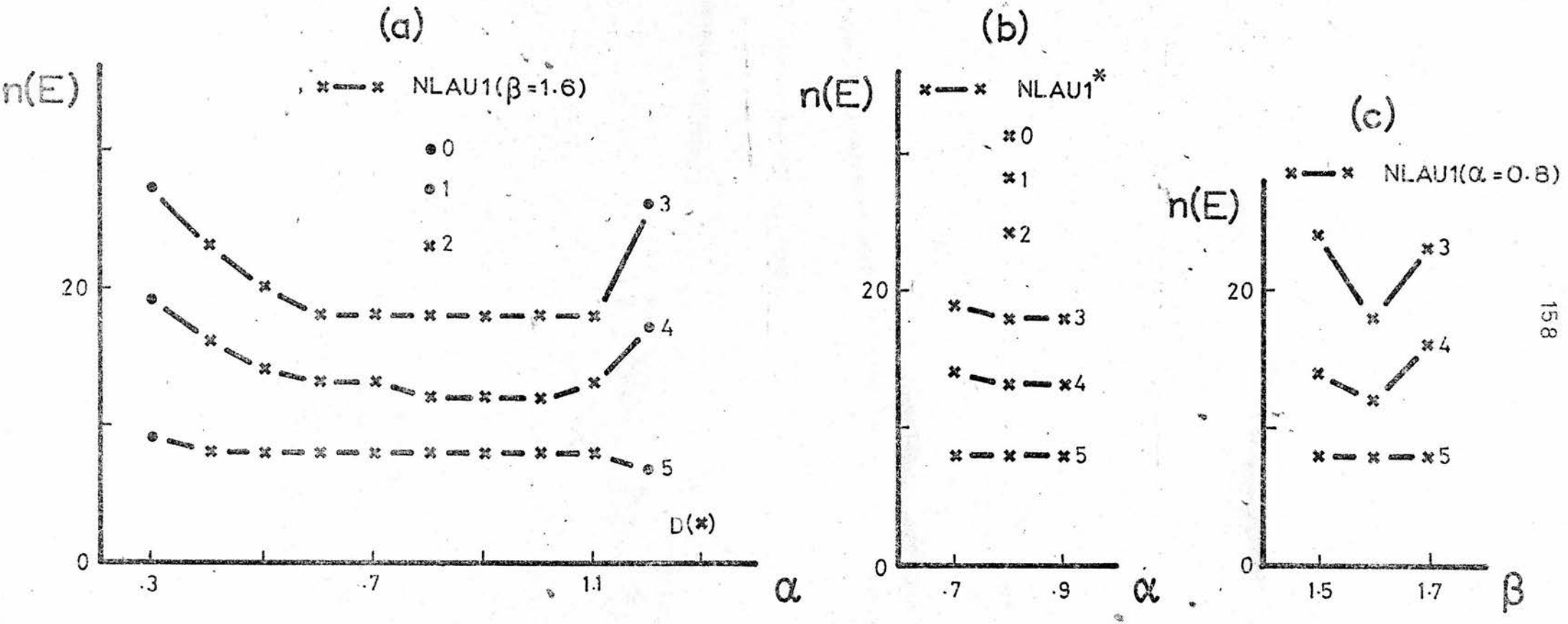
(a)
n(E)
NLAU1(β=1.6)
0
1
2
3
4
5
20
0
.3
.7
1.1
D(*)
α
(b)
n(E)
NLAU1*
0
1
2
3
4
5
20
0
.7
.9
α
(c)
NLAU1(α=0.8)
n(E)
3
4
5
20
0
1.5
1.7
β

FIGURE 3.11

this with Fig. 3.10a showed that Miyakoda's technique had little effect on the rate of convergence. But, Table 3.3 shows that it did increase the total count. Also it required the retention of an extra field of Ψ . Therefore Miyakoda's technique should only be used where necessary.

Fig. 3.10c shows how the convergence rate varied with β, when $\alpha = 0.8$. As expected, the optimum value of β was 1.6.

The above computations were repeated for NLAU1 and the results are shown in Figs. 3.11a, 3.11b and 3.11c.

A comparison of Figs. 3.10a and 3.11a shows that the constant E curves had a similar shape for both NLWH1 and NLAU1. With $\alpha = 0.8$ (taken to be the optimum value) NLAU1 was more efficient than NLWH1 (see Table 3.3). Therefore these results show that the optimum value of α is similar for both methods and that NLAU1 is the better method.

Fig. 3.11a also indicates that with $E > 10^2$ and $\alpha = 0.8$ there was non-monotonic convergence. Two methods were used to reduce this oscillation in the convergence rate. Firstly, Miyakoda's technique was used and the results are shown in Fig. 3.11b (NLAU1*). This, in conjunction with Table 3.3, shows that the convergence became monotonic and that the total count increased. The second technique used was that suggested by White (1969). This consisted of reducing α by 0.1 when the convergence became non-monotonic. The results of using this technique (NLAU1**) are shown in Table 3.3. This shows that NLAU1** is better than NLAU1*. Also, White's technique

does not require an extra field of Ψ , and thus it should be used rather than Miyakoda's technique.

Fig. 3.11c shows that with α =0.8, the optimum value of β for NLAU1 was 1.6.

With α = 1.0 and β = 1.6, NLAU1 is equivalent to NLSS1 (see Table 3.1). Fig. 3.11a shows that there is little difference between NLAU1 and NLSS1. But, it is likely that the difference between these will depend upon the same factors as the difference between NLWH1 and NLMB1.

With α = 1.0 and β = 1.0, NLAU1 is equivalent to NLMA1 (see Table 3.1). The results of NLMA1, shown in Table 3.3, indicate that this method is a very inefficient way of solving the balance equation.

So far, only the NLT1 form of the non-linear term has been considered. Therefore the results of using NLT2 will now be discussed.

The results of NLWH2 are shown in Fig. 3.12a. This shows that there was a sharp decrease in the convergence rate when $\alpha > 0.5$ and divergence for α = 0.7. This behaviour was due to the presence of Ψ_o in F (Ψ) (see Equ.(3.29)). Also, even with α = 0.5, monotonic convergence did not occur.

The techniques of both Miyakoda and White were used in an attempt to improve the convergence rate (NLWH2* and NLWH2**). The results of NLWH2* are shown in Fig. 3.12b. The optimum α was 0.8. With this value the convergence rate for NLWH2* was greater than that for NLWH2 with α =0.5. Also this technique produced convergence when α = 1.0. A summary of the results for NLWH2* and NLWH2** are shown in Table 3.3. This shows that there was

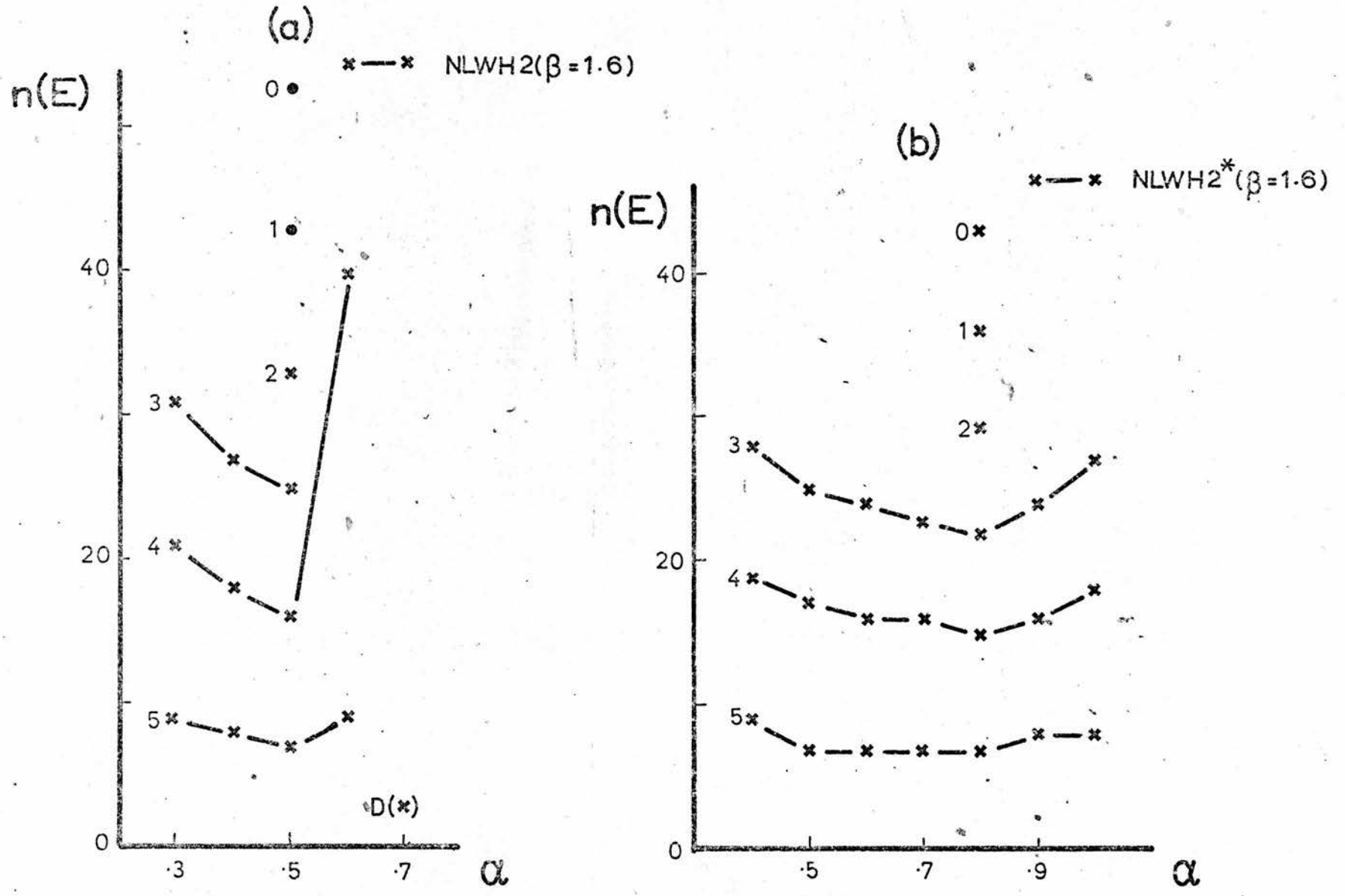
(a)
NLWH2(β=1·6)
n(E)
0
1
2
3
4
5
40
20
0
D(*)
·3
·5
·7
α
(b)
NLWH2*(β=1·6)
n(E)
0
1
2
3
4
5
40
20
0
·5
·7
·9
α

FIGURE 3.12

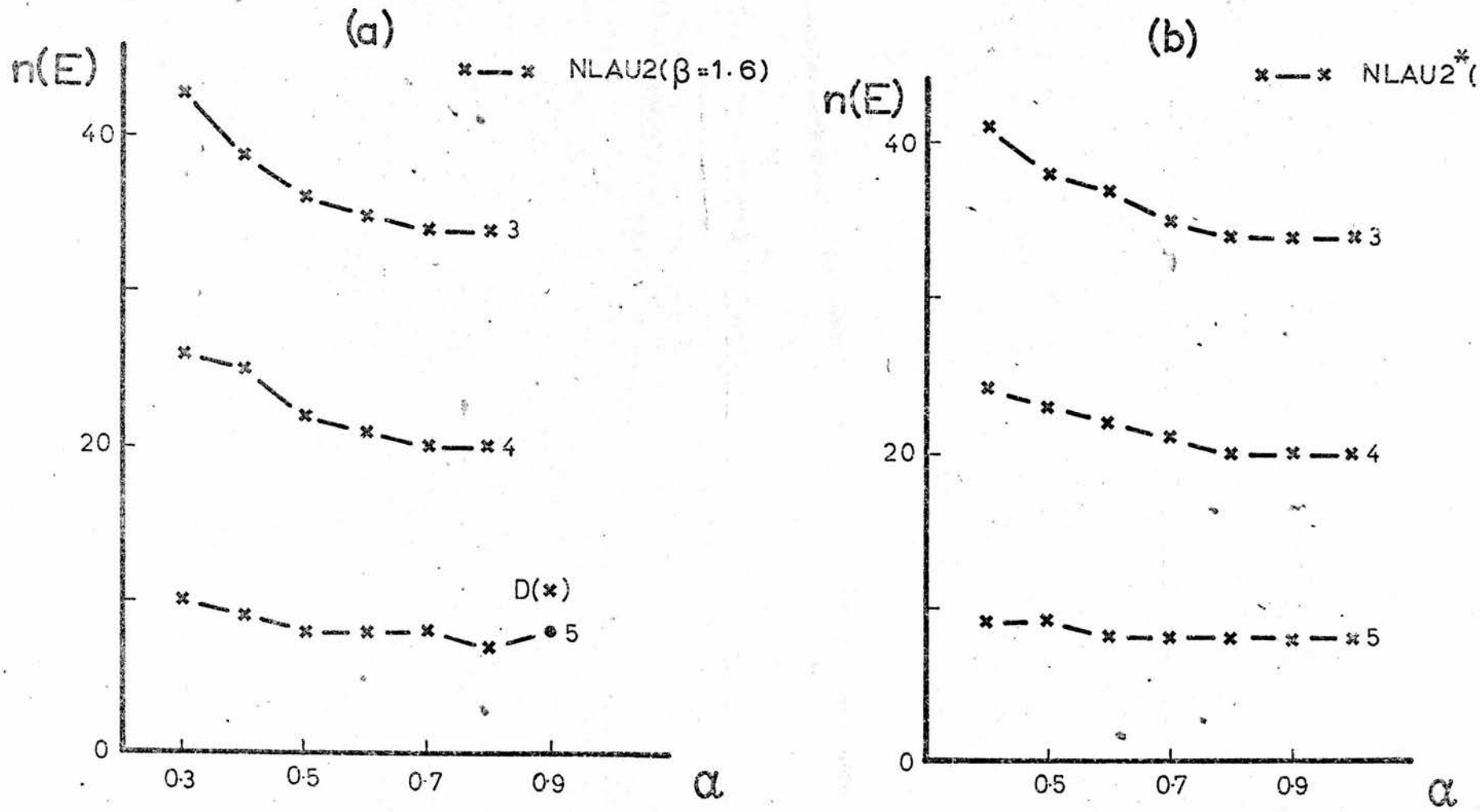
(a)
n(E)
NLAU2(β=1·6)
40
20
0
3
4
D(*)
5
0·3
0·5
0·7
0·9
α
(b)
n(E)
NLAU2*(β=1·6)
40
20
0
3
4
5
0·5
0·7
0·9
α

FIGURE 3.13

little difference between NLWH2, NLWH2* and NLWH2** when the optimum values of α are used. However a possible advantage of NLWH2* is that if α_o can be found for a given area ($\alpha_o = 0.8$, in this case), then this method ensures convergence with that α . Unfortunately, the author knows of no way in which α_o may be calculated.

The above computations were repeated with NLAU2 and the results are shown in Fig. 3.13a. Once again there was divergence when $\alpha = 1.0$. Also with $\alpha = 0.8$ and $E > 10^3$ the convergence was non-monotonic.

The effect of using Miyakoda's technique is shown in Fig. 3.13b (NLAU2*). This shows that the convergence rate for $E > 10^3$ hardly altered, and that it increased for $E < 10^3$. It also shows that the optimum value of α was in the vicinity of 0.8. The efficiency of NLAU2* can be compared with that for White's technique (NLAU2**) by referring to Table 3.3. This shows that NLAU2** was superior to NLAU2*.

In all the methods considered it was either better or essential to use $\alpha < 1.0$. Also, whenever there was monotonic convergence the optimum value of α was in the vicinity of 0.8. This implies that this value of α is characteristic of the area used.

The results in Table 3.3 show that it is better to use NLT1 rather than NLT2. Also, that when NLT2 is used, it is necessary to use the techniques of either Miyakoda or White in order to obtain monotonic convergence. The disadvantages of Miyakoda's technique are that two fields of Ψ are needed and that the operational count is increased. However it has an advantage in that it produces convergence

when $\alpha = 0.8$.

Table 3.3 also shows that, with $\alpha = 0.8$, the NLAU method is the most efficient (if NLSS1 is excluded). However the efficiency of the NLWH method could be improved by using a more efficient method of solving the Poisson equation. For example, the ADI method could be used (White (1969)).

3.7.4. A Discussion Of The Methods Of Solving The Balance Equation

The most important fact that emerges from the previous investigation is that it is best to use NLT2 with methods of the first and second types and NLT1 with those of the third type. With the converse proce dure, there tends to be non-monotonic convergence or divergence with unexpected values of α or β . However this difficulty can often be overcome by using either Miyakoda's technique or that of White.

For methods of the first and second types, the optimum value of β is almost the same as that for a Poisson equation. When this β is used the NLOR$^{\times}$ method is the most efficient. However, the NLOR$^{\times}$ method has never been studied theoretically or used operationally and thus there is neither theoretical nor statistical proof that it will always give a convergent solution.

For methods of the third type there appears to be a unique optimum value of α , provided that there is monotonic convergence. However, the author does not know how to calculate this value of α . With the optimum value of α , the NLAU method is the best method of the third type. Also a comparison of the results for this method with those for the NLOR$^{\times}$ method shows that NLAU is the better method.

3.8 The Boundary Conditions For The Balance Equation (A)

To solve an elliptic partial differential equation it is necessary to impose boundary conditions. It is usually desirable, and often necessary, to choose boundary conditions which satisfy the integral properties of the equation.

Consider the balance equation in the form

$$\nabla^2\Psi + F(\Psi,\Phi) = 0 \qquad (3.43)$$

Suppose that Equ. (3.43) has to be solved in an area bounded by curve C and that s and n are the coordinates parallel and perpendicular to C.

The first integral constraint on Ψ is almost trivial. Let the quantity I be defined by

$$I = \oint_C \frac{\partial\Psi}{\partial s}\, ds$$

The physical meaning of I is that it is the total inflow of air into the area considered. On both physical and mathematical grounds it is obvious that

$$I = 0 \qquad (3.44)$$

A second itegral property of Ψ is found by integrating Equ. (3.43) over the area (A) enclosed by C. The result is

$$\oint_C \frac{\partial\Psi}{\partial n}\, ds + \iint_A F(\Psi,\Phi)\, dA = 0 \qquad (3.45)$$

Whenever possible, the distribution of Ψ on the boundary should satisfy either Equs. (3.44) or (3.45).

The next few sections will deal with the types of boundary conditions that can be used with the linear balance equation and the balance equation.

3.8.1 The Boundary Conditions For The Linear Balance Equation

This section is concerned with the boundary conditions which are used with the linear balance equation.

In section 3.2 it was shown that the wind derived from the linear balance equation is very similar to the geostrophic wind. Therefore it is reasonable to assume that the distribution of Ψ on the boundary is such that the wind there is geostrophic.

If the wind normal to the boundary is geostrophic, then

$$\frac{\partial \Psi}{\partial s} = \frac{1}{f}\frac{\partial \phi}{\partial s}$$

However, if this is used in Equ. (3.44), it is found that that $I \neq 0$. This is because f varies around the boundary. This problem can be overcome by using

$$\frac{\partial \Psi}{\partial s} = \frac{1}{f}\frac{\partial \phi}{\partial s} - \delta_1 \qquad (3.46)$$

Here δ_1 is a constant and its value is given by

$$\delta_1 = \oint_C \frac{1}{f}\frac{\partial \phi}{\partial s}\, ds$$

If the gridpoints on the boundary are labelled 0 too n, then δ_1 is computed from

$$\delta_1 = \frac{1}{S}\sum_{q=0}^{n}\left(\frac{\phi(q+1)-\phi(q)}{\bar{f}}\right) \qquad \bar{f} = \frac{f(q+1)+f(q)}{2}$$

Here S is the length of the perimeter. Once δ_1 is known, the value of Ψ on the boundary is computed from

$$\Psi(0) = \frac{\phi(0)}{f(0)}$$

$$\Psi(q+1) = \Psi(q) + \frac{1}{\bar{f}}\left(\phi(q+1)-\phi(q)\right) - \delta_1 d \qquad q = 1,1,n \qquad (3.47)$$

Since it is the gradient of Ψ that is significant, the choice of the zero point and of $\Psi(0)$ is unimportant.

The above procedure for calculating Ψ on the boundary

was devised by Bolin (1956).

If f is taken to be a constant, $\bar{f}$ say, then $\delta_1 = 0$ (see Equ. (3.46)). In this case, if it is assumed that $\Psi(0) = \Phi(0) / \bar{f}$, then the values of Ψ are given by

$$\Psi(q) = \frac{\Phi(q)}{\bar{f}} \qquad q = 1,1,n \tag{3.48}$$

For a small area f will not vary much and thus these results will be similar to those using a variable f.

Benwell et al.(1971) used a boundary condition that was similar to that in Equ. (3.48), namely

$$\Psi = \frac{\Phi}{\bar{f}} - \delta_2 \tag{3.49}$$

The Coriolis parameter, f, was allowed to vary and δ_2 was calculated so that Equ. (3.44) was satisfied. This is a surprising choice of boundary condition because the component of velocity normal to the boundary that lies approximately east-west is not geostrophic, whereas the component normal to the other boundaries is geostrophic.

The boundary condition for Ψ derived from Equ. (3.46) is based on the assumption that the wind normal to the boundary is geostrophic. Alternatively, it can be assumed that the wind parallel to the boundary is geostrophic. In this case

$$\frac{\partial \Psi}{\partial n} = \frac{1}{f}\frac{\partial \Phi}{\partial n} - \delta_3 \tag{3.50}$$

This must satisfy the consistency condition given by Equ. (3.45). When the linear balance equation is used it is found that the value of δ_3 depends upon Ψ . However, if the $\nabla f.\nabla\Psi$ term is approximated by $\frac{1}{f}\nabla f.\nabla\Phi$, then the value of δ_3, is given by

$$S\delta_3 = \oint_C \frac{1}{f}\frac{\partial \Phi}{\partial n}\, ds - \iint_A \left[\frac{1}{f}\nabla^2\Phi - \frac{1}{f^2}\nabla f.\nabla\Phi\right] dA$$

Before discussing the effect of using different types of boundary conditions, it is worth considering the difference between the velocity components calculated from Ψ (u and v say) and the geostrophic components (u_g and v_g say). Consider the following form of the linear balance equation,

$$\nabla^2\Psi + \frac{1}{f^2}\beta\frac{\partial\phi}{\partial y} - \frac{1}{f}\nabla^2\phi = 0 \qquad (3.51)$$

If this is differentiated with respect to y and if the β^2 terms are ignored, then $u - u_g$ is given by

$$\nabla^2(u-u_g) = \frac{\beta}{f^2}\phi_{xx}$$

Similarly, if Equ. (3.51) is differentiated with respect to x, then

$$\nabla^2(v-v_g) = \frac{\beta}{f^2}\phi_{xy}$$

Suppose that $\Phi = A + B \sin(kx) \sin(hy)$. If $u - u_g \propto \sin(k'x) \sin(h'y)$ then it can easily be shown that

$$u - u_g = \frac{\beta}{f^2}\frac{k^2}{k^2+h'^2}(\Phi - A)$$

Therefore this simple analysis gives $(u - u_g) \propto (\Phi - A)$. There is no such simple relationship between $(v - v_g)$ and Φ.

3.8.2 A Case Study

The linear balance equation was solved with different types of boundary condition. The wind field was then computed and compared with the geostrophic wind. These computations were carried out for the 1000 mb surface of area 51. The distribution of Φ, for this area, is shown in Fig. 3.14 and the two components of the geostrophic wind are shown in Figs. 3.15a and 3.15b.

FIGURE 3.14

Φ for the 1000 mb surface of area 51

FIGURE 3.15

(a) u_g computed from Fig. 3.14

(b) v_g from the same Φ

FIGURE 3.16

(a) $(u-u_g)$ when Ψ is computed from the linear balance equation using Equ. (3.46) on the boundary

(b) $(v-v_g)$ from the same Ψ

FIGURE 3.17

(a) $(u-u_g)$ when Ψ is computed from the linear balance equation using Equ. (3.49) on the boundary

(b) $(v-v_g)$ from the same Ψ

FIGURE 3.18

(a) $(u-u_g)$ when Ψ is computed from the linear balance equation using Equ. (3.50) on the boundary

(b) $(v-v_g)$ from the same Ψ

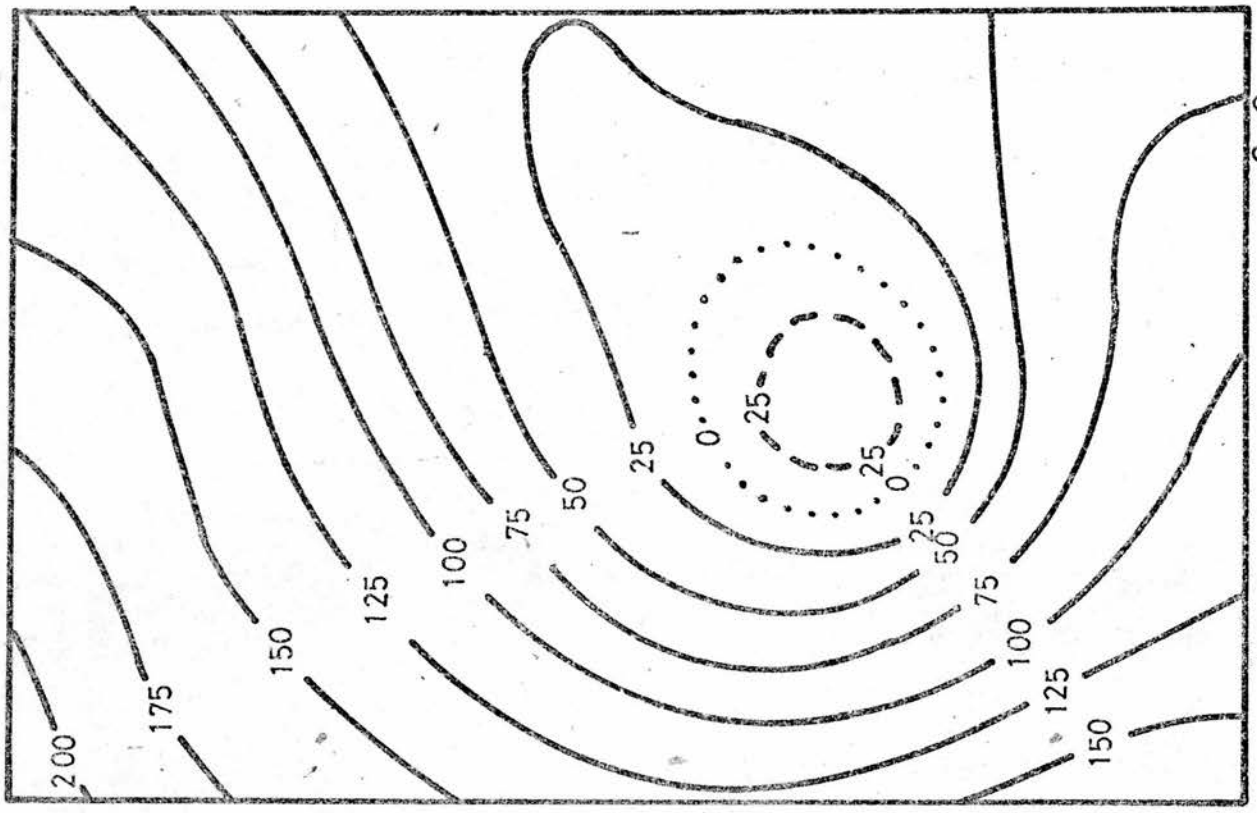

FIGURE 3.14

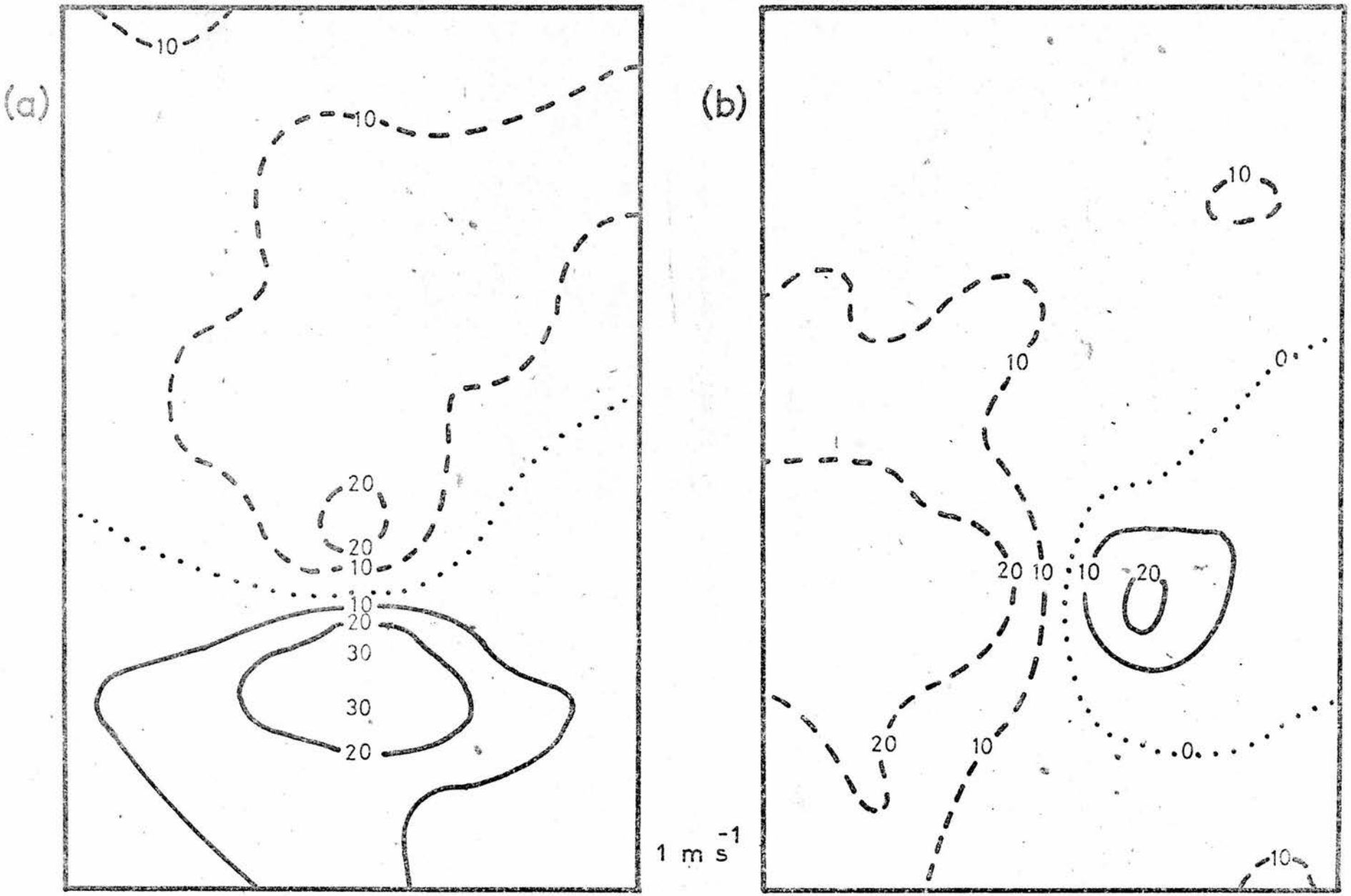
(a)
10
10
20
20
10
10
20
30
30
20
(b)
10
10
0
20
10
10
20
20
10
0
10
1 m s⁻¹
u_g
v_g

FIGURE 3.15

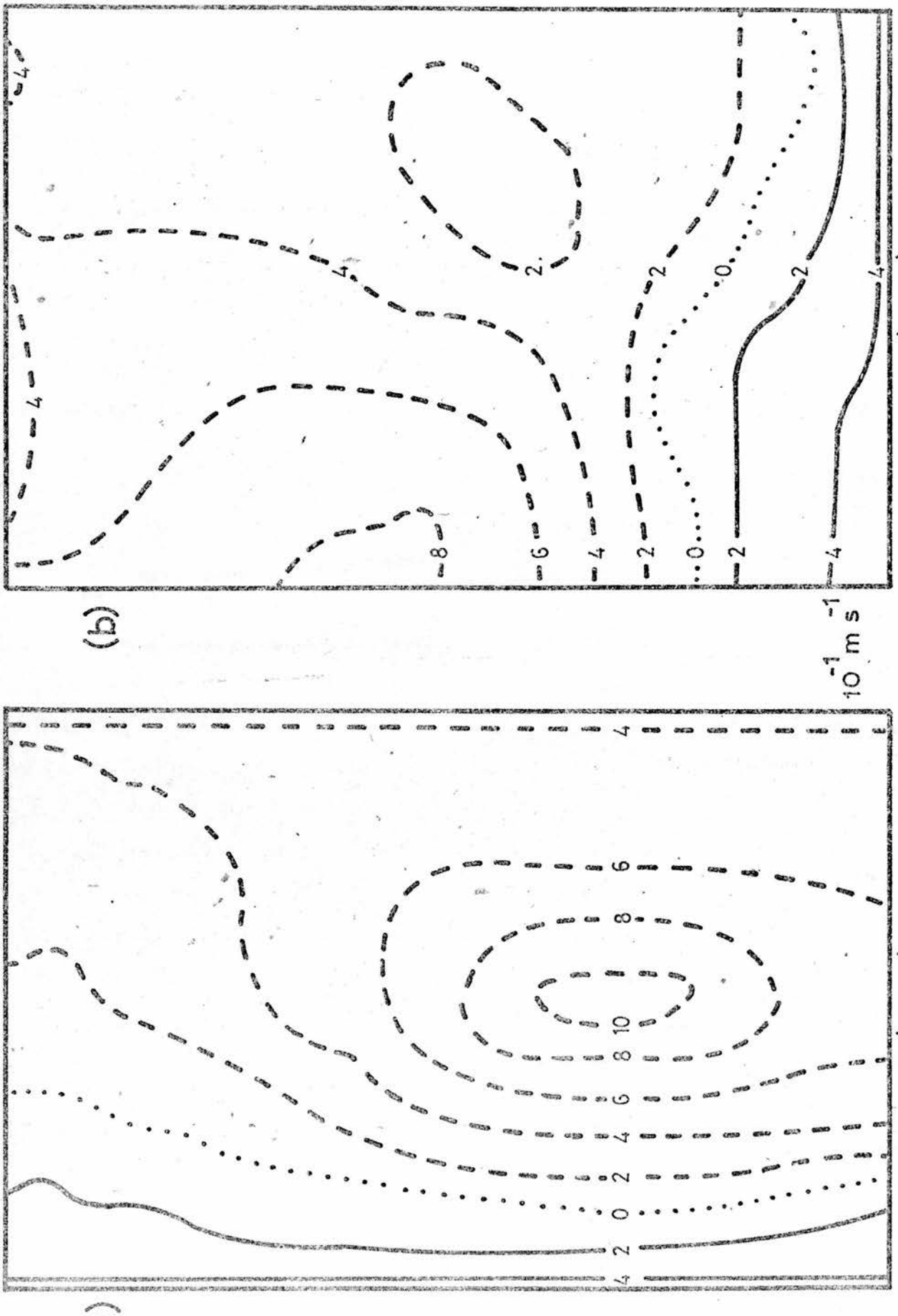

FIGURE 3.16

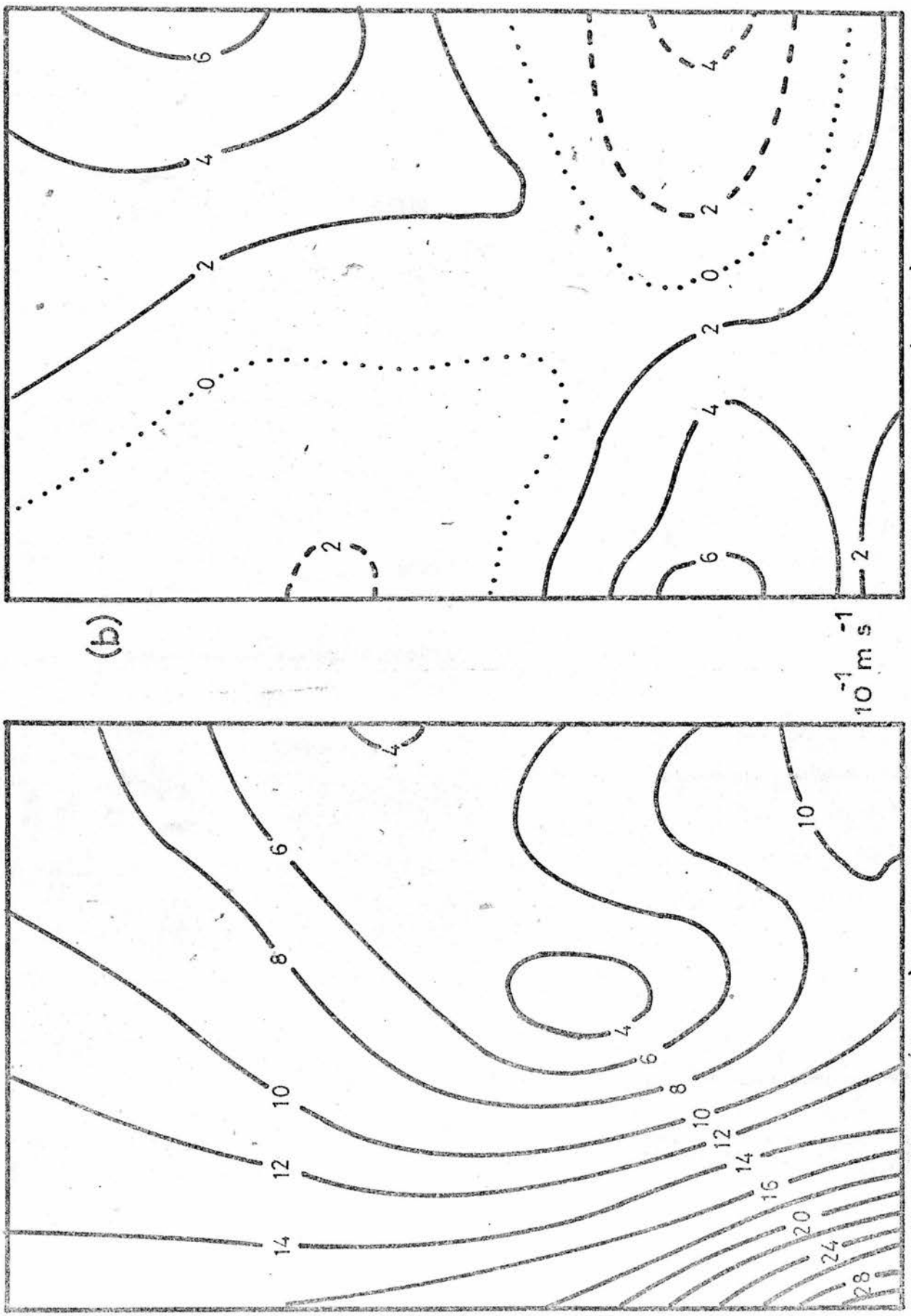

FIGURE 3.17

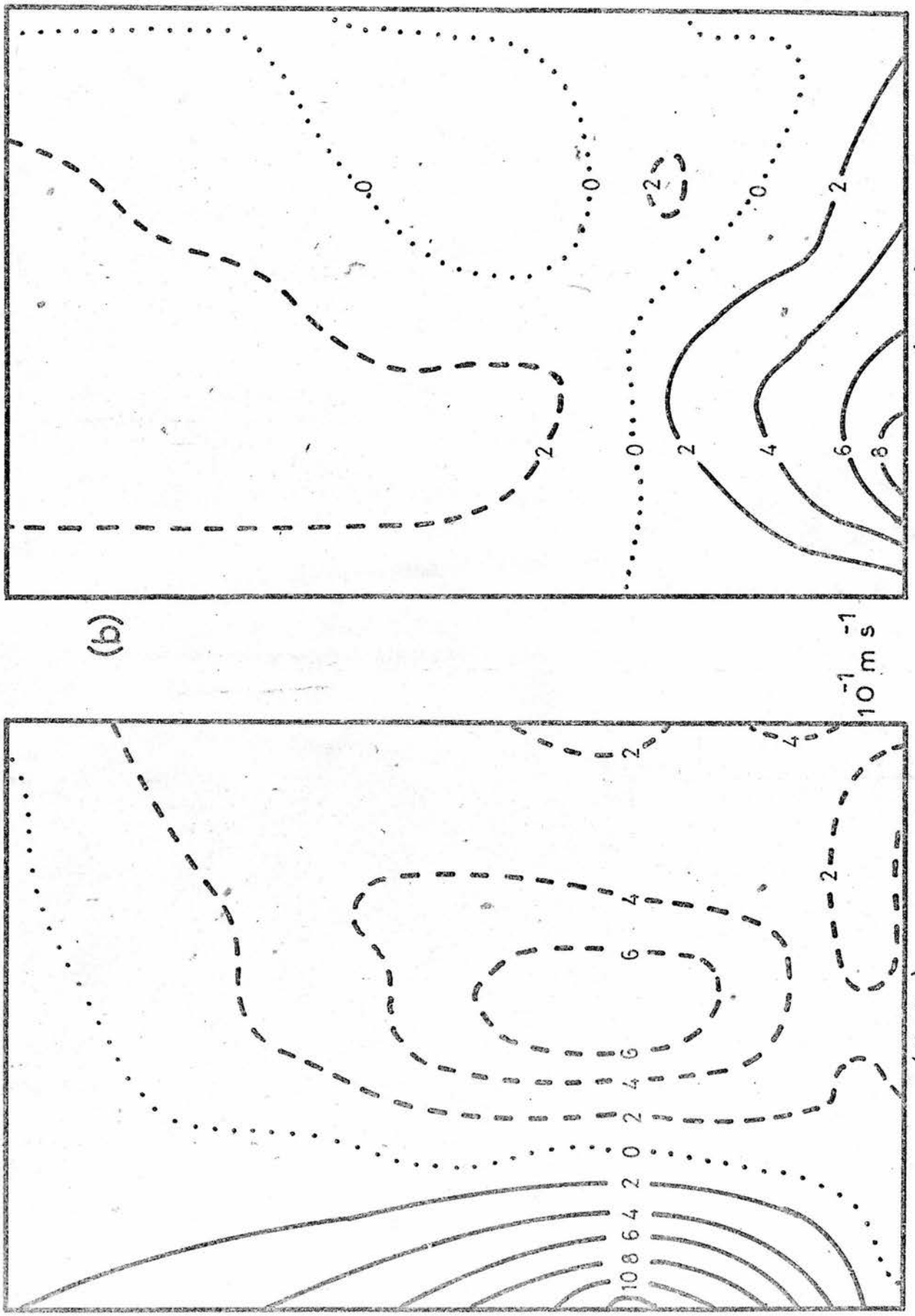

FIGURE 3.18

The first boundary condition considered was that given by Equ. (3.46). The distributions of $(u - u_g)$ and $(v - v_g)$ are illustrated in Figs. 3.16a and 3.16b. These show that the maximum geostrophic departure, for both components, was about 1 ms^{-1}. For $(u - u_g)$, this maximum occurred at the centre of the depression. This situation came about because $(u - u_g)$ was comparatively small round the boundary and Φ_{xx} was large and positive at the centre of the depression. Fig. 3.16a also shows that the distribution of $(u - u_g)$ is similar to that of Φ. This was anticipated in the previous section. The distribution of $(v - v_g)$ is more complicated and, as expected, there is no obvious relationship between this and Φ.

The geostrophic departures were also calculated from the solution of the linear balance equation for the case where Equ. (3.49), with $\delta_2 = 0$, was used to calculate the boundary conditions. The results are shown in 3.17a and 3.17b. As in the previous case, the distribution of $(u - u_g)$ is closely related to that of Φ. However, in this case the maximum geostrophic departure of 3 ms^{-1} is on the boundary. The reason for this becomes apparent when the boundary condition is considered in more detail.

It can easily be shown that on the east and west boundaries the geostrophic departure is

$$(u - u_g)_b = \frac{1}{f^2} \frac{\partial f}{\partial y} \Phi$$

In the previous section it was shown that, to a good approximation, $\nabla^2(u - u_g) \propto \Phi$. Therefore it is to be expected that $(u - u_g) \propto \Phi$ everywhere. Since Φ has its

maximum value on the boundary, so has $(u - u_g)$. On the north and south boundaries $(v - v_g)_b \simeq 0$ and thus the geostrophic departure of v tends to be small everywhere.

The last boundary condition considered was that described by Equ. (3.50). This allows Ψ to be computed only to within an arbitary constant. However this is not important since it is only the velocity components that are significant. The geostrophic departures are shown in 3.18a and 3.18b. Once again the distribution of $(u - u_g)$ is related to that of Φ. It is also worth noting that the boundary conditions implies, and Fig. 4.17a shows, that $(u - u_g) \simeq 0$ on the north and south boundaries. Fig. 3.18b shows that $(v - v_g) \simeq 0$ on the other two boundaries and that the magnitude of $(v - v_g)$ tends to be less than that of $(u - u_g)$.

The above results show that the boundary conditions described by Equs. (3.46) and (3.50) give more realistic results than that described by Equ. (3.49) with $\delta_2 = 0$. The reason for this becomes apparent when it is remembered that it is the gradients of Ψ that are used. Thus the gradients of Ψ on the boundary should be given by the first integral of Equ. (3.8). Therefore, on the boundary, $\nabla\Psi$ and $\nabla\Phi$ should be related by

$$f \nabla\Psi = \nabla\Phi + \nabla_x \underline{M}$$

Both Equs. (3.46) and (3.50) satisfy this kind of relationship.

The boundary conditions described by Equs. (3.46) and (3.50) are Dirichlet and Neumann boundary conditions respectively. Thus for the sake of efficiency it is better to use the former boundary condition (see Chapter

II).

In the next section the boundary conditions for the balance equation will be considered.

3.8.3 The Boundary Conditions For The Balance Equation(B)

Kuo (1956) has shown that the first integral of the balance equation is

$$(f + \nabla^2\psi)\nabla\psi = \nabla(\phi + \frac{V_1^2}{2}) + \nabla \times \underline{M}$$

Here $\nabla \times \underline{M}$ is a function of integration and $V_1 = | \underline{k} \times \nabla\psi |$. If the principle enunciated in the previous section is invoked then one possible boundary condition for the balance equation is

$$\frac{\partial\psi}{\partial s} = \frac{1}{(f+\zeta)} \frac{\partial}{\partial s}\left(\phi + \frac{V_1^2}{2}\right) + (\nabla \times \underline{M})_s \qquad (3.52)$$

In this equation s is the coordinate round the boundary and $(\nabla \times \underline{M})_s$ is the component of $\nabla \times \underline{M}$ is the s direction. The wind given by Equ. (3.52) is similar to the component of the gradient wind normal to the boundary.

If Equ. (3.52) is to be used in the same way as Equ. (3.46), then the righthand side must be made independent of ψ. This may be achieved by using $\nabla\psi = \frac{1}{f}\nabla\phi$ on this side of the equation. The result is

$$\frac{\partial\psi}{\partial s} = \frac{1}{(f+\zeta_g)}\left(\frac{\partial\phi}{\partial s} + \frac{1}{f^2}\frac{\partial}{\partial s}\left[\left(\frac{\partial\phi}{\partial x}\right)^2 + \left(\frac{\partial\phi}{\partial y}\right)^2\right] \right) - \delta_4 \qquad (3.53)$$

Thus, once δ_4 has been calculated by using Equ. (3.44), the above equation can be used to derive a boundary condition for ψ.

The wind derived from Equ. (3.53) by replacing s by x and y will be referred to as the quasi-gradient wind.

Some insight into the relationship between the geostrophic, quasi-gradient and balanced winds can be obtained by considering a set of circular isobars. If an

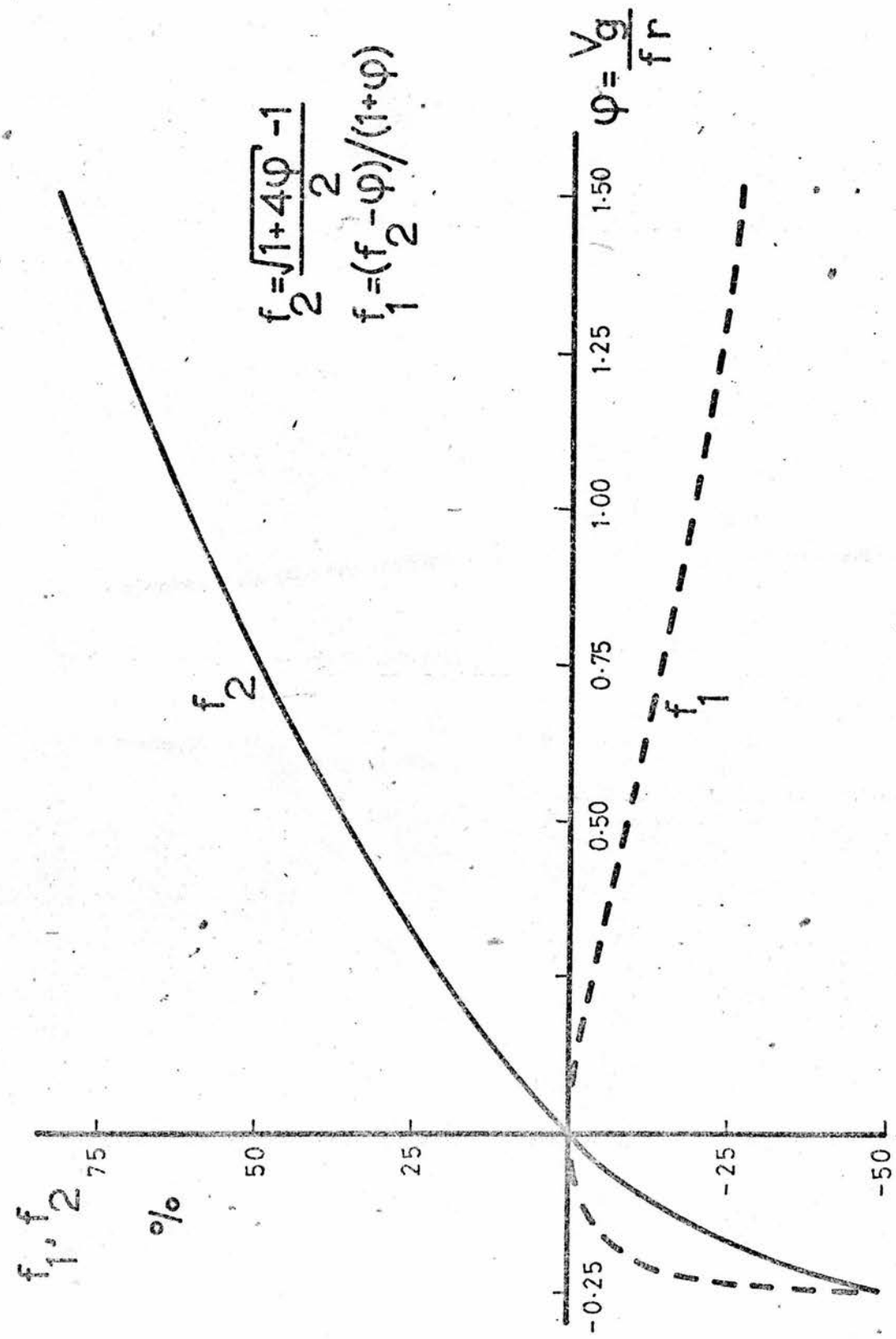
$f_2 = \frac{\sqrt{1+4\varphi} - 1}{2}$
$f_1 = (f_2 - \varphi)/(1+\varphi)$
$\varphi = \frac{V_g}{f r}$
f_1, f_2 %
75
50
25
-25
-50
-0·25
0·50
0·75
1·00
1·25
1·50
f_2
f_1

FIGURE 3·19

isobar has radius r, then the balanced wind along the isobars derived from the balance equation (V_{gr} say) is given by

$$\frac{V_{gr}^2}{fr} = V_g - V_{gr} \qquad (3.54)$$

In this particular case the balanced wind is the gradient wind. If V'_{gr} is the quasi-gradient wind, then

$$\frac{V_g V'_{gr}}{fr} = V_g - V'_{gr} \qquad (3.55)$$

It can easily be shown from Equs. (3.54) and (3.55) that

$$\frac{V'_{gr} - V_{gr}}{V_{gr}} = f_1 \left[\frac{V_g}{fr}\right] \qquad \frac{V_g - V_{gr}}{V_{gr}} = f_2 \left[\frac{V_g}{fr}\right]$$

The functions f_1 and f_2 are illustrated in Fig. 3.19. This shows that for both cyclonic and anticyclonic curvature V'_{gr} is a better approximation to V_{gr} than is V_g. Another interesting feature shown in the figure is that f_1 and f_2 are of opposite sign when there is cyclonic curvature. Thus for this type of curvature V'_{gr} is an underestimate V_{gr} whilst V_g is an overestimate.

The above discussion indicates that Equ. (3.53) can be used to make a good approximation to the gradient wind without the need to find the radius of curvature.

Consider the characteristics of the gradient wind equation (Equ. (3.54)). It can be shown that

(i) for cyclonic curvature $V_g - V_{gr} > 0$

(ii) $V_g - V_{gr}$ is large when r is small.

If Equ. (3.53) is to be of any use it is necessary that the quasi-gradient wind should have the same properties as V_{gr}. This was tested by comparing the quasi-gradient wind with the geostrophic wind in a case study.

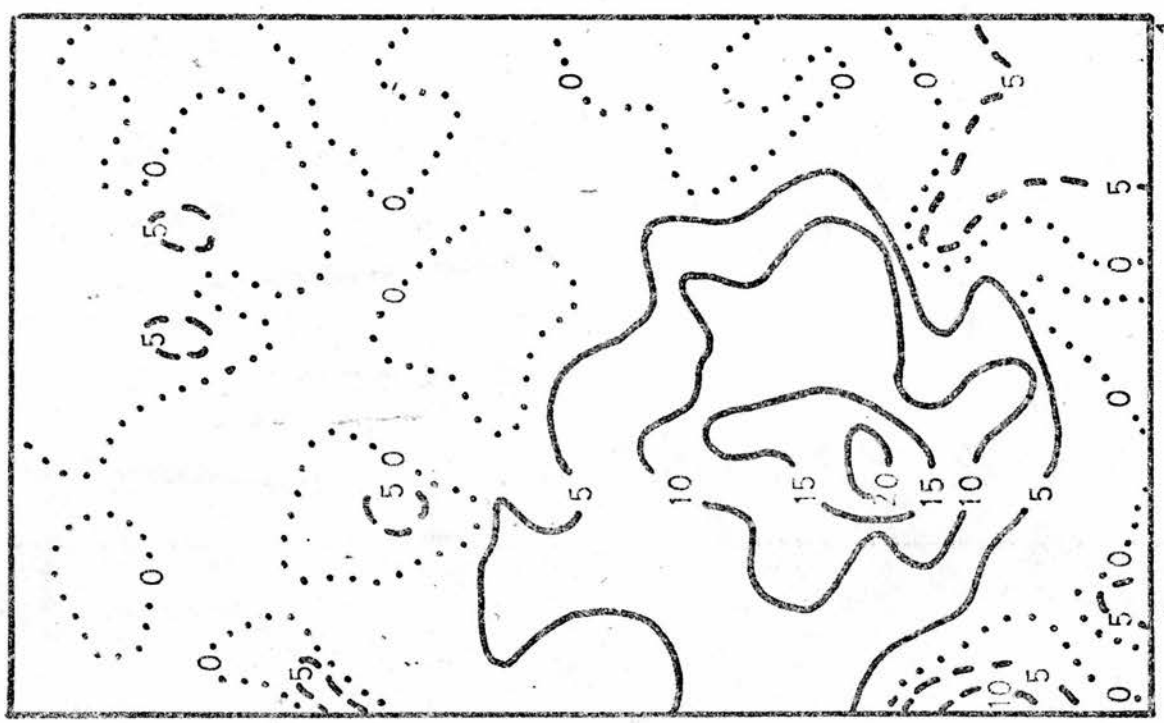

FIGURE 3.20

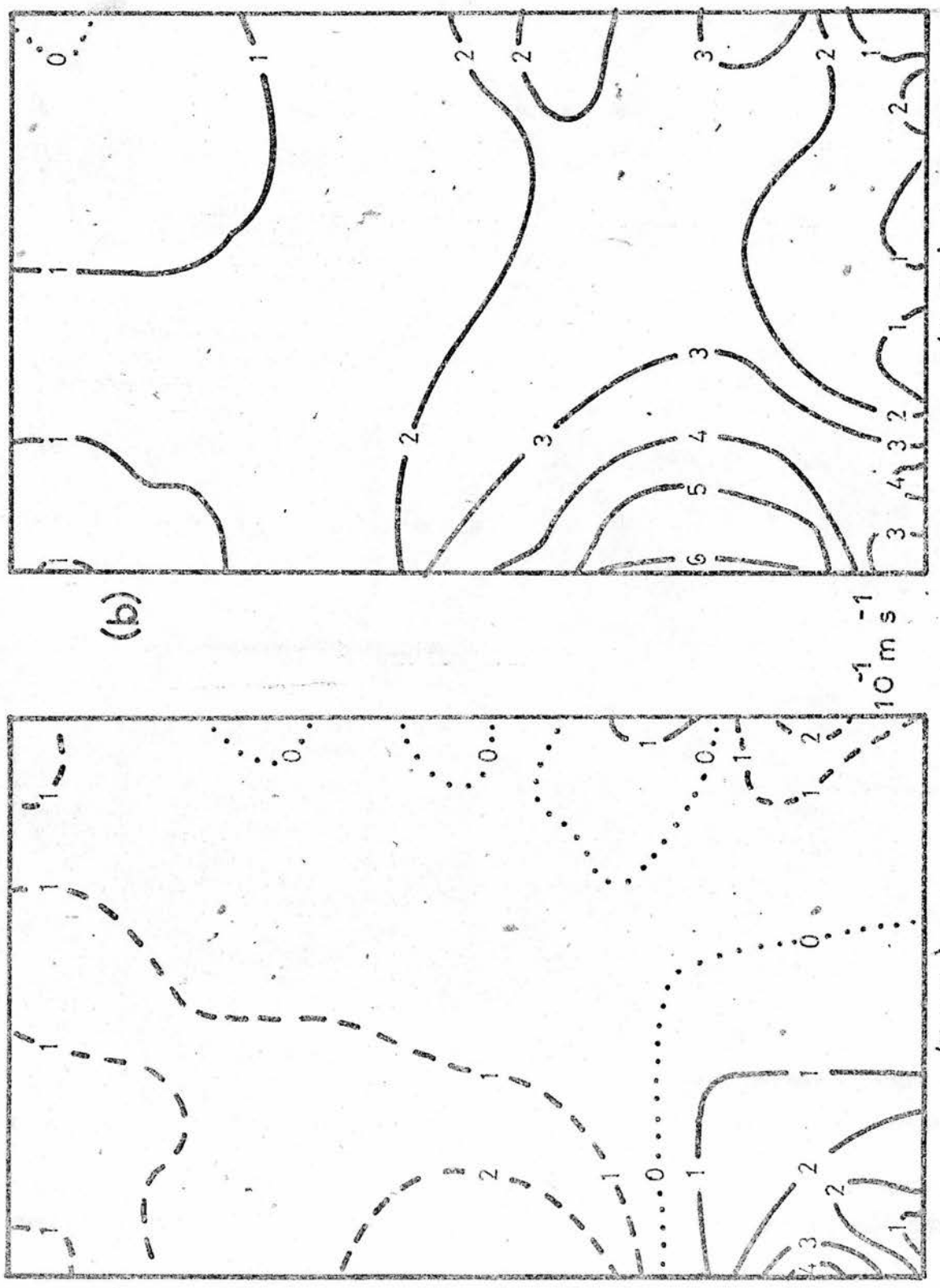

FIGURE 3.21

3.8.4 A Case Study

The data used was the same as that used in section 3.8.2.

The quasi-gradient wind, V'_{gr}, was calculated from equations similar to Equ. (3.53). This was then compared with the geostrophic wind, V_g. Fig. 3.20 shows $(V_g - V'_{gr})$. This shows that when the radius of curvature was large, $(V_g - V'_{gr})$ was both large and positive. Thus the behaviour of V'_{gr} is similar to that of V_{gr} described in (i) and (ii) of the previous section. However, when the radius of curvature was small $(V_g - V'_{gr})$ could be either positive or negative and its magnitude was small. This satisfies condition (ii) but not (i). This is reasonable because V'_{gr} is only an approximation to V_{gr} anyway. These results show that the quasi-gradient wind has similar properties to those of the gradient wind.

The balance equation was solved with the boundary condition described by Equ. (3.46). The velocity components computed from the solution will be denoted by u_1 and v_1. When Equ. (3.53) is used to calculate the boundary conditions the corresponding components are u_2 and v_2. Figs. 3.21a and 3.21b show $(u_1 - u_2)$ and $(v_1 - v_2)$. The root mean square values of these fields were also computed and they were found to be 1.2 ms^{-1} and 2.3 ms^{-1}. These results indicate that there is a significant difference between the velocity components when the two different boundary conditions are used. However no experiments have been carried out to find whether this difference is meaningful or not. It is hoped that in the future this problem will be resolved.

CHAPTER IV

PROBLEMS ASSOCIATED WITH THE SOLUTION OF THE ω-EQUATION

4.1 Introduction

This chapter is mainly concerned with the solution of a quasi-geostrophic system of equations. In particular great attention is paid to the ω-equation and vorticity equation.

First of all, the relationship between the elliptic criterion and the condition for convergence of the iterative scheme is considered. The choice of appropriate boundary conditions for ω is then studied in some detail. Next, the effect on ω and Φ_t of some of the common approximations made to the ω-equation are considered. Use is made of both simple "analytical" models and a case study. Also the meaning of partitioning introduced by Krishnamurti (1968) is discussed and use is made of this concept in the case study. Finally the consistency of the boundary conditions used for ω and Φ_t is discussed.

4.2 The Geostrophic ω-Equation

Haltiner (1971) has described a quasi-geostrophic system of equations which is consistent with the conservation of energy (see (iv) of section 1.4). However, as pointed out in the Introduction, the equations used in diagnostic studies do not necessarily have to conserve energy. Therefore other quasi-geostrophic systems of equations may be used.

If only terms of the order R^0 in Equs. (1.23), (1.24) and (1.25) are considered, and if $\underline{V}_1$ is replaced

by the geostrophic wind ($\underline{V}_g$), then an alternative quasi-geostrophic system of equations is

$$\underline{V}_g = \frac{1}{f}\,\underline{k} \times \nabla\Phi \tag{4.1}$$

$$-f\zeta + \nabla^2\Phi = 0 \tag{4.2}$$

$$\frac{\partial \zeta}{\partial t} + \underline{V}_g.\nabla\eta - f\frac{\partial \omega}{\partial p} = 0 \tag{4.3}$$

$$\frac{\partial \Phi_t}{\partial p} + \underline{V}_g.\nabla\frac{\partial \Phi}{\partial p} + \sigma\omega = 0 \tag{4.4}$$

The value of ζ given by Equ. (4.2) is usually called the geostrophic vorticity. However, it is important to note that this is derived from the divergence equation and not Equ. (4.1).

If Equs. (4.2), (4.3) and (4.4) are written as $DE_g = 0$, $VE_g = 0$ and $TE_g = 0$ the geostrophic ω-equation is derived from

$$\nabla^2(TE_g) - f\frac{\partial}{\partial p}(VE_g) - \frac{\partial}{\partial t}\frac{\partial}{\partial p}(DE_g) = 0$$

This comes from the definition of the ω-equation (see Equ. (1.29)). Substituting for TE_g, VE_g and DE_g gives

$$\nabla^2(\sigma\omega) + f^2\frac{\partial^2\omega}{\partial p^2} - f\frac{\partial}{\partial p}(\underline{V}_g.\nabla\eta) + \nabla^2(\underline{V}_g.\nabla\frac{\partial \Phi}{\partial p}) = 0$$

The third and fourth terms depend upon the differential vorticity advection and the laplacian of the thermal advection respectively. For the geostrophic ω-equation these terms depend only upon Φ . Due to this they are often thought of as being the cause of the vertical velocity. However just because Φ rather than ω is observed, it does not mean that the distributions of Φ and ω represent cause and effect. In fact an ω-equation simply states the condition which makes the local vorticity change ($\frac{\partial \zeta}{\partial t}$) and the local temperature change

$(\frac{\partial T}{\partial t})$ consistent with one another. In other words an ω-equation links the thermal and vorticity (i.e. wind) fields.

Although the terms depending upon Φ in the ω-equation do not cause the vertical velocity, there are some qualitative relationships between the vertical velocity and these terms. Let ω be divided into two parts, ω_1 and ω_2, such that

$$\nabla^2(\sigma\omega_1) + f^2\frac{\partial^2\omega_1}{\partial p^2} - f\frac{\partial}{\partial p}(\underline{V}_g.\nabla\eta) = 0$$

$$\nabla^2(\sigma\omega_2) + f^2\frac{\partial^2\omega_2}{\partial p^2} + \nabla^2(\underline{V}_g.\nabla\frac{\partial\Phi}{\partial p}) = 0$$

It is found that

(i) ω_1 is large and positive (negative) if the advection of vorticity, $\underline{V}_g.\nabla\eta$, increases (decreases) rapidly with height.

(ii) ω_2 is large and positive (negative) if the thermal advection, $-\underline{V}_g.\nabla\frac{\partial\Phi}{\partial p}$, has a sharp maximum (minimum).

The geostrophic ω-equation may be written as

$$\nabla^2(\sigma\omega) + f^2\frac{\partial^2\omega}{\partial p^2} + S = 0 \qquad (4.5)$$

Here S depends only upon Φ and therefore S is known. If Equ. (4.5) is elliptic it can be solved as a boundary value problem. Therefore once ω has been specified on the boundary the equation can be solved. The vorticity equation, Equ. (4.3), may be written as

$$\nabla^2\Phi_t + J(\Phi,\eta) - f^2\frac{\partial\omega}{\partial p} = 0 \qquad (4.6)$$

Therefore, once ω is known, this equation reduces to a Poisson equation in Φ_t. This equation is always elliptic and thus once the boundary conditions have been specified it can be solved for Φ_t.

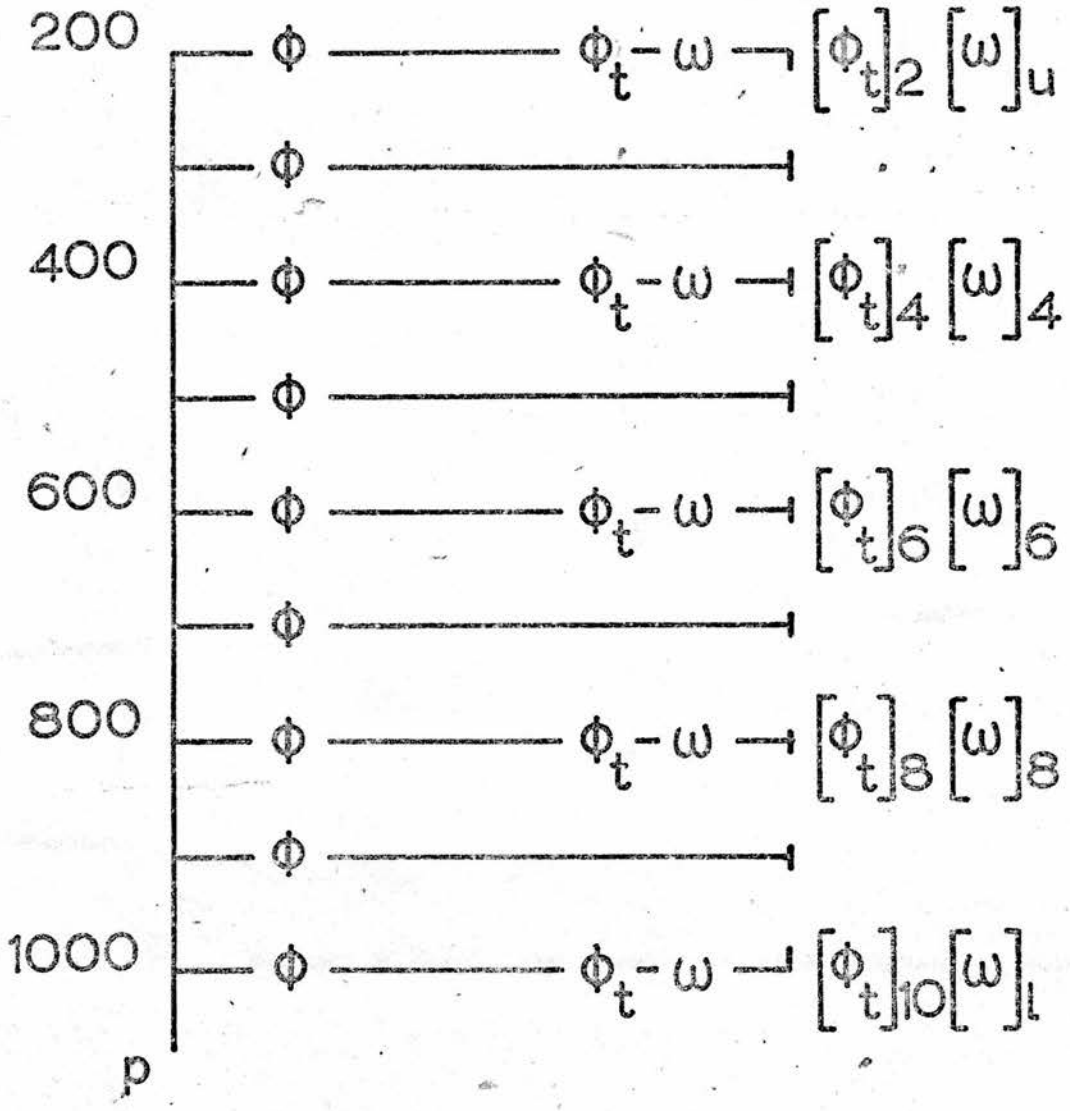

FIGURE 4.1

Often approximations to the first term of Equ. (4.5) are made. The most common is to neglect the derivatives of σ so that the equation becomes

$$\sigma \nabla^2 \omega + f^2 \frac{\partial^2 \omega}{\partial p^2} + S = 0 \qquad (4.7)$$

Let $\left[\Phi_t\right]_k$ denote that Φ_t is specified on the lateral boundaries of the k x 100 mb isobaric surface. Also let $\left[\omega\right]_u$ and $\left[\omega\right]_l$ denote that ω specified on the upper and lower boundaries. Using this notation, Fig. 4.1 shows the levels at which Φ was known and those at which ω and Φ_t were computed. It also shows the boundaries on which ω and Φ_t were specified.

4.3 The Elliptic Criteria For The Poisson Equation And The ω-Equation

Consider the Poisson equation

$$\nabla^2 \chi = F$$

Suppose that this is solved by using the SOR method. Let χ_{ij} be the exact solution and $\chi_{ij}^{(n)}$ the solution after n iterations. If $\varepsilon_{ij}^{(n)} = \chi_{ij}^{(n)} - \chi_{ij}$ then

$$\varepsilon_{ij}^{(n+1)} = \varepsilon_{ij}^{(n)}(1 - \beta) + \frac{\beta}{4}\left(\varepsilon_{i+1,j}^{(n)} + \varepsilon_{i-1,j}^{(n+1)} + \varepsilon_{i,j+1}^{(n)} + \varepsilon_{i,j-1}^{(n+1)} \right)$$

Here β is the overrelaxation factor. Let $\varepsilon_{ij}^{(n)}$ have a major Fourier component of

$$\varepsilon_{ij}^{(n)} = q^{(n)} e^{i\vartheta + j\varphi}$$

When this is substituted into the above equation it can be shown that

$$\frac{q^{(n+1)}}{q^{(n)}} = \frac{4 - 4\beta + \beta V + i'\beta W}{4 - \beta V + i'\beta W} \qquad i' = \sqrt{-1}$$

$$V = \cos(\vartheta) + \cos(\varphi)$$

$$W = \sin(\vartheta) + \sin(\varphi)$$

The iteration scheme is convergent if $\left| \frac{q^{(n+1)}}{q^{(n)}} \right| < 1$.

Therefore in this case there will be convergence if

$$(2 - V)(2 - \beta) > 0$$

The $(2-\beta)$ part of this inequality refers only to the iteration scheme that was used. From the theory of SOR it is known that $(2-\beta) > 0$ for convergence. The $(2-V)$ part of the inequality refers to the form of the equation that is solved. This may be thought of as the elliptic condition for the finite difference form of the original equation. The above considerations show that the elliptic criterion for the Poisson equation is

$$(2-V) > 0$$

This condition is always satisfied and thus the Poisson equation, with ∇^2 as the finite difference operator, is always elliptic.

Now consider the ω-equation given by Equ. (4.5). If the SOR method is used it can be shown that a very good approximation to the condition for convergence is

$$(1-2V)(2-\beta) > 0 \qquad (4.8)$$

$$2V = \frac{\cos(\vartheta)+\cos(\varphi)}{2 + \frac{\nabla^2\sigma}{\sigma} + \frac{f^2 d^2}{2 m^2 \sigma \Delta p^2}}$$

Equ. (4.8) shows that the finite difference form of the ω-equation is elliptic if $(1-2V) > 0$. Therefore, if $\frac{\nabla^2\sigma}{\sigma}$ is small, the elliptic condition is $\sigma > 0$. This result was anticipated in section 1.6.

If the $\nabla^2(\sigma\omega)$ term in the ω-equation is replaced by $\sigma\nabla^2\omega$ or if σ is assumed to be a function of pressure only, the condition for convergence is the same as above, with 2V given by

$$2V = \frac{\cos(\vartheta)+\cos(\varphi)}{2 + \frac{f^2 d^2}{2 m^2 \sigma \Delta p^2}}$$

Therefore the equation is elliptic if $\sigma > 0$.

The above results show that if it is ensured that $\sigma > 0$ it should be possible to compute the solution of an ω-equation.

The next step in solving the ω-equation is to impose suitable boundary conditions at both the lateral boundaries and the upper and lower boundaries. This will be discussed in the following sections.

4.4 The Upper and Lower Boundary Condition For ω

The kinematic boundary condition at $p = 0$ is $\omega = 0$. However it is convenient to replace this by $\omega = 0$ at the tropopause and to assume that the tropopause is at a fixed level. In the past this level has been taken to be at 200 mb (e.g. Danard (1964)) or at 100 mb (e.g. Haltiner et al.(1963) and Krishnamurti (1968a)). In the present investigation the 200 mb level was chosen as the upper boundary.

Now consider the lower boundary. If there is no topography then the kinematic boundary condition is

$$w = 0 \text{ at } z = 0$$

When pressure coordinates are used this is usually replaced by

$$\omega = 0 \text{ at } p = 1000 \text{ mb}$$

These are only equivalent if

(a) $p = 1000$ mb at $z = 0$

(b) $\omega = 0$ when $w = 0$

The surface pressure is not usually 1000 mb but the maximum error involved in assuming this value is 5%. Therefore it is reasonable to assume that (a) holds. However it is worth noting that it is possible to use

$\omega = 0$ at the surface pressure (p_s) instead of at 1000 mb. To do this it is first necessary to compute p_s (e.g. by using the altimeter equation). Then the pressure derivatives in the ω-equation can be derived from non-centre finite differences. This proce dure was carried out by Haltiner et al.(1963) but it is impossible to deduce from their results the effect of using p_s as the lower boundary instead of 1000 mb. For the situation studied in this thesis it was found that the effect was negligible. However this result will not hold when at the lower boundary is large or when $(p_s - 1000)$ is large.

Now consider (b). The relationship between w and ω is

$$gw = \Phi_t + \underline{V}.\nabla\Phi + \omega\frac{\partial\Phi}{\partial p} \qquad (4.9)$$

It is usually argued that Φ_t and $\underline{V}.\nabla\Phi$ are small so that to a good approximation

$$\omega = -\rho g w$$

This implies that $w = 0$ when $\omega = 0$. However this argument obscures an important point. If $w = 0$ at the lower boundary and if the wind is geostrophic then Equ. (4.9) gives

$$\omega = \rho\Phi_t \qquad (4.10)$$

Similarly, if $\underline{V} = k \times \nabla\Psi + \nabla X$ and only the largest terms are considered

$$\omega = \rho\Phi_t + \rho J(\Psi, \Phi) \qquad (4.11)$$

Thus at the lower boundary the values of ω and Φ_t are closely linked. However a typical value of Φ_t at 1000 mb is 10^{-1} $m^2 s^{-2}$. Therefore Equ. (4.10) implies

that the error involved by using $\omega = 0$ in place of $\omega = \rho \Phi_t$ at the lower boundary is of the order of 10^{-4} mb s^{-1}, which is small. Berkofsky (1964) investigated the fall-off with height of terrain-induced vertical motions. His results imply that if $\sigma \propto 1/p^2$ the error ($\varepsilon(p)$) induced by an incorrect lower boundary condition ($\varepsilon(1000)$) is approximately

$$\varepsilon(p) = \varepsilon(1000) \times \left[\frac{p}{1000}\right]^{2.3}$$

Therefore the small boundary errors fall-off rapidly.

The above results indicate that when there is no terrain or frictionally induced vertical velocities it is reasonable to use $\omega = 0$ at $p = 1000$ mb in place of $w = 0$ at $z = 0$ provided that $(p_s - 1000)$ and Φ_t are small.

In the following computations $\omega = 0$ was used as the boundary condition for both the upper (200 mb) and lower (1000 mb) boundaries.

It is worth noting that when Equ. (4.6) is solved for Φ_t on the 1000 mb surface, $\Phi_t = 0$ is usually specified on the lateral boundaries. Therefore away from the lateral boundaries neither Equ. (4.10) or (4.11) is satisfied and thus the values of ω and Φ_t on the lower boundary are not consistent.

The boundary conditions for ω on the lateral boundaries are considered next.

4.5 The Lateral Boundary Conditions For The ω-Equation

Nearly all previous investigations of the vertical velocity field have used the lateral boundary condition, $\omega = 0$, in conjunction with an ω-equation. For example, this procedure was used by Haltiner et al.(1963) and

Pedersen et al.(1969). O'Neill also computed ω in this way and he briefly investigated the effect of the boundary condition on the solution. He concluded that the main effect of using the "incorrect" boundary condition $\omega = 0$ was to change the vertical boundary near the boundary. Harwood (1969) also investigated the effect of using this boundary condition and he found that its use tended to underestimate the "correct" value of ω near the boundary. Because of this, Harwood decided to use the less restrictive condition $\frac{\partial \omega}{\partial n} = 0$ on the boundary. However, he did not investigate the effect on the solution of using this boundary condition.

Krishnamurti (1968a) used a combination of a rather strange cyclic boundary condition on two of the lateral boundaries, and Dirichlet boundary conditions on the others. It was decided that it was not worthwhile pursuing this sytem of boundary conditions.

In the light of the lack of information on the effect of using a particular kind of boundary condition, it was decided that it would be worthwhile making a detailed study of the different types of boundary condition that are used with an ω-equation. One, two-, and three- dimensional ω-equations are used with both real and artificial data. An examination is made of rates at which the boundary errors decrease away from the boundary. Also, the qualitative effect of using different types of boundary conditions is considered.

4.5.1 The One-Dimensional Error Equation

If $\omega = f(x) \sin(lp)$ then Equ. (4.7) becomes

$$\frac{d^2\omega}{dx^2} - \lambda^2\omega + S' = 0 \qquad \lambda^2 = \frac{f^2 l^2}{\sigma} \qquad S' = \frac{S}{\sigma} \qquad (4.12)$$

Here $l = 2\pi/L_p$ where L_p is the wavelength in the p direction. Let F and G be the correct values of ω at $x = 0$ and $x = L$ and let $\varepsilon(x)$ be the error in the vertical velocity produced by using the incorrect boundary conditions $\omega = 0$ at $x = 0$ and $x = L$. Since Equ. (4.12) is linear, $\varepsilon(x)$ is given by

$$\frac{d^2\varepsilon}{dx^2} - \lambda^2\varepsilon = 0 \qquad \varepsilon(0) = F \qquad \varepsilon(L) = G \tag{4.13}$$

This is the one-dimensional error equation and has a solution

$$\varepsilon(x) = \varepsilon(0)\, f_1(x, L, \lambda) + \varepsilon(L)\, f_2(x, L, \lambda) \tag{4.14}$$

$$f_1(x,L\,\lambda) = e^{-\lambda x} - e^{-\lambda L}\,\frac{\sinh(\lambda x)}{\sinh(\lambda L)} \qquad f_2(x,L,\lambda) = \frac{\sinh(\lambda x)}{\sinh(\lambda L)}$$

If L is large the distributions of $\varepsilon(x)$ near the $x = 0$ and $x = L$ boundaries are

$$\varepsilon(x) = \varepsilon(0)\, e^{-\lambda} \qquad\qquad \varepsilon(x) = \varepsilon(L)\, e^{-\lambda(L-x)}$$

These clearly show that in the vicinity of the boundaries, the boundary error decays exponentially. It can also be shown from Equ. (4.14) that, if F and G are finite,

$$\varepsilon(x) \longrightarrow \varepsilon(0)\, e^{-\lambda x} \quad \text{as } L \longrightarrow \infty.$$

The distribution of $\varepsilon(x)$ was found using the following parameters

$$\sigma = 4 \times 10^{-2}\ m^2\ mb^{-2}\ s^{-2} \qquad L_p = 1600\ mb \qquad f = 10^{-4}\ s^{-1}$$

$$d = 10^5\ m \qquad \lambda = 1.96 \times 10^{-6}\ m^{-1}$$

In units of mb s^{-1}, the two sets are boundary conditions used are

(a) $\varepsilon(0) = 30 \times 10^{-4}$ (b) $\varepsilon(0) = 30 \times 10^{-4}$

$\varepsilon(L) = 30 \times 10^{-4}$ $\varepsilon(L) = -30 \times 10^{-4}$

Also two values of L were used, namely $L = 13d$ and $L = 21d$. The results of these computations, presented in Fig. 4.2, shows that the boundary error near the

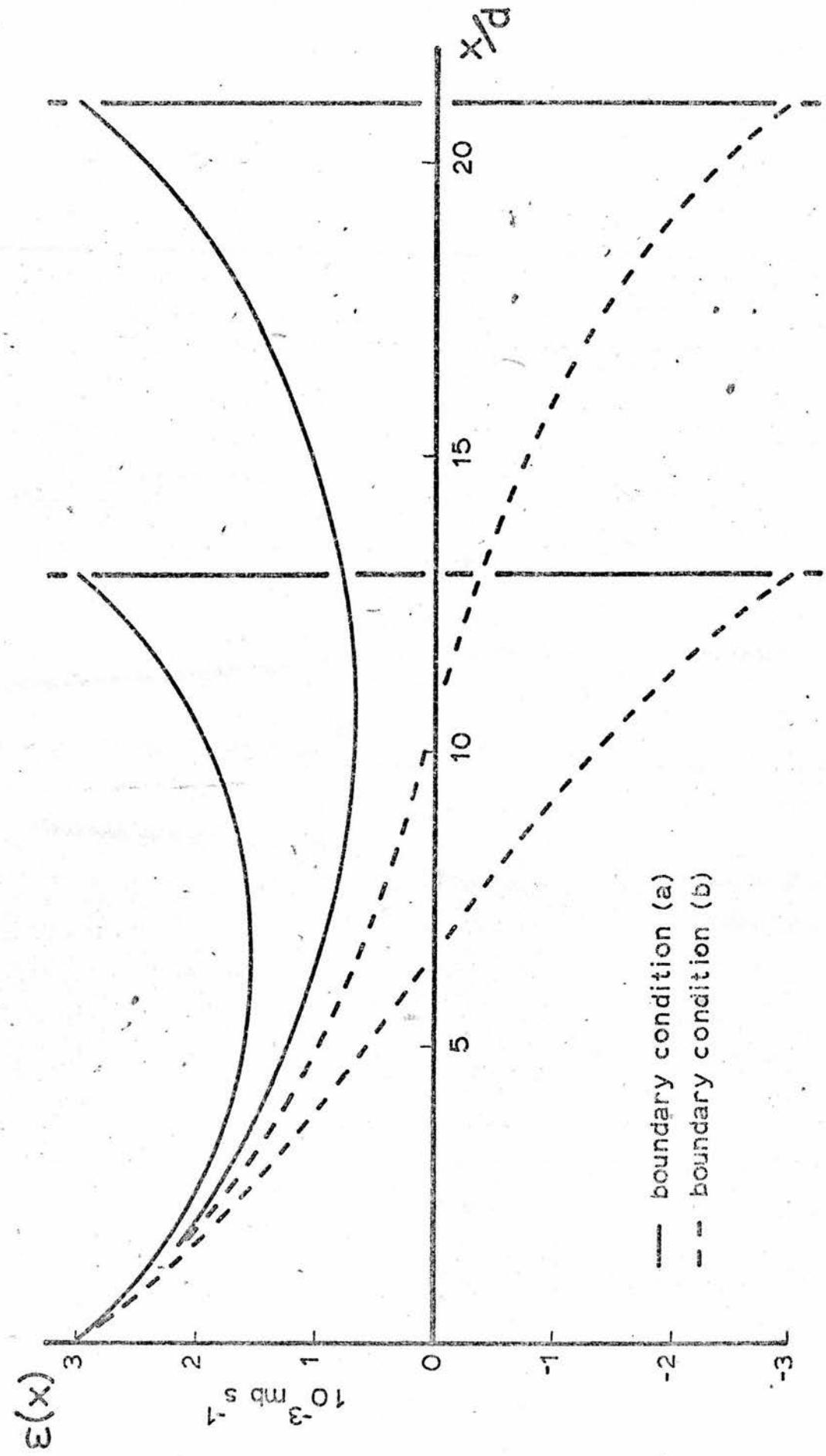
ε(x)
10⁻³ m s⁻¹
3
2
1
0
-1
-2
-3
x/d
5
10
15
20
boundary condition (a)
boundary condition (b)

FIGURE 4.2

p mb	$\sigma \times 10^{2}$ $m^{2}mb^{-2}s^{-2}$	$\lambda \times 10^{6}$ m^{-1}	d_{10}
400	4.16	1.9	12.0
600	2.15	2.7	8.5
800	1.18	3.6	6.4

TABLE 4.1

p mb	$\lambda \times 10^{6}$ m^{-1}	$\mu \times 10^{6}$ m^{-1}	d_{10}
400	1.9	2.8	8.2
600	2.7	3.4	6.8
800	3.6	4.2	5.5

TABLE 4.2 $\mu = \sqrt{\lambda^{2} + h^{2}}$ $\quad h = 2\pi / 30d$

	Units of 10^{-4} mb s^{-1}		Units of 10^{-6} m^{-1}	
	value at a = 0 from		decay rate at a = 0 from	
	Equ. (4.21) or Equ. (4.22)	Fig. 4.4	Equ. (4.21) or Equ. (4.22)	Fig. 4.4
dav(a)	9.8	10.8	1.95	1.91
rmse(a)	12.1	13.8	2.42	2.32

TABLE 4.3

$x = 0$ boundary decreased at the same rate for all combinations of L and boundary error. However, the value of $\varepsilon(x)$ after a few gridlengths depended upon $\varepsilon(0)$, $\varepsilon(L)$ and L.

Now consider the error at a distance 4d from the $x = 0$ boundary, $\varepsilon(4d)$. Fig. 4.2 shows that, for a given value of L, $\varepsilon(4d)$ decreased as $\varepsilon(L) / \varepsilon(0)$ decreased. Also, for given value of $\varepsilon(0)$ and $\varepsilon(L)$, $\varepsilon(4d)$ either increased or decreased according as $\varepsilon(L) / \varepsilon(0)$ was less than or greater than zero. Thus, in this simple case, an increase in the distance between the boundaries does not necessarily imply that the error at a given distance from the boundary will decrease.

The decay rate of the boundary error depends upon σ which is a function of pressure. The variation of λ with pressure, for a standard atmosphere is shown in Table 4.1. Also, the number of gridlengths (d_{10}) required for the error to decay to 1/10 of its boundary value is shown. These results show that when the pressure increases from 400 mb to 800 mb, the value of d_{10} is halved. However, it is important to bear in mind that the boundary error at the 400 mb level is usually less than that at the other two levels.

So far only a one-dimensional case has been considered. The results from this are not directly applicable to the two-dimensional case because in two dimensions the rate at which the boundary error decays must depend upon the distribution of the boundary error along the boundary. In the next section an error equation that is closely related to the two-dimensional

error equation is considered.

4.5.2 The $1\frac{1}{2}$-Dimensional Error Equation

Consider a two-dimensional problem where $\omega = f(x)\, g(y) \sin(lp)$. Equ. (4.7) then becomes

$$\frac{\partial^2 \omega}{\partial x^2} + \frac{\partial^2 \omega}{\partial y^2} - \lambda^2 \omega + S' = 0 \qquad (4.15)$$

Suppose that the actual distribution of ω on the boundary is

$$\omega_b = A \sin(kx + \alpha) \sin(hy + \beta)$$

The error produced by using $\omega_b = 0$ instead of the correct distribution is given by

$$\frac{\partial^2 \varepsilon}{\partial x^2} + \frac{\partial^2 \varepsilon}{\partial y^2} - \lambda^2 \varepsilon = 0 \qquad \varepsilon_b = A \sin(kx+\alpha)\sin(hy+\beta) \qquad (4.16)$$

Let two of the boundaries of a rectangular region be at $x = 0$ and $x = L_1$ and let the y = constant boundaries be distant from the region under consideration. Equ. (4.16) now reduces to the $1\frac{1}{2}$-dimensional error equation

$$\frac{\partial^2 \varepsilon}{\partial x^2} - \mu^2 \varepsilon = 0 \qquad \varepsilon_b = A \sin(kx+\alpha)\sin(hy+\beta)$$

$$\mu^2 = \lambda^2 + h^2 \qquad h = 2\pi / L_y \qquad (4.17)$$

Here L_y is the wavelength of ε_b in the y direction. The solution of Equ. (4.17) is

$$\varepsilon(x,y) = \varepsilon(0,y)\, f_1(x, L_1, \mu) + \varepsilon(L_1,y)\, f_2(x, L_1, \mu)$$

$$\varepsilon(0,y) = A \sin(\alpha) \sin(hy + \beta) \qquad (4.18)$$

$$\varepsilon(L_1,y) = A \sin(kL_1 + \alpha) \sin(hy + \beta)$$

As $L_y \longrightarrow \infty$ (i.e. the boundary error becomes constant along the x = constant boundaries), $\varepsilon(x,y)$ becomes identical to $\varepsilon(x)$ (see Equ. (4.14)). Also, as $L_y \longrightarrow 0$, $\varepsilon(x,y)$ becomes zero everywhere.

Near the $x = 0$ boundary

$$\varepsilon(x,y) = \varepsilon(0,y)\, e^{-\mu x}$$

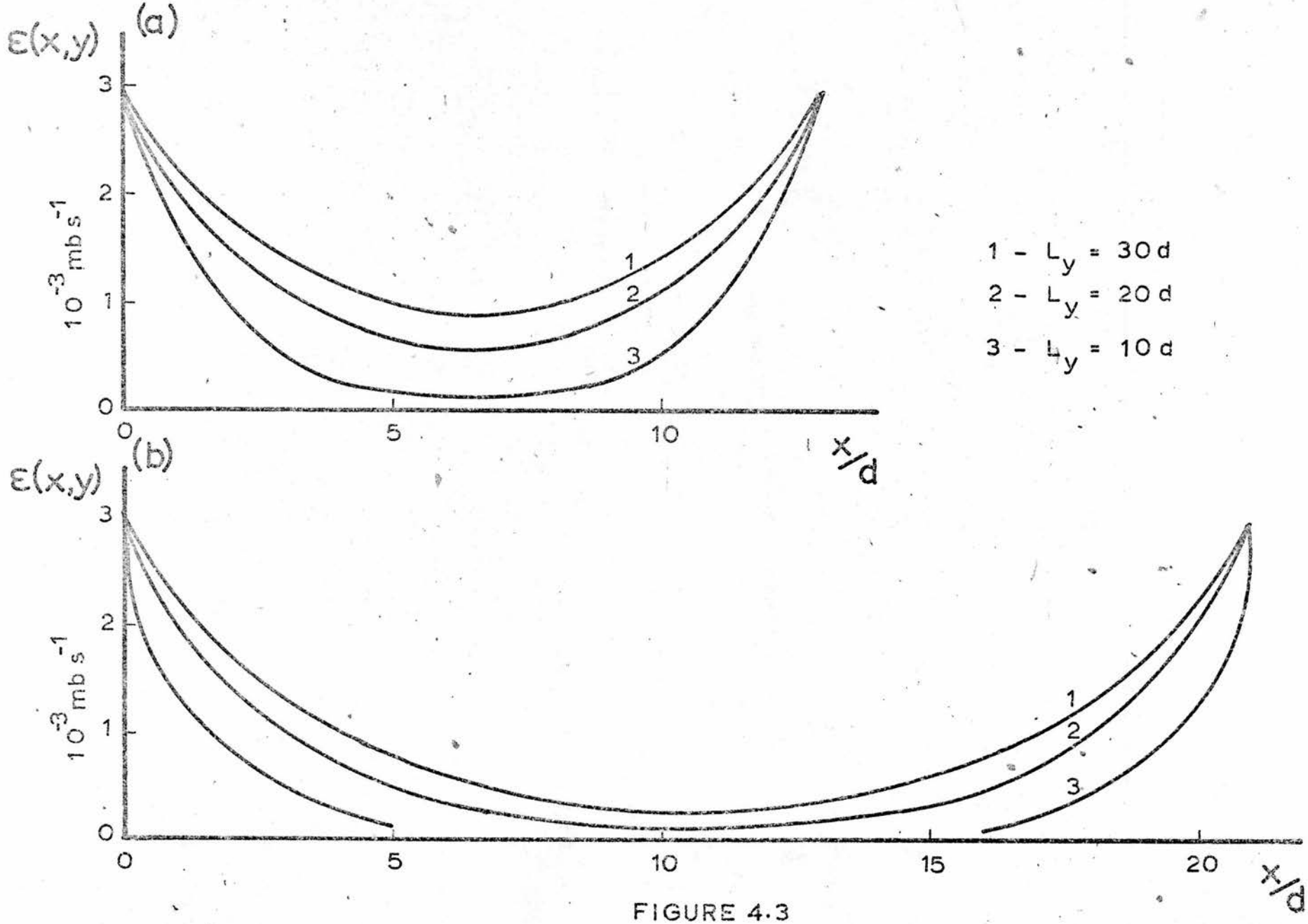
ε(x,y)
(a)
3
2
1
0
10^{-3} mb s^{-1}
0
5
10
x/d
1
2
3
1 - L_y = 30 d
2 - L_y = 20 d
3 - L_y = 10 d
ε(x,y)
(b)
3
2
1
0
10^{-3} mb s^{-1}
0
5
10
15
20
x/d
1
2
3

FIGURE 4.3

Therefore the boundary error decays exponentially away from the boundary. (This is also true near the $x = L_1$ boundary). As L_y increases, μ deceases and d_{10} increases. Thus the boundary error decays rapidly or slowly depending upon if the boundary error changes sign rapidly or slowly. Fig. 4.3 shows $\varepsilon(x,y)$ for various values of L_y and L_1. The boundary conditions were the same as that denoted by (a) in the previous section. Fig. 4.3 clearly illustrates the dependance of μ and $\varepsilon(x,y)$ upon L_1 and L_y.

A reasonable value for L_y is 3000 km (i.e. 30d). With this value of L_y, L_1 = 21d, and the static stability for a standard atmosphere, the values of μ and d_{10} were calculated (see Table 4.2). A comparison of these results with those in Table 4.1 shows that the one-dimensional model overestimates d_{10}. Further it is expected that the values of d_{10} for the $1\frac{1}{2}$-dimensional model are greater than (those for a 2-dimensional model (i.e. where the variation of the boundary error along the x = constant boundaries is taken into consideration).

Let dav and rmse be the difference in average and the root mean square error between the correct solution and that using $\omega = 0$ on the boundary. The variation of these quantities as a function of the distance from the boundary (a) can be investigated in terms of

$$\mathrm{dav}(a) = \frac{\int_a^{L_1-a}\int_a^{L_2-a} \varepsilon(x,y)\,dx\,dy}{\tilde{A}} \qquad (4.19)$$

$$\mathrm{rmse}(a)^2 = \frac{\int_a^{L_1-a}\int_a^{L_2-a} \varepsilon(x,y)^2\,dx\,dy}{\tilde{A}} \qquad (4.20)$$

$$\tilde{A} = \int_a^{L_1-a}\int_a^{L_2-a} dx\,dy$$

Here L_1 and L_2 are the dimensions of the original area in the x and y directions.

If Equ. (4.18) is substituted into Equs. (4.19) and (4.20) and if it is assumed that $a \ll L_1$ and $a \ll L_2$, and that $L_2 \simeq L_y$, then

$$dav\,(a) \simeq \frac{(\varepsilon(0) + \varepsilon(L))}{\mu L_1} e^{-a\left(\mu - \frac{2}{L_1}\right)} \qquad (4.21)$$

$$rmse\,(a) \simeq \sqrt{\frac{\varepsilon(0)^2 + \varepsilon(L)^2}{2\mu L_1}}\, e^{-a\left(\mu - \frac{1}{L_1}\right)} \qquad (4.22)$$

Here $\varepsilon(0)$ and $\varepsilon(L)$ are defined by

$$\varepsilon(0,y) = \varepsilon(0) \sin(hy + \beta) \qquad \varepsilon(L_1,y) = \varepsilon(L_1) \sin(hy + \beta)$$

Equs. (4.21) and (4.22) show that both dav (a) and rmse (a) decay exponentially with a.

The decay rates depend upon both μ and the dimensions of the region and that they are different for $\varepsilon(x,y)$, dav (a) and rmse (a). Equs. (4.21) and (4.22) also show that as μ increases (i.e. L_y decreases), both dav (0) and rmse (0) decrease and the rates of decay of dav (a) and rmse (a) increase.

The value of dav (0) can also be computed by integrating Equ. (4.17) w.r.t. x between 0 and L_1. This gives

$$dav(0) = \frac{\left.\frac{d\varepsilon}{dx}\right|_{L_1} - \left.\frac{d\varepsilon}{dx}\right|_0}{\mu^2 L_1} \qquad (4.23)$$

If Equ. (4.17) is multiplied by ε and a similar integration performed then

$$rmse(0) = \frac{\left.\varepsilon\frac{d\varepsilon}{dx}\right|_{L_1} - \left.\varepsilon\frac{d\varepsilon}{dx}\right|_0}{\mu^2 L_1} - \frac{\int_0^{L_1}\left(\frac{d\varepsilon}{dx}\right)^2 dx}{\mu^2 L_1} \qquad (4.24)$$

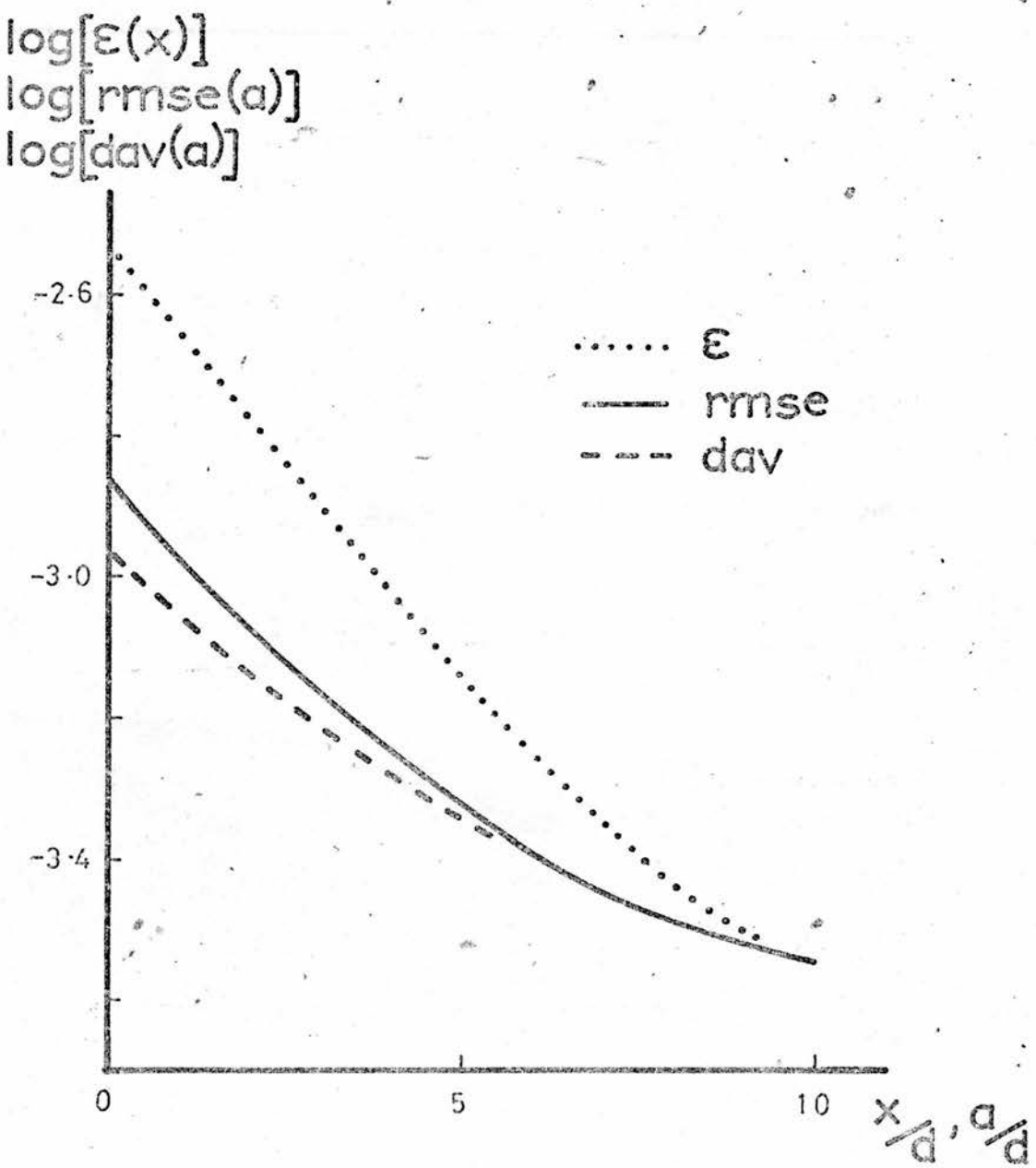

FIGURE 4.4

It is found that, provided $\mu L_1 > 3$, the values of dav (0) and rmse (0) derived from Equs. (4.21) and (4.22) agree to within 10% with those derived from the above equations. It is worth noting that there are similar equations to those above for the two-dimensional case.

From the distribution of $\varepsilon(x,y)$ with $L_y = 30d$ and $L_1 = 21d$ (see Fig. 4.3) dav (a) and rmse (a) were calculated.

These are shown, along with $\varepsilon(x,y)$, in Fig. 4.4. Clearly they all vary exponentially. Table 4.3 shows the values of dav (a) and rmse (a) at a = 0 and their decay rates. The corresponding approximates values calculated from Equs. (4.21 and (4.22) are also shown. A comparison shows that both Equs. (4.21) and (4.22) give good estimates of the values at a = 0 and the decay rates.

So far only the difference between the "correct" solution and that using $\omega = 0$ on the boundary has been considered. In the next section the difference between solutions using Dirichlet and Neumann boundary conditions is described.

4.5.3 A Comparison Between Dirichlet And Neumann Boundary Conditions For The One-Dimensional ω-Equation

Suppose that ω is given by Equ. (4.12) with

$$S' = F \sin (kx + \delta)$$

$$\frac{d^2\omega}{dx^2} - \lambda^2 \omega = F \sin (kx + \delta) \qquad \lambda^2 = \frac{f^2 l^2}{\sigma} \qquad (4.25)$$

The general solution of this is

$$\omega = A e^{\lambda x} + B e^{-\lambda x} - \frac{F}{\nu^2} \sin (kx + \delta)$$

Here $\nu^2 = k^2 + \lambda^2$ and the arbitary constants A and B must be determined from the boundary conditions.

(i) When $\omega(0) = 0$ and $\omega(L) = 0$ (Dirichlet)

$$\omega_1(x) = \frac{F}{\nu^2}\left[2\alpha \sinh(\lambda x) + e^{-\lambda x}\sin(\delta) - \sin(kx+\delta)\right]$$

(ii) When $\left.\frac{d\omega}{dx}\right|_0 = 0$ and $\left.\frac{d\omega}{dx}\right|_L = 0$ (Neumann)

$$\omega_2(x) = \frac{F}{\nu^2}\left[2\beta\cosh(\lambda x) - \frac{k}{\lambda}\, e^{-\lambda x}\sin(\delta) - \sin(kx+\delta)\right]$$

$$2\alpha = \left[\frac{\sin(kL+\delta) - \sin(\delta)\, e^{-\lambda L}}{\sinh(\lambda L)}\right]$$

$$2\beta = \left[\frac{\sin(kL+\delta) - \cos(\delta)\, e^{-\lambda L}}{\sinh(\lambda L)}\right]\frac{k}{\lambda}$$

If $\varepsilon(x) = \omega_2 - \omega_1$ and $\gamma = \frac{k}{\lambda}\cos(\delta) + \sin(\delta)$, then

$$\varepsilon(x) = \frac{F}{\nu^2}\left[e^{-\lambda x}(\alpha + \beta - \gamma) - e^{\lambda x}(\alpha - \beta)\right]$$

From this equation it can be shown that if $\lambda L \gg 3$, then

$$\varepsilon(0) \simeq -\frac{F}{\nu^2}\left[\frac{k}{\lambda}\cos(\delta) + \sin(\delta)\right]$$

$$\varepsilon(L) \simeq \frac{F}{\nu^2}\left[\sin(kL+\delta)\left(\frac{k}{\lambda} - 1\right)\right]$$

These values of $\varepsilon(0)$ and $\varepsilon(L)$ can be used in Equs. (4.21) and (4.22) to find the values of dav (a) and rmse (a) at a = 0 and their rates of decay. Further, due to the form of the boundary conditions, it is possible to put dav (a) and rmse (a) in terms of ω_2. The boundary conditions for ω_1 and ω_2 are such that

$$\varepsilon(0) = \omega_2(0) \qquad \left.\frac{d\varepsilon}{dx}\right|_0 = \left.\frac{d\omega_1}{dx}\right|_0$$

$$\varepsilon(L) = \omega_2(L) \qquad \left.\frac{d\varepsilon}{dx}\right|_L = \left.\frac{d\omega_1}{dx}\right|_L$$

Thus Equs. (4.21) and (4.22) can be put in terms of $\omega_2(0)$ and $\omega_2(L)$. At a = 0, these equations give

$$\text{dav}(0) = \frac{\omega_2(0) + \omega_2(L)}{\lambda L}$$

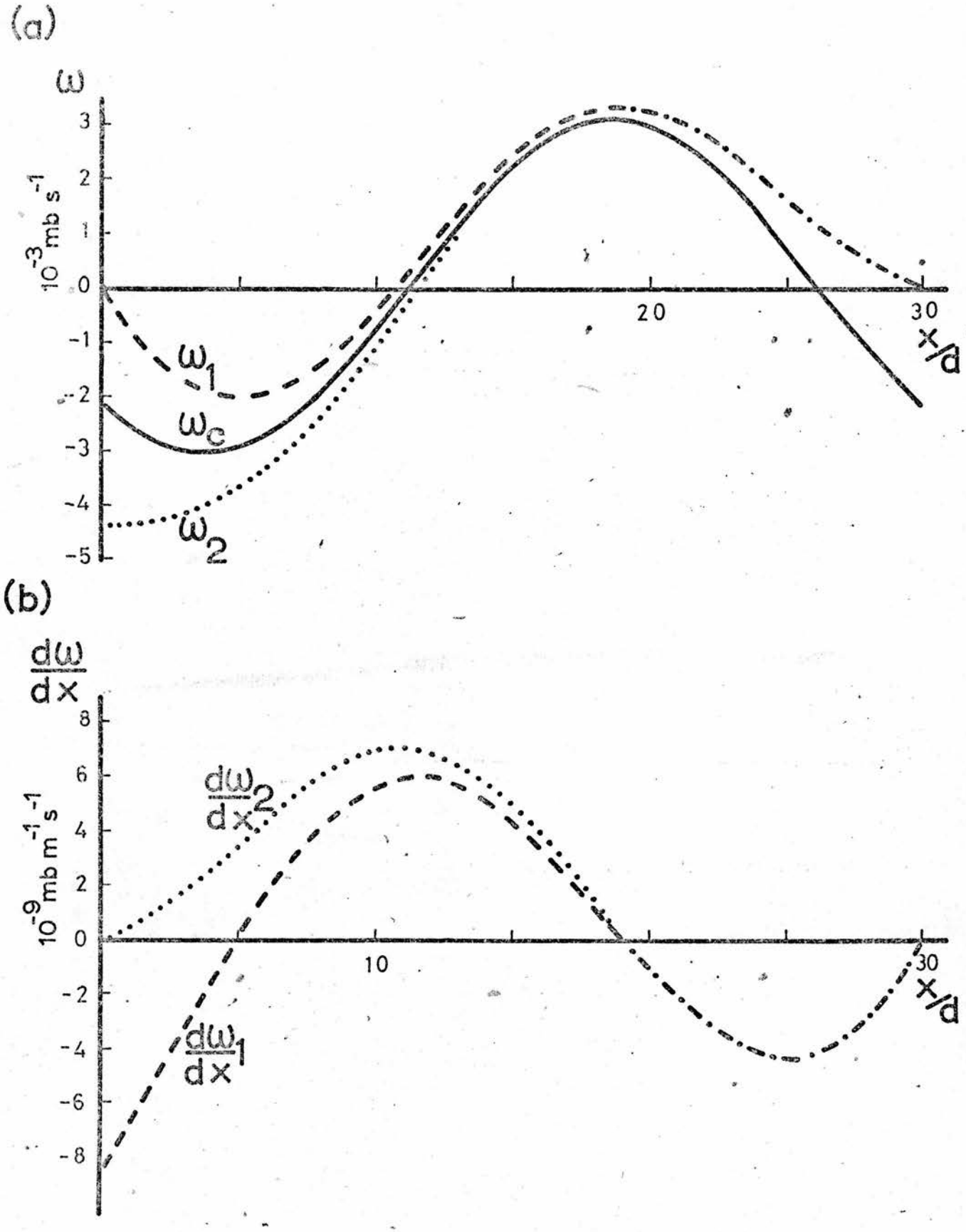
(a)
ω
10^-3 mb s^-1
3
2
1
0
-1
-2
-3
-4
-5
20
30
x/d
ω1
ωc
ω2
(b)
dω/dx
8
6
4
2
0
-2
-4
-6
-8
10^-9 mb m^-1 s^-1
10
30
x/d
dω/dx 2
dω/dx 1

FIGURE 4.5

$$\text{rmse (0)} = \sqrt{\frac{\omega_2 (0) + \omega_2 (L)}{2 \lambda L}}$$

Using Equ. (4.23) dav (0) can also be put in terms of ω_1. However the value of rmse (0) derived from Equ. (4.24) cannot be put solely in terms of ω_2.

It is reasonable to assume that the vertical velocity is zero when the forcing function is zero. Therefore the 'correct' solution of Equ. (4.25) (ω_c) is given by

$$\omega_c = - \frac{F \sin (kx + \delta)}{(\lambda^2 + k^2)}$$

This, along with ω_1 (x) and ω_2 (x), was computed using the following parameters.

$\lambda = 1.96 \times 10^{-6}$ m^{-1} $\quad d = 10^5$ m $\quad L = 30d$

$F = 2.5 \times 10^{-14}$ mb m^{-2} s^{-1} $\quad k = 2\pi/L \quad \delta = \pi/4$

The results shown in Fig. 4.5a indicate that both ω_1 and ω_2 have the same basic distribution (e.g. they have the same number of maxima and minima). However, there is a systematic difference between the solutions (i.e. $\omega_1 > \omega_2$ everywhere). The reason for this become apparent when Equ. (4.21) is written as

$$\text{dav (a)} = \text{dav (0)}\, e^{- a (\mu - \frac{2}{L})}$$

This indicates that the sign of dav (a) (and that of $\varepsilon(x)$) is determined by that of dav (0) which depends upon $\varepsilon(0) + \varepsilon(L)$. Therefore, if both $\varepsilon(0)$ and $\varepsilon(L)$ have the same sign or if one of these is much larger than the other, it is possible to determine the sign of $\varepsilon(x)$. In the case considered $\varepsilon(L) \simeq 0$ (because $\lambda \simeq k$) and thus the sign of both dav (0) and $\varepsilon(x)$ is determined by that of $\varepsilon(0)$ (i.e. ω_2 (0)). Since ω_2 (0) < 0, it follows that both dav (0) and $\varepsilon(x)$ are

negative and therefore $\omega_1 > \omega_2$. This means that at a positive maximum the magnitude of ω_2 is less than that of ω_1. The reverse is true at a negative minimum. However, if dav (0) > 0 the opposite is true.

Consider the distributions of ω_1, ω_2 and ω_c near the x = 0 boundary (see Fig. 4.5a). There is a negative minimum of ω_c at about 4d from the boundary. The effect of using the Neumann boundary condition is to increase the magnitude of the minimum and to shift it to the boundary. The corresponding effect of using the Dirichlet boundary condition is to shift the minimum slightly away from the boundary and to reduce its magnitude. The net effect is to produce a large difference between ω_1 and ω_2 near this boundary. Near the same boundary it is found that $|\omega_1| < |\omega_c|$ and that $\frac{1}{\omega_1} \frac{\partial \omega_1}{\partial n} > 0$. Also ω_2 is such that $\frac{\partial \omega_c}{\partial n} \frac{1}{(\omega_2 - \omega_c)} > 0$. By manipulating the equations for ω_1 and ω_2 it is found that these results will always apply near a boundary if S' is large.

Fig. 4.5b shows the gradients of ω_1 and ω_2. It is worth noting that, unlike ω_1 and ω_2, $\frac{d\omega_1}{dx}$ and $\frac{d\omega_2}{dx}$ have opposite signs over a region of 5d near the x = 0 boundary.

It will be shown later than in more realistic situations the differences between solutions using Dirichlet and Neumann boundary conditions resemble those between ω_1 and ω_2.

4.5.4 Two-Dimensional Error Equations

In previous sections the properties of one-and $1\frac{1}{2}$-dimensional error equations were investigated. Now

the two-dimensional error equations derived from a Poisson equation and a Helmholtz equation are considered.

First consider the Poisson equation

$$\nabla^2 X = F \qquad X = X_s \text{ on the boundary}$$

Knighting (1962) derived an expression for the average error, $\bar{\varepsilon}(a)$, in a circular region of radius a, where $X = 0$ is used in place of $X = X_s$ on the boundary. He showed that

$$\bar{\varepsilon}(a) = \frac{1}{2\pi} \int_0^{2\pi} X_s \, d\vartheta'$$

Here ϑ' is the coordinate around the boundary. Knighting argued that for large areas X_s and ϑ' are uncorrelated and therefore $\bar{\varepsilon}(a)$ is almost zero. However his analysis gives no information about $\bar{\varepsilon}(a)$ when the area is small or about how the boundary error changes away from the boundary.

The above problems are investigated for a Helmholtz equation derived from Equ. (4.7) by supposing that $\omega = f(x,y) \sin(lp)$. If ω on the boundary (ω_b) varies sinusoidally with x and y, then the equation for ω is

$$\nabla^2 \omega - \lambda^2 \omega + S' = 0 \qquad \omega_b = A \sin(kx + \alpha) \sin(hy + \beta)$$

The equation for the error, ε, introduced by using $\omega_b = 0$ is

$$\nabla^2 \varepsilon - \lambda^2 \varepsilon = 0 \qquad \varepsilon_b = A \sin(kx + \alpha) \sin(hy + \beta) \tag{4.26}$$

It is difficult, if not impossible to find an analytical solution of this equation. However it is possible to derive simple approximate expressions for rmse (a) and dav (a) (defined by Equs. (4.19) and (4.20)). The following analysis can also be applied to a Poisson

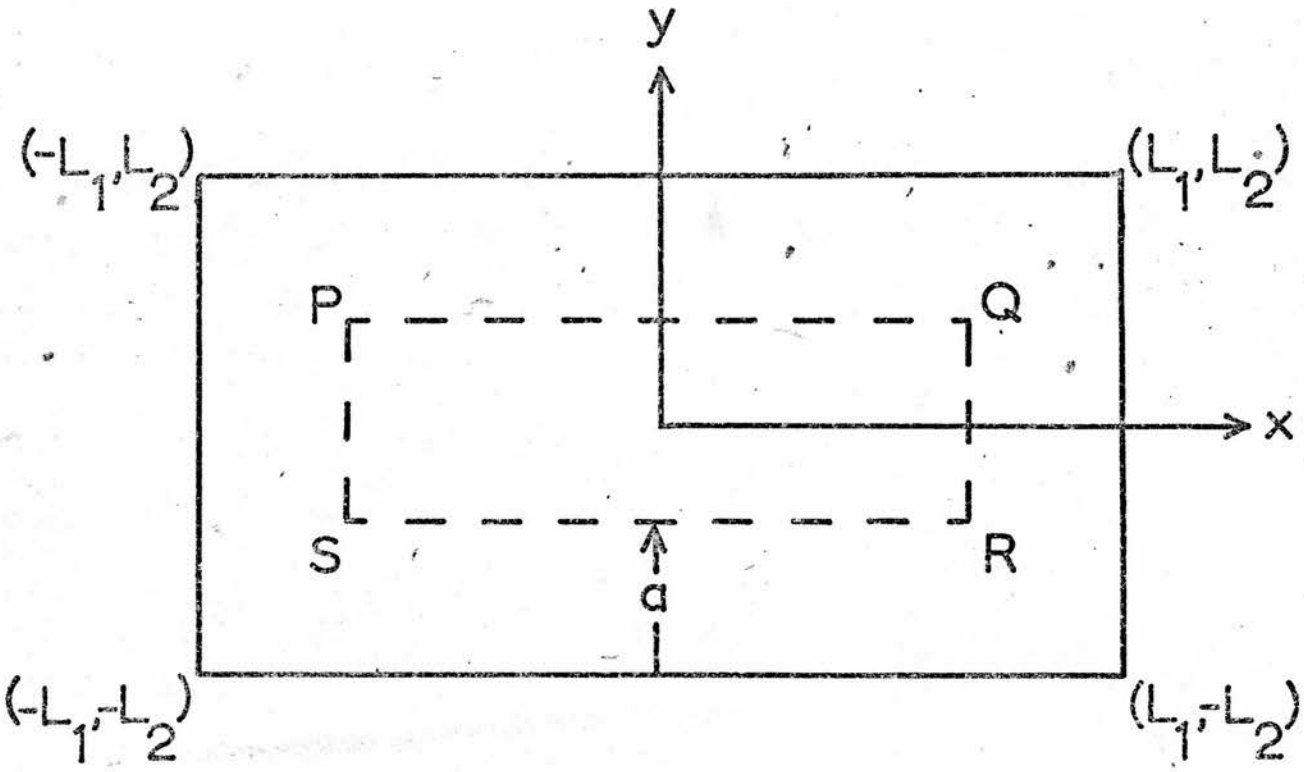

$$A = 4 L_1 L_2 \qquad C = 4(L_1 + L_2)$$

$$\text{area of PQRS} = \tilde{A} = A\left[1 - \frac{C}{A}a + \frac{4}{A}a^2\right]$$

$$\tilde{A} = A \exp\left[-\frac{C}{A}a\right] \quad \text{if } a \ll C$$

FIGURE 4.6

equation.

Suppose that Equ. (4.26) applies is a rectangular region with dimensions $2L_1$ and $2L_2$ (see Fig. 4.6). Let A and C be the area and circumference of this region. Near the $y = L_2$ boundary, an approximate expression for is

$$\varepsilon \approx \varepsilon_b \, e^{-\mu (L_2 - y)}$$

Here μ is related to both λ and k. There are similar expressions for ε near the other boundaries. Using these it can be shown that, when $k = h$, approximate expressions for dav (a) and rmse (a) are

$$\text{dav (a)}^* = \frac{d\ S_1}{\mu A \left(1 - \frac{Ca}{A}\right)} \, e^{-\mu a}$$

$$\text{rmse (a)}^* = \sqrt{\frac{d\ S_2}{2\mu A \left(1 - \frac{Ca}{A}\right)}} \, e^{-\mu a}$$

Here d is the gridlength and S_1 is the sum of the errors at the gridpoints around the boundary. Similarly S_2 is the sum of the square of the errors. When a is small, the above equations become

$$\text{dav (a)}^* = \frac{dS_1}{\mu A} \, e^{-a\left(\mu - \frac{C}{A}\right)} \tag{4.27}$$

$$\text{rmse (a)}^* = \sqrt{\frac{dS_2}{2\mu A}} \, e^{-a\left(\mu - \frac{C}{2A}\right)} \tag{4.28}$$

Before these equations can be used it is necessary to find μ. An examination of Equ. (4.26) suggests that $\mu = k^2 + \lambda^2$ when $k = h$. However, the situation is much more complicated when $k \neq h$. If $\mu_x = \sqrt{k^2 + \lambda^2}$ and $\mu_y = \sqrt{h^2 + \lambda^2}$, and if S_1 is divided into the sum of

the errors along the y = constant boundaries (Sx_1) and along the x = constant boundaries (Sy_1), then an approximate expression for dav (a) is

$$\left[\frac{Sx_1}{\mu_x} e^{-\mu_x a} + \frac{Sy_1}{\mu_y} e^{-\mu_y a} \right] \frac{d}{A} e^{\frac{C}{A} a}$$

A similar expression can be derived for rmse (a). However it will be shown later that it is not necessary to use these complicated expressions because Equs. (4.27) and (4.28) can be used with $\mu = \tilde{\mu}$ such that $\mu_1 < \tilde{\mu} < \mu_2$ (or vice versa).

The validity of Equs. (4.27) and (4.28) was tested for both Poisson and Helmholtz equations. In particular the values of dav (a)* and rmse (a)* at a = 0 and the decay rates were computed and compared with the actual values. These computations are described in the following section.

4.5.5 Computations Of dav (a) And rmse (a)

Equ. (4.26) was solved several times with different values of k and h. Different values of λ were also used and the computations were carried out for two areas. From the solution (ε) the values of dav (a) and rmse (a) were calculated for several values of a. The results were then compared with those derived from Equs. (4.27) and (4.28).

The two regions used had areas 13 x 21d and 29 x 21d with $d = 10^5$ m. Within these regions Equ. (4.26) was solved with $\lambda = 2 \times 10^{-6}$ m^{-1} (a Helmholtz equation) and $\lambda = 0$ (to avoid confusion this will be referred to as a Poisson equation). The values of k and h which were used corresponded to wavelengths of

		Units of 10^{-6} m^{-1}				Units of 10^{-4} mb s^{-1}							
							rmse(0)* using				dav(0)* using		
λ	Case	k_h	μ	μ_r	μ_a	rmse(0)	μ	μ_r	μ_a	dav(0)	μ	μ_r	μ_a
2×10^{-6} m^{-1}	SH_1	2.09	2.90	2.94	3.90	9	10	8	7	-6	-1	-1	-1
	SH_2	6.28	6.59	6.41	-	9	6	7	-	0	0	0	-
	SH_3	6.28 2.09	6.59 2.90	3.95	3.28	8	-	8	9	5	-	3	5
	SH_4	0	2.00	1.98	3.12	24	24	22	18	24	33	33	24
0	SP_1	2.09	2.09	2.37	3.21	10	10	0	9	-7	-1	-1	-1
	SP_2	6.28	6.28	5.93	-11.16	9	7	8	-	0	0	0	-
	SP_3	6.28 2.09	6.28 2.09	3.12	2.55	9	-	8	9	6	-	5	6

TABLE 4.4

$$C/A = 2.34 \times 10^{-6}\ m^{-1}$$

$$A = 273d^2$$

		Units of 10^{-6} m^{-1}				Units of 10^{-4} mb s^{-1}							
							rmse(0)* using				dav(0)* using		
λ	Case	k h	μ	μ_r	μ_a	rmse(0)	μ	μ_r	μ_a	dav(0)	μ	μ_r	μ_a
2×10^{-6} m^{-1}	LH_1	2.09	2.90	3.05	1.72	9	9	9	10	1	0	0	1
	LH_2	6.28	6.59	6.39	-0.07	8	6	6	-	-1	0	0	-
	LH_3	6.28 2.09	6.59 2.90	3.44	-0.05	8	-	7	-	-1	-	0	-
	LH_4	0	2.00	1.94	2.70	20	19	19	16	19	23	23	17
0	LP_1	2.09	2.09	2.35	0.89	9	9	8	9	1	1	1	1
	LP_2	6.28	6.28	5.89	-0.06	9	7	7	-	-1	0	0	-
	LP_3	6.28 2.09	6.28 2.09	2.40	-0.05	9	-	9	-	-1	-	0	-

TABLE 4.5

$C/A = 1.58 \times 10^{-6}$ m^{-1}

$A = 609\ d^2$

10d ($h = 6.28 \times 10^{-6}\ m^{-1}$), 30d ($h = 2.09 \times 10^{-6}\ m^{-1}$) and infinity ($h = 0$).

Once dav(a) and rmse(a) were known, their decay rates (γ_a and γ_r) were computed. The values of μ_a and μ_r were then calculated from

$$\mu_a = \gamma_a + \frac{C}{A} \qquad \mu_r = \gamma_r + \frac{C}{2A}$$

These were then used to give $dav(0)^*$ and $rmse(0)^*$. For the cases where $k = h$, $\mu = \sqrt{\lambda^2 + k^2}$ was also used to compute these quantities. The results for the small and large areas are shown in Tables 4.4 and 4.5 respectively.

Table 4.4 shows that when $k = h$, μ_r is similar to $\mu = \sqrt{\lambda^2 + k^2}$. It also shows that the use of both μ and μ_r in Equ. (4.28) gives good estimates of rmse(0). They can also be used effectively to give estimates of dav(0).

The value of μ_a for case SH_2 is missing because dav(a) changed sign between $a = 0$ and $a = d$. The results for case SH_2 (with those for LH_2) are shown in Fig. 4.7. This shows that although rmse(a) decreased exponentially, dav(a) increased and then decreased. This behaviour is due to the fact that the corners, which were ignored in the derivation of Equ. (4.27), sometimes have a large effect on dav(a). Therefore the use of μ_a to give $dav(0)^*$ and $rmse(0)^*$ sometimes produces inaccurate estimates of dav(0) and rmse(0) (e.g. see cases SH_2 and SP_2). However it is worth noting that in all cases $dav(0)^*$ has the same sign as dav(0). Thus Equ. (4.27) always predicted correctly if there would be an over-

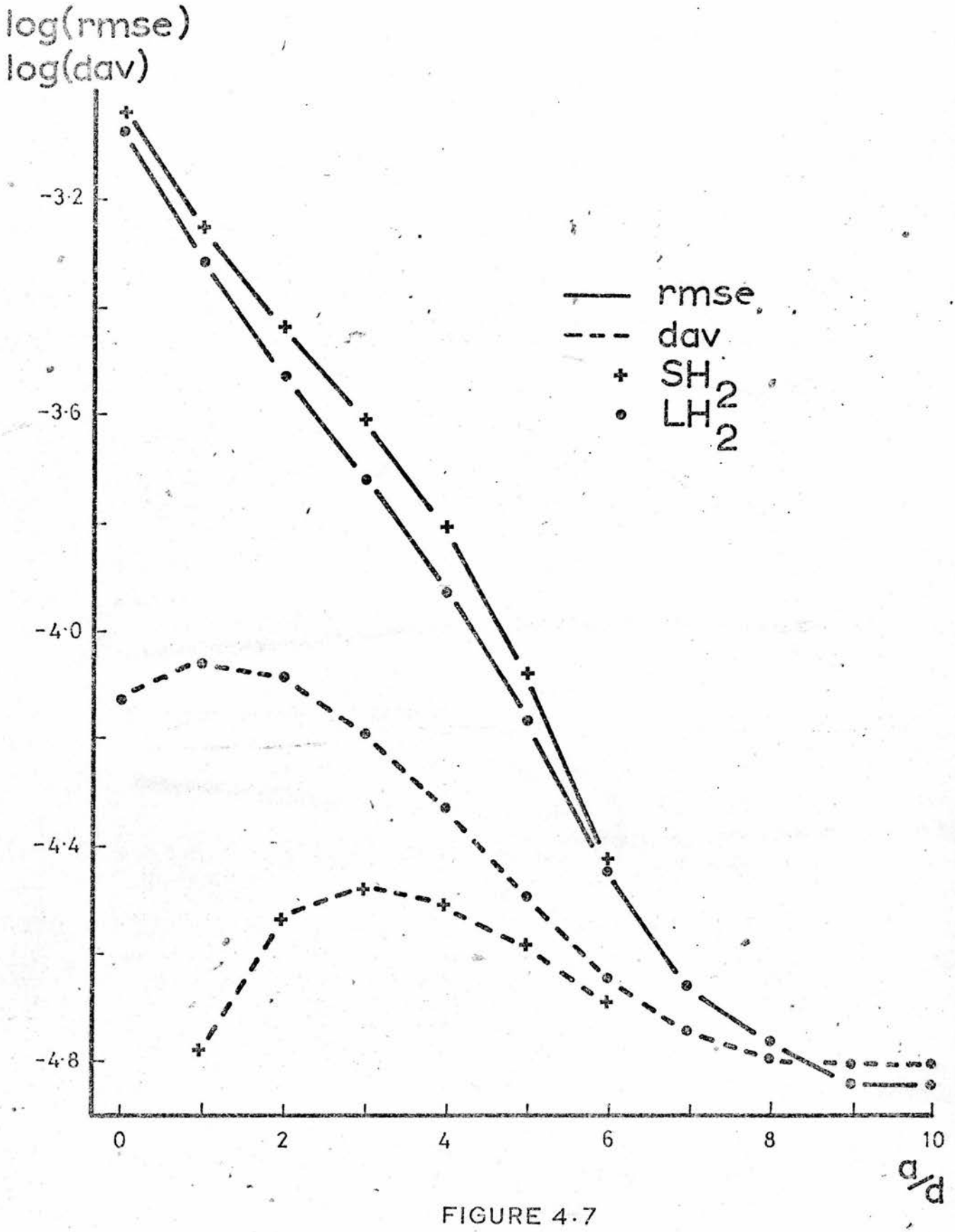

FIGURE 4.7

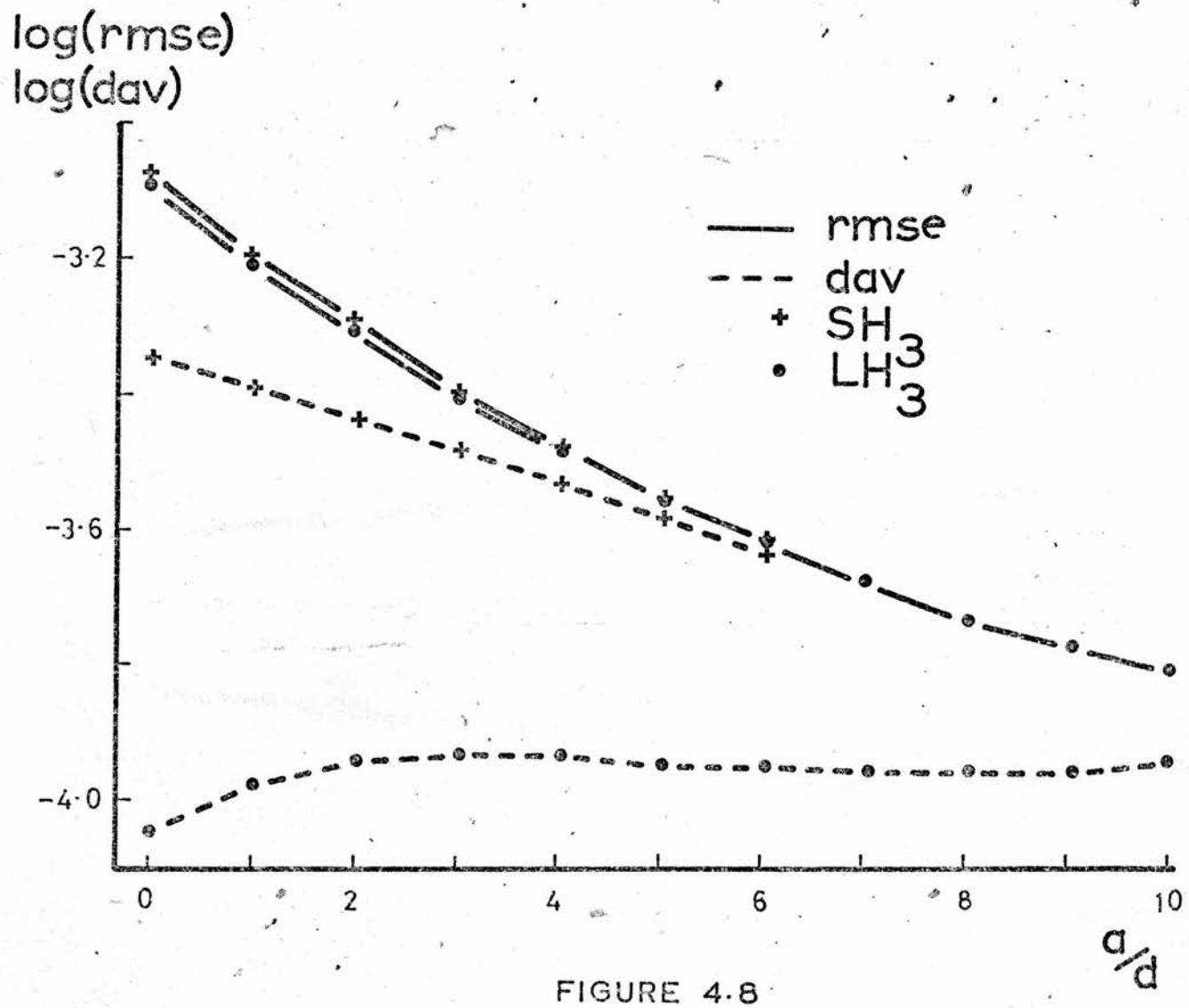

FIGURE 4.8

estimation, or underestimation, of the vertical velocity.

The cases denoted by subscript 3 have $k \neq h$. Fig. 4.8 shows the results for case SH_3 (with case LH_3). These results, with those in Table 4.4 indicate that the behaviour of rmse(a) can be described by Equ. (4.28) even when μ is not the same on all boundaries. Unfortunately there does not appear to be an easy way of estimating the appropriate value of μ.

The cases marked with subscript 4 used a constant value of boundary error. For the Helmholtz equation, $dav(a)^*$ and $rmse(a)^*$ produced good estimates of dav(0) and rmse(0). However for the Poisson equation both λ and μ are zero and thus Equs. (4.27) and (4.28) cannot be used.

The results for the large area are summarised in Table 4.5. An examination of this reveals that the above comments and conclusions also apply to the results for the large area.

The above results show that if the error on the boundary is known, and if μ can be estimated, then the behaviour of rmse(a) can be easily described. This also applies to a lesser extent to dav(a). For example, if a Helmholtz equation is solved with $\frac{\partial \omega}{\partial n} = 0$ on the boundary then it is easy to estimate the effect of using $\omega = 0$ on the boundary.

4.6 The Boundary Conditions For The Two-Dimensional ω-Equation

To evaluate the usefulness of a particular type of boundary condition, it would be necessary to solve the ω-equation with the boundary condition and to compare it

with the actual distribution of ω. Unfortunately the latter is not known. However, in the previous section it has been shown that the boundary error tends to decrease exponentially away from the boundary. Thus, if the ω-equation is solved in a large area (denoted by L), the values of ω near the centre should be almost independent of the boundary condition. If this is so, then the solution in a central area (denoted by S) is a good approximation to the actual vertical velocity. Thus the suitability of a boundary condition can be tested by using it to solve the ω-equation in area S. This solution may then be compared with the solution in area L.

Before the above procedure can be carried out, it is necessary to choose the boundary condition to be used in area L. In the past two types have been used. These are

(i) $(\omega)_b = 0$ (ii) $\left(\frac{\partial \omega}{\partial n}\right)_b = 0$

Since the distributions of ω, derived by using these, have given meaningful results in the past, it is reasonable to use one of them in area L. Since it is not known which one is best, computations were carried out for both.

The two-dimensional ω-equation used was

$$\nabla^2\omega - \lambda^2\omega + S' = 0 \qquad \lambda^2 = \frac{f^2 l^2}{\sigma} \qquad (4.29)$$

S' was calculated from Φ for the 600 mb level. The areas L and S corresponded to regions 11 and 51 with two gridpoints missing normal to their boundaries. In terms of the gridlength d, these regions had dimensions of 27d by 19d and 19d by 11d. The parameters used were

$f^2 = 1.226 \times 10^{-8}\ s^{-2}$ $\sigma = 1.97 \times 10^{-2}\ m^2\ mb^{-2}\ s^{-2}$ $\lambda = 3.1 \times 10^{-6}\ m^{-1}$

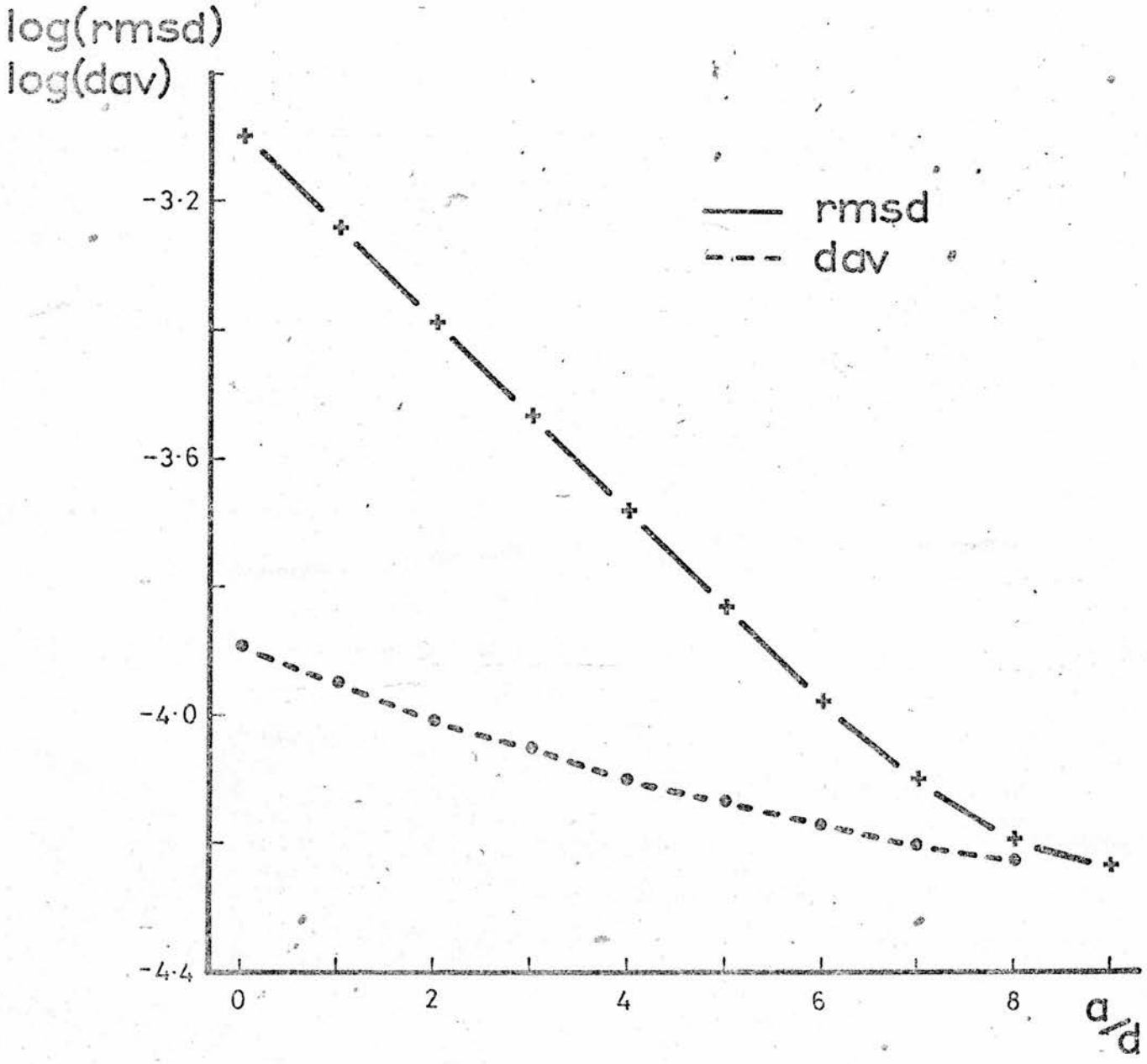

FIGURE 4·9

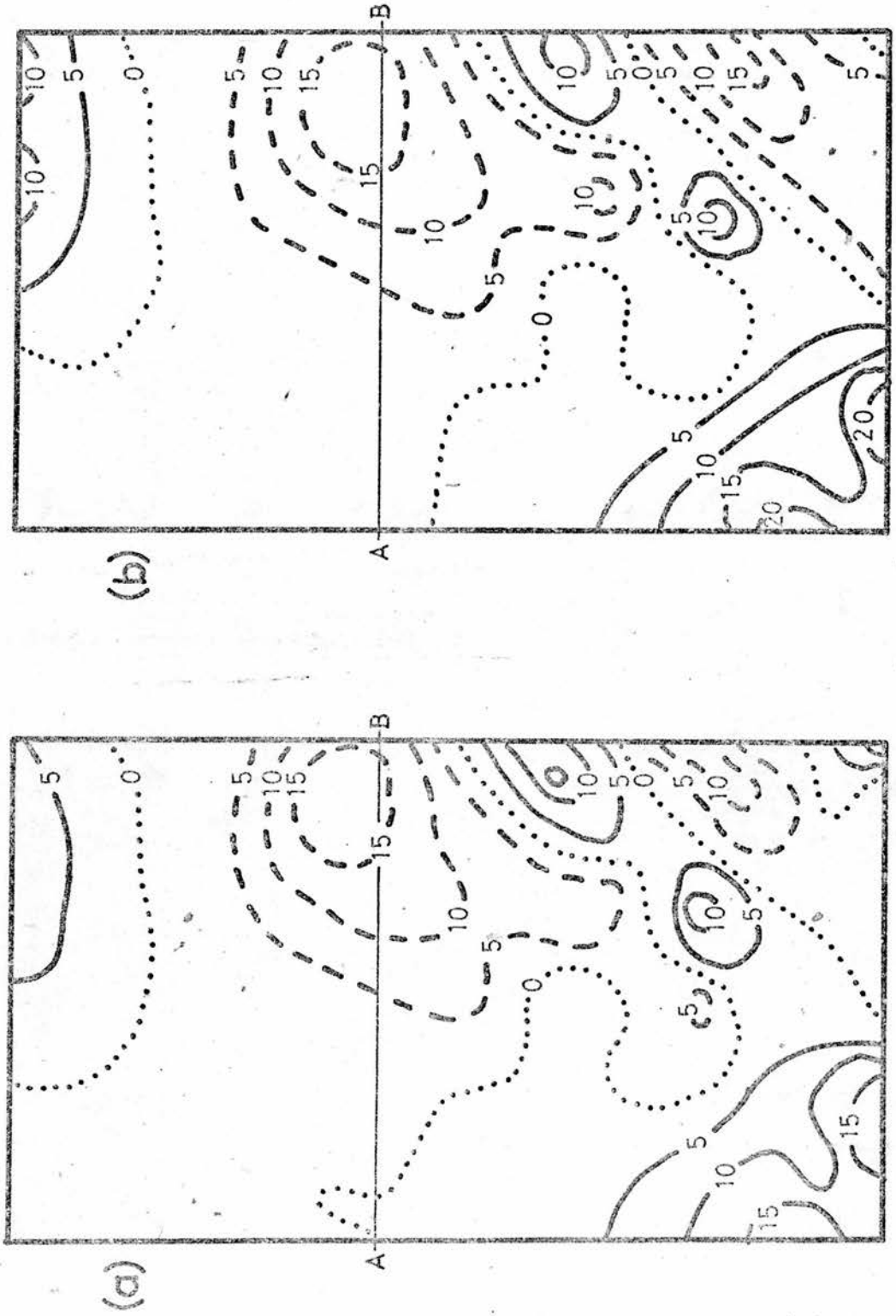

FIGURE 4.10

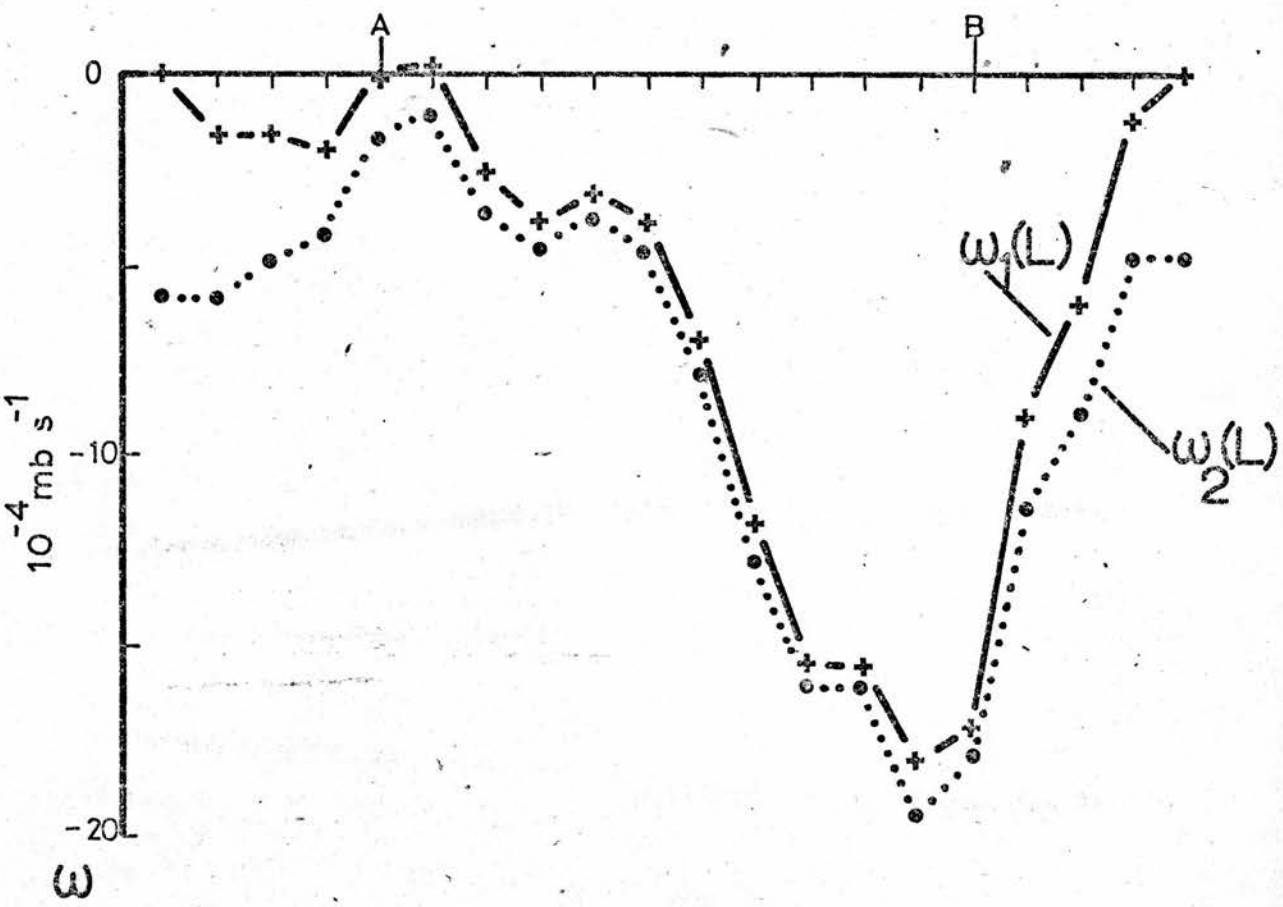

FIGURE 4.11

The solutions of the two-dimensional ω-equation in area L with boundary conditions (i) and (ii) will be called ω_1 (L) and ω_2 (L).

The root mean square difference (rmsd) and the difference in averages (dav) were computed for ω_1 (L) and ω_2 (L) as a function of a. The results are shown in Fig. 4.9. Since area S is the same as area L with a = 4d, this figure shows that in area S, rmsd = 2×10^{-4} mb s^{-1} and dav = $.8 \times 10^{-4}$ mb s^{-1}. These are far from negligible. Figs. 4.10a and 4.10b show ω_1 (L) and ω_2 (L) in area S. An examination of these figures shows that this area, the distributions of ω_1 (L) and ω_2 (L) are similar. This implies that the "correct" distribution of ω in area S is similar to that exhibited in either Figs. 4.10a or 4.10b. Thus the quality of a boundary condition can be tested by using it to solve Equ. (4.29) in area S and comparing the solution with either the distribution of ω_1 (L) or ω_2 (L).

The results in Figs. 4.10a and 4.10b can also be used to test Equs. (4.27) and (4.28). The values of μ_a and μ_r were calculated from the figures and they were then used to compute dav $(0)^*$ and rmsd $(0)^*$. It was found that these estimates of dav (0) and rmsd (0) were within about 15% of the correct values.

From the definition of dav (a), dav (0) = $\bar{\omega}_2(L) - \bar{\omega}_1(L)$. Further, Fig. 4.9 shows that dav (a) > 0 for all a. Thus the magnitude of ω_2 (L) is greater than that of ω_1 (L) over most of the area. This fact is illustrated by the profiles of ω_1 (L) and ω_2 (L) across AB (see

Figs. 4.10a and 4.10b) which are illustrated in Fig. 4.11. This behaviour was anticipated in section 4.5.3.

In the next two sections the characteristics of both Dirichlet and Neumann boundary conditions are considered. This work is based on the assumption that the "correct" distribution of ω in area S is similar to that of $\omega_1(L)$ or $\omega_2(L)$.

4.6.1 Dirichlet Boundary Conditions

A boundary condition of this type has the form

$$(\omega)_b = f(x, y)$$

The solution of Equ. (4.29) with this boundary condition can be split into two parts, $\tilde{\omega}$ and ω^*, which are given by

$$\nabla^2 \tilde{\omega} - \lambda^2 \tilde{\omega} + S' = 0 \qquad (\tilde{\omega})_b = 0$$

$$\nabla^2 \omega^* - \lambda^2 \omega^* = 0 \qquad (\omega^*)_b = f(x,y)$$

The solutions $\tilde{\omega}$ and ω^* can be thought of as the vertical velocity due to S' and that due to the boundary condition $(\omega^*)_b = f(x, y)$. In section 4.54 it was shown that ω^* decreases away from the boundary, and that the rate of decrease depends upon both λ and the variation of $f(x, y)$ along the boundary. This implies that $\tilde{\omega}$ is more important than ω^* near the centre of the region considered.

If Equ. (4.29) is solved with two different boundary conditions ($f_1(x, y)$ and $f_2(x, y)$) then the difference between the solutions (ε) is given by

$$\nabla^2 \varepsilon - \lambda^2 \varepsilon = 0 \qquad (\varepsilon)_b = f_1(x,y) - f_2(x,y)$$

Therefore the difference between the solutions decreases away from the boundary at a rate which depends upon λ and the variation of $(\varepsilon)_b$.

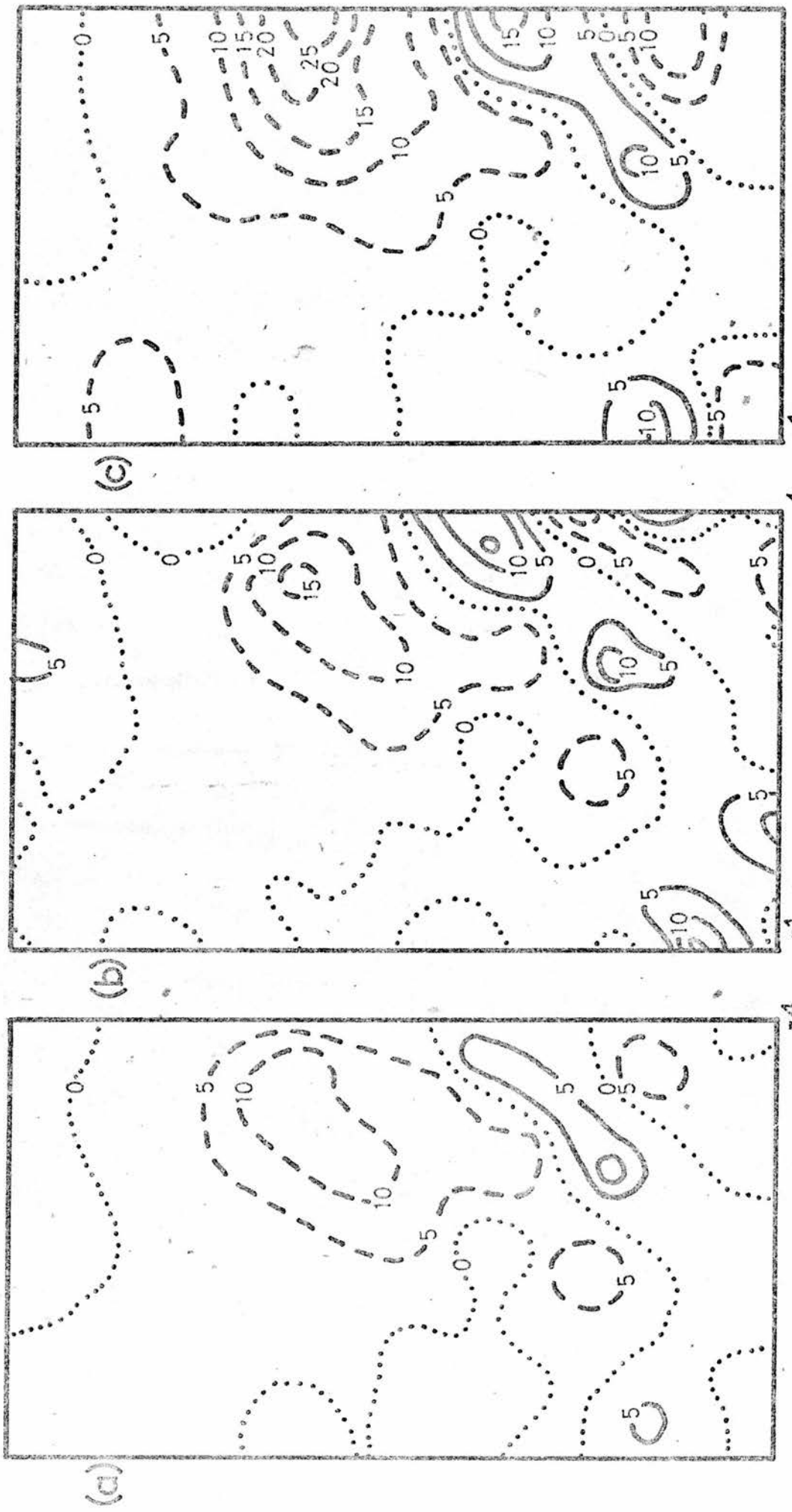

FIGURE 4.12

So far, only one Dirichlet boundary condition has been used, namely $(\omega)_b = 0$. However, others can be imposed. For instance, if it is assumed that ω varies sinusoidally with x and y along the boundary, Equ. (4.29) gives

$$(\omega)_b = \gamma^2 (S')_b \qquad \gamma^2 = \frac{1}{(\lambda^2 + h^2 + k^2)}$$

When this was used in area S, the solution was called ω_3 (S). The corresponding solution using $(\omega)_b = 0$ was ω_1 (S). These two solutions are illustrated in Figs. 4.12a and 4.12b. A comparison of these with Figs. 4.10a and 4.10b reveals that ω_1 (S) and ω_3 (S) are similar to both ω_1(L) and ω_2(L). However there are some important differences which will be discussed later. The value of rmsd between ω_1 (S) and ω_3 (S) was computed for various values of a. It was found that rmsd decreased very rapidly. The reason is that S' varies very rapidly along the boundary and therefore the decay of ε away from the boundary depends only upon the value of λ.

A comparison of ω_1(S) and ω_1 (L) (see Figs. 4.12a and 4.10a) shows that the use of $(\omega)_b = 0$ produces isolated maxima and minima near the boundaries. Also, in these regions the magnitude of ω tends to be underestimated. Another consequence of using this boundary condition is that there tends to be a relationship between the sign of the gradient of ω normal to the boundary and ω itself, in the vicinity of the boundary. This relationship is

$$\frac{1}{\omega} \quad \frac{\partial \omega}{\partial n} > 0$$

Now compare ω_3 (S) and ω_1 (L) (see Figs. 4.12b and 4.10a). Since ω is usually large when S' is large, the use of $(\omega)_b = \gamma^2 (S')_b$ ensures that areas of large ω on the boundary are located correctly. However, another effect of using this boundary condition is that it produces spurious results on parts of the boundary. These two effects are illustrated by the results on and near the eastern boundary. The overall effect of using this boundary condition is to make both ω, and its gradients, very irregular in the vicinity of the boundaries.

In the next section the effect of using a Neumann boundary condition is considered.

4.6.2 Neumann Boundary Conditions

Neumann boundary conditions have the form

$$\left(\frac{\partial \omega}{\partial n}\right)_b = f(x, y)$$

When this is used with Equ. (4.29) it is not possible to split ω into $\tilde{\omega}$ and ω^* (as was done for Dirichlet boundary conditions) because ω^* is a function of both f (x, y) and $\tilde{\omega}$.

Unfortunately the value of f (x, y) cannot be derived and thus f (x, y) $\equiv$ 0 is usually used. The solution of Equ. (4.29) with $\left(\frac{\partial \omega}{\partial n}\right)_b = 0$ in area S is denoted by ω_2(S) and is illustrated in Fig. 11c. A comparison of this with ω_1(S) and ω_3(S) (Figs. 4.12a and 4.12b) indicates that all three solutions are similar. However, ω_2 (S) has certain characteristics which differ from those of solutions that employ Dirichlet boundary conditions.

The gradient of ω_2(S) normal to the boundary is zero and so the contours of ω_2(S) must meet the boundaries at

right-angles. Thus the maxima and minima of $\omega_2(S)$ near the boundary are extended towards the boundary. This is especially noticeable on the eastern boundary.

A comparison of $\omega_2(S)$ with $\omega_1(L)$ also illustrates the elongation of the maxima and minima near the boundary (see Figs. 4.12c and 4.10a). Further examination of these figures reveals that, near the boundaries, $\omega_2(S)$ sometimes overestimates and sometimes underestimates the vertical velocity. In general it is found that if $\frac{\partial \omega}{\partial n_1}^{(L)} > 0$ near the boundary of ara S, then $\omega_2(S)$ tends to be greater than $\omega_1(L)$. The behaviour was anticipated in section 4.5.3.

It is worth noting that neither $\omega_1(S)$, $\omega_2(S)$ or $\omega_3(S)$ produced the correct distribution of ω in the vicinity of the south-west corner. However elsewhere these solutions were reasonable.

4.6.3 A Discussion Of The Results Of Using Different Boundary Condition With The Two-dimensional ω-Equation

From the results in the previous three sections, the characteristics of the different boundary conditions can be deduced. Let ω be the "correct" solution of Equ. (4.29) and let ω_1 be the solution when $(\omega)_b = 0$ is used. It is found that, near the boundaries, there tends to be

(a) maxima and minima of ω_1

(b) $|\omega_1| < |\omega|$

(c) gradients of ω_1 such that $\frac{1}{\omega_1} \frac{\partial \omega}{\partial n_1} > 0$

The corresponding results when $\left(\frac{\partial \omega}{\partial n}\right)_b = 0$ is used (with solution ω_2) are

(a) a displacement of the maxima and minima of ω onto the boundary

(b) a change in magnitude of the vertical velocity so that $\frac{\partial \omega}{\partial n} \frac{1}{\omega_2 - \omega_1} > 0$.

(c) a zero gradient of ω_2 normal to the boundary.

If ω_3 is the solution when $(\omega)_b = \gamma^2 (S')_b$ is used, then it is found that, near the boundary,

(a) ω_3 is often very similar to ω when ω is large.

(b) ω_3 often has a different sign from that of ω when ω is small.

(c) both ω_3 and its gradients are very irregular along the boundary.

It is not easy to choose the best boundary condition. Both ω_1 and ω_2 are systematic distortions of the "correct" solution. Further, the distortions are such that the differences $(\omega - \omega_1)$ and $(\omega - \omega_2)$ tend to be less than the difference between ω_1 and ω_2. The distortions caused by using $(\omega)_b = \gamma^2 (S')_b$ are not systematic. Thus ω_3 approaches ω very rapidly away from the boundary. This means that this boundary condition is useful provided the solution at the first few grid-points can be ignored. If this is not possible then one of the other two boundary conditions must be used. Due to the amount of computer time required to solve a Neumann problem it would be preferable to use $(\omega)_b = 0$.*

In the next section a three-dimensional ω-equation is considered.

4.6.4 The Boundary Conditions For The Three-Dimensional ω-Equation

Equ. (4.7) was used in an investigation of the effect of both Dirichlet and Neumann boundary conditions on the solution of a three-dimensional ω-equation. The

* In retrospect, it is clear that it can never be possible to draw general conclusions regarding the relative accuracy of ω_1 and ω_2 since this must depend on the particular form of the forcing function.

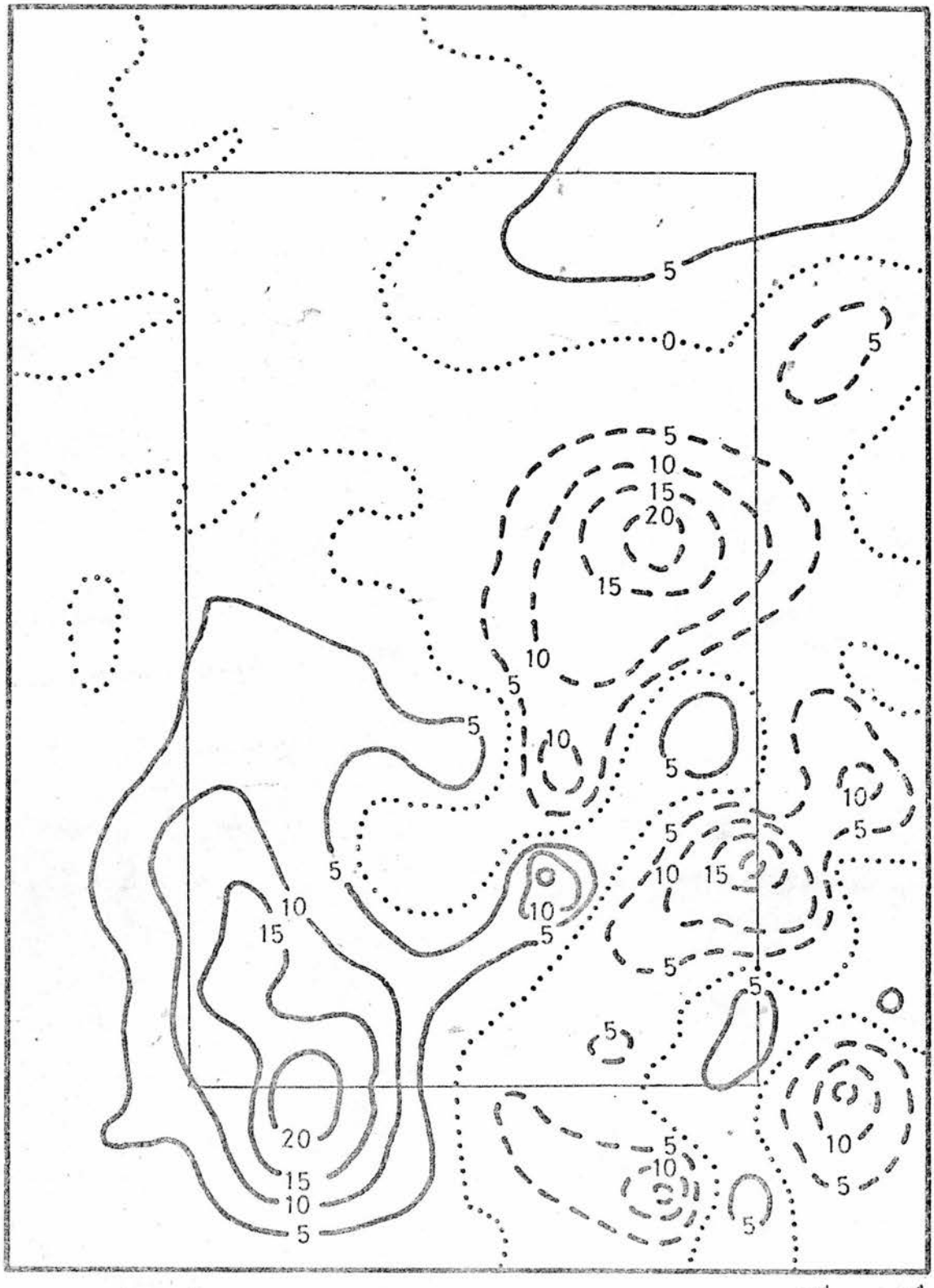

FIGURE 4.13

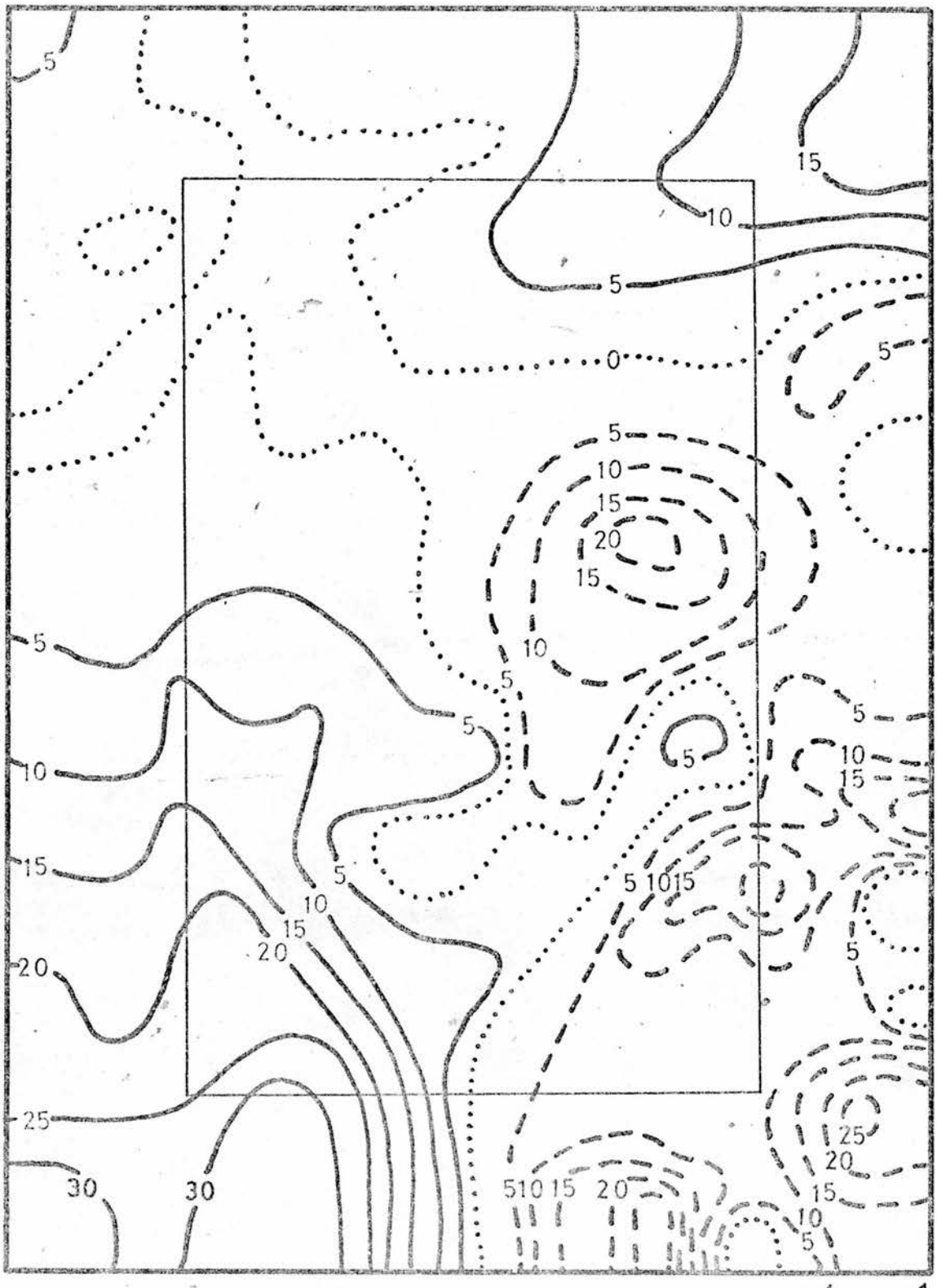

FIGURE 4.14

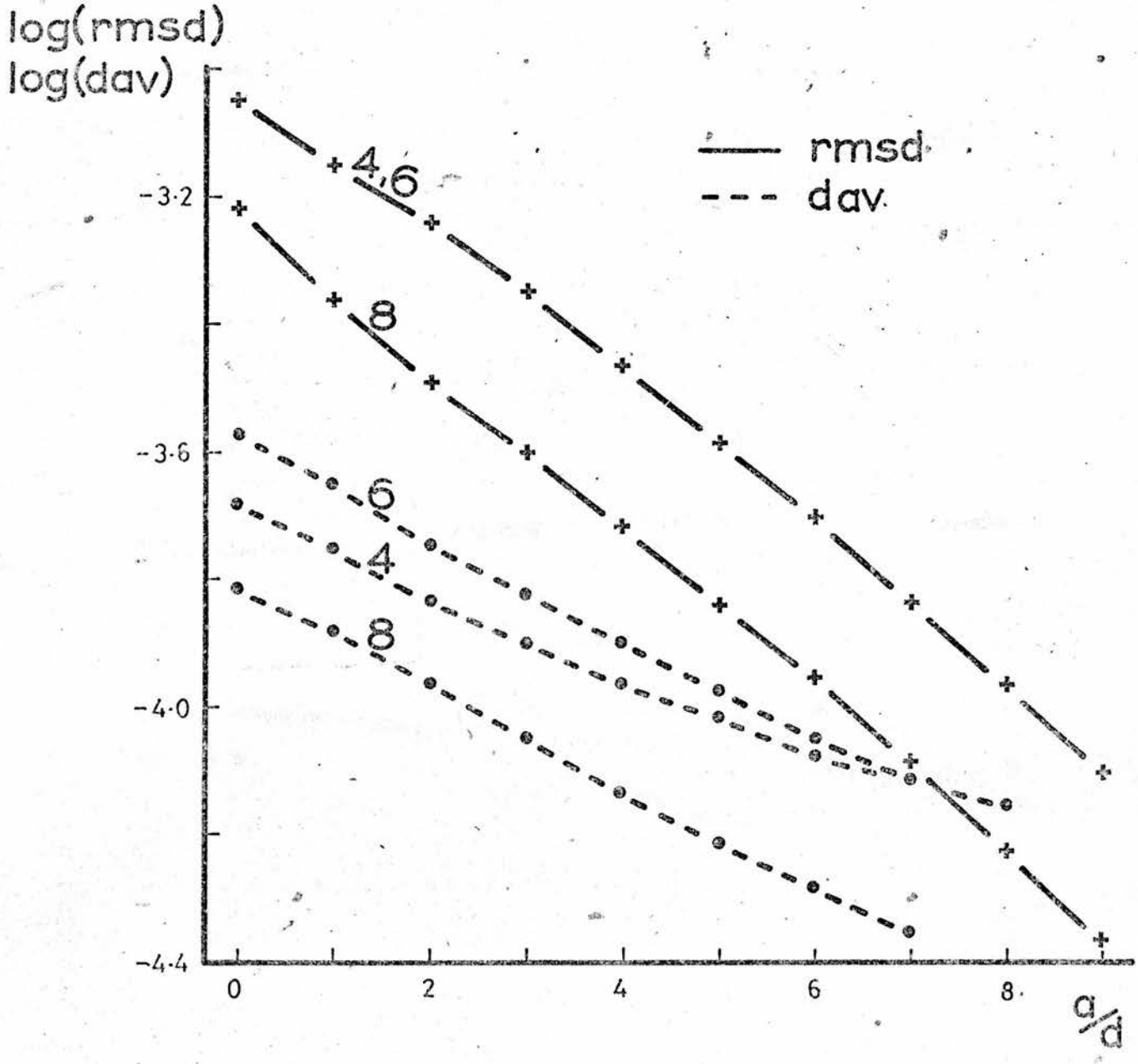

FIGURE 4.15

horizontal boundary conditions were $\omega = 0$ on the 200 mb and 1000 mb surfaces and the lateral boundary conditions were

(i) $(\omega)_b = 0$; giving a solution ω_1 (L).

(ii) $\left(\frac{\partial \omega}{\partial n}\right)_b = 0$; giving a solution ω_2 (L)

The computations were carried out in a region with horizontal dimensions 21d by 29d (using data from area 11). The region contained five isobaric surfaces with $\Delta p = 200$ mb.

The distributions of ω_1(L) and ω_2 (L) at the 600 mb level are illustrated in Figs. 4.13 and 4.14. An examination of these figures reveals that the characteristics of ω_1 (L) and ω_2 (L) near the boundary are the same as those found for the two-dimensional equation.

Now consider the central region corresponding to $a = 4d$. In this region ω_1 (L) and ω_2 (L) have similar distributions, but differences are still discernible. An estimation of this difference can be made by referring to Fig. 4.15. This shows the root mean square difference (rmsd) and the difference in averages (dav) between ω_1 (L) and ω_2 (L) at the three interior levels. As in previous cases, both rmsd and dav vary exponentially with a. At the 600 mb level, with $a = 4d$, rmsd $= 3.5 \times 10^{-4}$ mb s^{-1} and dav $= 1.3 \times 10^{-4}$ mb s^{-1}. Even with $a = 8d$, rmsd $= 1.1 \times 10^{-4}$ mb s^{-1} and dav $= .9 \times 10^{-4}$ mb s^{-1}. These results imply that, even near the centre of the region considered, the error due to the boundary condition is at least of the order of 10^{-4} mb s^{-1}. This is also true for the other two levels. Therefore, for this particular case, it is not worth computing ω to an accuracy

greater than 10^{-4} mb s^{-1}.

As in sections 4.61 and 4.62, boundary conditions (i) and (ii) were used to compute the vertical velocity in central region (corresponding to a = 4d). The solutions will be referred to as $\omega_1(S)$ and $\omega_2(S)$. A comparison of these with the "correct" solution (either $\omega_1(L)$ or $\omega_2(L)$) was made. It was found that the characteristics of the solutions using (i) and (ii) were the same as those for the two-dimensional case (see section 4.63).

As a by-product of these investigations, it is worth noting the similarity between Fig. 4.10a and the central portion of Fig. 4.13; and also between Fig. 4.10b and Fig. 4.14. Therefore, if only the general features of the vertical velocity field are required, it is sufficient to use the two dimensional ω-equation (Equ. (4.29)).

4.7 Previous Investigations Into The Relationship Between The Static Stability And The Vertical Velocity

The most comprehensive investigation into the effect of the static stability on the vertical velocity, was carried out by Haltiner et al.(1963). They defined the static stability (σ^*) as

$$\sigma^* = \frac{RT}{pc_p} - \frac{\partial T}{\partial p}$$

This is related to the static stability used in this thesis by $\sigma = \frac{R}{p_*}\sigma^*$. But, despite the difference between σ and σ^*, the general conclusions of Haltiner et al. are applicable to the use of σ. They used three different static stability parameters.

1. constant static stability, $\bar{\bar{\sigma}}^*$.
2. pressure variable static stability, $\bar{\sigma}^*$.

3. point variable static stability, σ^*.

The geostrophic ω-equation (without the terms depending upon the gradients of the stability) was solved with the above stabilities and the solutions will be referred to as $\bar{\bar{\omega}}$, $\bar{\omega}$ and ω.

They concluded that

(a) the greatest differences between $\bar{\bar{\omega}}$, $\bar{\omega}$ and ω occurred when the vertical velocity was greatest.

(b) $|\bar{\bar{\omega}}| < |\bar{\omega}|$ at maximum values of vertical velocity on the 700 mb and 500 mb surfaces. But, on the 300 mb surface at maximum values the opposite was found and the difference between $\bar{\bar{\omega}}$ and $\bar{\omega}$ was as high as 50%, compared with about 10% at the lower levels.

(c) the difference between $\bar{\omega}$ and ω was small.

From their results it can also be shown that at the maxima for a given isobaric surface, the ratio of $\bar{\omega}$ to $\bar{\bar{\omega}}$ was almost a constant.

These conclusions are limited because it is not obvious if they apply to all situations or just this particular one. Also no indication was given of the effect of the choice of the constant static stability on the results. Thus the conclusions cannot be used to estimate the difference between $\bar{\omega}$ and $\bar{\bar{\omega}}$ for given $\bar{\sigma}^*$ and $\bar{\bar{\sigma}}^*$. Also no method was suggested for estimating the difference between $\bar{\omega}$ and ω. Some of these outstanding problems will be considered later.

Danard (1964) solved the ω-equation using a point variable static stability, $\sigma(x, y, p)$, and a static stability derived from the average values of σ over each isobaric surface, $\sigma_o(p)$. He found that "one effect of

letting σ vary is to shift the maxima of upward and downward motions towards regions of lower stability and to increase their magnitudes. This amplification is due to the circumstance that $\sigma/\sigma_o < 1$ in these regions".

Harwood (1969) considered the effect of replacing $\sigma(p)$ by a constant value given by $\sigma(850)$. It was found that at 300 mb this prodiced a 100% change in ω. Harwood argued that because $\sigma(300) \approx 7 \times \sigma(850)$, the effect of replacing $\sigma(p)$ by $\sigma(850)$ should be a 600% change in ω at 300 mb. This argument is based on the assumption that if ω_1 and ω_2 are the solutions using $\sigma(p)$ and $\sigma(850)$, then

$$\sigma(p)\ \omega_1 \approx \sigma(850)\ \omega_2 \qquad (4.30)$$

Harwood was unable to resolve the discrepancy between the 100% change found experimentally and the 600% change deduced from the above equation. It will be shown later that the discrepancy was due to the inaccuracy of Equ. (4.30). It will also be explained why the change at the 300 mb level found by Haltiner et al. was different from that found by Harwood.

4.7.1 The Vertical And Horizontal Variations Of σ

In terms of Φ, σ is given by

$$\sigma = \frac{\partial^2 \Phi}{\partial p^2} + \frac{(1-\varkappa)}{p}\frac{\partial \Phi}{\partial p} \qquad \varkappa = \frac{R}{C_p}$$

For an atmosphere with a constant lapse rate Γ and a surface temperature and pressure of T_o and p_o, Equ. (4.31) gives

$$\sigma = \frac{R^2 T_o p_o^{\gamma}}{C_p}\, p^{\gamma-2} \qquad \gamma = \frac{R\Gamma}{g}$$

For a standard atmosphere $\gamma \approx 0.2$ and thus to a good approximation

$$\sigma(p) = \frac{S_o}{p^2} \qquad (4.32)$$

This is a simple and accurate analytical expression for the usual variation of static stability with pressure. Since $\sigma(p) \propto 1/p^2$, the static stability varies rapidly with pressure and therefore it is far from being a constant.

If T_o and p_o vary horizontally, then to a good approximation

$$\frac{\partial \sigma}{\partial x} \approx \frac{R\, p_o^{2}\, p^{\gamma-2}}{C_p} \frac{\partial T_o}{\partial x}$$

Thus the horizontal variations of σ will tend to be large when the horizontal gradients of T_o are large.

Suppose that the static stability is given by

$$\sigma(x, y, p) = \frac{S(x, y)}{p^2} \qquad (4.33)$$

It can then be shown that Equ. (4.31) gives

$$\Phi = \frac{S(x, y)}{\varkappa} \ln(p_o/p) \qquad p_o = p_o(x, y) \qquad (4.34)$$

If S (x, y) is eliminated between Equs. (4.33) and (4.34) then it is found that to a good approximation

$$\frac{\partial \sigma}{\partial x} \approx \frac{\varkappa}{p^2} \frac{1}{\ln(p_o/p)} \frac{\partial \Phi}{\partial x}$$

Therefore the horizontal variations of σ will tend to be large when the gradients of Φ are large.

4.7.2 A Simple Model Of The Atmosphere

Following the work of Nita (1967), Φ was separated into its zonal mean and the deviation from this mean. Thus

$$\Phi = \bar{\Phi}(y, p) + \Phi'(x, p)$$

It was also assumed that

$$u_g = U(p) \qquad f(y) = f_o + \beta y$$

$$\omega = \omega(x, p) \qquad \Phi_t = \Phi_t(x, p)$$

It can then be shown that the ω-equation and vorticity equation become

$$\frac{\partial^2(\sigma\omega)}{\partial x^2} + f_o^2 \frac{\partial^2 \omega}{\partial p^2} = f_o \left(\left[\frac{\partial U}{\partial p} \frac{\partial^2 v_g}{\partial x^2} + \beta \frac{\partial v_g}{\partial p} + U \frac{\partial^3 v_g}{\partial x^2 \partial p} \right] - \left[U \frac{\partial^3 v_g}{\partial x^2 \partial p} - \frac{\partial U}{\partial p} \frac{\partial^2 v_g}{\partial x^2} \right] \right) \quad (4.35)$$

$$\frac{\partial^2 \Phi}{\partial x^2 t} = -f_o \left[U \frac{\partial^2 v_g}{\partial x^2} + \beta v_g \right] + f_o^2 \frac{\partial \omega}{\partial p} \quad (4.36)$$

In Equ. (4.35), the two forcing functions enclosed by square brackets represent the differential vorticity advection and the laplacian of the thermal advection. The righthand side of Equ. (4.35) will be denoted by FF, so that

$$FF = f_o \left(2 \frac{\partial U}{\partial p} \frac{\partial^2 v_g}{\partial x^2} + \beta \frac{\partial v_g}{\partial p} \right)$$

The term enclosed by square brackets in Equ. (4.36) is the vorticity advection, and this will be denoted by VA.

It is assumed that the flow consists of a small perturbation in a uniform zonal flow. Therefore Φ is given by

$$\Phi = -f_o U(p) y + A(p) f_o \cos(kx + \gamma) \quad (4.37)$$

If $\gamma = \gamma(p)$ is used then the distribution of Φ would be similar to that used by Wiin-Nielsen (1961) and Sanders (1971). But, due to the general objectives of this analysis, it was decided that the use of a constant would not detract from the conclusions. Similarly, it was decided that it was not necessary to include the tropopause, although it could have been included in a manner similar to that used by Sanders (1971).

Using the above distribution of Φ it can be shown that

$$FF = f_o \left(2 \frac{\partial U}{\partial p} Ak^3 - \beta k \frac{\partial A}{\partial p} \right) \sin(kx+\gamma)$$

$$= \tilde{FF} \sin(kx+\gamma)$$

$$VA = Ak(k^2 U - \beta) \sin(kx+\gamma)$$

$$= \tilde{VA} \sin(kx+\gamma)$$

$$\sigma = -f_o y \left(\frac{\partial^2 U}{\partial p^2} + \frac{(1-\varkappa)}{p} \frac{\partial U}{\partial p} \right) + f_o \cos(kx+\gamma) \left(\frac{\partial^2 A}{\partial p^2} + \frac{(1-\varkappa)}{p} \frac{\partial A}{\partial p} \right)$$

Also, the thermal equation becomes

$$\frac{\partial \Phi}{\partial p}_t + TA + \sigma \omega = 0 \qquad (4.38)$$

$$TA = f_o \left(A \frac{\partial U}{\partial p} - U \frac{\partial A}{\partial p} \right) \sin(kx+\gamma)$$

Suitable distributions of U (p) and A (p) must be chosen. Since Φ varies with $\ln (p_o/p)$, the zonal wind must be given by

$$U(p) = Q \ln (p_o/p)$$

Both Wiin-Nielsen (1961) and Sanders (1971) used distributions of A (p) that increased as p decreased. Therefore the following distributions of A (p) were considered

$$A'(p) = a' \ln (p_o/p) \qquad A''(p) = a''/p$$

The use of these produced the forcing functions $\tilde{FF}'$ and $\tilde{FF}''$. Unfortunately, it was found that when the vertical variation of the static stability was considered, neither of these forcing functions gave simple analytical solutions for both Equs. (4.35) and (4.36). Thus the following distribution of A (p) was used

$$A(p) = ap$$

With this, it was found that

$$\tilde{FF} = f_o ka \left[-2Qk^2 - \beta \right]$$

$$\tilde{VA} = kap \left[Qk^2 \ln (p_o/p) - \beta \right] \qquad (4.39)$$

When the horizontal variations of σ were considered, it was found that it was advantageous to use $A'(p)$. In this case

$$\widetilde{FF}' = f_o\, ka' \left[-2Qk^2 \ln (p_o/p) + \beta \right]$$

$$\widetilde{VA}' = ka' \ln (p_o/p) \left[Qk^2 \ln (p_o/p) - \beta \right] \qquad (4.40)$$

When $A(p)$ and $A'(p)$ are used, the static stabilities become

$$\sigma = \frac{S_o}{p^2} + \frac{f_o (1 - \varkappa)\, a}{p} \cos (kx + \gamma) \qquad (4.41)$$

$$\sigma' = \frac{S_o}{p^2} + \frac{f_o \varkappa\, a'}{p^2} \cos (kx + \gamma) \qquad (4.42)$$

$$S_o = -f_o y \varkappa Q$$

In the following analysis it is assumed that $\omega = 0$ at $p = 0$ and $p = p_o$ (surface pressure). Also it is assumed that ω and Φ_t are zero when the forcing functions are zero.

4.7.3 The Effect Of The Vertical Variation Of σ On ω and Φ_t

The effect of the vertical variation of σ on ω and Φ_t was investigated by solving Equs. (4.35) and (4.36) with both a pressure variable and constant static stabilities. Since analytical solutions of these equations were required it was necessary to use the $\widetilde{FF}$ and $\widetilde{VA}$ given by Equ. (4.39).

The pressure variable static stability is denoted by $\sigma_1(p)$ and is given by the isobaric average of Equ. (4.41) in the region $0 < x < 2\pi/k$. Thus $\sigma_1(p)$ is given by Equ. (4.32) with $S_o = f_o \delta \varkappa Q$. The constant value of the stability was defined by $\sigma_2 = \vartheta S_o$.

If $\omega_1 = \tilde{\omega}_1 \sin (kx + \gamma)$ and $\omega_2 = \tilde{\omega}_2 \sin (kx + \gamma)$

are the solutions of the ω-equation using $\sigma_1(p)$ and σ_2, then

$$p^2 \frac{d^2\tilde{\omega}_1}{dp^2} - \lambda^2 \tilde{\omega}_1 = \frac{\tilde{F}\tilde{F}}{f_o^2} p^2 \qquad \lambda^2 = S_o k^2 / f_o^2 \tag{4.43}$$

$$\frac{d^2\tilde{\omega}_2}{dp^2} - \mu^2 \tilde{\omega}_2 = \frac{\tilde{F}\tilde{F}}{f_o^2} \qquad \mu^2 = \vartheta \lambda^2 \tag{4.44}$$

The solutions of these equations are

$$\tilde{\omega}_1 = -\frac{\tilde{F}\tilde{F}}{\sigma_1(p)} \frac{\lambda}{\xi} \frac{1}{k^2} \left[1 - \left(\frac{p}{p_o} \right)^{q-2} \right] \qquad q = \frac{1+\sqrt{1+4\lambda^2}}{2} \tag{4.45}$$

$$\xi = \frac{\lambda^2 - 2}{\lambda}$$

$$\tilde{\omega}_2 = -\frac{\tilde{F}\tilde{F}}{\sigma_2} \frac{1}{k^2} \left[(1 - e^{-\mu p}) - (1 - e^{-\mu p_o}) \frac{\sinh(\mu p)}{\sinh(\mu p_o)} \right] \tag{4.46}$$

The divergence $D_i = \tilde{D}_i \sin(kx + \gamma)$ is calculated from $\tilde{\omega}_i$ by using

$$\tilde{D}_i = \frac{-d\tilde{\omega}_i}{dp} \qquad i = 1, 2$$

With $\Phi_{ti} = \tilde{\Phi}_{ti} \sin(kx + \gamma)$, Equ. (4.38) gives

$$\tilde{\Phi}_{ti} = \frac{f_o \tilde{V}A + f_o^2 \tilde{D}_i}{k^2} \qquad i = 1, 2 \tag{4.47}$$

Let $R(\omega)$ and $R(\Phi_t)$ be the percentage errors in ω and Φ_t when σ_2 is used instead of $\sigma_1(p)$. Therefore

$$R(\omega) = \left(\frac{\omega_2 - \omega_1}{\omega_1} \right) \times 100$$

There is a similar expression for $R(\Phi_t)$. Using Equs. (4.45) and (4.46) it is found that when p is small, $R(\omega)$ is approximately

$$\left(\frac{1}{p\sqrt{\vartheta}} \xi - 1 \right) \times 100 \qquad \xi = \frac{\lambda^2 - 2}{\lambda}$$

If the equivalent pressure level (p_e) is defined as the pressure where $\sigma_2 = \sigma_1(p_e)$, then $\sqrt{\vartheta} = 1/p_e$ and the approximate expression for $R(\omega)$ is

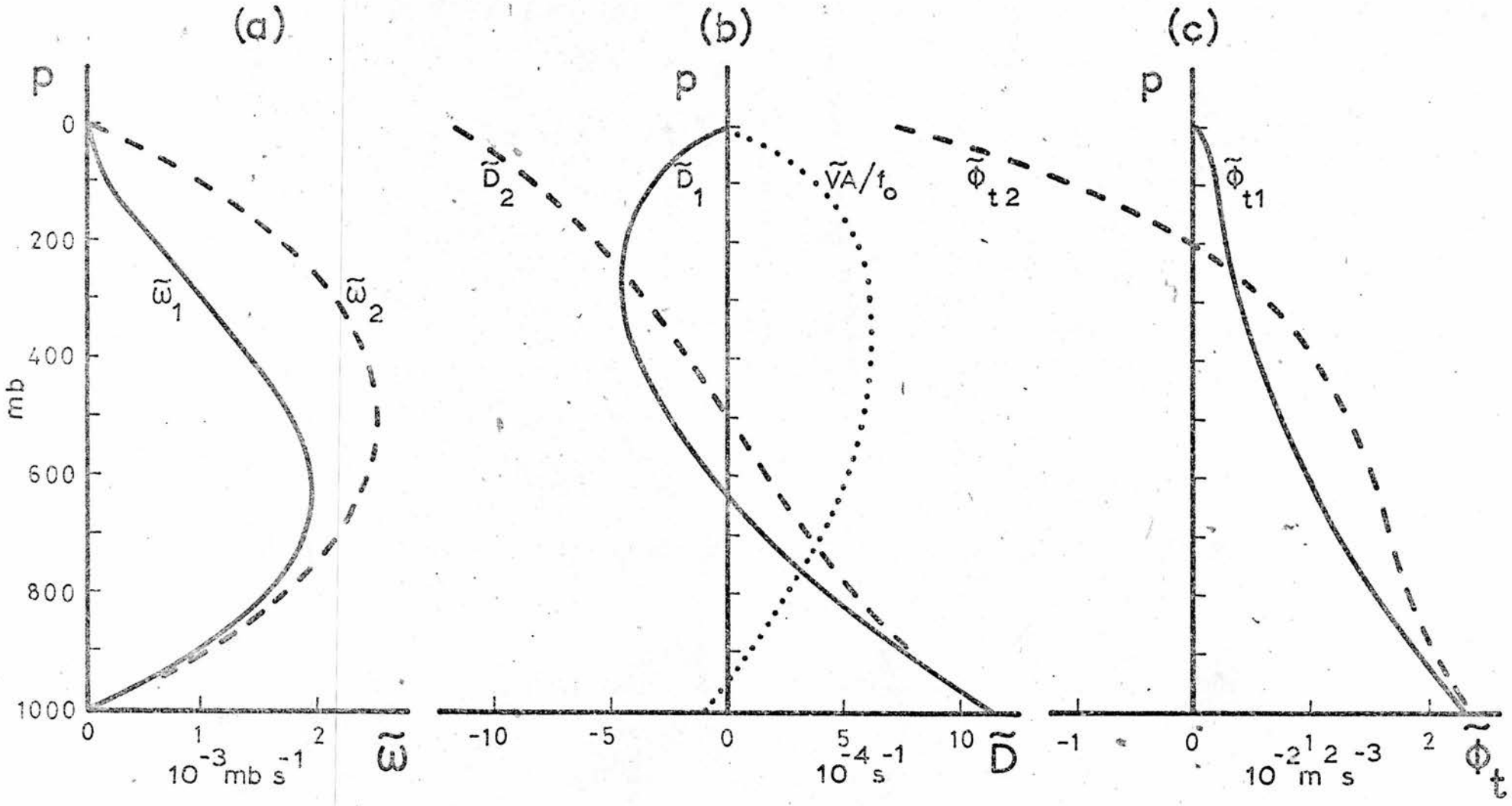
(a)
(b)
(c)
p
mb
0
200
400
600
800
1000
$\tilde{\omega}_1$
$\tilde{\omega}_2$
0
1
2
10^{-3} mb s^{-1}
$\tilde{\omega}$
$\tilde{D}_2$
$\tilde{D}_1$
$\tilde{V}A/f_o$
$\tilde{\Phi}_{t2}$
-10
-5
0
5
10
10^{-4} s^{-1}
$\tilde{D}$
$\tilde{\Phi}_{t1}$
-1
0
1
2
10^{-2} m^2 s^{-3}
$\tilde{\Phi}_t$

FIGURE 4·16

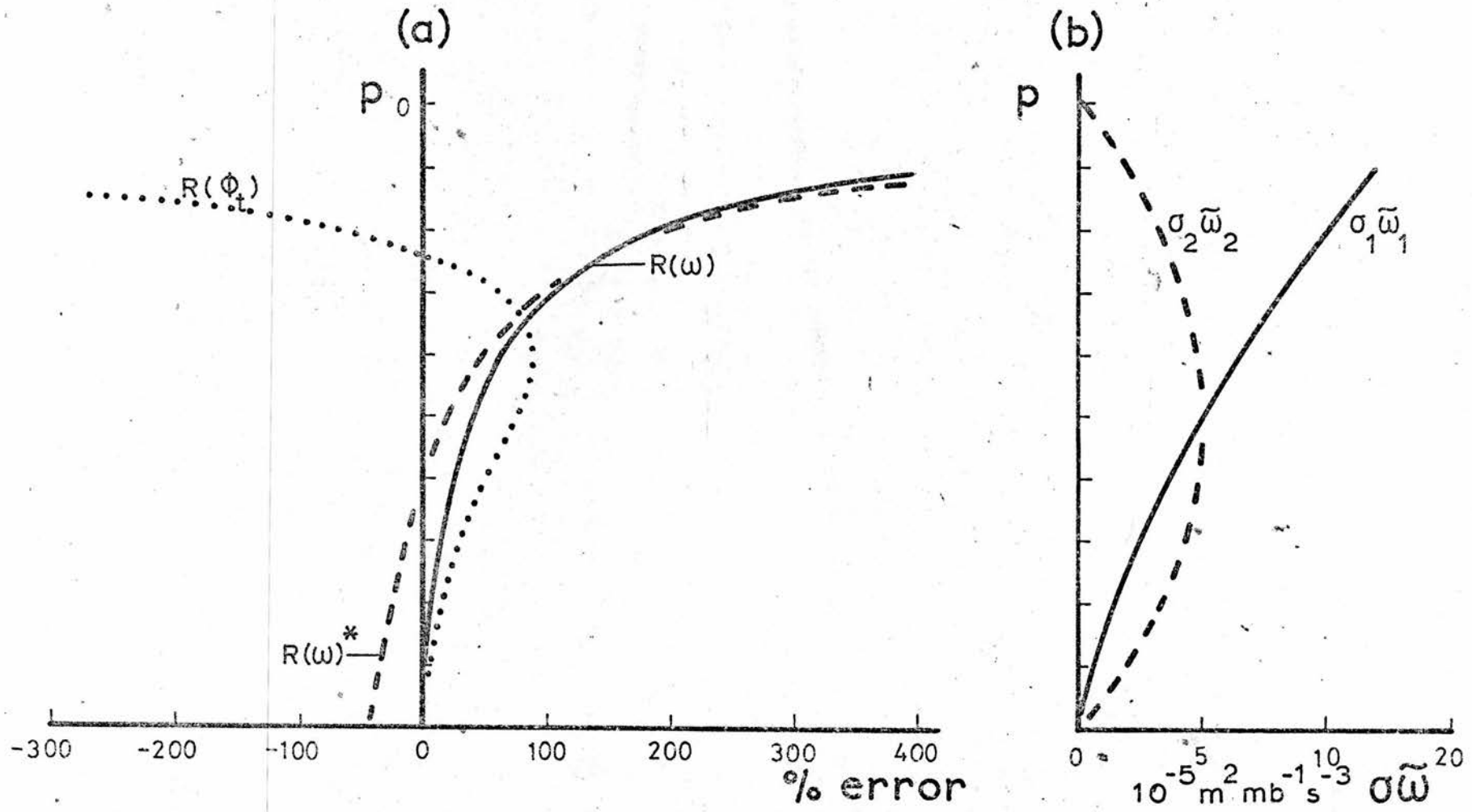
(a)
P 0
R(Φt)
R(ω)
R(ω)*
-300
-200
-100
0
100
200
300
400
% error
(b)
P
σ2ω̃2
σ1ω̃1
0
10^-5 m^2 mb^-1 s^-3 σω̃
20

FIGURE 4·17

$$R(\omega)^{*} = \left[\left(\frac{p_e}{p} \right)^{\xi} - 1 \right] \times 100 \qquad \xi = 1 \qquad (4.48)$$

It is difficult to find simple expressions for R (D) and R (Φ_t) but it can be shown that D_2/D_1 and Φ_{t2}/Φ_{t1} vary with p_e/p when p is small.

In the following discussion the conclusions that refer to $\tilde{\omega}_i$ will also apply to ω_i.

The distributions of $\tilde{\omega}_1$ and $\tilde{\omega}_2$ for p_e = 600 mb ($\vartheta = 2.78 \times 10^{-6}$) are shown in Fig. 4.16a. The other parameters used were

$f_o = 10^{-4}\ s^{-1}$ $L = 3 \times 10^6$ m $k = 2\pi/L$ $S_o = 6.9 \times 10^3\ m^2 s^{-2}$

$a = 5 \times 10^3\ m^2\ mb^{-1}\ s^{-1}$ $Q = 40\ m\ s^{-1}$ $\lambda = 2.7$

Fig. 4.16a shows that $\tilde{\omega}_2$ has an almost parabolic profile that is symmetric about 500 mb. However there would be asymmetry if FF was a function of pressure. A comparison of $\tilde{\omega}_1$ and $\tilde{\omega}_2$ indicates that the main effect of using σ_2 in place of σ_1 (p) is to increase the vertical velocity for small values of p. In the smaller values of p_e this may not be so at large pressures.

Fig. 4.17a shows that R $(\omega)^{*}$ is a good approximation to R (ω). Therefore Equ. (4.48) describes the dependence of R (ω) upon p_e and p. As p_e decreases (σ_2 increases) R $(\omega)^{*}$ decreases. For example, if $\sigma_2 = \sigma_1$ (700) then R (ω) = 230% at 200 mb whereas when $\sigma_2 = \sigma_1$ (500), R (ω) = 146%. Equ. (4.48) also shows that R (ω) changes rapidly when p is small. For example, when $\sigma_2 = \sigma_1$ (600) it is found that R (ω) $\approx$ 50% at 500 mb and that it is about 200% at 200 mb.

It was found that with p_e = 600 mb there was a 24% difference between $\tilde{\omega}_1$ and $\tilde{\omega}_2$ at the p_e level. As p_e

increased the difference increased. Therefore it is not valid to estimate the value of ω at level p^* with $\sigma = \sigma(p)$ by finding the value of ω for a constant stability of value $\sigma(p^*)$.

Fig. 4.17b shows that $\sigma_1 \tilde{\omega}_1$ is not equal to $\sigma_2 \tilde{\omega}_2$ and that the difference between them is large for small values of p. This explains the discrepancy between Harwood's (1969) theoretical and experimental results. Further, in terms of p_e, Harwood computed $R(\omega)$ from

$$R(\omega)_h = \left[\left(\frac{p_e}{p}\right)^2 - 1\right] \times 100 \qquad (4.49)$$

A qualitative examination of Equs. (4.43) and (4.44) indicates that the above results remain essentially unaltered if the upper boundary is at a higher pressure or if $\tilde{FF}$ is a function of pressure.

These considerations show that the values of $R(\omega)$ computed by Haltiner et al. (1963) and Harwood (1969) would only be the same if they both chose the same p_e. There is no indication that this is the case.

In the simple model considered so far both $R(\omega)$ and ω_1 / ω_2 are functions of pressure only. Therefore the largest changes in ω will occur when $|\omega_1|$ or $|\omega_2|$ have their maximum values. Also ω_1 / ω_2 will be a constant on an isobaric surface. These conclusions are essentially the same as those deduced by Haltiner et al. (1963) with reference to an actual case study.

Fig. 4.16b shows the profiles of $\tilde{D}_1$, $\tilde{D}_2$ and $\tilde{VA}$. Since $\tilde{D}_2(0)$ is large whilst $\tilde{D}_1(0) = 0$, the difference between $\tilde{D}_1$ and $\tilde{D}_2$ is large for small values of p. The profiles of $\tilde{\Phi}_{t1}$ and $\tilde{\Phi}_{t2}$ were computed (see Equ. (4.47))

and these are depicted in Fig. 4.16c. For small values of p the difference between $\tilde{\Phi}_{t1}$ and $\tilde{\Phi}_{t2}$ is large and the solutions have opposite signs. These facts are illustrated by the variation of R (Φ_t) shown in Fig. 4.17a. The behaviour of these solutions appears to remain unaltered if the upper boundary is at a different pressure.

4.7.4 The Effect Of The Horizontal Variation Of σ On ω And Φ_t

The effect of the horizontal variation of σ was investigated by splitting the static stability into two parts, namely $\bar{\sigma}(p)$ and $\sigma'(p, x)$. The vertical velocity was then divided into ω (which depends only upon $\bar{\sigma}(p)$) and ε (which depends upon $\bar{\sigma}(p)$ and $\sigma'(p, x)$.

Equ. (4.35) may be written as

$$\frac{\partial^2}{\partial x^2}\left[(\bar{\sigma}+\sigma')(\omega+\varepsilon)\right]+f_o^2\frac{\partial^2}{\partial p^2}\left[\omega+\varepsilon\right]=FF \qquad (4.50)$$

Since the static stability varies much less in the horizontal than in the vertical $\bar{\sigma} \gg \sigma'$ and thus $\omega \gg \varepsilon$. Therefore the above equation can be separated into two separate equations for ω and ε . Define $\Gamma(\omega)$as

$$\Gamma(\omega) = \bar{\sigma}\frac{\partial^2\omega}{\partial x^2}+f_o^2\frac{\partial^2\omega}{\partial p^2}$$

In terms of this the equations are

$$\Gamma(\omega) = FF \qquad (4.51)$$

$$\Gamma(\varepsilon) = FF_1(\sigma', \omega) \qquad (4.52)$$

$$FF_1(\sigma', \omega) = -\frac{\partial^2}{\partial x^2}(\sigma'\omega)$$

Once Equ. (4.51) has been solved for ω , Equ. (4.52) can be solved for ε .

If the terms that contain the derivatives of the

stability are ignored then Equ. (4.50) becomes

$$(\bar{\sigma} + \sigma') \frac{\partial^2}{\partial x^2}[\omega + \eta] + f_o^2 \frac{\partial^2}{\partial p^2}[\omega + \eta] = FF \qquad (4.53)$$

This can then be split into two equations for ω and η and it is found that ω is given by Equ. (4.51) and η by

$$\Gamma(\eta) = FF_2(\sigma', \omega) = -\sigma' \frac{\partial^2 \omega}{\partial x^2} \qquad (4.54)$$

For this investigation a logarithmic variation of A (p) was chosen. Therefore $\widetilde{FF}$ and $\widetilde{VA}$ are given by Equ. (4.40) and σ is given by Equ. (4.42). This means that $\bar{\sigma}$ and σ' are given by

$$\sigma(p) = \frac{f_o \delta \varkappa Q}{p^2} \qquad \sigma'(p, x) = \frac{f_o \varkappa a}{p^2} \cos(kx + \gamma)$$

The above distribution of A (p) was chosen because both Wiin-Nielsen (1961) and Sanders et al.(1971) had considerable success when they used it.

Using $\omega = \tilde{\omega} \sin(kx + \gamma)$ and $p^* = p/p_o$, Equ. (4.51) gives

$$\tilde{\omega} = \frac{G}{\lambda^2} p \ln(p^*) + \frac{Gp}{\lambda^4}\left[1 - (p^*)^{q-1}\right] \qquad (4.55)$$

$$G = \frac{-2Qk^3 a}{f_o} \qquad q = \frac{1 + \sqrt{1 + 4\lambda^2}}{2}$$

Here λ^2 is the same as in the previous section (see Equ. (4.43)).

If $\varepsilon = \tilde{\varepsilon} \sin(2kx + 2\gamma)$, then Equ. (4.52) becomes

$$p^2 \frac{d^2\tilde{\varepsilon}}{dp^2} - 4\lambda^2 \tilde{\varepsilon} = \frac{2\varkappa a k^2}{f_o} \tilde{\omega}$$

Therefore

$$\tilde{\varepsilon} = \frac{2\varkappa a k^2}{4\lambda^2 f_o}\left(-\tilde{\omega} - \frac{Gp}{12\lambda^4}\left[3 - 4(p^*)^{q-1} + (p^*)^{r-1}\right]\right)$$

$$r = \frac{1 + \sqrt{1 + 16\lambda^2}}{2}$$

It can be shown that to a good approximation

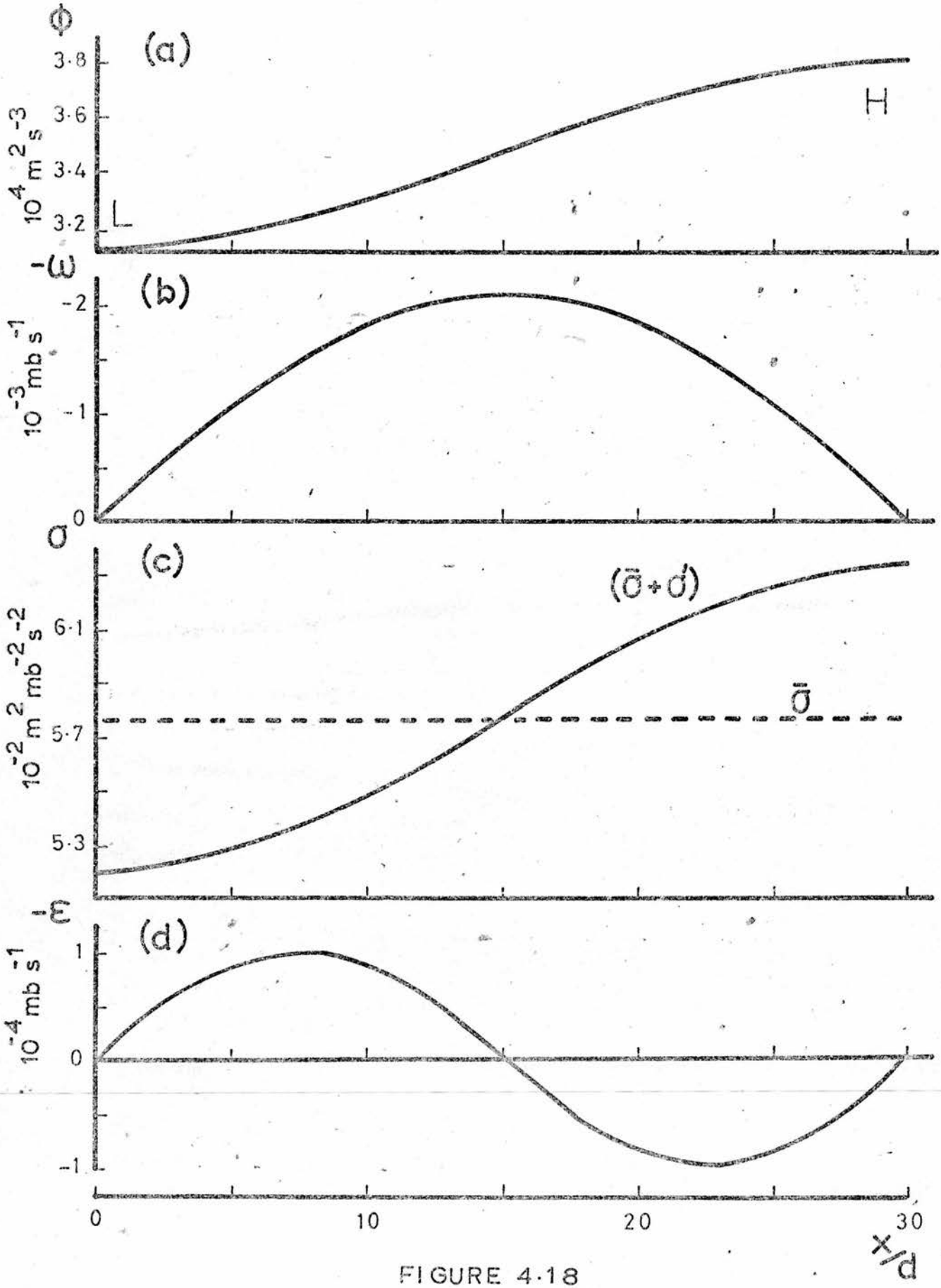
Φ
(a)
3·8
3·6
3·4
3·2
$10^{4}\ m^{2}\ s^{-3}$
H
L
ω
(b)
-2
-1
0
$10^{-3}\ mb\ s^{-1}$
σ
(c)
$(\bar{\sigma}+\sigma')$
$\bar{\sigma}$
6·1
5·7
5·3
$10^{-2}\ m^{2}\ mb^{-2}\ s^{-2}$
ω
(d)
1
0
-1
$10^{-4}\ mb\ s^{-1}$
0
10
20
30
x/d

FIGURE 4·18

$$\varepsilon = -\frac{\sigma'}{\bar{\sigma}}\,\omega \qquad (4.57)$$

Similarly it can be shown that

$$\eta = -\frac{\sigma'}{4\bar{\sigma}}\,\omega \qquad (4.58)$$

Let Φ_t be the geopotential tendency when ω is used in Equ. (4.47). Also let $\Phi_t + \nu(\varepsilon)$ and $\Phi_t + \nu(\eta)$ be the tendencies when $\omega + \varepsilon$ and $\omega + \eta$ are used. It can be shown that from Equs. (4.47), (4.57) and (4.58) that both $\nu(\varepsilon)$ and $\nu(\eta)$ are proportional to the divergence. Since this changes sign in mid-troposphere it is expected that $\nu(\varepsilon)$ and $\nu(\eta)$ will also change sign.

Rearranging Equ. (4.57) gives

$$(\bar{\sigma} + \sigma')(\omega + \varepsilon) = \omega\bar{\sigma} + \varepsilon\sigma' \qquad (4.59)$$

Since $\sigma'\varepsilon$ is small, the product of the vertical velocity and the stability for the solutions of Equs. (4.50) and (4.51) is almost a constant. Further from Equs. (4.59) and (4.38) it can be shown that

$$\frac{\partial \nu(\varepsilon)}{\partial p} = -\omega\sigma' - \varepsilon\bar{\sigma}$$

Therefore $\nu(\varepsilon)$ is small. Also a qualitative analysis of the equations suggests that $\nu(\eta) > \nu(\varepsilon)$.

Both ω and ε were computed using the following parameters (see Fig. 4.18)

$p = 500$ mb $\quad p_o = 1000$ mb $\quad \gamma = 0 \quad 0 < x < L/2$

$a = -5 \times 10^{7}\ m^2\ s^{-1} \quad Q = 5\ m\ s^{-1}$

Other parameters were the same as those described in the previous section.

Figs. 4.18a and 4.18b show the distributions of Φ and ω. As expected there is upward motion ($\omega < 0$) in front of the depression and downward motion ($\omega > 0$) behind

it (i.e. ω and Φ are 90° out of phase). Both $(\bar{\sigma} + \sigma')$ and $\bar{\sigma}$ are illustrated in Fig. 4.18c and it is clear that $(\bar{\sigma} + \sigma')$ and ω are also 90° out of phase. This difference in phase results in a distribution of ε that has a wavelength of L/2. Fig. 4.18d depicts ε. These results show that ε is zero when $\omega = 0$ and when $|\omega|$ is a maximum. Thus ω underestimates the magnitude of the correct vertical velocity $(\omega + \varepsilon)$ both in front of and behind the depression. For a high pressure region ω is an overestimate of the correct vertical velocity. These conclusions also apply to the use of ω in place of $(\omega + \eta)$.

4.8 A Case Study

A case study was carried out using the data described in section 1.8.2. The vertical velocity and geopotential tendency were calculated from the following equations

$$STAB_{x}\nabla^2\omega + f_o^2 \frac{\partial^2\omega}{\partial p^2} + S = 0 \qquad (4.60)$$

$$\nabla^2\Phi_t + f_o \underline{V}_g \cdot \nabla\eta - f_o^2 \frac{\partial\omega}{\partial p} = 0 \qquad (4.61)$$

The calculation were performed on a 22 x 30 horizontal grid (area 11), with a vertical grid spacing of 200 mb. In all the computations it was assumed that $\omega = 0$ and $\Phi_t = 0$ on the boundary.

All the figures referred to in this section illustrate the central portion of the computation area which is composed of 14 x 22 gridpoints.

The above equations were solved using three different forms of the stability, STAB.

(1) a point variable static stability (σ) given by Equ. (4.31).

(2) a pressure variable static stability ($\bar{\sigma}$) given by the average value of σ on each isobaric surface. The values of $\bar{\sigma}$ were

$$\bar{\sigma}(400) = 4.35 \times 10^{-2} \qquad \bar{\sigma}(600) = 2.09 \times 10^{-2}$$

$$\bar{\sigma}(800) = 1.42 \times 10^{-2}$$

The units are $m^2 mb^{-2} s^{-2}$.

(3) a constant static stability $\bar{\bar{\sigma}} = 2.62 \times 10^{-2}$ which is the average value of $\bar{\sigma}$.

The solutions of Equs. (4.60) and (4.61) using the three different forms of STAB will be denoted by

(1) ω and Φ_t

(2) $\bar{\omega}$ and $\bar{\Phi}_t$

(3) $\bar{\bar{\omega}}$ and $\bar{\bar{\Phi}}_t$

The distributions of $\bar{\omega}$ and $\bar{\bar{\omega}}$ at the 400 mb level are shown in Figs. 4.19a and 4.19b. These show that the areas of upward and downward motion are the same for both $\bar{\omega}$ and $\bar{\bar{\omega}}$. They also show that the maxima of both $|\bar{\omega}|$ and $|\bar{\bar{\omega}}|$ (marked by $\wedge$) are in the same position. An examination of the difference between $\bar{\bar{\omega}}$ and $\bar{\omega}$ clearly shows that at this level $|\bar{\bar{\omega}}| > |\bar{\omega}|$ nearly everwhere. A close examination shows that $\bar{\bar{\omega}} \approx f(p)\bar{\omega}$ with $f(400) \approx 1.3$. At the 800 mb level $f(800) \approx 0.7$. These results imply that $|\bar{\bar{\omega}}|$ tends to be greater than $|\bar{\omega}|$ when $\bar{\bar{\sigma}} < \bar{\sigma}$ and vice versa when $\bar{\bar{\sigma}} > \bar{\sigma}$.

At the 400 mb and 800 mb levels the percentage errors produced by replacing $\bar{\sigma}$ by $\bar{\bar{\sigma}}$ are approximately 30% and -30%. Using p_e = 550 mb and $\xi = 1$, Equ. (4.48) gives corresponding values of 37% and -31%. Thus $R(\omega)^*$ (see Equ. (4.48)) produces a good estimate of the percentage errors. It is worth noting that the correspond-

	RMS values in units of 10^{-4} mb s^{-1}								
p	$\bar{\bar{\omega}}$	$\bar{\omega}$	ω	$\hat{\omega}$	$\bar{\bar{\omega}} - \bar{\omega}$	ε	ε^*	$\hat{\omega} - \bar{\omega}$	$\hat{\omega} - \omega$
400	13.2	10.1	9.5	9.9	3.2	1.1	1.8	1.1	1.0
600	7.4	7.8	7.9	8.5	1.0	1.4	1.3	1.6	1.3
800	4.4	6.5	8.2	8.9	2.3	2.8	2.1	3.6	1.9

TABLE 4.6

	RMS values in units of 10^{-3} $m^2 s^{-3}$						
p	$\bar{\bar{\phi}}_t$	$\bar{\phi}_t$	ϕ_t	$\hat{\phi}_t$	$\bar{\bar{\phi}}_t - \bar{\phi}_t$	$\hat{\phi}_t - \bar{\phi}_t$	$\hat{\phi}_t - \phi_t$
200	24.4	23.5	23.3	23.3	10.0	7.1	2.3
400	17.3	17.3	17.3	17.3	0.4	1.7	1.0
600	3.9	4.2	4.3	4.3	5.5	1.9	1.4
800	4.5	4.5	4.5	4.5	0.4	1.5	1.0
1000	8.9	9.0	8.7	9.0	3.2	5.6	3.6

TABLE 4.7

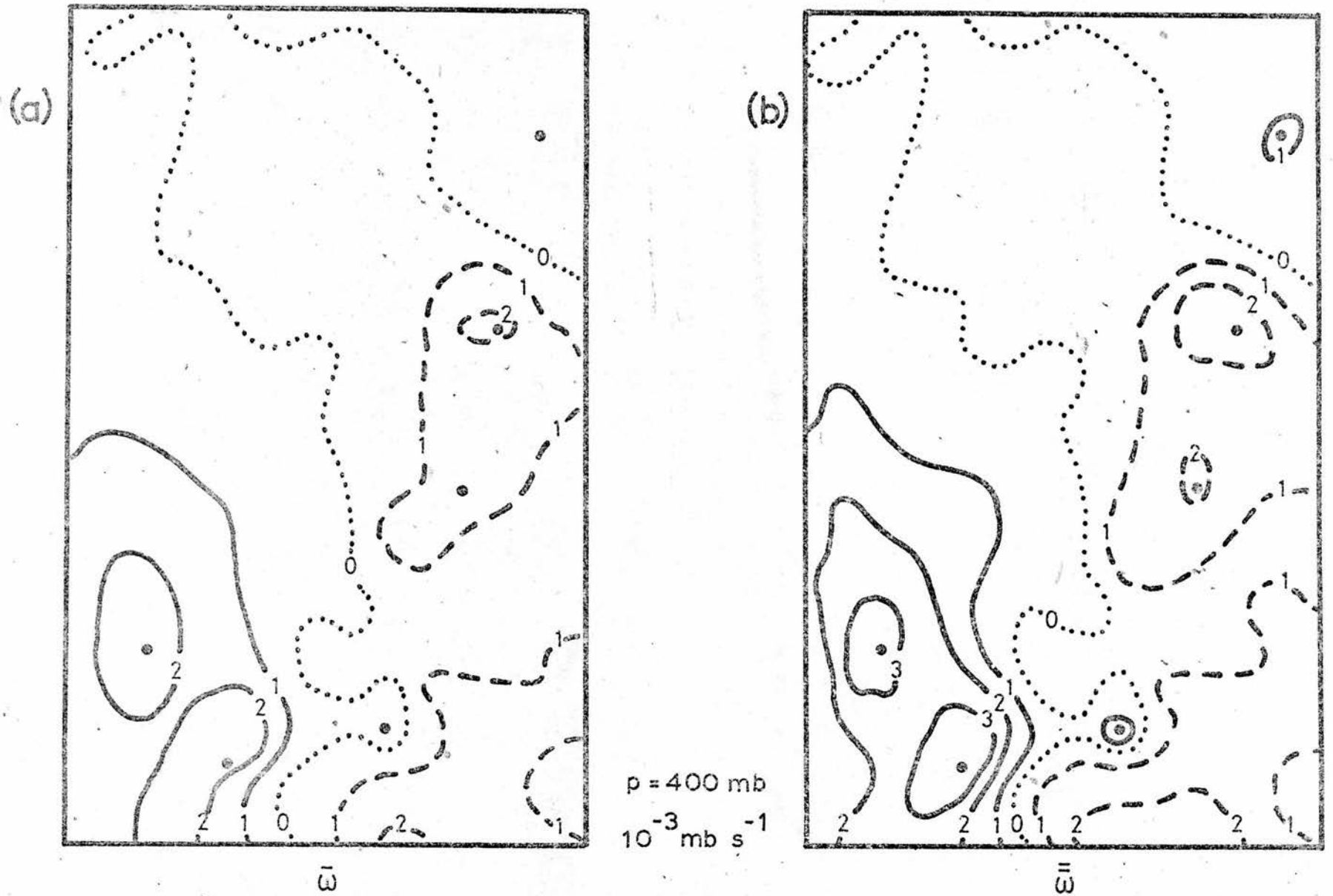

FIGURE 4.19

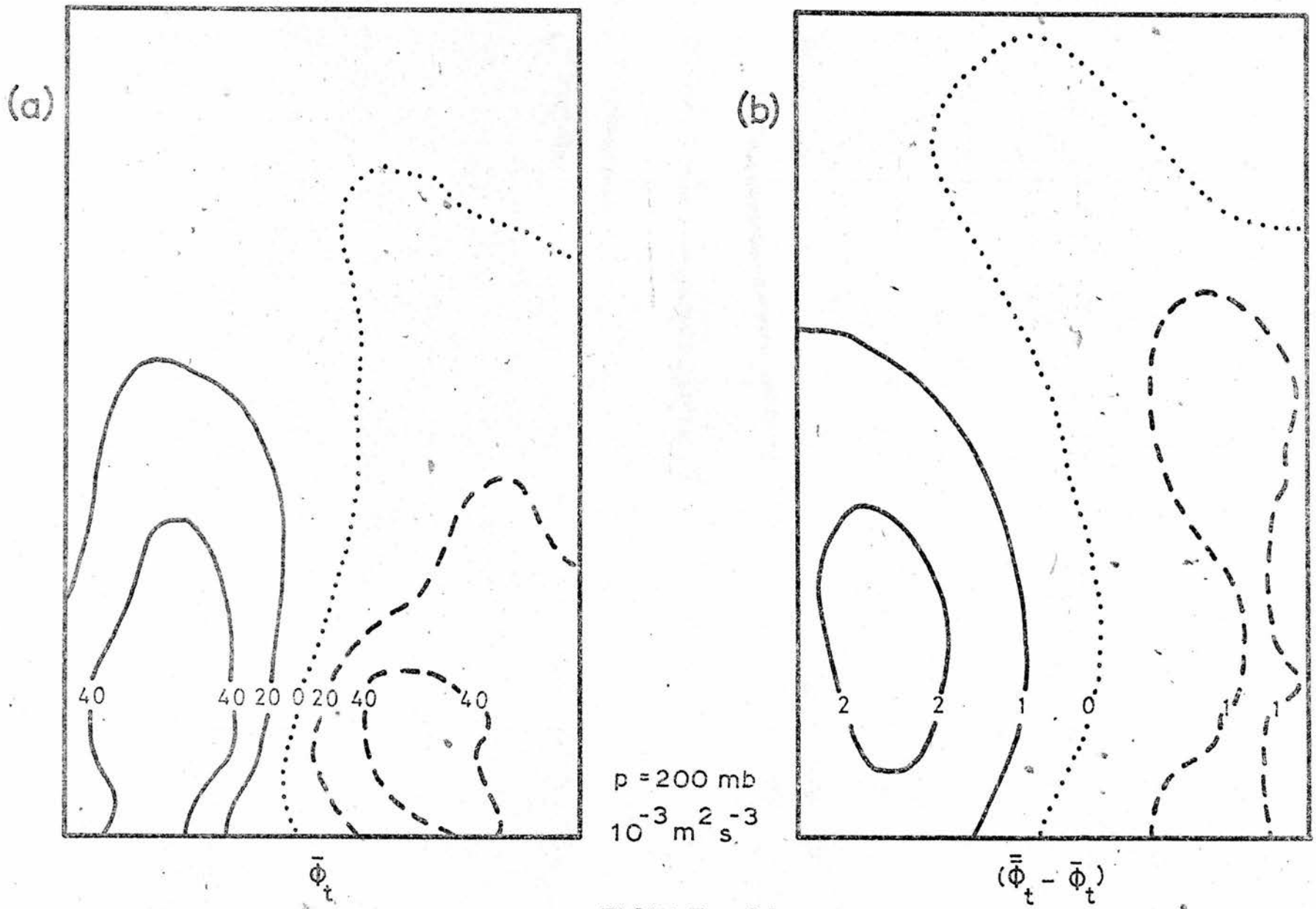
(a)
(b)
40
40 20 0 20 40
40
2
2
1
0
1
1
p = 200 mb
$10^{-3} m^2 s^{-3}$
$\bar{\Phi}_t$
$(\bar{\bar{\Phi}}_t - \bar{\Phi}_t)$

FIGURE 4.20

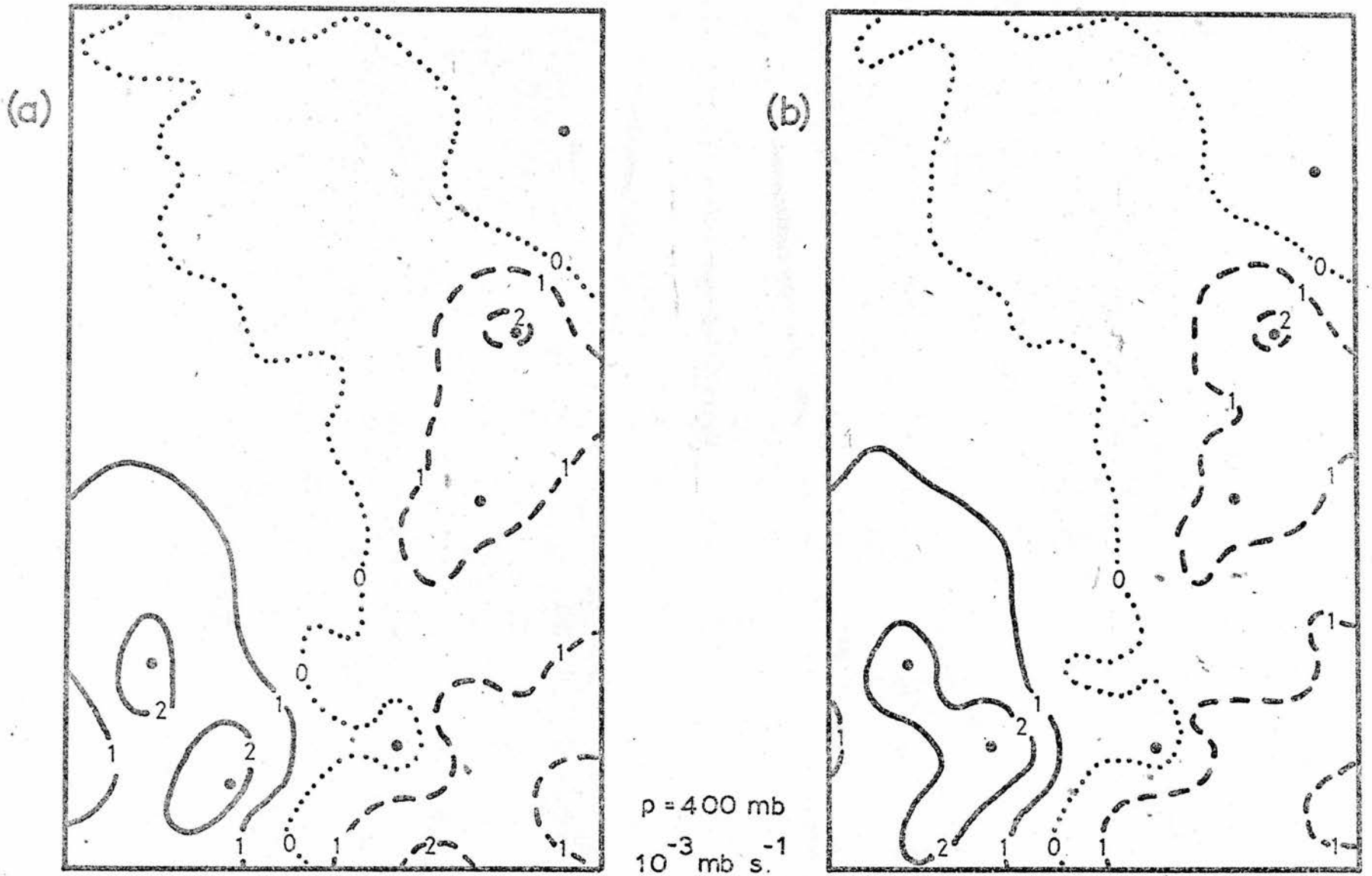

FIGURE 4·21

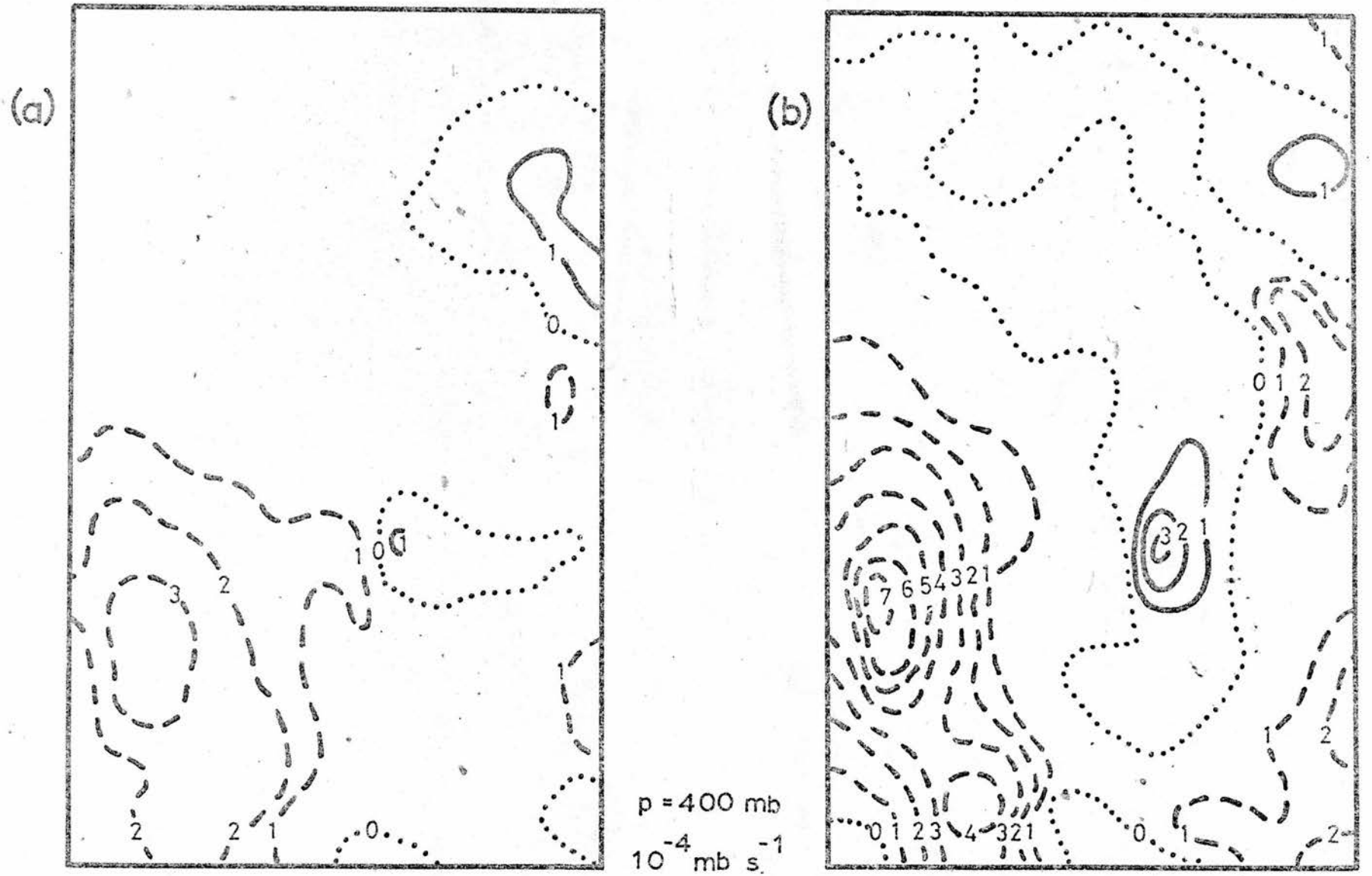

FIGURE 4.22

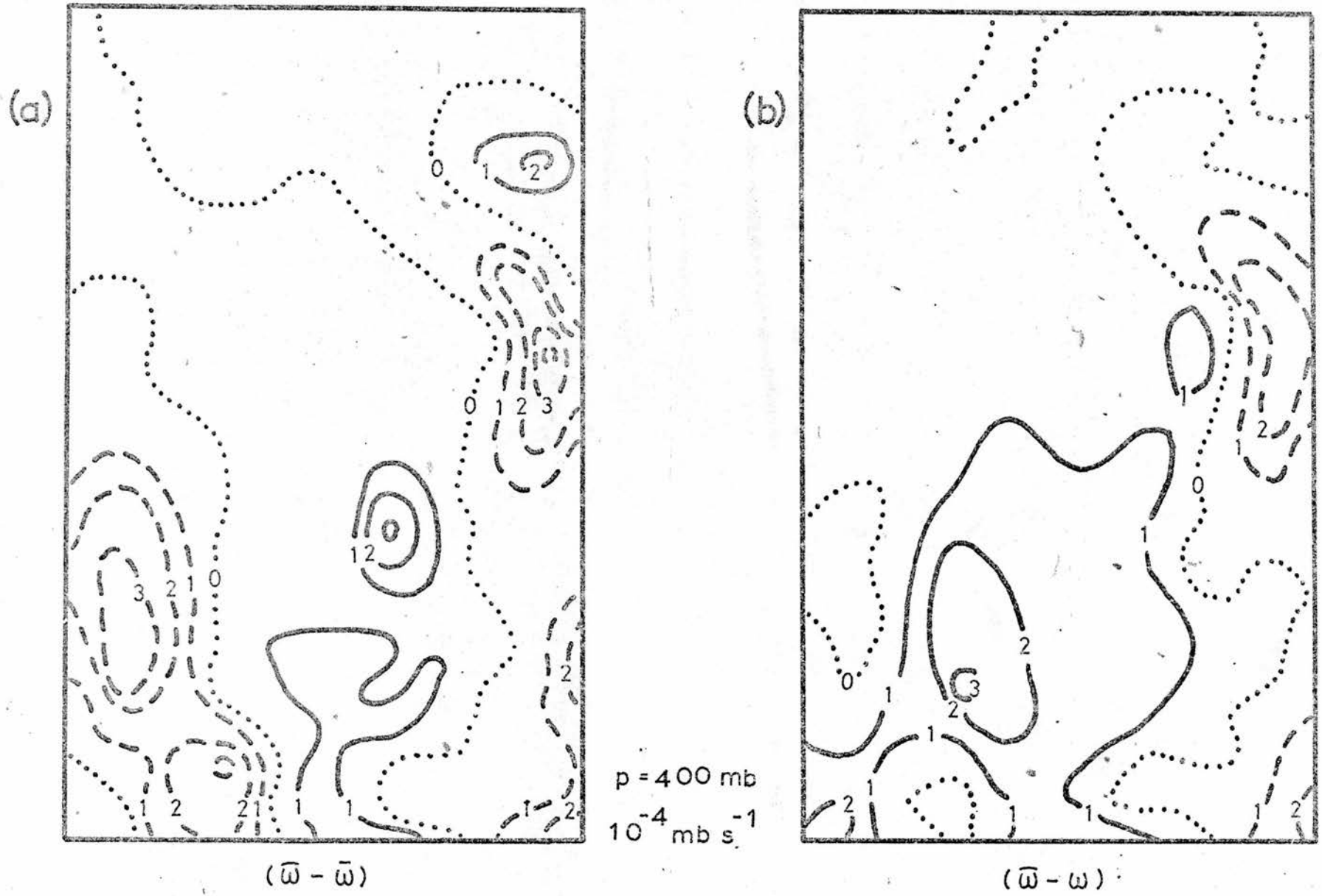

FIGURE 4·23

ing value derived from $R(\omega)_h$ (Equ. (4.49)) are 90% and 53%. This estimate is clearly inaccurate and this is because $\bar{\sigma}\bar{\omega}$ is not equal to $\bar{\bar{\sigma}}\bar{\bar{\omega}}$. The root mean square (RMS) values of $\bar{\omega}$, $\bar{\bar{\omega}}$ and $\bar{\bar{\omega}}-\bar{\omega}$ are shown in Table 4.6.

The distributions of $\bar{\Phi}_t$, at the 200 mb level, is shown in Fig. 4.20a and ($\bar{\bar{\Phi}}_t - \bar{\Phi}_t$) is depicted in Fig. 4.20b. These figures show that at this level $|\bar{\bar{\Phi}}_t| > |\bar{\Phi}_t|$. This result was anticipated in section 4.7.3. The RMS values of $\bar{\Phi}_t$, $\bar{\bar{\Phi}}_t$ amd ($\bar{\bar{\Phi}}_t - \bar{\Phi}_t$) are shown in Table 4.7 This shows that ($\bar{\bar{\Phi}}_t - \bar{\Phi}_t$) is largest at the 200 mb level although the largest percentage difference is at 600 mb.

Equ. (4.60) was solved with STAB = σ to give ω (see Fig. 4.21a). This solution is very similar to $\bar{\omega}$ and $\bar{\bar{\omega}}$ which are illustrated in Figs. 4.19a and 4.19b. In particular, their maxima and minima (denoted by •) are in the same position. This was found to be true at all levels. Therefore these results contradict those of Danard described in section 4.7. It is suspected that this is due to the large gridlength and small number of gridpoints used by Danard.

The quantities of $\sigma/\bar{\sigma}$ and $\bar{\omega}/\omega$ were compared and it was found that regions where $\sigma < \bar{\sigma}$ tended to coincide with regions where $|\bar{\omega}| < |\omega|$. This confirms the conclusions of Danard (1964) and is consistent with the relationship between vertical velocity and the static stability found for the simple model (see Equ. (4.59)).

Fig. 4.22a shows the difference between ω and $\bar{\omega}$. It would be useful if this difference could be estimated from a knowledge of σ ,$\bar{\sigma}$and $\bar{\omega}$. An equation that is

similar to Equ. (4.58) is

$$\varepsilon^{*} = -\frac{(\sigma - \bar{\sigma})}{\bar{\sigma}}\,\bar{\omega}$$

Here ε^{*} is an estimate of $(\omega - \bar{\omega})$ and its value at 400 mb is shown in Fig. 4.22b. A comparison of this with $(\omega - \bar{\omega})$ (see Fig. 4.22a) indicates that ε^{*} is large when $(\omega - \bar{\omega})$ is large but ε^{*} overestimates the magnitudes. For the 800 mb level $|\omega - \bar{\omega}|$ is underestimated. These results indicate that the dependence of $(\omega - \bar{\omega})$ upon σ, $\bar{\sigma}$ and ω is similar to that described by ε^{*}.

The reason why ε^{*} does not describe $(\omega - \bar{\omega})$ exactly becomes apparent if the ω-equations for ω and $\bar{\omega}$ are subtracted to give

$$\bar{\sigma}\,\nabla^{2}\varepsilon + f_{o}^{2}\frac{\partial^{2}\varepsilon}{\partial p^{2}} = -\sigma'\nabla^{2}\bar{\omega}$$

Here $\varepsilon = \omega - \bar{\omega}$, $\sigma' = \sigma - \bar{\sigma}$ and $\sigma'\nabla^{2}\varepsilon$ is neglected. Assuming that

$$\bar{\omega} \propto \sin(rx)\,\sin(sy)$$

$$\varepsilon \propto \sin(kx)\,\sin(hy)\,\sin(lp)$$

then

$$\varepsilon = \frac{\sigma'(r^{2}+s^{2})\,\bar{\omega}}{(k^{2}+h^{2})\bar{\sigma} + f_{o}^{2}l^{2}} \qquad (4.62)$$

If $r = k$, $s = h$ and $l = 0$ then this equation reduces to that for ε^{*}. However, if $h = 2s$ and $k = 2r$ there is a factor of 4 in the denominator and the expression is identical to Equ. (4.58). The above considerations clearly show that $(\omega - \bar{\omega})$ depends upon the wavelengths of $\bar{\omega}$ and ω as well as the magnitudes of $\bar{\omega}$, σ' and $\bar{\sigma}$.

A comparison of Φ_{t} and $\bar{\Phi}_{t}$ shows that at the 200 mb and 400 mb levels $\bar{\Phi}_{t} > \Phi_{t}$ nearly everywhere. The reverse was true at the 800 mb and 1000 mb levels. This behaviour is due to the divergence tending to have opposite signs in

the upper and lower troposphere and it was exhibited in the model described in section 4.74. Table 4.7 shows the RMS values of $(\Phi_t - \bar{\Phi}_t)$ and these indicate that the value are largest at the top and bottom of the atmosphere. However $(\Phi_t - \bar{\Phi}_t)/ \Phi_t$ is largest in the lower part of the atmosphere.

The last part of this case study is concerned with a comparison of ω and $\bar{\omega}$ with $\bar{\omega}$ where

$$\nabla^2(\sigma \bar{\omega}) + f_o^2 \frac{\partial^2 \bar{\omega}}{\partial p^2} + S = 0$$

Fig. 4.21b shows $\bar{\omega}$ at the 400 mb level. A comparison of this with ω (Fig. 4.21a) and $\bar{\omega}$ (Fig. 419a) indicates that both ω and $\bar{\omega}$ give a good representation of the 'correct' vertical velocity $\bar{\omega}$. Further, a comparison of $(\bar{\omega} - \bar{\omega})$ and $(\omega - \bar{\omega})$ (see Figs. 4.23a and 4.22a) shows that the difference between $\bar{\omega}$ and $\bar{\omega}$ tends to be greater than that between ω and $\bar{\omega}$ (see also Table 4.6). It is also worth noting that the distribution of $(\bar{\omega} - \bar{\omega})$ is very similar to that of ε^*.

Fig. 4.23b shows the distribution of $(\bar{\omega} - \omega)$ and Table 4.6 exhibits the RMS values. These values show that the difference between $\bar{\omega}$ and ω tends to be less than that between $\bar{\omega}$ and $\bar{\omega}$, ω and $\bar{\omega}$, and $\bar{\bar{\omega}}$ and $\bar{\omega}$. Thus the best approximation to $\bar{\omega}$ is found by using Equ. (4.60) with STAB = σ. However the difference between ω and $\bar{\omega}$ is by no means insignificant.

The geopotential tendency found by using $\bar{\omega}$ will be referred to as $\bar{\Phi}_t$. Table 4.7 shows the RMS values of $\bar{\Phi}_t$ and $(\bar{\Phi}_t - \Phi_t)$. These results indicate that the difference between $\bar{\Phi}_t$ and Φ_t was small and that the

largest difference was at the 1000 mb level.

4.8.1 The Concept Of Partitioning

The concept of partitioning was discussed and used in two papers by Krishnamurti (1968). He considered the solution of the equation

$$\nabla^2(\sigma\omega) + f^2\frac{\partial^2\omega}{\partial p^2} = \sum_{i=1}^{I} L_i(\omega) + \sum_{j=1}^{J} M_j \qquad (4.64)$$

He interpreted the forcing functions on the righthand side as the causes of the vertical velocity. An attempt was then made to evaluate the contribution of each of these causes (i.e. forcing function) to the total vertical velocity, ω . He computed ω and then calculated the vertical velocities

ω_i (i = 1,1, I) and ω'_j (j = 1, 1, J).

$$\nabla^2(\sigma\omega_i) + f^2\frac{\partial^2\omega_i}{\partial p^2} = L_i(\omega) \qquad i = 1,1,I \qquad (4.65)$$

$$\nabla^2(\sigma\omega'_j) + f^2\frac{\partial^2\omega'_j}{\partial p^2} = M_j \qquad j = 1,1,J \qquad (4.66)$$

This method of partitioning ω has the essential property that

$$\omega = \sum_{i=1}^{I}\omega_i + \sum_{j=1}^{J}\omega'_j \qquad (4.67)$$

It is worth noting that there are numerous other ways of partitioning ω that will satisfy the above equation.

The contribution ω'_j is the same as the error in the vertical velocity that would be introduced if the forcing function M_j is neglected in Equ. (4.64). Unfortunately the relationship between ω_i and $L_i(\omega)$ is not a simple one. Let $\bar{\omega}_i$ be the error introduced into the vertical velocity when the term $L_i(\omega)$ is not included in Equ. (4.64). It can be shown that $\bar{\omega}_i$ is given by

$$\nabla^2(\sigma\bar{\omega}_i) + f^2\frac{\partial^2\bar{\omega}_i}{\partial p^2} = L_i(\omega) + \sum_{\substack{k=1\\k\neq i}}^{I} L_k(\bar{\omega}_i) \qquad (4.68)$$

A comparison of Equs. (4.68) and (4.65) shows that $\omega_i \neq \bar{\omega}_i$.

It can be shown that, under the following circumstances, ω_i is almost the same as $\bar{\omega}_i$. If one of the forcing function M_j (j = 1, 1, J) is an order of magnitude greater than all of the forcing functions L_i (ω) (i = 1, 1, I), then ω_j' (and thus ω) will be an order of magnitude greater than ω_i and $\bar{\omega}_i$. Thus L_i (ω) will be an order of magnitude greater than $\sum_{\substack{k=1\\k\neq i}}^{I} L_k(\bar{\omega}_i)$ (see Equ. (4.68)). Hence ω_i will be almost the same as $\bar{\omega}_i$.

The circumstances described above prevail in all forms of the ω-equation. Thus ω_i is approximately the error introduced into the vertical velocity when the forcing function L_i (ω) is neglected in Equ. (4.64).

4.8.2 The Partitioning Of The Quasi-Geostrophic ω-Equation

Partitioning was employed to investigate the effect of the use of certain approximations in the geostrophic ω-equation (Equ. (4.5)). Let Γ be the differential operator such that

$$\Gamma(\omega) = \bar{\sigma}(p)\nabla^2\omega + f_o^2\frac{\partial^2\omega}{\partial p^2}$$

The parameters $\bar{\sigma}(p)$ and f_o are the average values over an isobaric surface of σ and f.

The vertical velocity was divided into five parts ω_i (i = 1, 1, 5) given by

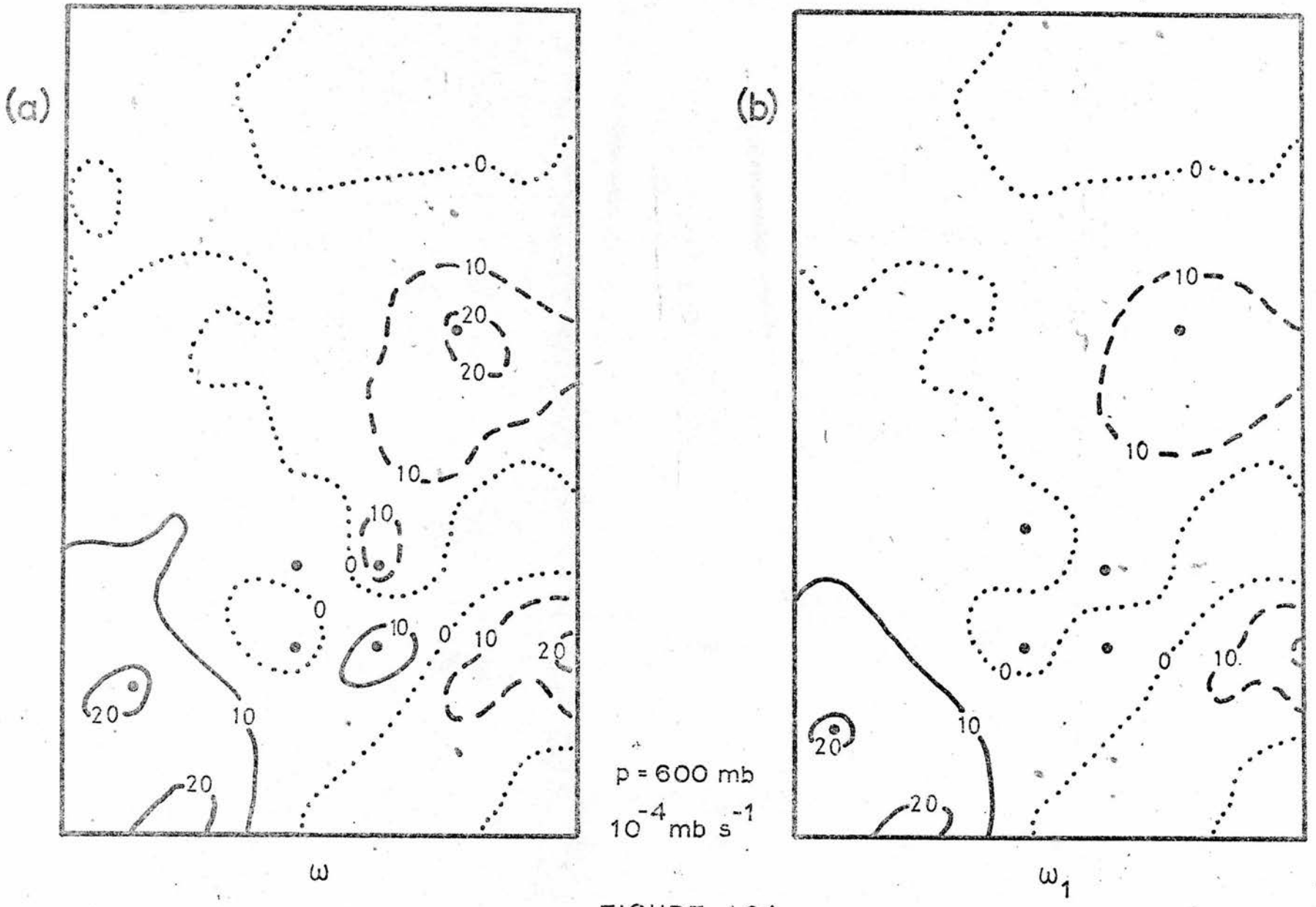

FIGURE 4.24

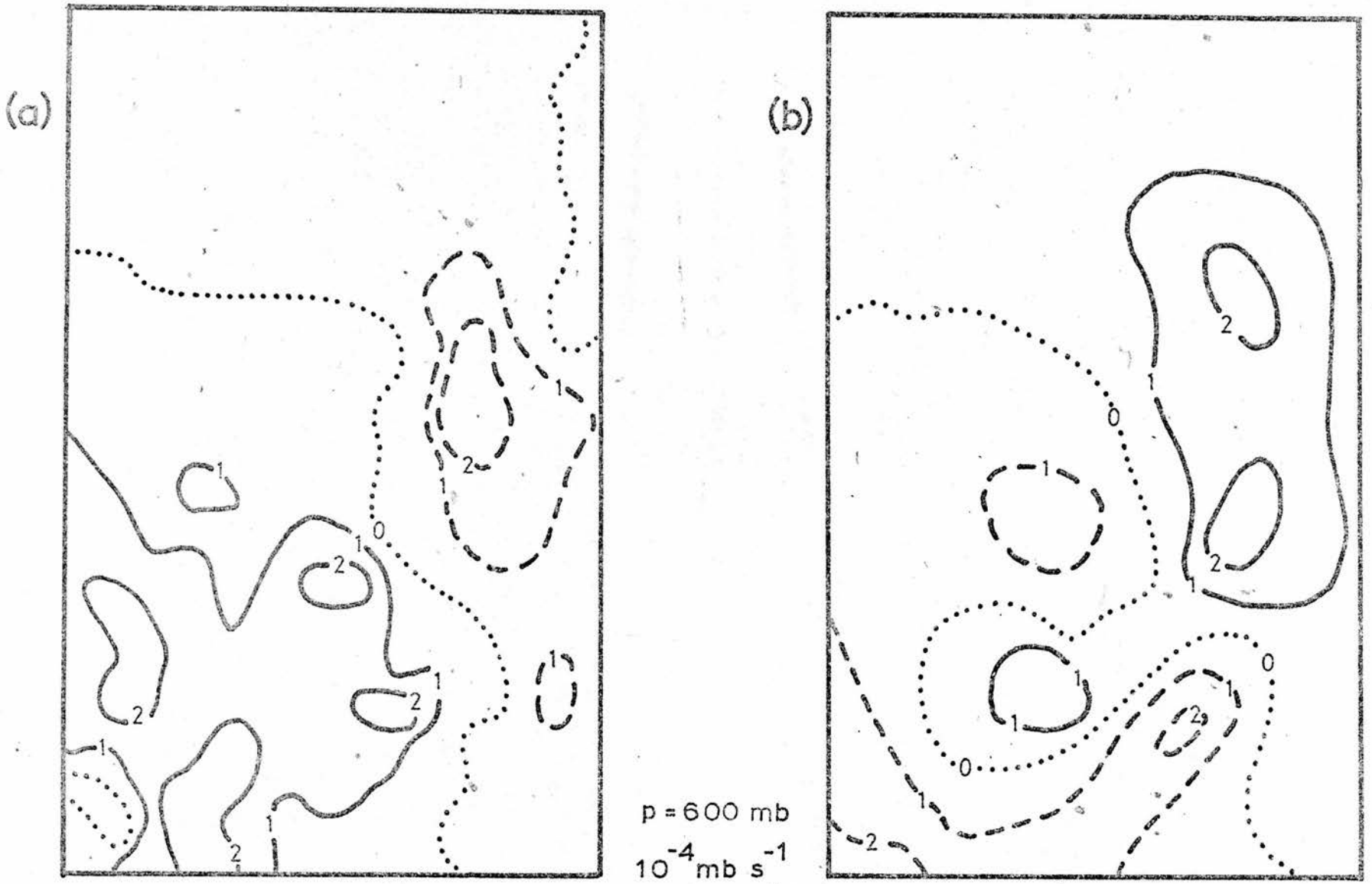

FIGURE 4·25

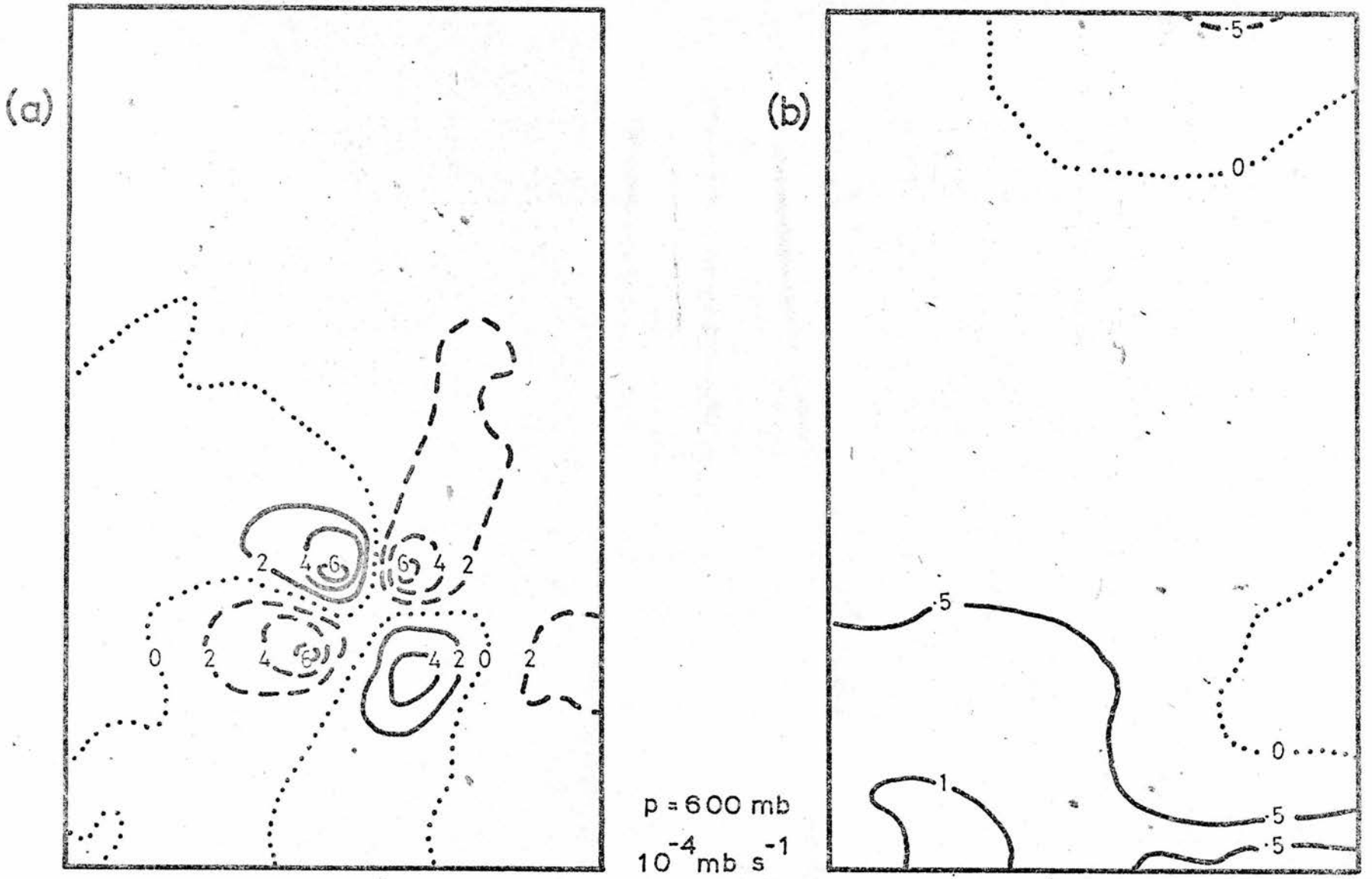

FIGURE 4·26

	AV and RMS in units of 10^{-4} mb s^{-1}					
	400 mb		600 mb		800 mb	
	AV	RMS	AV	RMS	AV	RMS
ω_1	0.7	8.1	0.8	6.4	1.0	5.8
ω_2	-0.1	0.5	0.1	0.8	-0.1	0.7
ω_3	0.3	0.7	-0.0	0.8	0.2	1.0
ω_4	-0.5	0.9	-0.3	1.1	-0.4	2.4
ω_5	-0.0	0.5	0.1	0.3	0.2	0.5
ω	0.4	8.4	0.7	6.8	0.9	0.7

TABLE 4.8

$$\Gamma(\omega_1) + S = 0$$

$$\Gamma(\omega_2) + \omega\nabla^2\sigma = 0$$

$$\Gamma(\omega_3) + 2\nabla\sigma.\nabla\omega = 0$$

$$\Gamma(\omega_4) + (\sigma - \bar{\sigma}(p))\nabla^2\omega = 0$$

$$\Gamma(\omega_5) + (f^2 - f_o^2)\frac{\partial^2\omega}{\partial p^2} = 0$$

Since S is the largest forcing function in the above equations, ω and ω_1 will tend to be greater than ω_i ($i = 2, 1, 5$). Thus the ω_i's represent approximately the effect on the vertical velocity of the omission of the relevant forcing function.

Using the above interpretation of the ω_i's it is obvious that ω_4 is a measure of the difference between the solutions of Equ. (4.60) using STAB = $\sigma(x, y, p)$ and STAB = $\sigma(p)$. Also $(\omega_2 + \omega_3)$ is closely related to the difference between the solutions of Equ. (4.63) and of Equ. (4.60) (with STAB = $\sigma(x, y, p)$). The effect of replacing the variable Coriolis parameter (f) by a constant (f_o), is represented by ω_5.

The solution of the geostrophic ω-equation is shown in Fig. 4.24a and the contributions ω_i ($i = 1, 1, 5$) at the 600 mb level are illustrated in Figs. 4.24b, 4.25a, 4.25b, 4.26a and 4.26b respectively.

A comparison of ω and ω_1 shows that ω_1 has the same areas of upward and downward motion as ω. Also the maximum magnitudes of ω and ω_1 (marked by •) almost coincide. The similarity of ω and ω_1 indicates that ω_1 is much larger than the other contributions. This is also shown by a comparison of the RMS values of these vertical velocities (see Table 4.8 which also shows the average (AV) values).

An examination of the distributions of ω_2 and ω_3 (Figs. 4.25a and 4.25b) shows that they tend to have opposite signs. Thus the effects of omitting the terms $\omega\nabla^2\sigma$ and $2\nabla\sigma.\nabla\omega$ tend to cancel. This implies that both of these terms should be neither omitted or included. Also, Table 4.8 shows that ω_3 tends to be larger than ω_2. Further, a comparison of ω_4 with ω_2 and ω_3 shows that ω_4 tends to be significantly larger than the other. Thus, even if the horizontal variations of σ are ignored in the $\omega\nabla^2\sigma$ and $2\nabla\sigma.\nabla\omega$ terms, it is important to include them in the $\sigma\nabla^2\omega$ term.

The distribution of ω_5 is illustrated in Fig. 4.26b. This, with Table 4.8, shows that the effect of replacing f by f_o tends to be small. However the table indicates that the effect may be comparable with that due to ignoring the $\sigma\nabla^2\omega$ and $2\nabla\sigma.\nabla\omega$ terms.

4.9 Inconsistent Boundary Conditions

Suppose that ω and z are related by

$$f_1\omega + g_1 z = A_1 \qquad (4.69)$$

$$f_2\omega + g_2 z = A_2 \qquad (4.70)$$

Here f_1, f_2, g_1 and g_2 are differential operators and A_1 and A_2 are known forcing functions. In order to solve this system of equations it is first necessary to eliminate one of the unknowns; z say, between the two equations. This gives

$$(g_2 f_1 - g_1 f_2)\omega = g_2 A_1 - g_1 A_2 \qquad (4.71)$$

If this is elliptic it can be solved as a boundary value problem using $\omega = \omega_b$ on the boundary. The solution is then substituted into either Equ. (4.69) or (4.70) (in this case Equ. (4.69)) and this is then solved for z, by using

$z = z_b$ on the boundary. The boundary conditions ω_b and z_b will be said to be inconsistent if they do not satisfy Equ. (4.70). It is suspected that the boundary conditions are inconsistent if the minimum number of boundary conditions are not used.

The inconsistency of boundary conditions can be illustrated by a simple example. Suppose the ω and z satisfy

$$\frac{d^2\omega}{dx^2} + z = A \qquad (4.72)$$

$$z + \omega = B \qquad (4.73)$$

Here A and B are constants. It can easily be shown that ω satisfies the equation $\frac{d^2\omega}{dx^2} - \omega = A-B$ and that if $\omega(0) = 0$ and $\omega(L) = 0$, then the solution

$$\omega(x) = (A-B)\,(1 - e^{L})\,\frac{\sinh(x)}{\sinh(L)} - (A-B)\,(1 - e^{x})$$

The solution for z can then be found from Equ. (4.73) and will be called z_1. An alt ernative method of finding z is to solve the equation

$$\frac{d^2z}{dx^2} - z = -A$$

If the boundary conditions $z(0) = 0$ and $z(L) = 0$ are chosen, then this equation can be solved for z and let the solution be z_2. It is found that

$$z_1 - z_2 = B\,(1 - e^{L})\,\frac{\sinh(x)}{\sinh(L)} + Be^{x}$$

The reason that $z_1 - z_2 \neq 0$ is that the boundary conditions for z and ω are inconsistent. That is they do not satisfy Equ. (4.73). An alternative approach is to say that z_1 and z_2 are not the same because too many boundary conditions were used in solving the equations for z_2. In the simple case considered, $(z_1 - z_2)$ decreases

exponentially away from the boundary.

4.9.1 The Inconsistency Of The Usual Boundary Conditions For ω And Φ_t

Suppose that the atmosphere is in geostrophic equilibrium and that its motions are governed by the following simplified forms of the vorticity and thermal equations.

$$\nabla^2 \Phi_t + J(\Phi, \eta) - f^2 \frac{\partial \omega}{\partial p} = 0$$

$$\frac{\partial \Phi_t}{\partial p} + \frac{1}{f} J\left(\Phi, \frac{\partial \Phi}{\partial p}\right) + \sigma \omega = 0$$

These correspond to Equs. (4.69) and (4.70) in the previous section. If Φ is known then the unknowns are ω and Φ_t. The elimination of Φ_t between these two equations results in the ω-equation given by Equ. (4.5). This is then solved for ω and it is usually assumed that $\omega = 0$ on the boundary. If b denoted the lateral boundaries then the boundary condition becomes $(\omega)_b = 0$ with $\omega = 0$ on the upper and lower boundaries. Once ω is known the vorticity equation is solved for Φ_t. This requires the specification of Φ_t on the boundary, b, and usually $(\Phi_t)_b = 0$ is used. If the boundary conditions for ω and Φ_t do not satisfy the thermal equation then they are inconsistent.

Since $\Phi_t = 0$ on the lateral boundary of each isobaric surface, $\left(\frac{\partial \Phi_t}{\partial p}\right)_b = 0$. Therefore $(\Phi_t)_b$ and $(\omega)_b$ do not satisfy the thermal equation unless the thermal advection is zero on the boundary. This is not usually so and therefore the boundary conditions are inconsistent.

The effect of using these inconsistent boundary conditions was investigated. Initially ω and Φ_t were computed in the above manner using the same grid and data as were used in section 4.8. The solution Φ_t was then

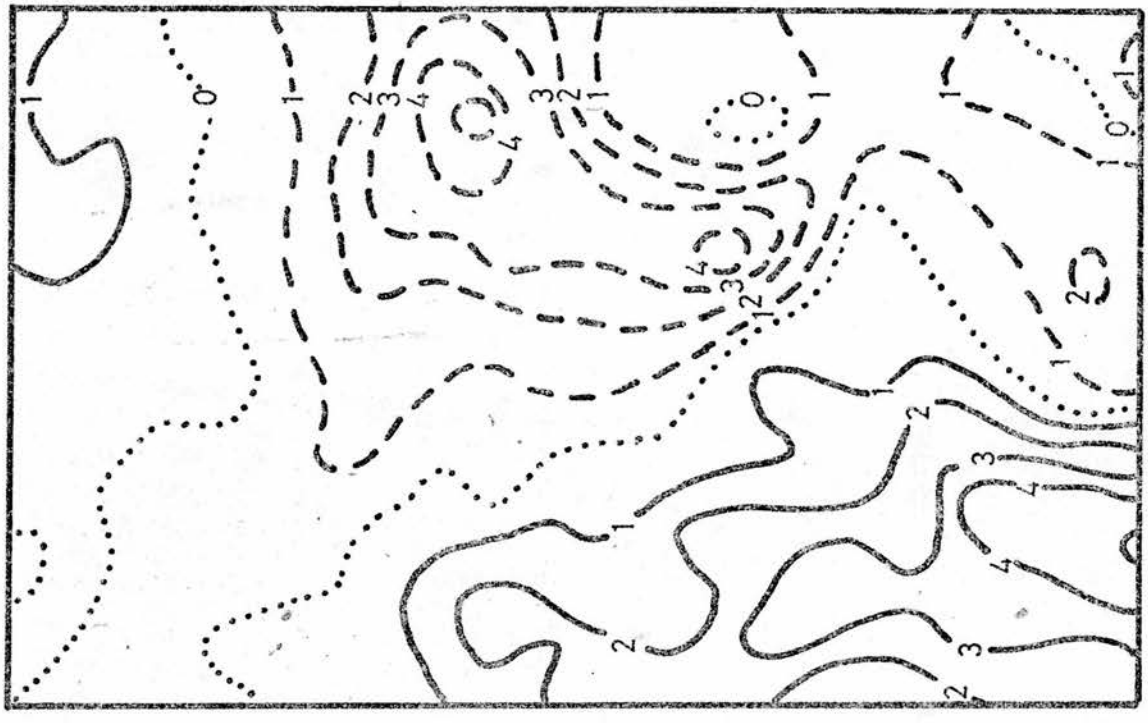

FIGURE 4.27

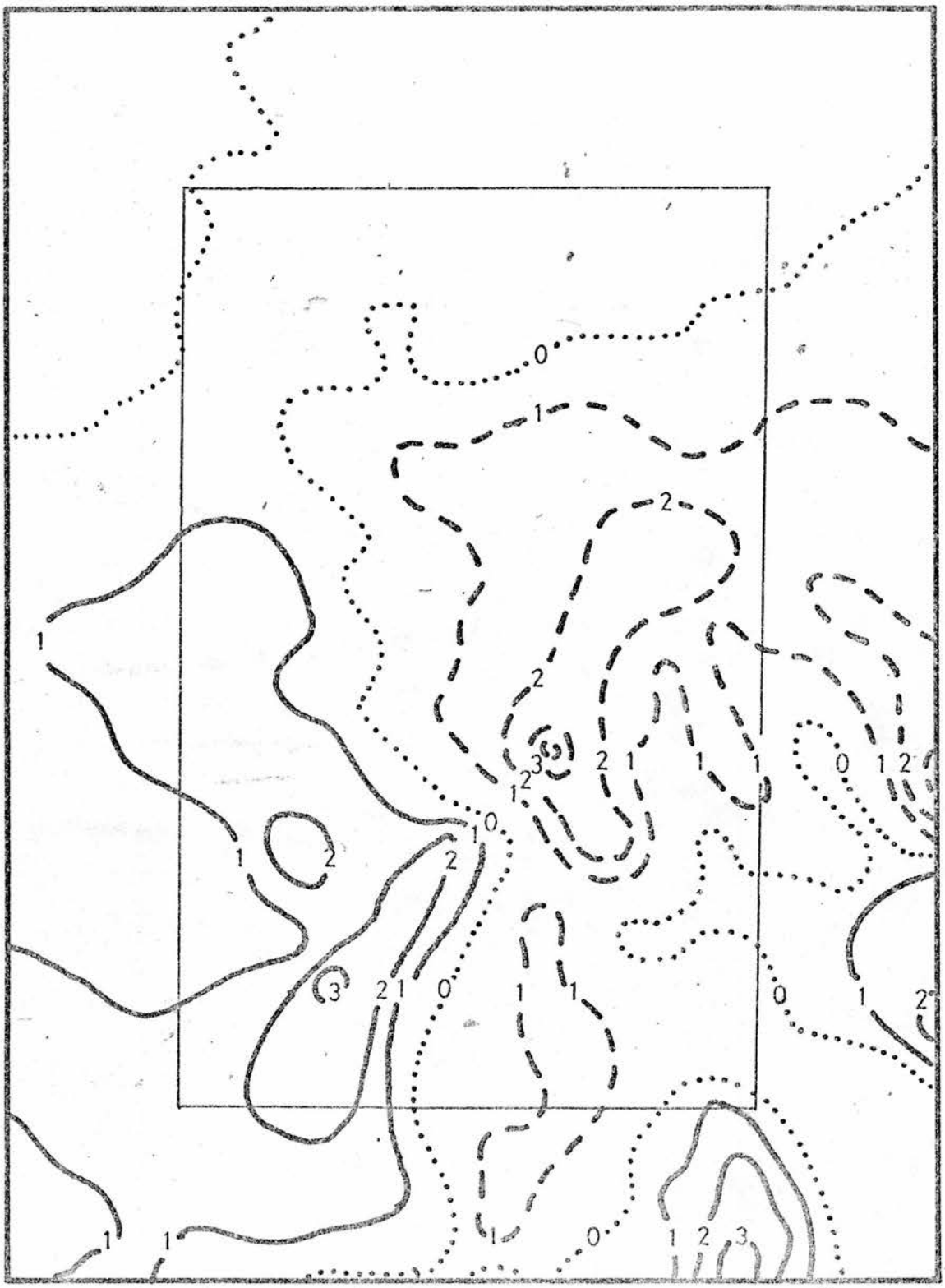

FIGURE 4·28

used to compute ω^*, where

$$\omega^* = \frac{-1}{\sigma}\left[\frac{\partial \Phi}{\partial p}_t + \frac{1}{f} J(\Phi, \frac{\partial \Phi}{\partial p})\right]$$

If the boundary conditions for ω and Φ_t were consistent, then ω^* would be almost the same as ω.

Fig. 4.27 shows the central portion of ω^* as the 600 mb level. The complete distribution of $(\omega^* - \omega)$ at this level is illustrated in Fig. 4.28. A comparison of ω^* and ω (see Figs. 4.27 and 4.24a) indicates that ω^* has the same sort of distribution as ω (e.g. the areas of upward and downard motions are almost the same). However ω^* is consistently larger than ω. This is illustrated by the fact that $(\omega^* - \omega)$ tends to be positive in the same areas in which $\omega^* > 0$ and $\omega > 0$. Fig. 4.28 also shows that $(\omega^* - \omega)$ does not decrease towards the centre of the region (this was also true at other levels). Therefore if ω and Φ_t are to be used in further computations it is desirable to find more consistent boundary conditions.

It can easily be shown that the above procedure for finding ω and Φ_t uses an excessive number of boundary conditions for Φ_t. If n_i, n_j and n_k are the number of gridpoints in the x, y and p directions, then the above proceedure requires the specification of Φ_t at $n_1 = n_k \times (n_i - 1)(n_j - 1) + 1$ gridpoints.

Two alternative methods of solving the system of equations both start by solving the ω-equation. The solution is then used to find Φ_t at the upper and lower boundaries. So far Φ_t has been specified at $n_2 = 2 \times (n_i - 1)(n_j - 1) + 1$ gridpoints. Two ways of proceeding from here are as follows.

(a) The thermal equation is solved as a two-point boundary value problem for Φ_t for all values of i and j.

(b) The procedure described in (a) is carried out only at the lateral boundary. The vorticity equation is then solved for Φ_t at all the interior gridpoints.

Neither (a) or (b) require the specification of Φ_t at any more gridpoints and therefore, for both methods, Φ_t has to be known at n_2 gridpoints. For a given n_i and n_j, n_2 is constant. However n_1 depends upon n_k and when $n_k = 5$ the usual method requires Φ_t to be specified at $2\frac{1}{2}$ times the number of gridpoints as is required by either of the alternative methods. It is suspected that the overspecification of Φ_t in the usual method is responsible for the inconsistencies.

The two alternative methods described above have not yet been tested. However it is likely that they will lead to an improvement in the consistency of the boundary conditions.

A P P E N D I X

The Computer Programs For Solving The Balance Equation

The computer programs were written in the IMP language (see Whitfield (1969)).

Figs. A1 and A2 illustrate the basic programs which were used to solve the balance equation. These differ from those actually used in that the real programs did not use the functions DX1 (SF) etc. All the programs used a maximum of five arrays that depended upon the map parameters (mapping factor, coriolis parameter and gridlength). These arrays were the same for each isobaric surface of a given area. The array Z (I, J) depended upon the geopotential and was therefore different for each isobaric surface. In all the programs it was necessary to store the streamfunction SF (I, J). Also some programs required the storage of extra fields (e.g. a streamfunction field SFX (I, J) or a vorticity field V (I, J)).

Fig. A1 shows the basic program which was used for methods of the first type. (The parts of the program enclosed by brackets were common to all the programs used in solving the balance equation). This program ensures that the ellipiticity condition is satisfied (see Equ. (3.13)) and that the absolute vorticity is greater than zero (see Equ. (3.11)). The lower limit of the vorticity was determined by the parameter γ (GAM in the program). The program ensures that

$$\zeta^{(n)} > -\gamma f$$

It was found that the condition $\zeta^{(n)} + f > 0$ was seldom violated and therefore the value of γ was not critical. In the computations GAM = 0.9 was used.

The program illustrated in Fig. A2a was slightly modified when the NLAS and NLSH methods were used.

```
GP(I,J) - GEOPOTENTIAL AT POINT (I,J)
SF(I,J) - STREAM FUNCTION
CP(I,J) - CORIOLIS PARAMETER
 M(I,J) - (MAPPING FACTOR/GRID LENTH)**2
BET - OVERRELAXATION FACTOR   E - TOLERANCE
GAM - A NUMBER <=1 SO THAT ABSOLUTE VORTICITY >=0
IN,IX,JN AND JX DEFINE THE AREA
 F(I,J)=CP(I,J)/M(I,J)  EY(I,J)=F(I,J)/8  C(I,J)=1/(2*F(I,J))
 Z(I,J)=(DX1(GP)+DY1(GP))/(4*CP(I,J))+EY(I,J)
 A(I,J)=(CP(I+1,J)-CP(I-1,J)/(16*CP(I,J))
 B(I,J)=(CP(I,J+1)-CP(I,J-1)/(16*CP(I,J))
SF(I,J)=GP(I,J)/CP(I,J) - INITIAL GUESS
DX1(X)=X(I+1,J)-2*X(I,J)+X(I-1,J)
DY1(X)=X(I,J+1)-2*X(I,J)+X(I,J-1)
DX2(X)=(X(I+1,J+1)-2*X(I,J)+X(I-1,J-1))/2
DY2(X)=(X(I+1,J-1)-2*X(I,J)+X(I-1,J+1))/2
DXY1(X)=(X(I+1,J+1)+X(I-1,J-1)-X(I+1,J-1)-X(I-1,J+1))/4
       =-(DY2(X)-DX2(X))/2
DXY2(X)=(X(I,J+1)+X(I,J-1)-X(I+1,J)-X(I-1,J))/2
       =(DY1(X)-DX1(X))/2
```

```
1:DET=0 ; MAXADD=0
%CYCLE I=IN+1,1,IX-1 ; %CYCLE J=JN+1,1,JX-1
LAPX=DX1(SF)+DY1(SF)
ELL=Z(I,J)-A(I,J)*(SF(I+1,J)-SF(I-1,J))-B(I,J)*(SF(I,J+1)-SF(I,J-1)
%IF ELL<0 %THEN ELL=0
%IF LAPX<-F(I,J) %THEN LAPX=-GAM*F(I,J)
LAPY=LAPX                                                    ;! NLOR1X
LAPY=2*LAPX                                                  ;! NLOR1
ADDX=DX1(SF)*DY1(SF)-((DX2(SF)-DY2(SF))**2)/16               ;! NLOR1 OR NLOR1X
LAPY=DX2(SF)+DY2(SF)                                         ;! NLOR2X
LAPY=2*(DX2(SF)+DY2(SF))                                     ;! NLOR2
ADDX=(DX2(SF)*DY2(SF)-(DX1(SF)-DY1(SF))**2)/4                ;! NLOR2 OR NLOR2X
ADD=BET*(ADDX*C(I,J)+LAPX/4+EY(I,J)-ELL)/(1+EX(I,J)*LAPY)
SF(I,J)=SF(I,J)+ADD
MADD=MOD(ADD)
%IF MADD>MAXADD %THEN MAXADD=MADD
%IF MADD>E %THEN DET=1
%REPEAT ; %REPEAT
NOS=NOS+1 ; WRITE(NOS,2) ; SPACES(4) ; PRINT(MAXADD/E,6,6)
NEWLINE
MA(NOS)=MAXADD
%IF NOS>2 %AND MA(NOS)>MA(NOS-1) %AND MA(NOS-1)>MA(NOS-2) %THEN ->2
%IF NOS>MAXNOS %THEN ->2
%IF DET#0 %THEN ->1
2:NEWLINE
```

FIGURE A1

(a)

```
SF(I,J)=SFX(I,J)=GP(I,J)/CP(I,J) - INITIAL GUESS

LXY=DXY1(SFX) ; DLX=DX1(SFX) ; DLY=DY1(SFX)          ;! NLAR1
LXY=DXY2(SFX) ; DLX=DX2(SFX) ; DLY=DY2(SFX)          ;! NLAR2
DD=1/(1+(DLX+DLY)*C(I,J)) ; XX=C(I,J)/2
AA=DLX*XX ; BB=DLY*XX ; CC=-LXY*C(I,J)
LXY=DXY1(SF) ; DLX=DX1(SF) ; DLY=DY1(SF)             ;! NLAR1
LXY=DXY2(SF) ; DLX=DX2(SF) ; DLY=DY2(SF)             ;! NLAR2
LAPX=DX1(SF)+DY1(SF)
ELL=Z(I,J)-A(I,J)*(SF(I+1,J)-SF(I-1,J))-B(I,J)*(SF(I,J+1)-SF(I,J-1))
%IF ELL<Ø %THEN ELL=Ø
%IF LAPX<-F(I,J) %THEN LAPX=-GAM*F(I,J)
ADD=BET*(DLX*BB+DLY*AA+LXY*CC+LAPX/4+EY(I,J)-ELL)*DD
SF(I,J)=SF(I,J)+ADD ; SFX(I,J)=SF(I,J)
```

(b)

```
 A(I,J)=(CP(I+1,J)-CP(I-1,J)/(2*M(I,J))
 B(I,J)=(CP(I,J+1)-CP(I,J-1)/(2*M(I,J))
 Z(I,J)=(CP(I,J)**2/M(I,J)+2*(DX1(GP)+DY1(GP))/M(I,J)
SF(I,J)=GP(I,J)/CP(I,J) - INITIAL GUESS
 V(I,J)=DX1(SF)+DY1(SF) - INITIAL GUESS
ALF - UNDERRELAXATION FACTOR   BET - OVERREALXATION FACTOR

ELL=Z(I,J)-A(I,J)*(SF(I+1,J)-SF(I-1,J))-B(I,J)*(SF(I,J+1)-SF(I,J-1))
%IF ELL<Ø %THEN ELL=Ø
H=(DY1(SF)-DX1(SF))**2+(DY2(SF)-DX2(SF))**2                          ;! NLAU1
H=2*((DY1(SF)-DX1(SF))**2)+4*DX1(SF)*DY1(SF)+4*DX2(SF)*DY2(SF)       ;! NLAU2
FF=-F(I,J)+SQRT(ELL+H)
V(I,J)=(1-ALF)*V(I,J)+ALF*FF
ADD=BET*((DX1(SF)+DY1(SF))/4-V(I,J)/4)
SF(I,J)=SF(I,J)+ADD
```

FIGURE A2

The program illustrated in Fig. A2a was slightly modified when the NLAS and NLSH methods were used.

The basic program for methods of the second type is shown in Fig. A2a. This program uses an extra array SFX (I, J). Also, when the coefficients of the linear equation were computed from $\frac{\Psi^{(n-1)} + \Psi^{(n-2)}}{2}$ a further array was required.

Fig. A2b shows the basic program for a method of the third type with a single scan.

REFERENCES

Ames, W.F. 1965 'Nonlinear partial differential equations in engineering', Academic Press, pp. 365-411.

Arnason, G. 1958 'A convergent method for solving the balance equation', J. Met., 15, pp. 220-225.

Asselin, R. 1967 'The operational solution of the balance equation', Tellus, 9, pp. 24-31.

Benwell, G.R.R., Gadd, A.J., Keers, J.F., Timpson Margaret S. and White, P.W. 1971 'The Bushby-Timpson 10-level model on a fine mesh', Meteorological Office, Scientific Paper No. 32.

Berkofsky, L. 1964 'The fall-off with height of terrain-induced vertical motion', J. Appl. Met., 3, pp. 410-414.

Bolin, B. 1955 'Numerical forecasting with the barotropic model', Tellus, 7, 27-49.

Bolin, B. 1956 'A improved barotropic model and some aspects of using the balance equational for three-dimensional flow', Tellus, 8, 61-73.

Carré, B.A. 1961 'The determination of the optimum accelerating factor for successive over-relaxation', Computer Journal, 4, pp. 73-78.

Danard, M.B. 1964 'On the influence of released latent heat on cyclone development', J. Appl. Met., 3, pp. 27-37.

Danard, M.B. 1966 'A quasi-geostrophic numerical model incorporating effects of release of latent heat', J. Appl. Met., 5, pp. 85-93.

Dixon, R. 1970 'An algorithm depending on the physical interpretation of the Laplacian', Met. Mag., London, 99, pp. 294-299.

Dixon, R. 1972 'The equation of a wind satisfying the balance equation', Quart. J.R. Met. Soc., 98, pp. 229-230.

Ellsaesser, H,W. 1968 'Comparative test of wind laws for numerical weather prediction', Mon. Weath. Rev., 96, pp. 277-285.

Endlich, R.M. 1970 'A method for solving the balance equation using vector alterations of the geostrophic wind', Tellus, 22, pp. 621-626.

REFERENCES (contd.)

Engeli, M. 1959 'Over-relaxation and related methods', Refined iterative methods for computation of the solutions and the eigenvalues of self-adjoint boundary value problems, by Engeli, M., Ginsburg, T.H., Rutishauser, H. and Stiefel, E., Birkhauser Verlag, Basel/Stuttgart, pp. 79-91.

Gambo, K. 1957 'The scale of atmospheric motions and the effect of topography are numerical weather prediction in the lower atmosphere', Papers in Meteorology and Geophysics, 8.

Haltiner, G.J., Clarke, L.C. and Lawniczak, G.E. 1963 'Computations of large scale vertical velocity', J. Appl. Met., 2, pp. 242-259.

Haltiner, G.J. 1971 'Numerical weather prediction', John Wiley and Sons, Inc, New York.

Harwood, R. 1969 'Vorticity patterns in extra-tropical cyclones', Ph. D. Thesis, Univ. of London.

Hinkelmann, K.H. 1965 'Lectures on numerical shortrange weather prediction', WMO Regional Training Seminar, Moscow.

Jenssen, D. and Straede, J. 1968 'The accuracy of finite difference analogues of simple differential operators', Proceedings of the WMO/I.U.G.G. symposium on numerical weather prediction in Tokyo November 26 - December 4, VII-59-VII-76.

Kirk, T.H. 1970 'The laplacian and its relevance for analysis', Met. Mag., 99, pp. 151-152.

Knighting, E. 1962 'Numerical weather prediction', Numerical solution of ordinary and partial differential equations, Ed. L. Fox, Pergamon Press, pp. 478-493.

Krishnamurti, T.N. 1968a 'A diagnostic balance model for studies of weather systems of low and high latitudes, Rossby number less than 1,' Mon. Weath. Rev., 96, pp. 197-207.

Krishnamurti, T.N. 1968b. 'A study of a developing wave cyclone', Mon. Weath Rev., 96, pp. 208-217.

Kuo, H.L. 1956 'Quasi-nondivergent prognostic equations', Tellus, 8, pp. 373-383.

REFERENCES (contd.)

Lorenz, E.N.	1960	'Energy and numerical weather prediction', Tellus, 12, pp. 364-373.
Miyakoda, K.	1956	'On a method of solving the balance equation', J. Met. Soc. Japan, 34, pp. 68-71.
Miyakoda, K.	1960	'Test of convergence speed of iterative methods for solving 2 and 3 dimensional elliptic-type differential equations', J. Met. Soc. Japan, 38, pp. 107-124.
Miyakoda, K.	1962	'Contributions to the numerical weather prediction - computations with finite difference', Japanese J. Geophysics, 3, pp. 76-190.
Nitta, T.	1967	'Dynamic interaction between the lower stratosphere and the troposphere', Mon. Weath. Rev., 95, pp. 319-339.
O'Brien, J.J.	1968	Correspondence. Mon. Weath Rev., 96, pp. 99-103.
O'Neill, T.H.R.	1966	'Vertical motion and precipitation computations', J. Appl. Met., 5 pp. 595-605.
Pedersen, K. and Gronskei, K.	1969	'A method of initialization for dynamic weather forecasting, and a balanced model', Geofus. Publikasjoner, 27, No. 7.
Sheldon, J.W.	1972	'Iterative methods for the solution of elliptic partial differential equations', Mathematical methods for digital computers, John Wiley and Sons, New York.
Shuman, F.G.	1957	'Numerical methods in weather prediction: I. the balance equation', Mon. Weath. Rev., 85, pp. 329-332.
Smebye, S.J.	1958	'Computations of preciptation from large-scale vertical motion', J. Met., 15, pp. 547-560.
Stuart, D.W. and O'Neill, T.H.R.	1967	'The overrelaxation factor in the numerical solution of the omega equation', Mon. Weath. Rev., 95, pp. 303-307.
Stuart, D.W.	1964	'A diagnostic case study of the synoptic scale vertical motion and its contribution to mid-tropospheric development', J. Appl. Met., 3, pp. 669-684.

REFERENCES (Contd).

Thomson, P.D.	1961	'Numerical weather analysis and prediction', The Macmillan Company, New York.
White, P.W.	1969	Unpublished Met. Office Papers.
Yamagishi, Y.	1968.	Correspondence. Mon. Weath. Rev., 5, pp. 323-324.
Young, D.	1954	'Iterative methods for solving partial difference equations of elliptic type', Trans. American Math. Soc., 76, pp. 92-111.

ACKNOWLEDGEMENTS

I would like to thank my supervisor, Dr. D.H. McIntosh, without whose patient help and encouragement I would neither have finished this work, nor improved my squash.

I would like to express my gratitude to Mr. J. Paton for allowing me to work in his department; to Mrs. M. Hallisey, Dr. A.S. Thom and my fellow research students for assorted help, advice and discussion; to Mr. F. Bushby and the Meteorological Office for allowing me to use data prepared for the 10-level model; to Mrs. M. Crowther for typing this thesis and to the Natural Environment Research Council for financial support during part of this work.

Finally, I would like to thank my wife who has both inspired, and distracted me. She also corrected my English, although any mistakes are my own.